Bottom-Hadron Production through Top Quark Decay

Dissertation
zur Erlangung des Doktorgrades
des Department Physik
der Universität Hamburg

vorgelegt von
Seyed Mohammad Moosavi Nejad
aus Yazd/Iran

Hamburg
2009

Erstgutachter der Dissertation:	Prof. Dr. B. A. Kniehl
Zweitgutachter der Dissertation:	Prof. Dr. G. Kramer
Erstgutachter der Disputation:	Prof. Dr. B. A. Kniehl
Zweitgutachter der Disputation:	Prof. Dr. J. Bartels
Datum der Disputation:	29.05.2009
Vorsitzender des Prüfungsausschusses:	Prof. Dr. G. Sigl
Vorsitzender des Promotionsausschusses:	Prof. Dr. R. Klanner
MIN-Dekan des Departments Physik:	Prof. Dr. H. Graener

Abstract

In this thesis we apply perturbative QCD to make precise predictions for some observables in high-energy processes involving bottom-quark.
Our first application is a prediction for the energy spectrum of b-flavored hadrons in top quark decay. For that purpose we calculate at NLO the QCD corrections for bottom fragmentation in top decay. The b-quark in the top quark decay is considered once as a massless and once as a massive particle in our calculations. The difference between the differential width calculated in both cases can give us the perturbative fragmentation function of the b-quark. After that using the obtained differential widths and applying ZM-VFNS and GM-VFNS, we make some predictions for the spectrum of B-hadrons produced in top quark decay. The comparison of both approaches shows that the mass effect of the b-quark in the top quark decay is negligible. We also investigate the mass effect of B-hadron in the energy distribution obtained in the previous calculations and we show that this increases the value of the differential width when the energy taken away by the produced parton in top decay is small.
Our second application is to obtain the helicity contributions of the W^+-boson in the energy distribution of b-flavored hadrons in top quark decay. For this reason we study the angular decay distribution for the cascade decay of the top-quark ($t \to b + W^+(\to e^+ + \nu_e)$). Using ZM-VFNS we make predictions for the NLO contributions of the longitudinal, the transverse-minus and the transverse-plus helicity of the W^+-boson in the energy distribution of B-hadron.

Zusammenfassung

In dieser Arbeit wenden wir störungstheoretische QCD an, um Präzisionsvorhersagen für einige Observablen in Hochenergieprozessen mit Bottom Quarks zu machen.

Als erste Anwendung berechnen wir das Energiespektrum von B Hadronen in Top Quark Zerfällen. Dafür berechnen wir in nächstführender Ordnung die QCD Korrekturen zur Bottom Fragmentierung in Top Zerfällen. Das b Quark im Top Zerfall wird dabei einmal als masselos und einmal als massiv angenommen. Die Differenz zwischen den beiden Ergebnissen ergibt uns die störungstheoretische Fragmentierungsfunktion des b Quarks. Danach machen wir Voraussagen für das Energiespektrum von B Hadronen in Top Quark Zerfällen, einmal im ZM-VFNS und einmal im GM-VFNS Schema. Der Vergleich beider

Ansätze zeigt, dass der Masseneffekt des b Quarks im Top Zerfall vernachlässigbar ist. Schließlich betrachten wir auch noch den B Hadron Massen-Effekt in der Energieverteilung der B Hadronen, die im Top Quark Zerfall erzeugt werden.

Unsere zweite Anwendung ist, die Händigkeitsverteilung von W^+ Bosonen in der Energieverteilung von B Hadronen im Top Zerfall zu berechnen. Dafür untersuchen wir die Winkelverteilung des Kaskadenzerfalls des Top Quarks ($t \to b + W^+(\to e^+ + \nu_e)$). Im dem ZM-VFNS Schema machen wir Vorhersagen für die NLO Verteilungen der longitudinalen, der negativ transversalen und der positiv transversalen Händigkeit des W^+ Bosons in den B Hadron Energieverteilungen.

Contents

List of Figures

Chapter 1

Introduction

The Standard Model(SM) of elementary particles has proved to be extremely successful during the past three decades. It has shown to be a well established theory. All predictions based on the SM have been experimentally verified and most of its parameters have been fixed. The only part of the SM that has not been directly experimentally verified yet is the Higgs sector and, in particular, the existence of a neutral massive spin-zero particle often simply referred to as Higgs. There is still no direct evidence for its existence and despite the many constraints from precision electro-weak physics, the Higgs mass is not known. Not all of the parameters of the Higgs potential are determined, and its Yukawa couplings to the fermions are determined through the measurements of the masses of the fermions (quarks and leptons). Experiments in the near future at the Large Hadron Collider (LHC) and at the Tevatron accelerator, either will confirm that particle's existence and fix the Higgs potential parameters, or will increase the limit on its mass.
The SM describes three of the four known interactions: Electromagnetic, Weak and Strong. The fourth one, Gravity, is not considered in the SM and we ignore its effect in our calculation. The gravity becomes important only at scales of the order of the Plank mass ($G_N^{-1/2} \sim 10^{18}$ GeV) thus it is completely irrelevant for present collider experiments.

The SM is a gauge-field theoretical model produced of two non-abelian gauge group and one abelian gauge group:

$$G_{SM} = SU(3)_C \times SU(2)_I \times U(1)_Y. \tag{1.1}$$

The gauge group is non-simple and involves three different dimensionless coupling constants corresponding to each of the three group factors above. The $SU(2)_I \times U(1)_Y$ part

corresponds to the Weinberg-Salaam model [1] and provides a unified description of the electromagnetic and weak interactions. There are four gauge bosons associated with that group: two neutral ones, γ and Z, and two charged ones, $W^{\pm}$. The photon γ is exactly massless due to the the unbroken $U(1)$ subgroup that is identified with electro-magnetism. The other three are heavy, with masses approximately $m_Z = 91$ GeV and $m_{W^{\pm}} = 80$ GeV; their masses arise as a result of electroweak symmetry breaking via the Higgs mechanism. The electroweak vector bosons couple to all fermions. The magnitude of those couplings is relatively small; the electromagnetic interactions are suppressed by powers of $\alpha = e^2/4\pi \approx 1/137$, while the effects of the weak interactions are typically proportional to powers of the Fermi constant $G_F = 1.166 \times 10^{-5} GeV^{-2}$. For that reason the quantum corrections introduced by electro-weak interactions are much smaller than the ones due to strong interactions[1].

The dependence of the dimensionless electroweak gauge couplings g and g' on energy is intuitive, i.e. the strength of the electroweak interactions increase with the energy scale. For that reason the $SU(2) \times U(1)$ theory of the electroweak interactions is a true perturbation theory formulated directly in terms of observable fields. The situation changes dramatically when one considers the strong interactions described by the $SU(3)_C$ factor in (1.1). First, the coupling constant is not small. Moreover, as it is well known, a non-abelian gauge theory with such a gauge group and with small number of active fermions (flavors) exhibits the behavior known as asymptotic freedom: the dimensionless coupling constant associated with th group decreases with the increasing of the energy scale and effectively such a theory behaves as a free theory at high energies, see Fig.(1.1). However , at small energies the coupling grows and eventually diverges at some finite value of the energy scale. That scale, usually denoted as Λ_{QCD} and called *the typical QCD scale*, has a value of the order of 200-300 MeV and quantifies the borderline between the perturbative and non-perturbative regimes in such a theory. From the above discussion it becomes clear that such a theory exhibits another considerable property: *confinement*.

The growing of the coupling at low energies (which corresponds to large distance) indicates that the particles which are described by such a gauge theory may not be able to exist as free (asymptotic) states at all. Instead, they will form bound states except top quark, since due to the large mass and the weak coupling constant, i.e. the top quark will

[1]This is also the case in the applications considered in this thesis as will be detailed in the subsequent sections.

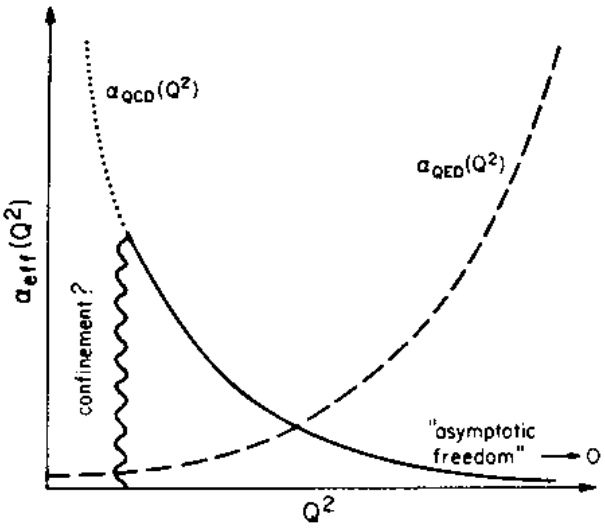

Figure 1.1: Illustration of the behavior of the QED and QCD effective coupling constant as a function of the energy scale, Q^2. In QED the effective coupling, $\alpha_{QED}(Q^2)$, is small at small Q^2, but becomes large at large Q^2 (i.e., short distance). In QCD the effective coupling is large at small Q^2 (i.e., large distance) where confinement occurs, but decreases to zero at large Q^2 (asymptotic freedom).

decay before forming a bound state. That expectation is confirmed by experiment: no free quarks have ever been observed experimentally.
Unlike the quarks that carry an additional quantum number called color, the observable strongly interacting particles - the hadrons- are colorless objects and have the quantum numbers of bound states of two-quarks (mesons) and three-quarks (baryons). The property of confinement is an assumption based on the above mentioned behavior of the strong coupling constant and the non-observation of free colored particles. Confinement is proved in lattice gauge theory. The derivation of the properties of the hadrons from QCD is one of the fundamental problems in theoretical physics nowadays.

It is a remarkable achievement that we are able to make precise predictions for the observed hadronic states in high energy experiments based on a theory formulated in terms of non-observable constituents, i.e. quarks. One of the main ingredients of the theory that makes this possible is the factorization theorem. In essence, it states that in hard scattering experiments with typical hard scale $Q \gg \Lambda_{QCD}$ an observable (e.g. a cross

section) can be written as a product(more precisely-convolution) of perturbative and non-perturbative parts. The former part can be calculated in perturbative theory based on an expansion in the strong coupling constant $\alpha_s(Q^2)$ while the latter part has to be extracted from experiment. It is possible to extend the factorization theorem even to processes where other scales besides Q are present, e.g. the mass of heavy quarks. As will be clear from discussions throughout this thesis, there is no absolute notion of heavy quarks, i.e. whether a quark is considered heavy or light depends on the particular problem is being studied. However, in general, light quarks are considered to be those with masses below Λ_{QCD} (i.e. u, d, s) while the ones with masses above that scale are usually considered to be heavy (c, b, t). The reason behind such a separation is easy to understand: for a heavy quark with mass $M, \alpha_s(M^2) \ll 1$ thus heavy quark production is a calculable process in perturbative QCD (pQCD). Studies of QCD involving processes with heavy quarks, are at present an important internal test for QCD as well as for obtaining precision predictions that will be needed to distinguish signals from new physics (Supersymmetry, Extra Dimension, etc.).

QCD has another particular feature: there are situations where the convergence of the perturbation series is spoiled because of the appearance of additional factors that multiply the coupling constant to any order in perturbation series. The presence of such terms effectively alters the expansion parameter to a larger value which in turn spoils the convergence of the series. To be able to obtain useful information in that case, one needs to resum classes of such terms to all orders in the coupling constant. These terms will be studied in next chapter.

There are many examples of physical processes involving heavy quarks where the factorization theorem plays a decisive role in studies of them and the application of the above mentioned resummation often leads to series improvement of the perturbative results. In this thesis we study one of these such processes in perturbative QCD with detailed phenomenological applications: the spectrum of b-flavored hadrons in top quark decay.

The top quark was discovered at the Tevatron in 1995. It is the heaviest elementary particle with a mass of 170.9 ± 1.8 GeV [2]. Since this is much larger than the mass of any other fermion and also twice as large as the mass of the electroweak gauge bosons, one may wonder that whether or not the top quark really is an elementary particle and if it is elementary, can its mass be generated by the same mechanism from the mass of the other particles?. After all, its mass is almost six orders of magnitude larger than the electron mass. On the other hand, the top quark is also essential for our understanding

of the standard model. The reason is that the precision of observables like the W-boson mass or the effective weak mixing angle depend on the top-quark mass through radiative corrections. If we want to reduce the errors on these quantities, it is therefore necessary to reduce the error on the top-quark mass as well. Therefore it is necessary to perform precision measurements of the top quark properties. Next to its mass, its total decay width and Yukawa coupling are of special interest. Concerning the mass, it is expected that the uncertainty will be reduced to about 1Gev at the LHC. However, the width and Yukawa coupling can not be measured to a very good accuracy either at the Tevatron or at the LHC. This would change at a future International Linear Collider (ILC). Such a collider offers the unique ability to measure the cross section with a very high experimental accuracy [3] and also provides the possibility to extract the strong coupling constant, α_s, with high precision. For example, it is expected that the t-quark mass can be measured with better than 100 MeV accuracy.

In the SM, it is the mass of the top that uniquely distinguishes it from the other five flavors. Top's large mass is responsible for its small lifetime, the latter prevents the top from forming bound states (a process known as hadronization). For that reason, the top quark behaves like a real particle and one can safely describe its decay in perturbative theory. Since the only experimental information about the top is through its decay products, it is very important to have a precise theoretical prediction for the decay products of the top. In this thesis we make a prediction for the spectrum of the hadrons resulting from the hadronization of the b-quark in the t-quark decay. We will show that there are two kinds of large logarithms into our partonic level calculation which should be resummed to all orders in α_s. These large logs are: *quasi-collinear* ones that are due to the large ratio of top-to-bottom mass and *soft* ones that are due to soft gluon radiation and affect the distribution in particular kinematical regions. Such results will be very important when the near future high energy experiments supply enough data on top decay.

This thesis is organized as follows: in the next chapter we discuss some general features of QCD from the perspective of our applications. In chapter 3, we present our results on differential decay rate of top decay when the b-quark is considered a massless particle. In chapter 4, we present our original results on the differential decay rate of top decay when the producing b-quark is considered to be a massive one and then by comparing them with the previous result we extract the perturbative fragmentation function of the b-massless into the b-massive. We show our results for the hadronization of the b-quark in top quark

decay and make predictions for the spectrum of b-flavored hadrons. We also show the effect of b-flavored hadron mass into the differential decay rate and energy spectrum of the B-hadron in the top decay process. In chapter 5 we concentrate on the contributions of the W^+-boson helicity in the cascade decay of the top quark followed by the leptonic decay of the W^+-boson. In chapter 6 are our conclusions. In the appendix we have listed some useful results.

Chapter 2

Perturbative QCD

In the previous chapter we made some general remarks about the importance of QCD as a theory of the strong interactions and also a few of its peculiar features. In this chapter we are going to review that theory and derive many of its properties. The organization of material in the present chapter does not follow any particular review on QCD but it is presented in a way that is suitable for our applications. There are many excellent reviews of QCD; some of those can be found in [5, 6, 7, 8, 9].

2.1 QCD as a Fundamental Model for the Strong Interactions

The strong interactions govern the interactions of hadrons at a wide range of energies: from the highest energies accessible to the present day colliders down to energies typical for the nuclear physics. At the same time the behavior of the strong interaction is very different in the low and high energy regimes. At low energies, i.e. energies characterized by a scale $\mu \ll \Lambda_{QCD}$, the hadrons behave as fundamental particles. However, no successful field-theoretical description in terms of the observed hadrons was found that was able to describe the high energy regime and explain the increasing data of observed hadrons at high energy colliders. Contrary to the early expectations, the understanding of the strong interactions was made in the study of the high energy behavior of the hadrons.

2.1.1 Quark Hypothesis

In 1964 Gell-Mann and Zweig [10] introduced the idea of quarks: a few elementary particles that are the building blocks of all hadrons. There are six known types of quarks (quark flavors); they are spin 1/2 fermions with rational electric charges (in units of the charge of the electron with the charge $-e$): u, c, t have charge $+2/3$ while d, s, b have charge $-1/3$. The quark hypothesis assumes that the wave function of a hadron is constructed from the one-particle wave functions of quarks and/or antiquarks. The mesons have the quantum numbers of a quark-antiquark pair while the baryons and anti baryons are combinations of three (anti)quarks. Also, in order to avoid a problem with the spin-statistics theorem, it was necessary to introduce the additional hidden quantum number-*color* [11]. From a comparison with experiment it was concluded that each quark flavor must have three different "copies" labeled by an additional color index. Since no colored particles have been observed it was postulated that the hadrons can only form "colorless" combinations of quarks, i.e. color was introduced as an exact global symmetry. It can be shown that the above observations plus the requirement that quarks and antiquarks transform under different (complex-conjugated) irreducible representations of the color symmetry group uniquely fixes the group to be $SU(3)_C$. The quarks transform under the fundamental representation 3 of that group, while the antiquarks transform under its conjugated representation $\overline{3}$.

2.1.2 Parton Model

The idea that the hadrons are built from elementary constituents - the partons [12]- was extremely successful not only in explaining the hadron spectroscopy but also in the description of the Bjorken scaling [13] observed in Deep Inelastic scattering (DIS) experiments [14]. The experimental data showed that at large scales the structure functions of the nucleons are (approximately) independent of the value of the hard energy scale Q and depend only on the Bjorken variable x. The parton model assumes that in high energy lepton-nucleon scattering, where the transferred momentum is large enough so the masses of the partons and their transverse motion inside the nucleon can be neglected, the virtual electroweak vector boson emitted from the initial lepton is scattered by a single free point-like parton a. The whole information about the structure of the hadron that is relevant to the high energy process is encoded in a scalar function $f_a(\xi)$ called the parton distribution function (pdf) representing the probability distribution for finding the parton a inside the

hadron and carrying a fraction ξ ($0 \leq \xi \leq 1$) of the momentum of the parent hadron. The philosophy of the parton model then suggests the following form of the cross section at high energy for the production of arbitrary number of final hadron in the state X, i.e. for the process $e + h \to e' + X$:

$$d\sigma(h, X) = \sum_a \int_0^1 d\xi f_a(\xi) d\hat{\sigma}(a, X), \tag{2.1}$$

where $d\sigma(h, X)$ is the cross-section for scattering of a hadron h and X stands for the other particles in the scattering process; $d\hat{\sigma}(a, X)$ is a parton level cross-section with the hadron h replaced by a free parton a, and $f_a(\xi)$ is a distribution function. Since the parton model is a free theory, to lowest order in the electroweak coupling the partonic cross-section is very simple: $d\hat{\sigma} \sim \delta(\xi - x)$, so that the momentum fraction ξ is identified with the Bjorken variable x. Therefore under the parton model assumption (2.1), the structure functions are simply proportional to the pdf $f_a(x)$ and naturally independent of the hard transferred momentum Q.

The success of the parton model goes beyond the description of Bjorken scaling. It also makes a prediction about various relations involving the measurable structure functions, one of them is the Callan-Gross relation [15] which leads to the fact that quarks have spin 1/2. The parton model can be generalized to other processes as well; one just needs to measure the pdfs for the various quarks in a specific process in order to predict a measurable quantity for another process. In that procedure, the following relations between the various parton distributions, following from iso-spin invariance, are often assumed:

$$f_u^{proton}(x) = f_d^{neutron}(x); \quad f_d^{proton}(x) = f_u^{neutron}(x). \tag{2.2}$$

2.1.3 QCD: the Dynamical Theory of Color

Although the parton model was quite successful in the description of many high energy processes, it was clear that it is a good hint toward a complete dynamical theory of the strong interactions. The complete theory would be able to explain one of the basic assumptions of the parton model-asymptotic freedom. Such a theory was constructed around 1973 after it was understood that the Yang-Mills theories play an important role in high energy physics; at that time the renormalizeability of those theories was proved and methods for their quantization were developed [16]. It was also shown that the non-abelian theories

were the only theories which may exhibit asymptotic freedom, or technically, have negative first coefficient in the $\beta-$function (see next section). All these developments led to the construction of QCD as the dynamical theory of the strong interactions [17] as follows:

QCD is a non-abelian gauge theory with six quark flavors. The gauge group can be naturally obtained by gauging the exact global color symmetry group $SU(3)_C$. The quarks transform under the fundamental representation of $SU(3)_C$. Since $\dim(SU(3))=8$, there are eight gauge bosons called *gluons* that are electrically neutral, carry color charge and, as usual, are hermitian fields that transform under the adjoint representation of the gauge group $SU(3)_C$.

The lagrangian of QCD has the following form:

$$L_{QCD} = -\frac{1}{4}F^a_{\mu\nu}F^{a,\mu\nu} + i\sum_q \overline{\psi^i}_q \gamma^\mu (D_\mu)_{ij}\psi^j_q - \sum_q m_q \overline{\psi^i}_q \psi^i_q, \tag{2.3}$$

where the index $i = 1, 2, 3$ runs over the different quark colors and q over the quark flavors: $q = u, b, s, c, b, t$. The field-strengths are given by:

$$F^a_{\mu\nu} = \partial_\mu A^a_\nu - \partial_\nu A^a_\mu - g_S f^{abc} A^b_\mu A^c_\mu, \tag{2.4}$$

and the gauge-covariant derivative is:

$$(D_\mu)_{ij} = \delta_{ij}\partial_\mu + ig_S \sum_a t^a_{ij} A^a_\mu. \tag{2.5}$$

In the above equations, g_S is the strong coupling constant, f^{abc} are the structure constants of the gauge group and t^a are the generators of the fundamental representation of the gauge group. In general, the lagrangian (2.3) must be supplemented with gauge-fixing and ghost terms. The quarks have non-zero masses but their origin is outside QCD; in the SM their masses result from the electroweak symmetry breaking. The only free parameters in QCD are the six quark masses and the single gauge coupling constant. The gauge group has the following matrix structure which, for generality, we present for arbitrary group SU(N); the fundamental representation has generators $t^a, a = 1, ..., N^2 - 1$ that satisfy:

$$\begin{aligned} tr(t^a t^b) &= \frac{1}{2}\delta^{ab} \\ \sum_a t^a_{ij} t^b_{jk} &= C_F \delta_{jk}, \quad i, j, k = 1, ..., N. \end{aligned} \tag{2.6}$$

For the group SU(3), the generator t^a are usually given by the Gell-Mann matrices λ^a : $t^a = \lambda^a/2$. Similarly, the adjoint representation has generator T^a that can be related to

the structure constants f^{abc} through:

$$(T^a)_{bc} = f^{abc}, \tag{2.7}$$

and

$$tr(T^c T^d) = \sum_{a,b} f^{abc} f^{abd} = C_A \delta^{cd}. \tag{2.8}$$

Above, C_F and C_A are the values of the quadratic Casimir of the gauge algebra in the fundamental and adjoint representation respectively:

$$C_F = \frac{N^2 - 1}{2N} \quad ; \quad C_A = N, \tag{2.9}$$

and for the case of SU(3):

$$C_F = \frac{4}{3} \quad ; \quad C_A = 3. \tag{2.10}$$

Once formulated, it must be shown that QCD indeed is capable of reproducing the success of the parton model as a first step. That in fact follows since from the formulation of QCD it is clear that the parton model corresponds to the Born approximation of QCD. The real challenge however is to derive the asymptotic freedom from first principles and also to derive the corrections to the Bjorken scaling.

2.1.4 Strong Coupling Constant

The running of the renormalized strong coupling $\alpha_S = \frac{g_S^2}{4\pi}$ is determined from the following equation:

$$\mu \frac{\partial \alpha_S}{\partial \mu} = 2\beta(\alpha_S). \tag{2.11}$$

The β-function $\beta(\alpha_S)$[1] has a series expansion in the coupling constant α_S. It can be determined up to a fixed order in perturbation theory from explicit evaluation of the gauge coupling renormalization constant Z_g:

$$\beta(g) = \lim_{\epsilon \to 0} \Big(-\epsilon g - \frac{\mu}{Z_g} \frac{dZ_g}{d\mu} g \Big). \tag{2.12}$$

[1] In contrast to most of the standard presentation (e.g [5]), we introduced $\beta(\alpha_S)$ through the relation: $\beta(\alpha_S) = \frac{g_S}{4\pi}\beta(g)$

At present, the β-function of QCD is known to four loops in the $\overline{MS}$ scheme [18]. However, since for all applications in this thesis we need the evolution of the strong coupling to two loops, we will present only the two loop result:

$$\beta(\alpha_S) = -b_0\alpha_S^2 - b_1\alpha_S^3 - \cdots , \tag{2.13}$$

with b_0 and b_1 given by:

$$b_0 = \frac{33 - 2n_f}{12\pi}, \quad b_1 = \frac{153 - 19n_f}{24\pi^2}. \tag{2.14}$$

The first two coefficients of the β-function are independent of the renormalization scheme. However, that is no longer true for the higher order terms. In Eq.(2.14), n_f is the number of active massless flavors. In the presence of quark masses, the value of the active flavors becomes scale dependent. If one considers the masses for the quarks, then for the scale $\mu : m_n \ll \mu \ll m_{n+1}$ all flavors with masses below m_{n+1} are effectively massless while the rest of the flavors are heavy and can be integrated out. An example is the case of top decay considered in Chapter 3 where the scale is running between the b and the t masses. However, in practical applications (especially with scales of the order of the b and the c quark) the assumption above is not always valid and therefore the choice of n_f is somehow ambiguous. The common practice is to change the value of n_f by one unit when the hard scale crosses the mass of the corresponding heavy quark, we will explain in more detail later. Changing of the number of the active flavors in crossing of the hard scale should be supplemented with an additional constraint that relates the values of the strong coupling evaluated in the two schemes at the switching point. In the $\overline{MS}$ renormalization scheme, the strong coupling is continuous at the switching points [19] (see also [4]), up to negligible corrections of order $\mathcal{O}(\alpha_S^3)$. We ignored this effect in our calculation.

Now it is easy to show that indeed QCD enjoys the property of asymptotic freedom [20]. In a regime where the strong coupling is small, from Eq.(2.14) and Eq.(2.11), it is easy to see that the strong coupling constant is a decreasing function of the scale μ if the number of flavors $n_f < 33/2$ and this requirement is satisfied in QCD. The exact solution of Eq.(2.11) to NLO is given by:

$$\alpha_S(\mu^2) = \frac{1}{b_0 \ln(\mu^2/\Lambda^2)}\left\{1 - \frac{b_1 \ln[\ln(\mu^2/\Lambda^2)]}{b_0^2 \ln(\mu^2/\Lambda^2)}\right\}. \tag{2.15}$$

One can use this expression in order to relate the values of the strong coupling at two

different scales with NLO accuracy [21]:

$$\alpha_S(k^2) = \frac{\alpha_S(\mu^2)}{1+b_0\alpha_S(\mu^2)\ln(k^2/\mu^2)}\Bigg(1-\frac{b_1}{b_0}\frac{\alpha_S(\mu^2)}{1+b_0\alpha_S(\mu^2)\ln(k^2/\mu^2)} \times \ln(1+b_0\alpha_S(\mu^2)\ln(k^2/\mu^2)) + \mathcal{O}(\alpha_S^2(\mu^2)[\alpha_S(\mu^2)\ln(k^2/\mu^2)]^n)\Bigg). \quad (2.16)$$

The constant Λ is the typical QCD scale [22] and contains all the information about the boundary condition. It is a low energy scale where the strong coupling diverges. As we mentioned in Chapter 1, Λ represents the border between the perturbative and non-perturbative regimes of QCD. In practice the value of Λ is ambiguous. In high energy experiments one typically obtains information about the strong coupling constant at some large scale and only from there the value of Λ is inferred. It is obvious that in this way the determination of Λ absorbs all ambiguities such as the dependence on the order of α_S (LO, NLO, etc.) and dependence on the scheme, the choice of the value of n_f and the choice of the renormalization scheme. In this thesis we use the following value of the strong coupling at NLO [4]:

$$\alpha_S(m_Z^2) = 0.1181. \quad (2.17)$$

It leads to $\Lambda^{(5)} \simeq 227$ MeV appropriate for $n_f = 5$. The precise values used in our applications will be discussed in the next chapter.

2.2 QCD Factorization Theorem

QCD is formulated in terms of quarks and gluons while the experimentally observed states are hadrons. Since at present we are not able to describe the non-perturbative regime of QCD, therefore to apply QCD to study the hadronic interactions, we require a universal way to split the contributions of short- and long-distance physics. Such a separation is possible. It is known at the (QCD) factorization theorem [23, 24] and states that for processes that have initial and/or observed final state hadrons the differential cross-section has the following form:

$$d\sigma(x,Q^2,m^2) = \prod_{h,h'}\sum_{i,f} f_{i/h}(x,\mu^2)\otimes d\hat{\sigma}_{i\to f}(x,Q^2,m^2,\mu_r^2,\mu_f^2) \otimes D_{h'/f}(x,\mu^2)+\mathcal{O}(\Lambda/Q). \quad (2.18)$$

The factor $f_{i/h}$ stands for the parton distribution function of the parton i inside the hadron h present in the initial state, and Q and x represent the hard scale and some kinematical variable respectively. Unlike the simple parton model (2.1), the parton distributions also depend on the factorization/renormalization scale μ^2. The second factor $d\hat{\sigma}_{i\to f}$, also known as the (Wilson) coefficient function, represents the partonic hard scattering cross section for the reaction $i \longrightarrow f$ that depends on the unphysical renormalization and factorization scales μ_r^2 and μ_F^2 and on the masses of the heavy quarks m^2. The last factor in Eq(2.18) is the so called fragmentation function D. It contains the information for the hadronization of the hard parton f (that is produced in the hard process described by the partonic cross-section $d\hat{\sigma}$) into an observed hadron $h^{'}$. The integral convolution appearing in (2.18) is defined as:

$$(f \otimes g)(x) = \int_x^1 dz g(z) f(\frac{x}{z}), \tag{2.19}$$

where f and g are two functions with argument x: $0 \leq x \leq 1$. The real power of the factorization theorem is in the fact that the distribution/fragmentation functions are universal: they depend only on the non-perturbative transition which they describe and not on the hard scattering process. That is why once they are measured in one process, they can be applied to any other process. At the same time, the coefficient function contains all the information about the hard scattering process and is independent of the details of the non-perturbative transitions. Although the $\otimes$-product of coefficient function and distribution/fragmentation function is an observable and therefore free from any ambiguity, the distribution, fragmentation and the coefficient functions are separately ambiguous. In particular, they are scheme dependent; the origin of that scheme dependence is in the treatment of the IR divergences associated with their computation. Infrared (IR) means collinear divergence in this case. As we will show later the IR singularities cancel between real and virtual contributions. Let us describe the scheme dependence of the coefficient function and the distribution/fragmentation function in more detail:

The evaluation of the coefficient function proceeds in the following way: one calculates the hadronic process $d\sigma$ that is under study by formally replacing each initial hadron h with an *on-shell* parton a. To that end, and in accordance with the factorization theorem (2.18) we just described, one introduces (also formally) new parton distributions $f_{i/a}$ which have the meaning of a distribution of a parton i inside parton a; we treat the fragmenting partons in a similar fashion. Therefore the differential cross-section can be factorized as

the following:

$$d\sigma = d\hat{\sigma} \otimes f_{i/a} \quad . \tag{2.20}$$

The main purpose of the fictitious distribution $f_{i/a}$ is to absorb all the IR singularities from the calculated cross-section. As a next step, one simply discards the functions $f_{i/a}$ and what is left is the needed coefficient function $d\hat{\sigma}$. The extraction of the partonic pdfs is physically equivalent to the absorption of the IR sensitive contributions into the pdfs $f_{i/h}$ (see also section (2.4.1)).

Clearly, such a procedure is very similar to th UV renormalization where one introduces appropriate counter-terms to absorb (and thus cancel) the UV divergences appearing in the Feynman diagrams. In the $\overline{MS}$ subtraction scheme, which is most often used, the partonic pdfs read:

$$f_{i/a}(x) = \delta_{ia}\delta(1-x) + \frac{\alpha_S}{2\pi}\left(-\frac{1}{\epsilon} + \gamma_E - \ln 4\pi \right) P_{ia}^{(0)}(x) + \mathcal{O}(\alpha_S^2), \tag{2.21}$$

where $P_{ij}^{(0)}(x)$ are the leading order Altarelli-Parisi splitting functions that will be defined and thoroughly discussed in the next section, and $\epsilon = (4-D)/2$ (see the next Chapter for more details). The subtraction scheme for the IR divergences emerging in $d\sigma$ in the limit $\epsilon \to 0$ is related to the renormalization scheme used to remove the UV divergences appearing in the formal (operator) definition of the parton densities. For a more detailed discussion see [23], [25] and [26].

The Factorization theorem in the presence of massive quarks is accurate up to terms $\mathcal{O}\ (\Lambda/Q)$; see Eq.(2.18). The proof of the factorization theorem presented in [24] uses a variable flavor number scheme (VFNS). The VFNS treats the light quark u, d and s as massless and always includes them as active flavors in the running of the strong coupling α_S. The treatment of the heavy flavors c, b and t is process dependent. In some references people apply this convention if the typical energy scale is below the corresponding quark mass then that quark is treated as heavy and is integrated out. In particular it does not contribute to the evaluation of the strong coupling constant and does not have an associated parton density. The quarks with masses below the hard scale are treated in a different way: they contribute to the strong coupling as if they are exactly massless, and they have their own distribution functions[2] which are evolved with the energy scale via

[2]These are introduced in order to systematically resum large logs of collinear origin that appear to all

evolution equation with massless kernels (see next section). We will explain this scheme in Chapter 4 but there we use other assumptions to specify the number of the active flavors.

The physical picture behind the factorization theorem is quite simple. One formally introduces a scale μ_F which separates the short- from long-distance physics involved in the process. It is intuitively clear that such separation must indeed occur in the limit of large values of the hard scale Q. The time scale for the hard interaction is of the order of Q^{-1} and therefore quite small, while the typical time for the hadronization effects is not smaller than $\Lambda_{QCD}^{-1} \gg Q^{-1}$. As a result, in the limit $Q \to \infty$, short - and long-distance effects cannot interfere with each other and therefore factorize. More formally, the separation between small and large scales means that all contributing Feynman diagrams that have lines with small virtuality can be separated from the lines with large (of the order of the hard scale Q) virtuality. The former diagrams constitute the distribution functions while the latter give the hard coefficient function. Such non-trivial factorization for the terms with leading power in $1/Q^2$ (the so-called leading twist terms) was proved by Libby and Sterman [28].

2.3 Perturbative Evolution: DGLAP Equations

In this section we will turn our attention to the dependence of the various factors in Eq.(2.18) on the renormalization and factorization scales which incorporate the scaling-violation effects. To better illuminate our point, we are going to make the following two simplifications throughout this section: first, we will set the renormalization and the factorization scales to the scale μ, i.e. $\mu_r = \mu_F = \mu$. This is a standard choice in the studies of pQCD which, however, will not restrict the generality of our discussion. If needed, the separate dependence on both scales can be easily restored with the use of the running of the strong coupling (see Eq.(2.16)). The second simplification is that we will consider Eq.(2.18) with a single fragmentation or distribution function multiplying the coefficient function $d\hat{\sigma}$. We will consider those two *"representative"* cases (only initial or final observed hadrons) of Eq.(2.18) separately.

orders in α_S. Schemes without heavy quark densities exist and are called Fixed Flavor Number Scheme (FFNS). An example is the GRV 98 set of parton distribution [27].

We start with:

$$d\sigma(x, Q^2, m^2) = \sum_i f_{i/N}(x, \mu^2) \otimes d\hat{\sigma}_{i\to X}(x, Q^2, m^2, \mu^2), \tag{2.22}$$

which corresponds to the case of a single hadron (nucleon N) in the initial state and no observed hadrons in the final state. A prominent example is the case of inclusive Neutral Current (NC) or Charged Current (CC) DIS:

$$l + N \to l' + X, \tag{2.23}$$

with l and l' being leptons, N a hadron (usually a nucleon) and X stands for any unobserved hadrons produced in the reaction (2.23). This case describes reactions with so-called space-like evolution.

As a representative for a reaction with a single fragmentation function we take:

$$d\sigma(x, Q^2, m^2) = \sum_f d\hat{\sigma}_{e^+e^-\to f}(x, Q^2, m^2, \mu^2) \otimes D_{h/f}(x, \mu^2), \tag{2.24}$$

which corresponds to the case of inclusive production of a single hadron h in a non-hadronic collision. These reactions are known as having time-like evolution. An example is the inclusive e^-e^+ annihilation:

$$e^+ + e^- \to h + X, \tag{2.25}$$

with h being an observed hadron and, as usual, X stands for any unobserved hadrons produced in the reaction (2.25). Also, for brevity, we have omitted the remainders in Eqs.(2.22) and (2.24).

2.3.1 The Case of Space-like Evolution

Let us concentrate on Eq.(2.22). Since the left hand side is independent of μ in the full perturbative theory with all orders then we can set that scale to any value we like. Among all the possible values, the choice $\mu^2 = Q^2$ is particularly convenient as will become clear below.

From dimensional considerations the coefficient function can be written as:

$$d\hat{\sigma}_{i\to X}(z, Q^2, \mu^2) = \sigma_B C(z, \frac{Q^2}{\mu^2}, \alpha_S(\mu^2)), \tag{2.26}$$

where for the present we consider the case when no heavy quark are present; we will generalize our considerations in the next section. In Eq.(2.26) σ_B is the Born cross-section for the partonic subprocess and the function C is a dimensionless function that has a power series decomposition in the strong coupling α_S.

It is now obvious that by setting $\mu^2 = Q^2$ the coefficient function takes the form $C(1, \alpha_S(Q^2))$ and depends only on the strong coupling and on no other large (or small) parameters. Since α_S is evaluated at the large scale Q^2 therefore it is small, the coefficient function can be easily and efficiently calculated to some fixed order in perturbation theory. However, as a result of the choice of scale we have made, the distribution function has now become Q-dependent. That dependence is very important. It indicates that the universality of a distribution function may be reduced since the PDF is specific to the experimental energy where it is extracted and therefore can not be applied to processes with different hard scale.

Fortunately, there exists a way to relate distribution functions at different scales. The scale dependence of the partonic fragmentation functions $f_i (i = q, \overline{q}, g)$ is perturbatively controlled and is given as a solution to a system of integro-differential equations known as Dokshitzer-Gribov-Lipatov-Altarelli-Parisi (DGLAP) equations [29, 30]. That way the universality of the distribution functions is retained; we only need to extract from experiment the distribution functions at one given scale Q_0. Then that input can be used as the initial condition for the DGLAP equations and the PDF at any other scale can be predicted. In practice that procedure works in the following way: at some low scale $Q_0 \sim 1$ GeV one writes down a function of z, that contains small number of free parameters. Then one evolves that initial condition via the DGLAP equations to different scales where experimental data exist, and one tries to fit those data by adjusting the parameters of the initial condition.

The DGLAP equations are:

$$\frac{d}{d \ln \mu^2} f_i(z, \mu) = \sum_j \int_z^1 \frac{d\xi}{\xi} P_{ij}\big(\frac{z}{\xi}, \alpha_S(\mu)\big) f_j(\xi, \mu), \tag{2.27}$$

and describe in general a system of $2n_f + 1$ equations for the distribution functions of all flavors of quarks, antiquarks and the gluon. The kernels P_{ij} have perturbative expansions in powers of the strong coupling:

$$P_{ij}(z, \alpha_S(\mu)) = \frac{\alpha_S(\mu)}{2\pi} P_{ij}^{(0)}(z) + \left(\frac{\alpha_S(\mu)}{2\pi}\right)^2 P_{ij}^{(1)}(z) + \mathcal{O}(\alpha_S^3). \tag{2.28}$$

$P_{ij}^{(0)}(z)$ are the Altarelli-Parisi splitting functions [29] that also appeared in Eq.(2.21) and the higher order terms $P_{ij}^{(1)}(x_b)$ can be found in [31, 32, 33, 34]. The one-loop splitting functions $P_{ij}^{(0)}(z)$ are renormalization scheme independent. However, that is not true for the higher order functions which are renormalization scheme dependent. The most common choice is to work in the $\overline{MS}$ scheme.
Because color and flavor commute, $P_{ij}^{(0)}(z)$ are independent of the quark flavor i.e. $P_{q_iq_j}^{(0)}(z) = \delta_{ij}P_{qq}^{(0)}(z)$. They also satisfy other relations as a result of probability conservation:

$$\int_0^1 dz P_{qq}^{(0)}(z) = 0, \tag{2.29}$$

and momentum conservation:

$$\begin{aligned} \int_0^1 dz\ z\Big(P_{qq}^{(0)}(z) + P_{gq}^{(0)}(z)\Big) &= 0, \\ \int_0^1 dz\ z\Big(2n_f P_{qg}^{(0)}(z) + P_{gg}^{(0)}(z)\Big) &= 0. \end{aligned} \tag{2.30}$$

Note that because of the property (2.29), the functions $P_{qq}^{(0)}(z)$ are not positive definite. They are distributions instead. The kernels P_{ij} satisfy also the following important relations as a result of charge invariance and the $SU(n_f)$ flavor symmetry:

$$\begin{aligned} P_{q_iq_j} = P_{\overline{q}_i\overline{q}_j} \quad &; \quad P_{q_i\overline{q}_j} = P_{\overline{q}_iq_j} \\ P_{q_ig} = P_{\overline{q}_ig} = P_{qg} \quad &; \quad P_{gq_i} = P_{g\overline{q}_i} = P_{gq} \end{aligned} \tag{2.31}$$

The explicit expressions for the four splitting functions at leading order are:

$$\begin{aligned} P_{qq}^{(0)}(z) &= C_F\left(\frac{1+z^2}{(1-z)_+} + \frac{3}{2}\delta(1-z)\right), \\ P_{qg}^{(0)}(z) &= \frac{1}{2}\big(z^2 + (1-z)^2\big), \\ P_{gq}^{(0)}(z) &= C_F\left(\frac{1+(1-z)^2}{z}\right), \\ P_{gg}^{(0)}(z) &= 2C_A\left(\frac{z}{(1-z)_+} + \frac{1-z}{z} + z(1-z)\right) \\ &\quad + \frac{11C_A - 2n_f}{6}\delta(1-z). \end{aligned} \tag{2.32}$$

In equations above the " + "–prescription of a function $f(z)$, which is singular at $z = 1$, is defined as:

$$\int_0^1 dz g(z)[f(z)]_+ = \int_0^1 dz f(z)[g(z) - g(1)]. \tag{2.33}$$

A complete explanation of the distribution $(F(z))_+$) and its properties can be found in Appendix C.

One can simplify the study of the DGLAP equations if one takes advantage of the flavor symmetry. As we mentioned earlier, the DGLAP equations describe the evolution of $2n_f + 1$ partons that are all massless (see also the discussion following). From the form of the QCD lagrangian with n_f massless quarks (2.3), it is evident that the theory has an additional global $SU(n_f)$ flavor symmetry. Since the gluons are flavor-neutral, they transform as singlet under the flavor group. The quarks in general transform non trivially under that group. One can split the $2n_f$ (anti)quark fields into one singlet:

$$\Sigma(x,\mu) = \sum_i^{n_f} \big(f_{q_i}(x,\mu) + f_{\overline{q}_i}(x,\mu)\big), \tag{2.34}$$

and $2n_f - 1$ non-singlet(NS) combinations. n_f of the NS fields can be taken as the different $M_i^- = f_{q_i}(x,\mu) - f_{\overline{q}_i}(x,\mu)$. The other $n_f - 1$ combinations, which we denote by M_j^+, depend on the value of n_f and can be found in [6]. Clearly, the NS combinations do not mix with the singlet; in particular they do not mix with the gluon. To LO, all NS fields also split from each other so we have a separate equation for each NS field:

$$\frac{d}{d\ln\mu^2} f^{NS}(z,\mu) = \frac{\alpha_S(\mu)}{2\pi} \int_0^1 \frac{d\xi}{\xi} P_{qq}^{(0)}\left(\frac{z}{\xi}\right) f^{NS}(\xi,\mu), \tag{2.35}$$

with $P_{qq}^{(0)}$ given in Eq.(2.32). Beyond the leading order, however, the evolution kernels are no longer flavor diagonal. One can still write the evolution equations in diagonal form that is similar to the LO case Eq.(2.35), but the kernels $P_{NS}^{(1)+}$ and $P_{NS}^{(1)-}$ corresponding to the fields M^+ and M^- are now different. Their explicit expressions can be found in [6] as well.

In the singlet sector, there is non-trivial mixing between the gluon density g and the quark singlet state Σ. The kernels of the evolution equations for the *"two-vector"* $(\Sigma(z,\mu), g(z,\mu))$ form a 2×2 matrix:

$$\begin{pmatrix} P_{qq}(z,\alpha_S(\mu^2)) & 2n_f P_{qg}(z,\alpha_S(\mu^2)) \\ P_{gq}(z,\alpha_S(\mu^2)) & P_{gg}(z,\alpha_S(\mu^2)) \end{pmatrix}. \tag{2.36}$$

The NLO kernels in the singlet sector can be found in [6]. Similarly to the NS case, we do not present them here because of their length. The original derivations are presented in [26, 35]. For future references we will only present the large z behavior of the $\overline{MS}$ splitting

functions at NLO:

$$\begin{aligned}\lim_{z\to 1} P_{qq} &= C_F \frac{\alpha_S}{\pi}\left(1 + K\frac{\alpha_S}{2\pi} + O(\alpha_S^2)\right)\frac{1}{(1-z)_+} \\ \lim_{z\to 1} P_{gg} &= C_A \frac{\alpha_S}{\pi}\left(1 + K\frac{\alpha_S}{2\pi} + O(\alpha_S^2)\right)\frac{1}{(1-z)_+},\end{aligned} \tag{2.37}$$

where:

$$K = C_A\left(\frac{67}{18} - \frac{\pi^2}{6}\right) - \frac{5}{9}n_f. \tag{2.38}$$

The origin of the DGLAP equations is in renormalization group invariance. That invariance is manifested as independence of physical quantities (for example a cross-section) of the renormalization scale μ_r that is introduced as a result of the renormalization procedure. Eq.(2.22) is a typical example.

2.3.2 The Case of Time-like Evolution

All the considerations that were made for the case of Eq.(2.22) can also be made for the fragmentation case (2.24). There are, however, a few difference between those two cases and we will discuss them now.

The fragmentation functions D have a expression different from that of the parton distribution functions. The function $D_{i/h}(z, \mu^2)$ represents the probability density that a parton i produced at scale μ will fragment to an observed (and therefore on-mass-shell) hadron h. Similarly to the distribution functions, the evolution of the fragmentation functions is also described by the DGLAP equations. The one-loop splitting functions $P^{(0)}_{time-like,ij}(x)$ coincide with those in the space-like case (2.32). However the time-like and the space-like evolution kernels differ beyond the leading order. The NLO time-like functions can be found in [26, 35]. The large z behavior of the NLO time-like evolution kernels is the same as for the space-like kernels, Eq.(2.37).

2.4 Infrared Effects

In our previous discussion we neglected the presence of masses of the quarks. However for a theory which is sensitive to the IR such as QCD, a detailed account for those effects is needed.

It is well known that in a gauge theory with massless fields, in addition to the usual UV divergences, there is another type of divergences that occurs in the evaluation of the Feynman diagrams. These are known as infrared (IR) divergences and as shown by Sterman for QCD in [36] can be divided into two types: collinear and soft.

The collinear divergences are due to the vanishing mass of the radiating particle (usually the quarks). When a quark radiates a gluon that is almost collinear to it, the corresponding real or virtual emission diagrams diverge. One can regulate such a divergence by introducing a small quark mass or by working in D space-time dimensions. Then a collinear divergence shows up as a logarithmitic singularity $\sim \ln(m^2)$ or as an $1/\epsilon$ pole, respectively. In principle, since quarks have non-vanishing masses, the quantities calculated should be finite and free of collinear singularities. That is not the case, however. In the perturbative regime it is not the absolute value of the quark that is important but its value with respect to some typical scale. If that typical scale - usually the hard scale Q - is much larger than the quark mass, then in a perturbative calculation there appear large logs $\ln(m^2/Q^2)$. Although these logs are finite, they appear to any order in perturbation theory and systematically multiply the strong coupling constant. Thus, the effective perturbation parameter is not α_S any more but $\alpha_S\times$ (a power of $\ln(m^2/Q^2)$). The latter can be quite large and can even invalidate the perturbation series. In effect, small but non-zero quark mass leaves the result finite but unphysical; one should sum up to all orders terms of this type in order to be able to make different perturbative predictions. Such large logs are called quasi-collinear logs and are classified in the following way: a term at order α_S^n has the form:

$$\alpha_S^n \sum_{k=0}^{n} c_k \ln^k \left(\frac{m^2}{Q^2}\right). \tag{2.39}$$

Terms with $k = n$ are known as leading logarithmic (LL) terms, the ones with $k = n - 1$ are the next-to-leading logarithms (NLL) etc.
It is a peculiar feature of QCD that due to its non-abelian gauge group not only quarks but also gluons can radiate collinear gluons. Unlike the quarks however the gluons are exactly massless due to the gauge symmetry.

The origin of the soft divergences is in the vanishing mass of the gauge fields (the gluon). These divergences manifest themselves as singularities in the loop integrals over gauge boson lines in the kinematical region where the energy E_g of the gluon vanishes or in the real emission diagrams where gluons with vanishing energy are emitted. The most

convenient way to regularize those divergences is to work with dimensional regularization since it preserves gauge invariance (unlike gluon-mass regularization).

It was understood long ago [37] that the problem of IR divergences is rooted in the way the physical observables are defined. It is intuitively clear that a state containing a hard parton can not be distinguished from a state containing in addition arbitrary number of soft (or collinear) gluons. In those singular limits the particle nature of the real soft (or collinear) gluon is not well defined and as a result we need to deal with degenerate states. The conditions for cancellation of the IR divergences are stated in the following theorem:

Kinoshita-Lee-Nauenberg Theorem[38]: In a theory with massless fields, transition rates are free of IR divergences if a summation over the initial and final degenerate states is carried out.

The proof of the theorem can be found in [5]. Its content is however clear: a physical state is one that contains arbitrary number of soft (collinear) gluons. When applied to perturbative calculations, the KLN theorem means that to some fixed order in the coupling constant one should take into account the contributions from virtual and real emission diagrams with arbitrary numbers of radiated gluons. Only their sum will be IR finite. That way we arrive at the idea of an inclusive observable: a calculated cross-section will be IR finite if it does not distinguish a state with one particle from a state with a number of soft (collinear) gluons. We will see examples in the next Chapter when we discuss the decay of the top quark.

In terms of Feynman diagrams (to all orders), the IR divergences are generated only from real or virtual emission lines connected exclusively to external (hard) lines in the diagram. The reason is that the internal lines are typically off-shell and thus regulate any possible divergences. That observation is important for constructing an explicit proof of cancellation of the soft divergences and was used first by Weinberg [39] in the context of QED. Let us also mention that in fact that property leads in the context of QCD to the factorization of the IR singularities in the hard diagrams. This is a very important property that we will use in the next section. For an excellent discussion see [40].

2.4.1 Heavy Quark Masses

Let us return to Eq.(2.22) or (2.24) and now take into account the masses of the quarks that we neglected in the discussion in the previous section. For example, Eq.(2.26) is now

generalized to:

$$d\hat{\sigma}_{i\to X}(x,Q^2,m^2,\mu^2)=\sigma_B C\bigg(x,\frac{Q^2}{\mu^2},\frac{m^2}{\mu^2},\alpha_S(\mu^2)\bigg). \tag{2.40}$$

It is clear that whatever choice we make for the scale μ, we can not set equal to one both mass ratios that appear in the right hand side of Eq.(2.40), an example is given in chapter 4 when the b-quark is considered a massive one in top decay. Let us set as before $\mu^2=Q^2$. Then (2.40) takes the form:

$$d\hat{\sigma}_{i\to X}(x,Q^2,m^2,\mu^2=Q^2)=\sigma_B C\bigg(x,1,\frac{m^2}{Q^2},\alpha_S(Q^2)\bigg). \tag{2.41}$$

Since the ratio m^2/Q^2 can take any non-negative real value, we anticipate a strong dependence on the value of the quark mass. The case when $m^2\gg Q^2$ was already discussed in section (2.2): one can simply integrate out the heavy quark and work in an effective theory where that flavor is omitted . As a result , the definition of the coupling constant becomes dependent on the number of flavors lighter than Q. To understand the dependence on m^2 in the case when m^2 is not (much) larger than Q^2, we first need to know if the cross-section $d\hat{\sigma}$ is IR safe, i.e. if it is finite in the limit $m^2\to 0$. If it is collinearly safe, we can represent it as:

$$C(x,1,\frac{m^2}{Q^2},\alpha_S(Q^2))=C\bigg(x,1,0,\alpha_S(Q^2)\bigg)+\mathcal{O}\bigg(\frac{m^2}{Q^2}\bigg). \tag{2.42}$$

Such cross-sections are well behaved and can be obtained by explicit calculation to any order in perturbation theory. A typical example is the case when $d\hat{\sigma}$ is a total partonic cross-section, e.g. for the process $e^-e^+\to$ hadrons.

The case when $d\hat{\sigma}$ is not IR safe is more complicated and at the same time perhaps more common. In this case the limit $m\to 0$ is singular, i.e. $d\hat{\sigma}$ diverges. Examples are the cases where $d\hat{\sigma}$ is an inclusive differential cross-section for production of a parton, or a process which is initiated by a single parton (the generalization to multiple partons is straightforward). According to (2.18), the hadron level result is a convolution of the partonic cross-section with distribution/fragmentation function. However in the presence of IR divergences we should first understand how to make sense of such divergent results.

Let us first consider the case when the parton in consideration is light i.e. we take $m^2\approx 0$ (the case of having a heavy one: $m^2\neq 0$, will be considered in chapter 4). The first thing to note is that since it is experimentally measurable, the physical process of

creation of a hadron or the process that is initiated by a single hadron is not IR divergent. Such a process includes complicated stages but to simplify the calculation we assume that the produced hadron has been created from a single parton, which non-perturbatively hadronizes later. This hadronization process is described by the fragmentation function D. Such a description is typical for production of light hadrons (i.e. hadrons that are constructed out of light quarks). Thus in simplifying the process we necessarily introduce mass singularities. The understanding of their origin suggests the method to cure them: one calculates the partonic cross-section in perturbation theory that is (usually) regulated in dimensional regularization. As we discussed in section (2.2) those divergences factorize and can be subtracted in a particular scheme(usually $\overline{MS}$). Then the subtracted partonic cross-section is convoluted with a non-perturbative fragmentation function which is process independent but subtraction scheme dependent. The same considerations apply for a process with space-like evolution. The justification for such a procedure is that the subtraction is physically equivalent to the absorption of the effects sensitive to long-distance physics into the distribution/fragmentation functions (see Eq.(2.20)).

After the subtraction of the mass singularities and defining the corresponding distribution/fragmentation functions now we use the factorization formula. We shall explain in more detail later.

2.4.2 Perturbative Fragmentation Function Formalism

Let us turn our attention to the processes that involve heavy quarks and typical hard scale Q somewhat larger than the quark mass. As usual, by heavy we mean c, b or t quarks. Although the partonic cross-section for such processes is divergent in the zero-mass limit, we can not really set the masses of the heavy quarks to zero since they are not so small. We are then in a situation that we previously described: the results are formally finite but in practice, perturbation theory can not be applied in a straightforward way since, as shown in Eq.(2.39), large logs $\ln(m^2/Q^2)$ appear to all orders in α_S. There are two physically different cases where such a situation can occur:
The first case is the partonic processes that are initiated by quarks with non-zero mass. We will indicate that in such situations we would subtract the divergent part of the coefficient function and then convolute it with the usual massless parton density. An example is given in [41] where the strange quark was treated as having non-zero mass and after the

subtraction of the quasi-collinear logs the effect of the (finite) power corrections of the mass of the strange quark was studied.

The second case is the process where a heavy quark (usually c or b) is created in a hard collision with a typical scale Q. Such processes lead to the creation of $c-$ or $b-$flavored hadrons and can be described within the formalism of the perturbative fragmentation function (PFF)[42]. This approach has been used for e^-e^+ annihilation [43, 44, 45, 46, 47], hadron collisions [48, 49] and photo production [50, 45]. In the next Chapter we describe its application for bottom quark production in top quark decay, $t \to bW$ [51].

According to the factorization theorem (2.18), we can write the cross-section for creating a heavy-flavored hadron H in the following way:

$$\frac{1}{\sigma_0}\frac{d\sigma^H}{dz}(z,Q,m) = \frac{1}{\sigma_0}\int_z^1 \frac{d\xi}{\xi}\frac{d\sigma^q}{d\xi}(\xi,Q,m)D_{np}^H\left(\frac{z}{\xi}\right), \tag{2.43}$$

where $\sigma^H(\sigma^q)$ is the cross-section for production of hadron H (heavy quark q) and D_{np} is a non-perturbative fragmentation function that describes the transition $q \to H$ at the scale set by the mass m of the heavy quark q. That function is to be obtained from a comparison with experiment. The kinematical variable z describes the parameter(s) of the observed final state and typically is an normalized energy fraction. We also normalize the cross-section in such a way that the Born term equals $\delta(1-z)$.

The partonic cross-section σ^q can be calculated in perturbation theory. It is finite because of the finite mass m but is not IR safe since the process is not completely inclusive, i.e. it does not include all number of soft (collinear) gluons. It contains large quasi-collinear logs to all orders in α_S that must be resummed as we previously discussed. To make a resummation of those, One writes:

$$\frac{1}{\sigma_0}\frac{d\sigma^q}{dz}(z,Q,m) = \frac{1}{\sigma_0}\sum_i\int_z^1 \frac{d\xi}{\xi}\frac{d\hat{\sigma}^i}{d\xi}(\xi,Q,\mu)D_i\left(\frac{z}{\xi},\mu,m\right), \tag{2.44}$$

where $\hat{\sigma}$ is the cross-section for production of massless parton i with the collinear singularity subtracted in the $\overline{MS}$ scheme. The function $D_i(z,\mu,m)$ is a perturbative fragmentation function (PFF) and it describes the transition of a massless parton i to a massive quark q.

The ansatz (2.44) has the following physical interpretation: in a hard collision set by the large scale Q a massive parton is produced at large transverse momentum. For that reason it behaves like a massless parton. The replacement of a massive parton with a massless one (after the collinear divergence is subtracted) is justified up to powers of

m^2/Q^2. The formalism of the PFF is applicable when such power correction are small and can be neglected. For that reason, the cross-section $\hat{\sigma}$ is insensitive to low energy physics and depends on Q. The scale μ is the factorization scale that, as usual, separates the low from the high energy regimes. Similarly, the function $D_i(z, \mu, m)$ depends only on the mass and the factorization scale, but is sensitive to the high energy part of the process. In particular, the perturbative fragmentation function is universal, i.e. independent of the process.

The PFF satisfy the DGLAP equation (2.27). The latter can be solved with NLL accuracy. To completely specify the solution one needs to specify at some scale μ_0 an initial condition $D_i^{ini}(z, \mu_0, m)$ that is also valid to NLL accuracy. Clearly, such a condition is also universal and can be obtained from a perturbative calculation [42]. To complete this procedure one needs to observe that if the scale μ_0 is chosen of the order of the mass m then no large logs will be present in the initial condition. Therefore, the initial condition can be simply calculated in perturbative theory:

$$D_i^{ini}(z, \mu_0, m) = d_i^{(0)}(z) + \frac{\alpha_S(\mu_0)}{2\pi} d_i^{(1)}(z, \mu_0, m) + \mathcal{O}(\alpha_S^2). \tag{2.45}$$

To obtain the above functions one need to independently compute to order α_S both σ^q and $\hat{\sigma}$ for some process and then plug the results into Eq.(2.44), for a more detailed discussion see section (4.7).
Comparing the terms by the first order in α_S one gets in the $\overline{MS}$ scheme [42]:

$$\begin{aligned}
d_i^{(0)}(z) &= \delta_{iq}\delta(1-z) \\
d_{i=q}^{(1)}(z, \mu_0, m) &= C_F \left[\frac{1+z^2}{1-z} \left(\ln \frac{\mu_0^2}{m^2} - 2\ln(1-z) - 1 \right) \right]_+ \\
d_{i=g}^{(1)}(z, \mu_0, m) &= \frac{1}{2}\left(z^2 + (1-z)^2\right) \ln\left(\frac{\mu_0^2}{m^2}\right) \\
d_{i\neq q,g}^{(1)}(z, \mu_0, m) &= 0.
\end{aligned} \tag{2.46}$$

In section (4.7), the second relation ($d_{i=q}^{(1)}(z, \mu_0, m)$) shall be obtained in the top quark decay process but process independent derivations of these initial conditions also exist in [43, 52].

The most convenient way to solve the DGLAP equations is to work with the Mellin moments of the fragmentation functions. We do not apply this method in this thesis therefore we refer a reader to see [51] for more detailed discussion.

Chapter 3

QCD Corrections for Top Quark Decay using the Dimensional Regularization Scheme

We present the QCD corrections at order α_s to the t-quark decay with $t \to b$ transition: $t \to b + W^+$. The QCD corrections receive contributions from both virtual and real gluon corrections. In our calculation to extract singularities we use dimensional regularization. Then both Infrared and Ultraviolet singularities appear in forms of $\frac{1}{\epsilon}$ and $\frac{1}{\epsilon^2}$, where as mentioned in the previous Chapter ϵ denotes the deviation of the number of space-time dimensions from 4 and defined as $\epsilon = \frac{4-D}{2}$. To specify the type of singularities, we label ϵ_{IR} for the infrared singularities and ϵ_{UV} for the ultraviolet singularities.

3.1 Kinematic Variables

In the processes $t \to b + W^+$ and $t \to b + W^+ + g$, which we are going to consider, a t-quark decays into a b-quark, a W^+-boson and possibly a gluon. Thus it is convenient to define scaled momenta as kinematic variables. First of all, we denote the four-momenta of the t-quark, b-quark, W^+-boson, real gluon and virtual gluon as p_t, p_b, p_W, p_g, q respectively. The t-quark mass and the W^+ boson mass are denoted as m_t and m_W, respectively. The gluon is massless and for our present calculations we neglect the b-quark mass, therefore we have ${p_g}^2 = {p_b}^2 = 0$. In next chapter we consider the case $m_b \neq 0$.
We define z-variable as the scaled energy fraction of the b-quark in the rest frame of t-quark,

i.e. $\overrightarrow{p_t} = 0$:

$$z = \frac{2p_b \cdot p_t}{{m_t}^2} = \frac{2E_b}{m_t}.$$

Neglecting the b-mass, this variable takes values in the region of $0 \leq z \leq 1-\omega$ in which ω is defined as the ratio $\omega = \frac{m_W^2}{m_t^2}$. From now on we use the normalized b-energy fraction x_b that is defined as:

$$x_b = \frac{z}{1-\omega} \qquad 0 \leq x_b \leq 1.$$

3.2 Born Approximation

The t-quark decay Feynman diagram in the tree level (or in the leading order) is depicted in Fig.3.1. The amplitude of the Born approximation is given by:

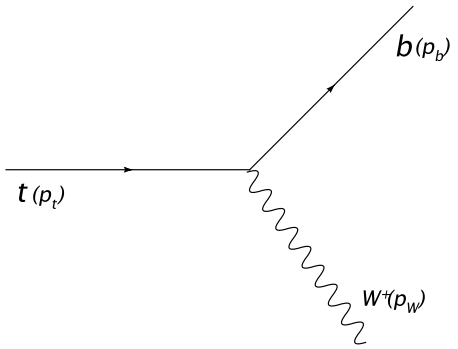

Figure 3.1: Feynman diagram in the Born approximation in top decay

$$M^{Born} = \frac{-e|V_{tb}|}{2\sqrt{2}\sin\theta_W}\epsilon^{\star\mu}(p_W)\overline{u}(p_b)\gamma_\mu(1-\gamma_5)u(p_t), \tag{3.1}$$

in which e is the charge of the electron, $\epsilon^\mu(p_W)$ is the polarization vector of the W^+-boson, $u(p_t)$ and $\overline{u}(p_b)$ are the spinors of the t-quark and the b-quark, respectively. The angle θ_W is known as the weak mixing angle or the Weinberg angle and V_{tb} is the CKM matrix element for the $t \to b$ flavor transition. For this transition we have $V_{tb} \simeq 1$ since our assumption for the branching ratio of the top quark decay is $B(t \to bW) = 1$. This result is consistent with recent measurements of the CDF [53] collaboration of the ratio $R^{-1} = \frac{B(t\to kW)}{B(t\to bW)}$, where k is a d, s or b quark.

The Born approximation of the decay rate (or Born width) is obtained as:

$$\Gamma_0 = \frac{m_t\alpha(1-\omega)^2(1+2\omega)}{16\omega\sin^2\theta_W} + \mathcal{O}(\epsilon),$$

but in order to get the correct finite terms in the normalized differential decay rate, the Born width Γ_0 will have to be evaluated in the dimensional regularization at $\mathcal{O}(\epsilon^2)$. We obtain:

$$\begin{aligned}\Gamma_0 &= \frac{m_t\alpha(1-\omega)^2(1+2\omega)}{16\omega\sin^2\theta_W}\Big\{1-\epsilon[\gamma_E-\log\frac{4\pi\mu^2}{m_t^2}+2\log(1-\omega)-2\frac{1+\omega}{1+2\omega}]+ \\ &\epsilon^2\big[\frac{1}{2}\big(\gamma_E-\log\frac{4\pi\mu^2}{m_t^2}+2\log(1-\omega)-2\frac{1+\omega}{1+2\omega}\big)^2-\frac{\pi^2}{4}+\frac{2(1+\omega)(1+3\omega)}{(1+2\omega)^2}\big]\Big\}+\mathcal{O}(\epsilon^3),\end{aligned} \tag{3.2}$$

where α is the electromagnetic coupling constant, $\gamma_E = 0.577216\cdots$ is the Euler constant and μ is the arbitrary reference mass that appears in the dimensional regularization.
Using the definition of the differential decay rate from appendix A, the normalized decay width reads:

$$\frac{1}{\Gamma_0}\frac{d\Gamma_0}{dx_b} = \delta(1-x_b). \tag{3.3}$$

Now we are ready to calculate the QCD corrections from α_s order (Next-to-leading order) in the t-quark decay.

3.3 QCD Radiative Corrections

The Born approximation of the decay rate receives radiative corrections from perturbative QCD that can be indicated as a power series of the strong coupling constant α_s:

$$d\Gamma = d\Gamma^{Born} + d\Gamma^{\alpha_s} + d\Gamma^{\alpha_s^2} + \cdots .$$

We now present the calculation of the first order of α_s corrections. The virtual gluon contributions are denoted by $d\Gamma^V$ and the real gluon contributions by $d\Gamma^R$, so the total radiative corrections of α_s order can be written as:

$$d\Gamma^{\alpha_s} = d\Gamma^V + d\Gamma^R.$$

The virtual corrections $d\Gamma^V$ contain the vertex correction and the self-energy corrections of quarks. All these types of corrections contain both ultraviolet divergences (UV) and infrared divergences (IR). The UV singularities are regulated and canceled out after renormalization of the fields, vertices and coupling constants. Likewise, the $d\Gamma^R$ has the infrared

divergences due to emission of the soft gluon and the collinear emitted gluon with the b-quark. These divergences must be regulated in the same way like the virtual corrections. The UV divergences in the virtual gluon corrections appear when the integration region of the internal momentum of the virtual gluon goes to infinity.

There are many regularization and renormalization schemes [5]. In this work we adopt the on-shell mass-renormalization scheme, choose the physical mass of the t-quark as the renormalization point(the position of the pole of a heavy t-quark propagator in perturbation theory). Dimensional regularization is better suited to regularize gauge theories, because it is compatible with gauge invariance. The main idea in the dimensional regularization is to change the number of space-time dimensions in the phase space integrals from 4 to $D = 4 - 2\epsilon$ and also in the calculation of the matrix elements. In this case, the singularities are extracted in terms of $\frac{1}{\epsilon}$ and $\frac{1}{\epsilon^2}$.
Now we provide the explicit procedure to calculate the virtual and real corrections using dimensional regularization.

3.4 Virtual Gluon Corrections

First we consider the one-loop corrections to the decay width which are called virtual corrections.
Expressing the virtual corrections amplitude M^V in terms of the phase space variables, the contribution of the virtual corrections to the differential decay width reads:

$$d\Gamma^{Vir} = \frac{\mu^{4-D}}{2m_t}\frac{d^{D-1}\mathbf{p}_W}{(2\pi)^{D-1}2E_W}\frac{d^{D-1}\mathbf{p}_b}{(2\pi)^{D-1}2E_b}(2\pi)^D\delta^D(p_t - p_b - p_W)|\overline{2\mathrm{Re}(M^{\star Born}M^V)}|, \quad (3.4)$$

where the $(\star)$ sign shows the complex conjugate of the Born amplitude. With respect to the definition of the kinematic variables, the equation above is simplified to:

$$\begin{aligned}\frac{d\Gamma^{Vir}}{dx_b} &= \frac{(1-\omega)}{16\pi m_t}\delta(1-x_b)\Big\{1-\epsilon\big[\gamma_E - \log\frac{4\pi\mu^2}{m_t^2} + 2\log(1-\omega) - \frac{2(1+\omega)}{1+2\omega}\big] + \\ &\epsilon^2\big[\frac{1}{2}\big(\gamma_E - \log\frac{4\pi\mu^2}{m_t^2} + 2\log(1-\omega) - \frac{2(1+\omega)}{1+2\omega}\big)^2 - \frac{\pi^2}{4} + \frac{2(1+\omega)(1+3\omega)}{(1+2\omega)^2}\big]\Big\}\times \\ &\overline{|2Re(M^{\star Born}M^V)|} + \mathcal{O}(\alpha_s^2), \end{aligned} \quad (3.5)$$

where the Dirac delta function shows the momentum-energy conservation of the particles system and the amplitude M^V contains 2 graphs, which are depicted in Fig.3.2.

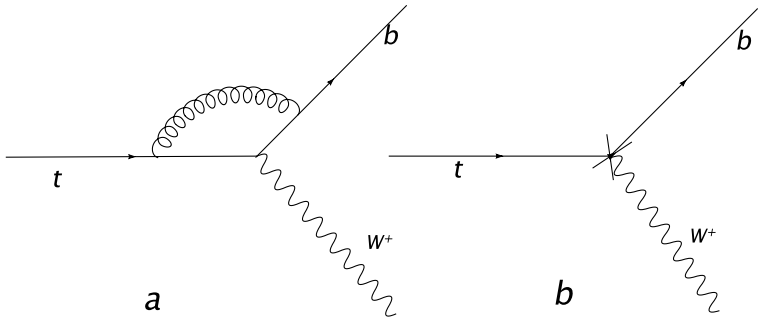

Figure 3.2: Feynman diagram for the virtual corrections. (a): vertex correction (b): renormalization of the fields and coupling constants.

In fact, in the α_s order there are several other Feynman diagrams depicted in Fig.3.3. But we do not have to consider them since in the on-shell renormalization scheme,the self-energy diagrams, Figs.3.3a and 3.3c, are canceled by the additional counter terms contributions, which arise from the quark wave function and mass renormalization, Figs.3.3b and 3.3d,[54]. The amplitude M_1^V which includes the one-loop vertex correction, shown in

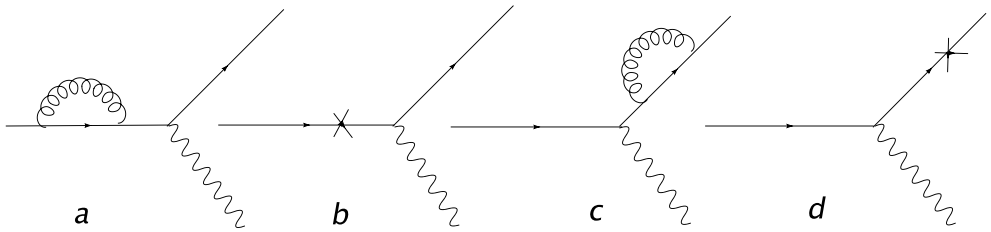

Figure 3.3: Virtual corrections: graphs a, c show the self-energy of quarks and graphs b, d are counter term contributions.

Fig.3.4, reads:

$$M_1^V = \frac{-e}{2\sqrt{2}\sin\theta_W}\epsilon^{\star\mu}(p_W)\overline{u}(p_b)\Lambda_\mu(p_W,p_b)u(p_t), \tag{3.6}$$

in which,

$$\begin{aligned}\Lambda_\mu(p_W,p_b) \;&= \mu^{4-D}\;\; \frac{g^2}{i(2\pi)^4}\int d^Dq \quad [g_{\beta\nu}-(1-\eta)\frac{q_\beta q_\nu}{q^2}]\times \\ &\quad \times[\frac{T^a_{ji}\gamma^\beta(\not{q}+\not{p}_b)\gamma_\mu(1-\gamma_5)(\not{p}_b+\not{p}_W+\not{q}+m_t)\gamma^\nu T^a_{il}}{q^2(q+p_b)^2[(p_b+p_W+q)^2-m_t^2]}].\end{aligned} \tag{3.7}$$

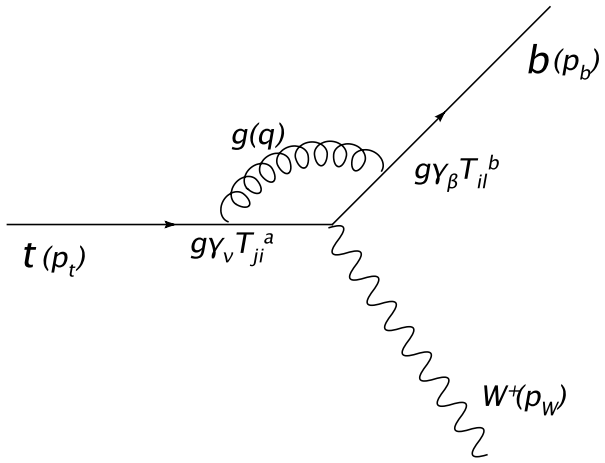

Figure 3.4: Feynman diagram for the one-loop vertex correction

In the one-loop integral calculation we used the dimensional regularization in which we replaced $\int \frac{d^4q}{(2\pi)^4}$ by $\mu^{4-D} \int \frac{d^Dq}{(2\pi)^D}$.
Since Λ_μ is directly connected to the measurable quantity $d\Gamma$, it is gauge independent thus we can choose the t'Hooft-Feynman gauge ($\eta = 1$). The γ_5 matrix is not well defined in D dimensions. The anti-commutation relation $\{\gamma^\mu, \gamma_5\} = 0$ produces the ambiguity, and one can not simply apply the anti-commutation relation in general D dimensions. There are several prescriptions to prevent the ambiguity of γ_5 [55, 56, 57, 58]. We employ the Breitenlohner-Maison (BM) scheme that is summarized by two principle rules. The first rule is that one should not commute γ_5 with other γ matrices, i.e.$\{\gamma_\mu, \gamma_5\} \neq 0$, and the other one is that the trace of $\gamma_5\gamma_\alpha\gamma_\beta\gamma_\gamma\gamma_\delta$ is expressed with the conventional anti-symmetric metric $\varepsilon-$tensor, i.e. $\mathrm{Tr}[\gamma_5\gamma_\alpha\gamma_\beta\gamma_\gamma\gamma_\delta] = 4i\varepsilon_{\alpha\beta\gamma\delta}$. To avoid the anti-commutation relation of γ_5, one does not contract two γ matrices with a γ_5 matrix between them. A more detailed explanation is found in [55, 57, 58].
After applying the on-shell evaluations, $p_t^2{=}m_t^2$ and $p_b^2{=}0$ in Eq.(3.7), we sum and average over the color of the quarks with respect to this property that $T^a_{ji} \cdot T^a_{il} = Tr(T^aT^a) = 4$ (the 'a' sign stands for the gluon color index which takes the values $1, 2, \cdots, 8$ and the indices i and j label the quarks colors). The result is:

$$\Lambda_\mu(p_W, p_b) = \frac{4g^2\mu^{4-D}}{3i(2\pi)^4} \int d^Dq [\frac{\gamma^\beta(\not{q} + \not{p}_b)\gamma_\mu(1-\gamma_5)(\not{p}_b + \not{p}_W + \not{q} + m_t)\gamma_\beta}{q^2(q+p_b)^2[(p_b+p_W+q)^2 - m_t^2]}].$$

Now we calculate contribution of the one-loop vertex correction to the differential decay

width (Eq.(3.4)), namely:

$$\overline{|2Re(M^{\star Born}.M_1^V)|} = \frac{\alpha\pi}{2\sin^2\theta_W}\big(-g^{\mu\nu}+\frac{p_W^\mu.p_W^\nu}{m_W^2}\big)Tr\big[\not{p}_b\Lambda_\mu(\not{p}_b+\not{p}_W+m_t)\gamma_\nu(1-\gamma_5)\big]. \tag{3.8}$$

Here we used the definitions (3.1) and (3.6) for $M^{\star Born}$ and M_1^V, respectively.

In our calculation we used the program Feyncalc and in conclusion we obtain:

$$\begin{aligned}&\overline{|2Re(M^{\star Born}.M_1^V)|} = \\ &\frac{m_t^2\alpha\alpha_s}{\sin^2\theta_W}\Bigg[\frac{4(1-\omega)(1+2\omega)}{3\omega}\big(-1+B_0(0,0,0)+m_t^2(1-\omega)C_0(m_t^2,m_W^2,0,0,m_t^2,0)\big)\\ &+4\omega B_0(m_W^2,0,m_t^2)-\frac{2}{3\omega}(4\omega^2+\omega+1)B_0(m_t^2,0,m_t^2)\Bigg].\end{aligned} \tag{3.9}$$

Here B_0 and C_0 functions are the Passarino-Veltman 2-point and 3-point integrals which are defined as:

$$B_0(p_1^2,m_0^2,m_1^2)=\frac{(2\pi\mu)^{4-D}}{i\pi^2}\int d^Dq\frac{1}{(q^2-m_0^2+i\epsilon)((q+p_1)^2-m_1^2+i\epsilon)},$$

and

$$\begin{aligned}C_0(p_1^2,(p_1-p_2)^2,p_2^2,m_0^2,m_1^2,m_2^2) &= \frac{(2\pi\mu)^{4-D}}{i\pi^2}\times\\ &\int d^Dq\frac{1}{(q^2-m_0^2+i\epsilon)((q+p_1)^2-m_1^2+i\epsilon)((q+p_2)^2-m_2^2+i\epsilon)}.\end{aligned}$$

The B_0 and C_0 functions which we need, are:

$$\begin{aligned}B_0(m_t^2,0,m_t^2) &= \Delta_{UV}+\log\frac{\mu^2}{m_t^2}+2\\ B_0(m_W^2,0,m_t^2) &= \Delta_{UV}+\log\frac{\mu^2}{m_t^2}+\frac{(1-\omega)}{\omega}\log(1-\omega)+2\\ B_0(0,0,0) &= \frac{1}{\epsilon_{UV}}-\frac{1}{\epsilon_{IR}}\\ C_0(m_t^2,m_W^2,0,0,m_t^2,0) &=\\ &-\frac{1}{4m_t^2(1-\omega)}\Bigg(\frac{1}{\epsilon_{IR}^2}+(\log\frac{\mu^2}{m_t^2}-2\log(1-\omega)+\Delta_{IR})^2+4Li_2(\omega)+\frac{\pi^2}{6}\Bigg),\end{aligned} \tag{3.10}$$

in which $\Delta_{UV} = \frac{1}{\epsilon_{UV}} + \log 4\pi - \gamma_E$, $\Delta_{IR} = \frac{1}{\epsilon_{IR}} + \log 4\pi - \gamma_E$, [59, 60].
Using these relations the final result for Eq.(3.9) is:

$$\begin{aligned}
&\overline{|2Re(M^{\star Born} M_1^V)|} \;=\; \\
&\frac{m_t^2 \alpha \alpha_s (1-\omega)(1+2\omega)}{3\omega \sin^2\theta_W}\Bigg(\frac{-2}{\epsilon_{IR}^2} + 2\Big(\frac{2\log(1-\omega) - \log\frac{4\pi\mu^2}{m_t^2} + \gamma_E - 2}{\epsilon_{IR}}\Big) + \frac{2}{\epsilon_{UV}} \\
&\quad -(\log^2\frac{4\pi\mu^2}{m_t^2} + 2(1-\gamma_E)\log\frac{4\pi\mu^2}{m_t^2} + \gamma_E(\gamma_E - 2) + \frac{\pi^2+48}{6}) \\
&+4(\log\frac{4\pi\mu^2}{m_t^2} - \log(1-\omega) + \frac{3\omega}{(1+2\omega)} - \gamma_E)\log(1-\omega) - 4Li_2(\omega)\Bigg), \qquad (3.11)
\end{aligned}$$

where $Li_2(\omega) = -\int_0^\omega \frac{dt}{t}\log(1-t)$ is the Spence function and ω is the ratio $\omega = \frac{m_W^2}{m_t^2}$, already introduced in section 3.1.

The contribution M_2^V, due to renormalization of the wave-functions, electric charge and masses, which are shown by the countervertex graph, Fig.3.2.b, reads:

$$M_2^V = \frac{-e}{2\sqrt{2}\sin\theta_W}\epsilon^{\star\mu}(p_W)\overline{u}(p_b)\{\delta z_e - \frac{\delta s_W}{s_W} + \frac{\delta z_W}{2} + \frac{\delta z_t}{2} + \frac{\delta z_b}{2}\}\gamma_\mu(1-\gamma_5)u(p_t), \quad (3.12)$$

in which δz_b, δz_t and δz_W are the renormalization constants of the b-quark, t-quark and W^+-boson wave functions respectively and δs_W ($s_W = \sin\theta_W$) is the renormalization constant based on the Weinberg angle and δz_e is the electric charge renormalization constant. In the α_s order, there is no self-energy correction for the W boson, thus $\delta z_W = 0$. On the other hand $\delta z_e = -\frac{1}{2}\delta z_A$ where δz_A is the electromagnetic field renormalization constant [5], which can be written as $\delta z_A = \sum_T'(0)$ which $\sum_T(k)$ (the transverse part of photon self-energy) is zero in the α_s order, therefore $\delta z_e = 0$. Likewise the contribution of $\frac{\delta s_W}{s_W}$ is expressed by:

$$\frac{\delta s_W}{s_W} = \frac{-c_W^2}{2s_W^2}(\frac{\delta m_W^2}{m_W^2} - \frac{\delta m_z^2}{m_z^2}),$$

where $s_W = \sin\theta_W$ and $c_W = \cos\theta_W$. On the one hand $\delta m_W^2 = Re\{\sum_T^W(m_W^2)\}$ and on the other hand in the α_s order there is no the W^+ boson self-energy thus $\sum_T^W = 0$ so $\delta m_W^2 = 0$ and analogously we obtain $\delta m_z^2 = 0$, therefore we obtain: $\delta s_W/s_W = 0$.
Now we have to calculate the b-quark and t-quark wave functions renormalization constant.
At first I explain the general method to calculate the wave functions renormalization constant of one particle with mass m and momentum p. This constant is obtained from

calculating the self-energy of that particle in the α_s order($\sum_m(p)$) which is depicted in Fig.3.5. In the t'Hooft-Feynman gauge, the self-energy $\sum_m(p)$ in D-dimension reads:

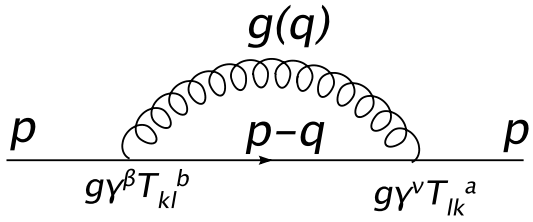

Figure 3.5: Feynman diagram for the self-energy of a particle with mass m in α_s order.

$$\sum\!\!\!\!\!\!-_m(p) = \frac{-4g^2\mu^{4-D}}{3i(2\pi)^4}\int d^Dq \quad \frac{\gamma^\beta(\not p - \not q + m)\gamma_\beta}{q^2((p-q)^2-m^2)}. \tag{3.13}$$

If we decompose the self-energy $\sum_m(p)$ into the vector and scalar parts to the face:

$$\sum\!\!\!\!\!\!-_m(p) = \not p \sum\!\!\!\!\!\!-_V(p^2) + m\sum\!\!\!\!\!\!-_s(p^2),$$

using the following relation:

$$\delta z_\psi = -\sum\!\!\!\!\!\!-_V(m^2) - 2m^2(\sum\!\!\!\!\!\!-'_V(m^2) + \sum\!\!\!\!\!\!-'_s(m^2)), \tag{3.14}$$

in which $\sum'_V(m^2) = \frac{\partial\sum_V(p^2)}{\partial\not p^2}\Big|_{\not p=m}$ and $\sum'_s(m^2) = \frac{\partial\sum_S(p^2)}{\partial\not p^2}\Big|_{\not p=m}$, we obtain the field renormalization constant δz_ψ . For t-quark with mass m_t we obtain:

$$\begin{aligned}\sum\!\!\!\!\!\!-_{m_t}(p_t) &= \frac{-g^2}{12\pi^2}\Big(\not p_t(\frac{m_t^2}{p_t^2}B_0(0,0,m_t^2) - \frac{m_t^2}{p_t^2}B_0(p_t^2,0,m_t^2) - B_0(p_t^2,0,m_t^2)+1)\\ &\quad + m_t(-2+4B_0(p_t^2,0,m_t^2))\Big),\end{aligned} \tag{3.15}$$

in which $B_0(0,0,m_t^2) = C_{\epsilon_{UV}}(\frac{1}{\epsilon_{UV}}+1)$.
The field renormalization constant δz_t reads:

$$\delta z_t = -\frac{\alpha_s}{3\pi}(\frac{1}{\epsilon_{UV}} + \frac{2}{\epsilon_{IR}} - 3\gamma_E + 3\ln\frac{\mu^2}{m_t^2} + 4), \tag{3.16}$$

where the strong coupling constant α_s is defined as $\alpha_s = \frac{g^2}{4\pi}$.
To calculate the field renormalization constant of the b-quark with mass $m_b = 0$, the self-energy $\sum_{m_b}(p_b)$ is:

$$\begin{aligned}\sum\!\!\!\!\!\!-_{m_b}(p_b) &= \frac{\alpha_s}{3\pi}B_0(p_b^2,0,0)\ \not p_b,\\ &= \not p_b\sum\!\!\!\!\!\!-_V(p_b^2).\end{aligned} \tag{3.17}$$

If we consider $\delta z_b = -\sum_V (m_b^2 = 0)$ from Eq.(3.14), therefore:

$$\begin{aligned}\delta z_b &= -\frac{\alpha_s}{3\pi} B_0(0,0,0) \\ &= -\frac{\alpha_s}{3\pi}\left(\frac{1}{\epsilon_{UV}} - \frac{1}{\epsilon_{IR}}\right),\end{aligned} \tag{3.18}$$

where the $B_0(0,0,0)$ function has been expanded in the powers ϵ_{UV} and ϵ_{IR}. The contribution of renormalization of the wave functions to the decay width reads:

$$\begin{aligned}&|\overline{2Re(M^{\star Born} M_2^V)}| \;= \\ &\frac{m_t^2 \alpha \alpha_s (1-\omega)(1+2\omega)}{3\omega \sin^2\theta_W}\Big(-\frac{1}{\epsilon_{IR}} - \frac{2}{\epsilon_{UV}} - 3\log\frac{4\pi\mu^2}{m_t^2} + 3\gamma_E - 4\Big) + \mathcal{O}(\epsilon_{IR}, \epsilon_{UV}).\end{aligned} \tag{3.19}$$

After summing up the vertex and the fields renormalization corrections we expand the obtained result in the powers of ϵ_{IR} and ϵ_{UV}. Obviously, all the UV singularities will be eliminated and the rest just contains the IR singularities in the forms $\frac{1}{\epsilon_{IR}^2}$ and $\frac{1}{\epsilon_{IR}}$. From now on we label the infrared singularities as ϵ. In conclusion, we have:

$$\begin{aligned}&|\overline{2Re(M^{\star Born} M^V)}| \;= \\ &|\overline{2Re(M^{\star Born} M_1^V + M^{\star Born} M_2^V)}| = \frac{m_t^2 \alpha \alpha_s (1-\omega)(1+2\omega)}{3\omega \sin^2\theta_W}\Big(\frac{4\pi\mu^2}{m_t^2}\Big)^{\epsilon}\Gamma[1+\epsilon] \times \\ &\Big[\frac{-2}{\epsilon^2} + \frac{4\log(1-\omega) - 5}{\epsilon} - 4\log^2(1-\omega) - 4Li_2(\omega) + \frac{12\omega\log(1-\omega)}{1+2\omega} - 12\Big],\end{aligned} \tag{3.20}$$

where the polylogarithm function $Li_2(\omega)$ can be written as: $-Li_2(1-\omega) - \ln\omega\ln(1-\omega) + \frac{\pi^2}{6}$. The contribution of the virtual corrections to the differential decay rate, Eq.(3.5) reads:

$$\frac{1}{\Gamma_0}\frac{d\hat{\Gamma}^{\rm vir}}{dx_b} = \frac{\alpha_s}{2\pi} C_F \delta(1-x_b)\Big[\frac{6\omega}{1+2\omega}\log(1-\omega) - F\Big], \tag{3.21}$$

where F is defined as:

$$\begin{aligned}F &= \frac{1}{2}\Big(-\log\frac{4\pi\mu^2}{m_t^2} + 2\log(1-\omega) + \gamma_E\Big)^2 + \frac{5}{2}\log\frac{4\pi\mu^2}{m_t^2} - 2Li_2(1-\omega) \\ &\quad -2\log(1-\omega)\log\omega + \frac{5\pi^2}{12} - \frac{5\gamma_E}{2} + 6 + \frac{1}{\epsilon^2} \\ &\quad -\frac{1}{\epsilon}\Big(-\log\frac{4\pi\mu^2}{m_t^2} + 2\log(1-\omega) + \gamma_E - \frac{5}{2}\Big),\end{aligned} \tag{3.22}$$

in which the color factor,C_F, is 4/3.

3.5 Real Gluon Corrections

The Feynman diagrams of the real gluon corrections are shown in Fig.3.6.

The amplitude M_a^R of the real gluon correction for graph (3.6a) is:

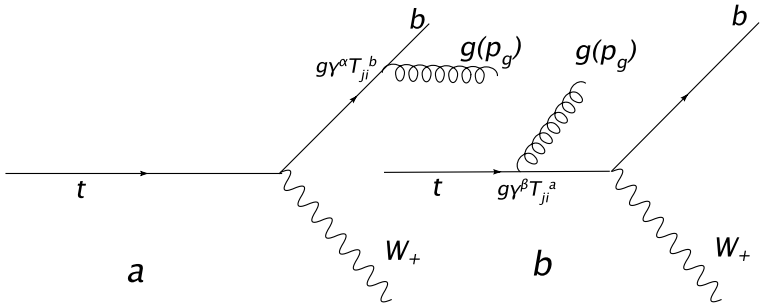

Figure 3.6: Feynman diagrams for emission of real gluons from t-quark and b-quark in α_s order

$$M_a^R = \frac{eg|V_{tb}|T_{ji}^b}{2\sqrt{2}\sin\theta_W}\epsilon'^{\alpha\star}(p_g)\epsilon^{\star\mu}(p_W)\overline{u}(p_b)\gamma^\alpha\left(\frac{\not{p}_b+\not{p}_g}{(p_b+p_g)^2}\right)\gamma_\mu(1-\gamma_5)u(p_t), \tag{3.23}$$

and the amplitude M_b^R for graph (3.6b) is:

$$M_b^R = \frac{eg|V_{tb}|T_{ji}^a}{2\sqrt{2}\sin\theta_W}\epsilon'^{\beta\star}(p_g)\epsilon^{\star\mu}(p_W)\overline{u}(p_b)\gamma_\mu(1-\gamma_5)\left(\frac{\not{p}_t-\not{p}_g+m_t}{(p_t-p_g)^2-m_t^2}\right)\gamma^\beta u(p_t). \tag{3.24}$$

As it was already explained $V_{tb} \simeq 1$.

The amplitude M_b^R leads to singularities of the form $\frac{1}{\epsilon}$ when $E_g \to 0$. These singularities are the soft gluon singularities. The amplitude M_a^R leads to both the soft singularities and the collinear singularities (see section 2.4).

To evaluate the contribution of the real corrections to the differential decay rate we use the dimensional regularization scheme and define $p_g^2 = 0$ and $D = 4-2\epsilon$. For this work we square the amplitude in general D-dimension, replace $D \to 4-2\epsilon$ and expand the squared amplitude in the powers of ϵ. In the squaring of amplitude we make a summation over the color and spin freedom degrees of the particles and obtain the average over the t-quark color and its spin degrees. We obtain:

$$\overline{|M^{Real}|^2} = \overline{|M_a^R|^2} + \overline{|M_b^R|^2} + 2Re\overline{|M_a^R.M_b^{\star R}|},$$

where for example: $\overline{|M_a^R|^2}$ is $\frac{1}{3\times 2}\sum_{spin,color}(M_a \cdot M_a^\star)$ and so on.

The differential decay rate for the real corrections, from appendix A, reads:

$$\frac{d\hat{\Gamma}}{dx_b} = 2^{4-3D}\pi^{\frac{3}{2}-D}\mu^{2(4-D)}\int dE_g\ d\cos\theta\ \delta(\cos\theta - a)\frac{(1-\omega)^{D-3}}{\Gamma[\frac{D}{2}-1]\Gamma[\frac{D-1}{2}]} \times (E_g m_t x_b)^{D-4}(1-\cos^2\theta)^{\frac{D-4}{2}} \times \overline{|M^R|^2}. \tag{3.25}$$

With respect to the momentum-energy conservation: $p_t^\mu = p_W^\mu + p_b^\mu + p_g^\mu$ we choose the 4-momentum of W^+ boson and b-quark as independent momenta and the 4-momentum of gluon dependent on them. Therefore as it can be found in appendix B, the range of the real gluon energy variations reads:

$$\frac{m_t(1-\omega)(1-x_b)}{2} \leq E_g \leq \frac{m_t(1-\omega)(1-x_b)}{2(1-x_b(1-\omega))}, \tag{3.26}$$

then the differential width is formulated in terms of the x_b kinematic variable which takes the values between 0 and 1 ($0 \leq x_b \leq 1$). The limit $x_b \to 1$ is equal to emission of a soft gluon. Now we investigate the terms in the squared amplitude $\overline{|M^R|^2}$ in detail and classify these terms to four types, i.e. we write down $\overline{|M^R|^2} = T_1 + T_2 + T_3 + T_4$. The contribution of the differential decay rate of each to the following four groups of terms are listed in appendix D.

- **First type terms** have no factors of singularities such as $\cos\theta$ or E_g^2 in their denominator. These are:

$$\begin{aligned} T_1 = {} & \frac{\pi^2\alpha\alpha_s}{\sin^2\theta_W}\Big\{\Big[32\frac{(D-2)E_gE_b^2}{3m_tm_W^2} + 64\frac{E_b^2}{3m_W^2}\Big]\cos^2\theta + \\ & \Big[-32\frac{2(D-2)E_b + m_t(10-3D)}{3m_tm_W^2}E_bE_g - 32\frac{2m_t^2 - 4E_bm_t + (D-3)m_W^2}{3E_gm_W^2}E_b \\ & -16\frac{2(D-6)m_t^2 - 2(D-2)E_bm_t + (D^2-5D+6)m_W^2}{3m_tm_W^2}E_b\Big]\cos\theta + \\ & \frac{16}{3m_tm_W^2}\Big[D^2(E_b-2m_t)M_W^2 + 2(8m_t^3 - 6E_bm_t^2 - 12m_tm_W^2 + 3E_bm_W^2) + \\ & D(-4m_t^3 + 6E_bm_t^2 - 2E_b^2m_t + 14m_tm_W^2 - 5E_bm_W^2)\Big] + \\ & \frac{32E_g}{3m_tm_W^2}\Big[(D-2)E_b^2 + (10-3D)m_tE_b + (3D-10)m_t^2\Big] + \\ & \frac{32(E_b+m_t)}{3E_gm_W^2}\Big[-2m_t^2 + 4E_bm_t - (D-3)m_W^2\Big]\Big\}. \end{aligned} \tag{3.27}$$

  In Eq.(D.1) the result is shown after integrating over E_g and $cos\theta$ and before expanding in ϵ. It is obvious that there is no singularity. We could even evaluate them in

4-dimension instead of D-dimension. The contribution of the real correction to the differential decay rate due to these terms reads:

$$\frac{1}{\Gamma_0}\frac{d\hat{\Gamma}^{Real,1}}{dx_b} = \frac{\alpha_s}{2\pi(1+2\omega)}C_F\Big\{\big[2(\omega-1)x_b^2+(1+2\omega)(1+x_b)\big]\log(1-x_b(1-\omega)) - \frac{x_b}{2(1-(1-\omega)x_b)^2}\big[7x_b^3(\omega-1)^3+2x_b^2(\omega+9)(1-\omega)^2 + 2(\omega^2+3\omega+2)+x_b(3\omega^3+5\omega^2+7\omega-15)\big]\Big\}. \quad (3.28)$$

- **Second type terms** which have the factor of $\cos\theta$ in their denominator in the form:$(1-\cos\theta)$. These are:

$$T_2 = \frac{16\pi^2\alpha\alpha_s}{3E_b m_W^2\sin^2\theta_W}m_t\Big\{-16m_tE_b^2-2E_b(-4m_t^2+(D+2)m_tE_g-2(D-3)m_W^2) +(D-2)E_g(2m_t^2-2m_tE_g+(D-3)m_W^2)\Big\}\frac{1}{E_g(1-\cos\theta)}. \quad (3.29)$$

According to the following differential decay rate:

$$\frac{d\hat{\Gamma}}{dx_b} = 2^{2(3\epsilon-4)}\pi^{-5/2+2\epsilon}\mu^{4\epsilon}\int dE_g\; d\cos\theta\;\delta(\cos\theta-a)\frac{(1-\omega)^{1-2\epsilon}}{\Gamma[1-\epsilon]\Gamma[\frac{3}{2}-\epsilon]} \times(E_g m_t x_b)^{-2\epsilon}(1+\cos\theta)^{-\epsilon}(1-\cos\theta)^{-\epsilon}\times\overline{|M^R|^2}, \quad (3.30)$$

if the scattering angle θ approaches zero they will create collinear singularities. The integrations of these terms have to be down in $D\neq 4$ dimensions and their infrared singularity appears in the form of $\frac{1}{\epsilon}$. The contribution of these terms to the differential decay rate reads:

$$\frac{1}{\Gamma_0}\frac{d\hat{\Gamma}^{Real,2}}{dx_b} = \frac{\alpha_s}{2\pi}C_F\Big\{\big(1+x_b-2x_b^2\frac{1-\omega}{1+2\omega}\big)\Big(-\frac{1}{\epsilon}+\gamma_E-\log\frac{4\pi\mu^2}{m_t^2}+2\log(1-x_b) -\log(1-x_b(1-\omega))+2\log(1-\omega)+2\log x_b+2\frac{1+\omega}{1+2\omega}\Big) - \frac{1}{2(1-x_b(1-\omega))^2(1+2\omega)}\Big(5(\omega-1)^3x_b^4+2(\omega-1)^2(3\omega+8)x_b^3 +5(\omega^3+\omega^2+\omega-3)x_b^2+2(3\omega^2+3\omega+1)x_b+2\Big). \quad (3.31)$$

- **Third type terms** have the factor E_g^2 in their denominator which produce the soft gluon singularities. These terms are:

$$T_3 = -\frac{32\pi^2\alpha\alpha_s}{3m_W^2\sin^2\theta_W}\Big\{E_b m_t\big(2m_t^2-2m_tE_b+(D-3)m_W^2\big)\Big\}\times\frac{1}{E_g^2}. \quad (3.32)$$

As already explained, radiation of a soft-gluon in top decay(the limit of $E_g \to 0$) corresponds to the limit $x_b \to 1$. When we integrate over E_g in the differential width $\frac{d\hat{\Gamma}}{dx_b}$, Eq.(3.30), terms of the form $(1-x_b)^{-1-2\epsilon}$ will appear(Eq.(D.3)). If we want to integrate over x_b and take the limit $\epsilon \to 0$ they will produce the IR singularities therefore we replace the terms $(1-x_b)^{-1-2\epsilon}$ by the following relation:

$$(1-x_b)^{-1-2\epsilon} = -\frac{1}{2\,\epsilon}\delta(1-x_b) + \Big(\frac{1}{1-x_b}\Big)_+ - 2\epsilon\Big(\frac{\log(1-x_b)}{1-x_b}\Big)_+. \tag{3.33}$$

A detailed discussion of the " + "–prescription is given in appendix C.
The contribution of the real corrections to the differential decay rate from these terms after integration over Eg reads:

$$\begin{aligned}\frac{1}{\Gamma_0}\frac{d\hat{\Gamma}^{\rm Real,3}}{dx_b} &= \frac{\alpha_s}{2\pi}C_F\Big\{\delta(1-x_b)\Big(\frac{1}{\epsilon} - 2\log(1-\omega) + 2\frac{\omega}{\omega-1}\log\omega + \log\frac{4\pi\mu^2}{m_t^2} - \gamma_E\Big)\\ &\quad -2x_b^2\frac{x_b(\omega-1)+\omega+2}{(1+2\omega)(1-x_b)_+}\Big\}.\end{aligned} \tag{3.34}$$

- **Fourth type terms** have both E_g and $(1-\cos\theta)$ factors in their denominators:

$$T_4 = \frac{64\pi^2\alpha\alpha_s}{3m_W^2\sin^2\theta_W}\Big\{m_tE_b\big(2m_t^2 - 2E_bm_t + (D-3)m_W^2\big)\Big\}\frac{1}{E_g^2(1-\cos\theta)}. \tag{3.35}$$

They contain both soft gluon and collinear singularities at the same time.
The terms $(1-x_b)^{-1-2\epsilon}$ appear after integrating over E_g and $cos\theta$ as well, Eq.(D.4), that they must again be replaced by Eq.(3.33) which leads to the singularities of the kind of $\frac{1}{\epsilon}\frac{1}{(1-x_b)_+}$. The contribution of the real corrections to the differential decay rate from these terms reads:

$$\begin{aligned}\frac{1}{\Gamma_0}\frac{d\hat{\Gamma}^{\rm Real,4}}{dx_b} &= \\ &\frac{\alpha_s}{2\pi}C_F\Big\{\delta(1-x_b)\Big(\frac{1}{\epsilon^2} + 2Li_2(1-\omega) + \frac{1}{2}\big(\gamma_E + 2\log(1-\omega) - \log\frac{4\pi\mu^2}{m_t^2}\big)^2 - \frac{\pi^2}{4}\\ &\frac{1}{\epsilon}\Big[-\gamma_E - 2\log(1-\omega) + \log\frac{4\pi\mu^2}{m_t^2}\Big]\Big) + 4x_b^2\frac{x_b(\omega-1)+\omega+2}{1+2\omega}\Big(\frac{\log(1-x_b)}{1-x_b}\Big)_+\\ &+\frac{2}{(1-x_b)_+}\Big[-\frac{1}{\epsilon}\big(\frac{x_b(\omega-1)+\omega+2}{1+2\omega}x_b^2\big) - 2\frac{x_b^2(1-x_b)(1-\omega)}{(1+2\omega)^2}\omega +\\ &\frac{x_b^2(x_b(\omega-1)+\omega+2)}{1+2\omega}\big(2\log x_b + 2\log(1-\omega) + \gamma_E - \log\frac{4\pi\mu^2}{m_t^2}\big)\Big]\Big\}.\end{aligned} \tag{3.36}$$

Summing all the contributions up, Eqs.(3.28,3.31,3.34,3.36), the real gluon contributions read:

$$\begin{aligned}\frac{1}{\Gamma_o}\frac{d\hat{\Gamma}^{Real}}{dx_b} &= \frac{\alpha_s}{2\pi}C_F\Bigg\{\delta(1-x_b)\Bigg[\frac{1}{\epsilon^2}+\frac{1}{\epsilon}\Big(\log\frac{4\pi\mu^2}{m_t^2}-2\log(1-\omega)-\gamma_E+1\Big)+\\ &+\frac{1}{2}\Bigg(-\log\frac{4\pi\mu^2}{m_t^2}+2\log(1-\omega)+\gamma_E\Bigg)^2-\Big(-\log\frac{4\pi\mu^2}{m_t^2}+2\log(1-\omega)+\gamma_E\Big)\\ &+\frac{2\omega}{\omega-1}\log\omega+2Li_2(1-\omega)-\frac{\pi^2}{4}\Bigg]+2(1+x_b^2)\Big(\frac{\log(1-x_b)}{1-x_b}\Big)_+ +\\ &\frac{1}{\big(1-x_b\big)_+}\Bigg[-\frac{1+x_b^2}{\epsilon}+2(1+x_b^2)\log x_b+(1+x_b^2)\Bigg(-\log\frac{4\pi\mu^2}{m_t^2}+\\ &2\log(1-\omega)+\gamma_E\Bigg)+x_b^2-4x_b+1+4\frac{x_b\omega(1-\omega)(1-x_b)^2}{(1+2\omega)(1-x_b(1-\omega))}\Bigg]\Bigg\}.\end{aligned} \tag{3.37}$$

3.6 Differential Decay Rate with α_s Corrections Using Fixed x_b

In the previous two sections we calculated the virtual and the real gluon corrections and showed both of them have singularities of the types $\frac{1}{\epsilon}$ and $\frac{1}{\epsilon^2}$. The singularities of the types $\frac{1}{\epsilon^2}$ cancel each other when the two corrections are summed up. The resulting differential decay rate in the variable x_b with α_s corrections is:

$$\frac{1}{\Gamma_o}\frac{d\hat{\Gamma}_b}{dx_b}=\delta(1-x_b)+\frac{\alpha_s}{2\pi}C_F\Bigg\{(-\frac{1}{\epsilon}+\gamma_E-\log 4\pi)\Bigg(\frac{1+x_b^2}{(1-x_b)_+}+\frac{3}{2}\delta(1-x_b)\Bigg)+\hat{A}(x_b)\Bigg\}, \tag{3.38}$$

where,

$$\begin{aligned}\hat{A}(x_b) &= \Bigg\{\delta(1-x_b)\Bigg[-\frac{3}{2}\log\frac{\mu^2}{m_t^2}+\frac{-2+2\omega}{1+2\omega}\log(1-\omega)+2\log(1-\omega)\log\omega-\frac{2\pi^2}{3}+\\ &4Li_2(1-\omega)-\frac{2\omega\log\omega}{1-\omega}-6\Bigg]+\frac{1}{(1-x_b)_+}\Bigg[-(1+x_b^2)\log\frac{\mu^2}{m_t^2}+(x_b^2-4x_b+1)+\\ &2(1+x_b^2)\log[x_b^2(1-\omega)]+\frac{4x_b\omega(1-\omega)(1-x_b)^2}{(1+2\omega)(1-x_b(1-\omega))}\Bigg]+2(1+x_b^2)\Bigg(\frac{\log(1-x_b)}{1-x_b}\Bigg)_+\\ &-2\frac{(1+x_b^2)\log x_b}{1-x_b}\Bigg\}+\mathcal{O}(\alpha_s^2).\end{aligned} \tag{3.39}$$

As we explained in section 2.2, to remove the IR collinear singularities remaining in equation above we define a fictitious distribution function $f_{i/a}$ which depends on the renormalization scheme. One of the most economical of renormalization schemes is the *modified minimal subtraction scheme($\overline{MS}$)*[62]. This scheme is due to 't Hooft and is specific to dimensional regularization. In this scheme we absorb the pole term $\frac{1}{\epsilon}$ accompanied by the natural constant γ_E and $\log 4\pi$ (in the combination $\frac{1}{\epsilon} - \gamma_E + \log 4\pi$) in the dimensionally regularized expression of the Green functions.

According to this approach to get the $\overline{MS}$-subtracted coefficient function we shall have to subtract from Eq.(3.38) the $\mathcal{O}(\alpha_s)$ term multiplying the characteristic $\overline{MS}$ constant $(\frac{1}{\epsilon} - \gamma_E + \log 4\pi)$ therefore we obtain:

$$\frac{1}{\Gamma_o}\frac{d\hat{\Gamma}_b^{\overline{MS}}}{dx_b} = \delta(1-x_b) + \frac{\alpha_s}{2\pi}C_F\hat{A}(x_b). \tag{3.40}$$

Having this result and obtaining the $\overline{MS}$ coefficient function for decay of the top quark to a massive b-quark, which will be discussed in the next chapter, we will be able to produce initial conditions for the partonic perturbative fragmentation functions(pFF). We also need Eq.(3.40) to evaluate B-hadronization of the b-quark in top decay. Later we explain about it in detail.

To obtain Eq.(3.40) we used the definition of the plus-function to simplify our calculations. For example, when summing up the coefficients of $\frac{1}{\epsilon}$ in Eqs.((3.31),(3.36)) using the plus function definition we obtain:

$$\frac{-x_b^2}{(1-x_b)_+}\left(\frac{x_b(\omega-1)+\omega+2}{1+2\omega}\right) - \frac{1}{2}(1+x_b-2\frac{1-\omega}{1+2\omega}x_b^2) = -\frac{1}{2}\frac{1+x_b^2}{(1-x_b)_+},$$

and also when we sum up Eq.(3.31) and Eq.(3.36), we can write:

$$\begin{aligned}(1+x_b+2\frac{\omega-1}{1+2\omega}x_b^2)\log(1-x_b) \quad + \quad & \frac{2x_b^2}{1+2\omega}(x_b(\omega-1)+\omega+2)\left(\frac{\log(1-x_b)}{1-x_b}\right)_+ \\ & = (1+x_b^2)\left(\frac{\log(1-x_b)}{1-x_b}\right)_+.\end{aligned}$$

The same applies use to the terms $\frac{1}{(1-x_b)_+}$.

We close the discussion of the radiative $\mathcal{O}(\alpha_s)$ corrections by stating that our final result (3.40) agrees with [51] and also this result is in agreement with the result of [63] after integration over x_b, see appendix G. It is remarkable that in the total width the IR divergences disappear together with the dependence on the unphysical scale μ.

3.7 Differential Decay Rate with α_s Corrections using Fixed x_g

In order to study the B-hadron production in top quark decay precisely, we need to know the differential width for the production of a gluon in top quark decay with the gluon scaled energy fraction x_g defined as:

$$x_g = \frac{2E_g}{m_t(1-\omega)} \qquad 0 \leq x_g \leq 1. \tag{3.41}$$

As usual we start from Eq.(A.1)and fixing the momentum of the gluon, the differential width for the real correction reads:

$$\begin{aligned} \frac{d\hat{\Gamma}}{dx_g} &= 2^{2(3\epsilon-4)}\pi^{-\frac{5}{2}+2\epsilon}\mu^{4\epsilon}\int dE_b\; d\cos\theta\; \delta(\cos\theta - a)\frac{(1-\omega)^{1-2\epsilon}}{\Gamma[\frac{3}{2}-\epsilon]\Gamma[1-\epsilon]} \\ &\quad \times (E_b m_t x_g)^{-2\epsilon}(1-\cos^2\theta)^{-\epsilon} \times \overline{|M|^2}, \end{aligned} \tag{3.42}$$

where $a = \frac{2E_gE_b+m_t^2-m_W^2-2m_tE_g-2m_tE_b}{2E_gE_b}$. The range of the variation of the b-quark energy is, (see appendix B):

$$\frac{m_t(1-\omega)(1-x_g)}{2} \leq E_b \leq \frac{m_t(1-\omega)(1-x_g)}{2(1-x_g(1-\omega))}. \tag{3.43}$$

It is obvious that because of fixing the momentum of the gluon, there will be no soft singularity. Therefore we will not have the plus prescription, because such terms arise after integration over the phase space of the real gluon. The only singularity which will appear, is due to the collinearity of the real emitted gluon and the massless parent quark.

Now we study the terms in the squared amplitude $\overline{|M|^2}$ in details and classify them as before.

- **First type terms** have no factor of singularity. they are:

$$
\begin{aligned}
T_1 = \frac{\pi^2\alpha\alpha_s}{\sin^2\theta_W}\Big\{ & \frac{-64Dm_t^2}{3m_W^2} + \frac{256m_t^2}{3m_W^2} + \frac{32DE_bm_t}{m_W^2} - \frac{64E_bm_t}{m_W^2} + \frac{32DE_gm_t}{m_W^2} - \frac{320E_gm_t}{3m_W^2} \\
& - \frac{32D^2}{3} + \frac{224D}{3} - \frac{32DE_b^2}{3m_W^2} - \frac{32DE_bE_g}{m_W^2} + \frac{16D^2E_b}{3m_t} - \frac{80DE_b}{3m_t} + \frac{32E_b}{m_t} + \frac{32DE_b^2E_g}{3m_tm_W^2} \\
& - \frac{64E_b^2E_g}{3m_tm_W^2} + \frac{320E_bE_g}{3m_W^2} - 128 + \Big[\frac{32DE_gE_b}{m_W^2} - \frac{320E_gE_b}{3m_W^2} + \frac{128E_gE_b^2}{3m_W^2m_t} - \frac{64DE_b^2E_g}{3m_tm_W^2} \\
& + \Big(- \frac{64E_gE_b^2}{3m_tm_W^2} + \frac{32DE_gE_b^2}{3m_tm_W^2} + \frac{64E_b^2}{3m_W^2}\Big)\cos\theta + \frac{64E_bm_t}{m_W^2} - \frac{64E_b^2}{3m_W^2} - \frac{32DE_bm_t}{3m_W^2} - \frac{32E_b}{m_t} \\
& + \frac{32DE_b^2}{3m_W^2} - \frac{16D^2E_b}{3m_t} + \frac{80DE_b}{3m_t}\Big]\cos\theta + \Big[- \frac{64m_t^3E_g}{3m_W^2} - \frac{64E_bm_t^3}{3m_W^2} + \frac{64E_bE_gm_t^2}{3m_W^2} \\
& + \frac{64m_t^2E_b^2}{3m_W^2} + \frac{128E_b^2E_gm_t}{3m_W^2} + 32E_bE_g - \frac{64m_t^2E_bE_g\cos\theta}{3m_W^2} + \frac{128m_tE_b^2E_g\cos\theta}{3m_W^2} + \\
& 32E_bE_g\cos\theta - \frac{32E_bE_gD\cos\theta}{3} - \frac{32DE_bE_g}{3} - \frac{32Dm_tE_g}{3} + 32m_tE_g - \frac{32DE_bm_t}{3} \\
& + 32E_bm_t\Big] \times \frac{1}{E_g^2}\Big\}.
\end{aligned}
$$

These terms can be calculated in 4-dimensions. The contribution of the real correction to the differential decay rate due to these terms reads:

$$
\begin{aligned}
\frac{1}{\Gamma_0}\frac{d\hat{\Gamma}^{Real,1}}{dx_g} = & \\
& \frac{\alpha_s(1-x_g)C_F}{12\pi x_g(1+2\omega)(1-x_g(1-\omega))^3}\Big\{4(1-\omega)^4x_g^5 + (1-\omega)^3(20\omega-11)x_g^4 + \\
& (1-\omega)^2(22\omega^2-65\omega+10)x_g^3 + 3(1-\omega)(-10\omega^2+23\omega-5)x_g^2 \\
& + 12(1-\omega)(\omega+2)x_g - 12(1+2\omega)\Big\}.
\end{aligned}
\tag{3.44}
$$

- **second type terms** have a factor of $(1-\cos\theta)$ in their denominator. These are:

$$
\begin{aligned}
T_2 = & \frac{\pi^2\alpha\alpha_s}{\sin^2\theta_W}\Big\{\Big[\frac{32Dm_t^3}{3E_bm_W^2} - \frac{64m_t^3}{3E_bm_W^2} + \frac{64E_gm_t^2}{3E_bm_W^2} + \frac{32m_t}{E_b} - \frac{32Dm_t^2}{3m_W^2} - \frac{32DEgm_t^2}{3E_bm_W^2} + \\
& \frac{16D^2m_t}{3E_b} - \frac{80Dm_t}{3E_b} - \frac{64m_t^2}{3m_W^2}\Big]\frac{1}{1-\cos\theta} + \Big[\frac{128m_t^3E_g}{3m_W^2} + \frac{128E_bm_t^3}{3m_W^2} - \frac{256E_bE_gm_t^2}{3m_W^2} \\
& - \frac{128E_b^2m_t^2}{3m_W^2} + \frac{64E_gDm_t}{3} + \frac{64Dm_tE_b}{3} - 64E_bm_t - 64E_gm_t\Big]\frac{1}{E_g^2(1-\cos\theta)}\Big\}.
\end{aligned}
$$

If the scattering angle θ approaches zero they will create collinear singularities. The integrations of these terms have to be down in $D \neq 4$ dimensions and their infrared singularity appears in the form of $\frac{1}{\epsilon}$. The contribution of the real correction to the differential decay rate from these terms reads:

$$\begin{aligned}\frac{1}{\Gamma_0}\frac{d\hat{\Gamma}^{Real,2}}{dx_g} &= \\ &\frac{\alpha_s C_F}{\pi}\Bigg\{\frac{1}{6(1+2\omega)(1-x_g(1-\omega))^3}\Big[2(1-\omega)^4x_g^5+3(1-\omega)^3(\omega-2)x_g^4+ \\ &3\omega(1-\omega)^2(9\omega-8)x_g^3+(1-\omega)(20\omega^3-102\omega^2+57\omega+16)x_g^2- \\ &3(16\omega^3-43\omega^2+18\omega+6)x_g+(1-\omega)(30\omega+6)\Big]+\frac{1+(1-x_g)^2}{2x_g}\Big[2\log(1-x_g) \\ &+2\log x_g-\log(1-x_g(1-\omega))+2\log(1-\omega)-\frac{1}{\epsilon}+\gamma_E-\log\frac{4\pi\mu^2}{m_t^2}\Big]\Bigg\}.\end{aligned} \tag{3.45}$$

The resulting differential decay rate in the variable x_g with α_s corrections is:

$$\begin{aligned}\frac{1}{\Gamma_o}\frac{d\hat{\Gamma}}{dx_g} &= \frac{1}{\Gamma_0}\frac{d\hat{\Gamma}^{Real,1}}{dx_g}+\frac{1}{\Gamma_0}\frac{d\hat{\Gamma}^{Real,2}}{dx_g}= \\ &\frac{\alpha_s}{2\pi}C_F\Bigg\{\frac{1+(1-x_g)^2}{x_g}\Big(-\frac{1}{\epsilon}+\gamma_E-\log 4\pi\Big)+\hat{B}(x_g)\Bigg\},\end{aligned} \tag{3.46}$$

where,

$$\begin{aligned}\hat{B}(x_g) &= \frac{1+(1-x_g)^2}{x_g}\Big(-\log\frac{\mu^2}{m_t^2}+2\log x_g+2\log(1-x_g)+2\log(1-\omega) \\ &-\log(1-x_g(1-\omega))\Big)+\frac{1}{2(1+2\omega)(1-x_g(1-\omega))^2}\Big((1-\omega)^2(6\omega-1)x_g^3 \\ &+2(1-\omega)(1-2\omega)(\omega+3)x_g^2+(-6\omega^3+25\omega^2-13)x_g-4(2\omega-3)(1+2\omega) \\ &-\frac{4(1+2\omega)}{x_g}\Big),\end{aligned} \tag{3.47}$$

and $C_F(1+(1-x_g)^2)/x_g = P_{gq}^{(0)}(x_g)$, see Eq.(2.32).

As we explained in sections 2.2 and 3.6, if we eliminate $\mathcal{O}(\alpha_s)$ the term multiplying the characteristic $\overline{MS}$ constant $(\frac{1}{\epsilon}-\gamma_E+\log 4\pi)$ in the above result the coefficient function in the $\overline{MS}$ scheme is obtained.

In the integration over E_b in Eq.(3.42) we deal with some specific kind of Hypergeometric functions. To obtain a finite result we use a useful relationship between Hypergeometric functions (see [67]):

$$\begin{aligned} {}_2F_1[a,b,c,x] &= \frac{\Gamma(c)\Gamma(b-a)}{\Gamma(b)\Gamma(c-a)}(1-x)^{-a} \times {}_2F_1[a,c-b,a-b+1,(1-x)^{-1}] \\ &+\frac{\Gamma(c)\Gamma(a-b)}{\Gamma(a)\Gamma(c-b)}(1-x)^{-b} \times {}_2F_1[b,c-a,b-a+1,(1-x)^{-1}]. \end{aligned} \tag{3.48}$$

In our calculations a, b, c and x are functions of ϵ and to expand the Hypergeometric functions in ϵ we used the program HYPEXP (see [68]).

Chapter 4

b-Quark Fragmentation Function to NLO QCD and B-Hadron Production in Top Quark Decay

In the previous chapter to simplify our calculation we assumed the b-quark is to be a massless particle. In the present chapter at first we attend to consider a non-zero mass m_b for b-quark and try to find out the differential width for the production of a massive b quark in top quark decay precisely. After that we will study the perturbative fragmentation function (pFF) of the b quark at NLO QCD by comparing the results obtained for the top quark decay width considering a massless and a massive b-quark separately, within the framework of perturbative fragmentation.

In the next section we try to find out the energy distribution of b-flavored hadron in top decay using two famous approaches: *zero-mass* and *general-mass variable-flavor-number scheme* applying realistic non-perturbative fragmentation functions. These non-perturbative FFs are obtained through a global fit to e^+e^- data from CERN LEP1 and SLAC SLC exploiting their universality. We show the b-energy distribution and make predictions for the energy spectrum of b-flavored hadrons in top decay comparing the two approaches mentioned above. We also study the B-hadron mass effect in the B-hadron energy distribution.

4.1 Kinematic Variables

In this section we introduce all kinematic quantities which we need to derive the NLO differential decay rate in presence of the b-quark mass. The kinematic variables needed are:

$$
\begin{aligned}
& b = \frac{m_b^2}{m_t^2} \qquad , \qquad \omega = \frac{m_W^2}{m_t^2} \qquad , \qquad S = \frac{1}{2}(1+b-\omega), \\
& x_b = \frac{E_b}{m_t S}, \\
& \beta = \frac{\sqrt{b}}{S}, \\
& Q = S\sqrt{1-\beta^2}, \\
& G_0 = \frac{1}{2}(1+b-2\omega+\frac{(1-b)^2}{\omega}), \\
& \Phi(x_b) = S\bigg(\sqrt{x_b^2-\beta^2} - \log(\frac{\beta}{x_b-\sqrt{x_b^2-\beta^2}})\bigg),
\end{aligned}
\tag{4.1}
$$

where as before, x_b is the normalized b-quark energy fraction and it is simple to show that $\beta \leq x_b \leq 1$:

$$
\begin{aligned}
& E_{b,min} = m_b = m_t\sqrt{b} \Rightarrow S m_t x_{b,min} = m_t\sqrt{b} \Rightarrow x_{b,min} = \beta, \\
& p_g = 0 \Rightarrow p_t = p_b + p_W \Rightarrow m_t^2 + m_b^2 - 2m_t E_b = m_W^2 \Rightarrow x_{b,max} = 1.
\end{aligned}
$$

4.2 The NLO Differential Width with the Full Inclusion of the b Mass

In this part we repeat all calculations which we had in the previous chapter but considering a massive b-quark. For the virtual and real corrections we have the same graphs like in the previous chapter.

4.2.1 Born Approximation

The amplitude of the Born approximation using Fig.3.1 is given by Eq.(3.1). Therefore the squared Feynman amplitude $\overline{|M^{Born}|^2}$ will be:

$$
\overline{|M^{Born}|^2} = \frac{\pi\alpha m_t^2}{sin^2\theta_W}\big(1+b-2\omega+\frac{(1-b)^2}{\omega}\big) = \frac{2\pi\alpha m_t^2}{sin^2\theta_W}G_0. \tag{4.2}
$$

In order to get the correct finite terms in the normalized differential decay rate, the Born width Γ_0 will have to be evaluated in dimensional regularization up to $\mathcal{O}(\epsilon)$. Therefore we have:

$$\overline{|M^{Born}|^2} = \frac{2\pi\alpha m_t^2}{sin^2\theta_W}\big(G_0 - 2S\epsilon\big). \tag{4.3}$$

Using the following two-body phase space:

$$\Gamma_0 = \frac{\mu^{2\epsilon}\ Q^{1-2\epsilon}}{8(4\pi)^{\frac{1}{2}-\epsilon} m_t^{1+2\epsilon}\Gamma[\frac{3}{2}-\epsilon]}\overline{|M^{Born}|^2}, \tag{4.4}$$

the Born width reads:

$$\Gamma_0 = \frac{\alpha m_t}{4sin^2\theta_W}(QG_0)\bigg\{1 - \epsilon\big[-\log\frac{4\pi\mu^2}{m_t^2} + \gamma_E + \log 4Q^2 + 2\frac{S-G_0}{G_0}\big]\bigg\} + \mathcal{O}(\epsilon^2). \tag{4.5}$$

To obtain Eq.(4.4), we used the differential decay rate of the two particles top decay in D-dimensions, (see Eq.(A.1)).

As we know the Born approximation of the decay rate receives the radiative corrections from virtual gluons and real gluon radiation. Now we are in situation to calculate the virtual gluon corrections to the differential decay rate.

4.2.2 Virtual Gluon Corrections

In section 3.4 we showed that in the one-loop correction the amplitude M^V contains 2 graphs, which are shown in Fig.3.2.
The amplitude M_1^V which includes the one-loop vertex correction, shown in Fig.3.4, in the t'Hooft-Feynman gauge reads:

$$M_1^V = \frac{-e}{2\sqrt{2}\sin\theta_W}\epsilon^{\star\mu}(p_W)\overline{u}(p_b)\Lambda_\mu(p_W,p_b)u(p_t), \tag{4.6}$$

where:

$$\Lambda_\mu(p_W,p_b) \ = \ \mu^{4-D}\frac{g^2}{i(2\pi)^4}\int d^Dq \quad [g_{\beta\nu}]\times[\frac{T^a_{ji}\gamma^\beta(\not{q}+\not{p}_b+m_b)\gamma_\mu(1-\gamma_5)(\not{p}_b+\not{p}_W+\not{q}+m_t)\gamma^\nu T^a_{il}}{q^2[(q+p_b)^2-m_b^2][(p_b+p_W+q)^2-m_t^2]}].$$

After applying the on-shell relations: $p_t^2 = m_t^2$ and $p_b^2 = m_b^2$, taking sum and average over the quark colors, the result will be:

$$\Lambda_\mu(p_W,p_b) = \frac{4g^2\mu^{4-D}}{3i(2\pi)^4}\int d^Dq[\frac{\gamma^\beta(\not{q}+\not{p}_b+m_b)\gamma_\mu(1-\gamma_5)(\not{p}_b+\not{p}_W+\not{q}+m_t)\gamma_\beta}{q^2[(q+p_b)^2-m_b^2][(p_b+p_W+q)^2-m_t^2]}].$$

Therefore the contribution of the one-loop vertex correction to the differential decay rate (Eq.(3.4)) reads:

$$\overline{|2Re(M^{\star Born}.M_1^V)|} = \frac{\alpha\pi}{2\sin^2\theta_W}\big(-g^{\mu\nu}+\frac{p_W^\mu.p_W^\nu}{m_W^2}\big)Tr\big((\not{p}_b+m_b)\Lambda_\mu(\not{p}_b+\not{p}_W+m_t)\gamma_\nu(1-\gamma_5)\big). \tag{4.7}$$

The final result gets the following form:

$$\begin{aligned}\overline{|2Re(M^{\star Born}.M_1^V)|} &= \frac{m_t^2\alpha\alpha_s}{\sin^2\theta_W}\Big\{\frac{16}{3}G_0Sm_t^2C_0(m_b^2,m_t^2,m_W^2,m_b^2,0,m_t^2)\\ &+\frac{4}{3\omega}\Big[b(b-1)B_0(0,m_t^2,m_b^2)-(-2G_0\omega+4b^2-3bS)B_0(m_b^2,0,m_b^2)+\\ &(2G_0\omega+3S+b-3)B_0(m_t^2,0,m_t^2)+3\omega^2B_0(m_W^2,m_t^2,m_b^2)-2G_0\omega+b^2-b\Big]\Big\}.\end{aligned} \tag{4.8}$$

It is simple to show that in the limit $m_b\to 0$ this result is converted to Eq.(3.9).
In the equation above, the new B_0 and C_0 functions which we need, are:

$$\begin{aligned}B_0(m_b^2,0,m_b^2) &= \Delta_{UV}+2-\log\frac{m_b^2}{\mu^2},\\ B_0(0,m_t^2,m_b^2) &= \Delta_{UV}+1-\frac{m_t^2\log\frac{m_t^2}{\mu^2}-m_b^2\log\frac{m_b^2}{\mu^2}}{m_t^2-m_b^2},\\ B_0(m_W^2,m_t^2,m_b^2) &= \Delta_{UV}+2-\log\frac{m_bm_t}{\mu^2}+\frac{m_t^2-m_b^2}{m_W^2}\log\frac{m_b}{m_t}\\ &+\frac{2Q}{\omega}(\log(Q+S)-\log S-\log\beta)\\ C_0(m_b^2,m_t^2,m_W^2,m_b^2,0,m_t^2) &= \frac{x_S}{m_bm_t(1-x_S^2)}\Big\{\frac{1}{2}\log^2(\frac{m_t}{m_b})-\frac{1}{2}\log^2x_S\\ &+\log x_S(2\log(1-x_S^2)-\log(\frac{\mu^2}{m_bm_t})-\Delta_{IR})+\\ &Li_2(1-x_S\frac{m_b}{m_t})+Li_2(1-x_S\frac{m_t}{m_b})+Li_2(x_S^2)-\frac{\pi^2}{6}\Big\},\end{aligned} \tag{4.9}$$

in which $\Delta_{UV} = \frac{1}{\epsilon_{UV}} + \log 4\pi - \gamma_E$, $\Delta_{IR} = \frac{1}{\epsilon_{IR}} + \log 4\pi - \gamma_E$ and $x_S = \frac{S-Q}{S\beta}$,[59, 60]. Therefore the final result for Eq.(4.8) is:

$$
\begin{aligned}
|\overline{2Re(M^{\star Born} M_1^V)}| \;=\; & \\
& \frac{\alpha\alpha_s m_t^2}{Sin^2\theta_W} C_F \Big\{ \frac{b - 3S + 2S^2}{\omega} \log b + 6Q \log \frac{S+Q}{\sqrt{b}} + \\
& G_0 (\frac{1}{\epsilon_{UV}} - \gamma_E + \log \frac{4\pi\mu^2}{m_t^2}) + \frac{SG_0}{Q} \Big(\frac{3}{2} \log^2 b - 2 \log b \log \frac{(S-Q)^2}{2Q} + \\
& 3 \log^2 (S-Q) + 4 \log 2Q \log (S-Q) - 2 \log \frac{S-Q}{\sqrt{b}} (\frac{1}{\epsilon_{IR}} - \gamma_E + \log \frac{4\pi\mu^2}{m_t^2}) \\
& + 2Li_2(1 + Q - S) + 2Li_2(\frac{b+Q-S}{b}) + 2Li_2(\frac{S-Q}{S+Q}) - \frac{\pi^2}{3} \Big) \Big\}.
\end{aligned}
\tag{4.10}
$$

Now we consider the contribution M_2^V, due to renormalization of the wave functions which are shown by the countervertex graph, Fig.3.2b:

$$
M_2^V = \frac{-e}{2\sqrt{2}\sin\theta_W} \varepsilon^{\star\mu}(p_W) \overline{u}(p_b) \{ \frac{\delta z_t}{2} + \frac{\delta z_b}{2} \} \gamma_\mu (1 - \gamma_5) u(p_t). \tag{4.11}
$$

As we showed in section 3.4 , the general field renormalization constant δZ_ψ for a quark with mass m_q is:

$$
\delta z_\psi = \frac{\alpha_s}{3\pi} (-B_0(0,0,m_q^2) + 4m_q^2 \frac{\partial B_0(p^2,0,m_q)}{\partial p^2}\Big|_{p^2=m_q^2} + 1), \tag{4.12}
$$

in which $\frac{\partial B_0(p^2,0,m_q)}{\partial p^2}\Big|_{p^2=m_q^2} = -\frac{1}{2m_q^2}(\frac{1}{\epsilon_{IR}} - \gamma_E + \log\frac{4\pi\mu^2}{m_q^2} + 2)$. With respect to the equation above, δz_b and δz_t read:

$$
\begin{aligned}
\delta z_b &= -\frac{\alpha_s}{3\pi} (\frac{1}{\epsilon_{UV}} + \frac{2}{\epsilon_{IR}} - 3\gamma_E + 3 \log \frac{\mu^2}{m_b^2} + 4) \\
\delta z_t &= -\frac{\alpha_s}{3\pi} (\frac{1}{\epsilon_{UV}} + \frac{2}{\epsilon_{IR}} - 3\gamma_E + 3 \log \frac{\mu^2}{m_t^2} + 4).
\end{aligned}
\tag{4.13}
$$

The contribution of the wave functions renormalization to the decay rate reads:

$$
\begin{aligned}
|\overline{2Re(M^{\star Born} M_2^V)}| = & \\
& \frac{\alpha\alpha_s G_0 m_t^2 C_F}{Sin^2\theta_W} (\frac{3}{2} \log b - 3 \log \frac{4\pi\mu^2}{m_t^2} - \frac{2}{\epsilon_{IR}} - \frac{1}{\epsilon_{UV}} + 3\gamma_E - 4).
\end{aligned}
\tag{4.14}
$$

Obviously, when we sum up the vertex and renormalization corrections (Eqs.(4.10,4.14)), the UV singularities cancel each other and the remaining singularities will be the IR singularities. From now on we label the infrared singularities as ϵ.

In order to obtain the differential decay rate due to the contribution of the virtual corrections we start from Eq.(3.4). With respect to the definition of the kinematic variables and considering the following relations in the t-quark rest frame:

$$\begin{aligned}
|\overrightarrow{p_b}| &= m_t(S^2-b)^{\frac{1}{2}}, \\
\frac{d^{D-1}\mathbf{p}_W}{2E_W} &= \int d^D\mathbf{p}_W\delta(p_W^2-m_W^2), \\
\delta(p_W^2-m_W^2) &= \delta((p_t-p_b)^2-m_W^2)=\frac{1}{2m_t}\delta(E_b-m_tS)=\frac{1}{2m_t^2S}\delta(1-x_b),
\end{aligned}$$

if we integrate over the four-momentum $\mathbf{p}_W$ in Eq.(3.4), therefore we obtain:

$$\begin{aligned}
\frac{d\tilde{\Gamma}^{Vir}}{dx_b} &= \frac{Q}{8\pi m_t}\delta(1-x_b)\Big\{1-\epsilon\big[\gamma_E-\log\frac{4\pi\mu^2}{m_t^2}+2\log(2Q)+\frac{2(S-G_0)}{G_0}\big]\Big\}\times \\
&\quad \overline{|2Re(M^{\star Born}(M_1^V+M_2^V))|}+\mathcal{O}(\alpha_s^2). \qquad (4.15)
\end{aligned}$$

This result is converted to Eq.(3.5) when we take the limit $m_b \to 0$.
Finally, the virtual correction contributes to the differential decay rate as:

$$\begin{aligned}
\frac{1}{\Gamma_0}\frac{d\tilde{\Gamma}^{\rm vir}}{dx_b} &= \frac{\alpha_s\delta(1-x_b)}{\pi}C_F\Big\{-\frac{Q+S\log\frac{S-Q}{\sqrt{b}}}{Q\epsilon}+\frac{S}{4Q}\log^2 b+\frac{3bS-3S+2\omega G_0}{4\omega G_0}\log b \\
&\quad -(\log\frac{4\pi\mu^2}{m_t^2}-\gamma_E)(1+\frac{S}{Q}\log\frac{S-Q}{\sqrt{b}})-\frac{S\log(1+Q-S)\log(Q+S)}{Q} \\
&\quad +\frac{3Q}{G_0}\log\frac{S+Q}{\sqrt{b}}-\frac{S\log(Q+S)\log(-b+Q+S)}{Q}+\frac{S\log(Q+S)\log(\omega)}{Q} \\
&\quad +\frac{SLi_2(\frac{2Q}{Q-S+1})}{Q}-\frac{SLi_2(\frac{2Q}{-b+S+Q})}{Q}-2\Big\}. \qquad (4.16)
\end{aligned}$$

To obtain the above result, we used the following relations between the Spence Functions

(or di-logarithms)[69]:

$$\begin{aligned} Li_2(x) &= \frac{\pi^2}{6} - \log x \log(1-x) - Li_2(1-x), \\ Li_2(-x) &= -Li_2(\frac{x}{1+x}) - \frac{1}{2}\log^2(1+x), \\ Li_2(\frac{1}{x}) &= \frac{\pi^2}{3} - Li_2(x) - \frac{1}{2}\log^2 x, \\ Li_2(xy) &= Li_2(x) + Li_2(y) - Li_2(\frac{x(1-y)}{1-xy}) - Li_2(\frac{y(1-x)}{1-xy}) - \log\frac{1-x}{1-xy}\log\frac{1-y}{1-xy}. \end{aligned} \tag{4.17}$$

4.2.3 Real Gluon Corrections

The Feynman diagrams corresponding to real gluon corrections are shown in Fig.3.6. The amplitude M_a^R for graph (3.6a) is given by:

$$M_a^R = -\frac{egT_{ji}^b}{2\sqrt{2}\sin\theta_W}\epsilon^{\star\prime\alpha}(p_g)\epsilon^{\star\mu}(p_W)\overline{u}(p_b)\gamma^\alpha\left(\frac{m_b + \not{p}_b + \not{p}_g}{m_b^2 - (p_b+p_g)^2}\right)\gamma_\mu(1-\gamma_5)u(p_t),$$

while the amplitude M_b^R for the graph (3.6b) is the same as before, Eq.(3.24). As we include now the mass of the b-quark, unlike in the previous case there is no collinear singularity in our calculations and only a soft singularity arises from the emission of a real soft gluon. We apply now the previous method to the new expressions.

The real correction contributions to the decay width are presented via Eq.(A.1), where $\overline{|M^R|^2}$ has been given by:

$$\overline{|M^R|^2} = \overline{|M_a^R|^2} + \overline{|M_b^R|^2} + 2Re\overline{|M_a^R.M_b^{\star R}|^2}. \tag{4.18}$$

To simplify our calculation we choose the p_t-rest frame as before. With this selection we have:

$$p_g^\mu.p_b^\mu = E_g(E_b - \sqrt{p_b^2}cos\theta) \quad \text{where} \quad p_b^2 = E_b^2 - m_b^2 \quad \text{and} \quad p_g^2 = E_g^2. \tag{4.19}$$

The differential decay rate for the real corrections in D-dimension will get the following form:

$$\begin{aligned} \frac{d\Gamma}{dx_b} &= 2^{-2D}\pi^{\frac{3}{2}-D}\mu^{2(4-D)}\int dE_g\; d\cos\theta\; \delta(\cos\theta - a)\frac{(1+b-\omega)}{\Gamma[\frac{D}{2}-1]\Gamma[\frac{D-1}{2}]} \\ &\quad \times E_g^{D-4}p_b^{D-4}(1-\cos^2\theta)^{\frac{D-4}{2}} \times \overline{|M^R|^2}, \end{aligned} \tag{4.20}$$

where $a = \frac{2E_gE_b+m_t^2-m_W^2+m_b^2-2m_tE_g-2m_tE_b}{2E_gp_b}$.
Obviously, the above result will be converted to Eq.(A.4) if $m_b \to 0$. In the next step we have to obtain the range of variation of E_g. In appendix B we showed that the range of E_g when the b-quark is considered to be a massive one, reads:

$$\frac{m_tS(1-x_b)(1-Sx_b-S\sqrt{x_b^2-\beta^2})}{1+b-2Sx_b} \leq E_g \leq \frac{m_tS(1-x_b)(1-Sx_b+S\sqrt{x_b^2-\beta^2})}{1+b-2Sx_b}.$$

Now we study the terms in the squared amplitude $\overline{|M^R|^2}$ in detail and classify them according to the singularities. We classify them into two groups:

First type terms have no factor of singularity. They are:

$$\begin{aligned}
&\frac{\pi^2\alpha\alpha_s}{\omega Sin^2\theta_W}\Big\{E_g\big(\frac{32(D-2)}{3m_t^3}(E_b^2+P_b^2cos^2\theta-2E_bP_bcos\theta)+32\frac{3D-10}{3m_t^2}(P_bcos\theta-E_b)+\\
&\frac{96D-320}{3m_t}\big)+\frac{1}{E_b-P_bcos\theta}\big(\frac{16\omega}{3}m_t(D^2-5D+6)-\frac{32}{3}(D+2)E_b-\frac{32}{3}(D-2)E_g+\\
&\frac{32m_t}{3}(D(1+b)-6b-2)\big)+\frac{32P_bcos\theta}{3m_t^2}((D-2)E_b-m_t(D(1+b)-2b-6))\\
&+\frac{64bm_t^2}{3(E_b-P_bcos\theta)^2}-32\frac{DE_b^2}{3m_t^2}+32\frac{(b+3)(D-2)E_b}{3m_t}+64\frac{p_b^2cos^2\theta}{3m_t^2}-\frac{64}{3}(1+b)(D-4)+\\
&\frac{16\omega(D^2-5D+6)}{3m_t}(E_b-P_bcos\theta)-\frac{32\omega}{3}(D^2-7D+12)\Big\}.
\end{aligned} \tag{4.21}$$

Due to absence of factor of singularity we can calculate them in 4-dimensions instead of D-dimensions. The contribution of the real correction to the differential decay rate due to these terms is giving by:

$$\begin{aligned}
&\frac{1}{\Gamma_0}\frac{d\tilde{\Gamma}^{Real,1}}{dx_b} \quad = \\
&\frac{(x_b-1)\alpha_s}{\pi Q\omega G_0}C_F\bigg(S^2\sqrt{x_b^2-\beta^2}(-3b+4Sx_b-3-\frac{4S\omega}{1+b-2Sx_b})-S\Phi(x_b)(-3b+4S(1+x_b)-3)\bigg).
\end{aligned} \tag{4.22}$$

Second type terms have the factor of E_g in their denominator. They are:

$$\frac{\pi^2\alpha\alpha_s}{3\omega(E_b-P_bcos\theta)^2Sin^2\theta_W}\Big\{\frac{1}{E_g^2}\Big(-64E_b^4+64E_b^2p_b^2cos^2\theta-32bm_t^3E_b(2b+(D-3)\omega+2)+$$
$$32E_bm_t(2b+(D-3)\omega+2)(E_b^2-P_b^2cos^2\theta)+64b^2m_t^4+64bm_t^2P_b^2cos^2\theta\Big)+$$
$$\frac{32}{E_g}\Big((2b+(D-3)\omega+6)(-E_b^3+P_bE_b^2cos\theta+E_bP_b^2cos^2\theta+bE_bm_t^2)+\frac{4E_b^4}{m_t}-\frac{4P_bE_b^3cos\theta}{m_t}$$
$$+\frac{4E_bP_b^3cos^3\theta}{m_t}-(2b+(D-3)\omega+2)(bm_t^3+P_b^3cos^3\theta+m_tP_b^2cos^2\theta+bm_t^2P_bcos\theta)$$
$$+m_tE_b^2(-2b+(D-3)\omega+2)+4bP_bE_bcos\theta-\frac{4P_b^2E_b^2cos^2\theta}{m_t}\Big)\Big\}. \tag{4.23}$$

When we integrate over E_g and $cos\theta$ in Eq.(4.20) terms of the form $(1-x_b)^{(-1-2\epsilon)}$ will appear, see Eq.(D.5). These terms are due to integrating over the soft part of phase space. This part of phase space includes the radiation of a soft gluon in top decay (i.e. the limit of $E_g \to 0$). This corresponds to the limit $x_b \to 1$. For a massive b quark, where $x_{b,min} \neq 0$, we replace the term $(1-x_b)^{(-1-2\epsilon)}$ by the plus-function in the following way:

$$(1-x_b)^{-1-2\epsilon}=\Big(-\frac{1}{2\,\epsilon}\delta(1-x_b)+\frac{1}{(1-x_b)_+}\Big)(x_b-\beta)^{-2\epsilon}.$$

To obtain the contribution of the real corrections to the differential decay rate from these terms we need to know the expansion of some Hypergeometric functions which appear in our calculations while integrating over the gluon phase space. To obtain the expansion of these type of Hypergeometric functions the XSummer-program [70] has been used.
The general results for the related functions, are:

$${}_2F_1(2\epsilon,\epsilon;1+\epsilon;x)=1+2\epsilon^2Li_2(x)+\mathcal{O}(\epsilon^3),$$
$${}_2F_1(1+2\epsilon,\epsilon;2+\epsilon;x)=1+\epsilon\Big(1+\frac{1-x}{x}\log(1-x)\Big)+$$
$$\epsilon^2\Big(-\frac{1-x}{x}\log^2(1-x)+\frac{1-x}{x}\log(1-x)+\frac{1+x}{x}Li_2(x)\Big)+\mathcal{O}(\epsilon^3).$$

Taking these into account, we obtain:

$$\frac{1}{\Gamma_0}\frac{d\tilde{\Gamma}^{Real,2}}{dx_b} = \frac{\alpha_s}{\pi}C_f\Big\{\delta(1-x_b)\Big(\frac{Q+S\log\frac{S-Q}{\sqrt{b}}}{Q\epsilon}-\frac{S\log^2 b}{4Q}+\frac{S\log(\frac{-b+S+Q}{2S(1-\beta)})\log b}{Q}-2\log(\frac{2S(1-\beta)}{\sqrt{\omega}})+ (\log\frac{4\pi\mu^2}{m_t^2}-\gamma_E)\big(1+\frac{S}{Q}\log(\frac{S-Q}{\sqrt{b}})\big)-\frac{S\log(S+Q)\log(1+Q-S)}{Q}+\frac{(S-b)\log(\frac{Q+S}{\sqrt{b}})}{Q} -\frac{S\log(S+Q)\log(-b+S+Q)}{Q}+\frac{2S\log(S+Q)\log(2S(1-\beta))}{Q}+\frac{(1-b)\log(\frac{1+Q-S}{\sqrt{\omega}})}{Q} +\frac{SLi_2(\frac{2Q}{1+Q-S})}{Q}-\frac{SLi_2(\frac{2Q}{S+Q-b})}{Q}\Big)+2\frac{\Phi(x_b)+\frac{\left(S(x_b-1)\sqrt{x_b^2-\beta^2}-x_b\Phi(x_b)\right)(2S^2(1-x_b)^2+\omega G_0)}{G_0\omega}}{Q(1-x_b)} -2\frac{\Phi(x_b)}{Q(1-x_b)_+}\Big\}. \tag{4.24}$$

If we sum up Eqs.(4.22),(4.24) the final contribution due to real corrections is:

$$\frac{1}{\Gamma_0}\frac{d\tilde{\Gamma}^{Real}}{dx_b} = \frac{\alpha_s}{\pi}C_f\Big\{\delta(1-x_b)\Big(\frac{Q+S\log\frac{S-Q}{\sqrt{b}}}{Q\epsilon}-\frac{S\log^2 b}{4Q}+\frac{S\log(\frac{-b+S+Q}{2S(1-\beta)})\log b}{Q}-2\log(\frac{2S(1-\beta)}{\sqrt{\omega}})+ (\log\frac{4\pi\mu^2}{m_t^2}-\gamma_E)\big(1+\frac{S}{Q}\log(\frac{S-Q}{\sqrt{b}})\big)-\frac{S\log(S+Q)\log(1+Q-S)}{Q}+\frac{(S-b)\log(\frac{Q+S}{\sqrt{b}})}{Q} -\frac{S\log(S+Q)\log(-b+S+Q)}{Q}+\frac{2S\log(S+Q)\log(2S(1-\beta))}{Q}+\frac{(1-b)\log(\frac{1+Q-S}{\sqrt{\omega}})}{Q} +\frac{SLi_2(\frac{2Q}{1+Q-S})}{Q}-\frac{SLi_2(\frac{2Q}{S+Q-b})}{Q}\Big)-2\frac{\Phi(x_b)}{Q(1-x_b)_+}+2\frac{\Phi(x_b)}{Q}-\frac{S(1-x_b)(1+b+2\omega)\Phi(x_b)}{QG_0\omega} +\frac{S\sqrt{x_b^2-\beta^2}}{G_0Q}\big(4\frac{(1-x_b)S^2}{1+b-2Sx_b}+\frac{(1-x_b)(1+b+2\omega)S}{\omega}-2G_0\big)\Big\}. \tag{4.25}$$

4.3 Differential Decay Rate with α_s Corrections using Massive b-Quark

In the last two sections we calculated the real and the virtual gluonic corrections to the top decay. Summing them up, the singularities cancel each other and the resulting differential decay rate in the variable x_b is:

$$\frac{1}{\Gamma_0}\frac{d\tilde{\Gamma}}{dx_b} = \delta(1-x_b) + \frac{\alpha_s}{2\pi}C_F\tilde{A}(x_b) \tag{4.26}$$

where:

$$\begin{aligned}
\tilde{A}(x_b) \;=\; & \frac{2}{Q}\Big\{\Big[2SLi_2(\frac{2Q}{1-S+Q}) - 2SLi_2(\frac{2Q}{S-b+Q}) + \frac{Q}{4}\log b\big(6\frac{(\omega-b)(S-b)}{\omega G_0} - 1\big) \\
& -2S\log(S+Q)\big(\log(\frac{1-S+Q}{\sqrt{\omega}}) + \log(\frac{S-b+Q}{2S(1-\beta)})\big) + S\log b\log(\frac{S-b+Q}{2S(1-\beta)}) + \\
& \big(3\frac{Q^2}{G_0} + S - b\big)\log(\frac{S+Q}{\sqrt{b}}) + (1-b)\log(\frac{1-S+Q}{\sqrt{\omega}}) \\
& -2Q\log(\frac{2S(1-\beta)}{\sqrt{\omega}}) - 2Q\Big]\delta(1-x_b) - 2\frac{\Phi(x_b)}{(1-x_b)_+} - 2\frac{S\Phi(x_b)}{G_0}(1+\frac{1+b}{2\omega})(1-x_b) \\
& +2\Phi(x_b) + 2S\sqrt{x_b^2-\beta^2}\bigg(2\frac{S^2}{G_0}(\frac{1-x_b}{1+b-2Sx_b}) + \frac{S}{G_0}(1-x_b)(1+\frac{1+b}{2\omega}) - 1\bigg)\Big\}.
\end{aligned} \tag{4.27}$$

In the calculations above the relations 4.17 have been used. Note that the above result is in agreement with [51]. In Fig 4.1 the b-quark energy distribution in top decay is shown when the b-quark is a massive particle (Eq.(4.27)). In this graph x_b can not be less than $\beta = 0.0729$. As it is seen, this graph diverges when $x_b \to 1$, due to a behavior proportional to $\frac{1}{(1-x_b)_+}$. In this plot we set $m_t = 174$ GeV and $m_b = 5$ GeV.

4.4 Subtraction Terms at NLO

Up to now to calculate the top decay width we assumed $m_b \neq 0$ from the beginning. We call it the massive decay rate. One might expect that the partonic decay rate calculated in the $\overline{MS}$ renormalization scheme with the massless b-quark should correspond to the massive decay rate in the limit $m_b \to 0$ if the collinear singular terms proportional to $\log(\frac{m_b^2}{m_t^2})$ are subtracted. It means the subtracted massive decay rate differs from the massless decay

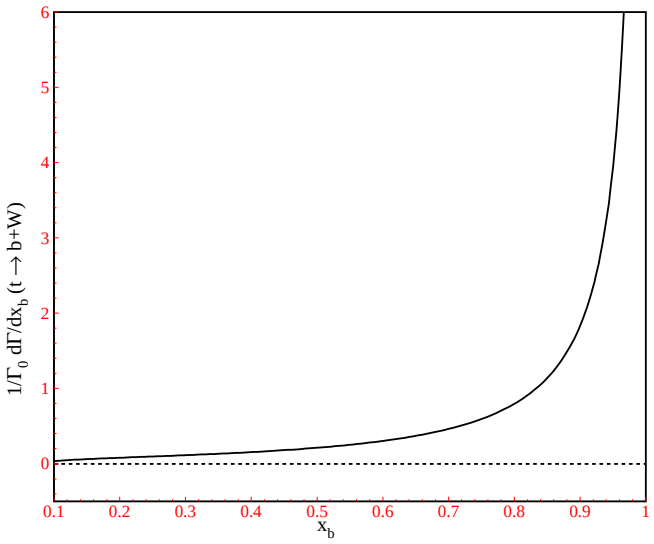

Figure 4.1: b-quark energy distribution in top decay according to the exact NLO calculation, with inclusion of powers of $\frac{m_b}{m_t}$. We set $m_t = 174$ GeV and $m_b = 5$ GeV.

rate only by terms $\sim \log(\frac{m_b^2}{m_t^2})$. This expectation is not true, as it was first demonstrated by Mele and Nason [42] for inclusive heavy quark production in e^-e^+ annihilation at NLO ($e^-e^+ \to Q\overline{Q}g$, where Q is the heavy quark). They found that the limit $m \to 0$ of the cross section for $e^-e^+ \to Q\overline{Q}g$ and the cross section calculated with $m = 0$ from the beginning (in the $\overline{MS}$ scheme) differ by finite terms of $\mathcal{O}(\alpha_s)$. Of course the reason for the occurrence of these finite terms is the different definition of the collinear singular terms in the two approaches. In the zero mass b-quark approach, the mass of b-quark is set to zero from the beginning and the collinearly divergent terms are defined with the help of dimensional regularization. This fixes the finite terms in a specific way and their form depends on the chosen regularization method. If one starts with $m_b \neq 0$ and performs the limit $m_b \to 0$ afterward, the finite terms can be different. In the following we compare the obtained result for the decay rate with a massless b-quark from the beginning (Eq.(3.40)) and the limit $m_b \to 0$ of the massive decay rate, Eq.(4.27). Afterward we will show that the difference between their finite terms will be the perturbative fragmentation function $d_{b\to b}(x_b, \mu)$. We also show the simplest way to connect the truly massless decay rate in the $\overline{MS}$ scheme with the massive decay rate is to subtract the finite pieces $d_{b\to b}$ from the massive theory. Now we start from Eq.(4.27) and we neglect powers of $\frac{m_b}{m_t}$. To do that we have to use the

following substitutions for the kinematic variables (Eq.(4.1)):

$$
\begin{aligned}
&S \to \frac{1}{2}(1-\omega),\\
&\beta \to 0,\\
&Q \to S,\\
&G_0 \to \frac{1}{2\omega}(1+2\omega)(1-\omega),\\
&\Phi(x_b) \to S(x_b - \log(2Sx_b) + \frac{1}{2}\log\frac{m_b^2}{m_t^2}).
\end{aligned}
$$

Rewriting Eq.(4.27) we find:

$$
\begin{aligned}
\lim_{m_b\to 0}\frac{1}{\Gamma_o}\frac{d\tilde{\Gamma}_b}{dx_b} \quad = \\
\delta(1-x_b) + \frac{\alpha_s}{2\pi}C_F\Bigg\{\delta(1-x_b)\Bigg[4Li_2(1-\omega) - \frac{2\pi^2}{3} + 2\log\omega\log(1-\omega) - \frac{2\omega}{1-\omega}\log\omega \\
-\frac{2(1-\omega)}{1+2\omega}\log(1-\omega) + \frac{3}{2}\log\frac{m_t^2}{m_b^2} - 4\Bigg] + 4x_b\Big(\frac{\omega(1-\omega)(1-x_b)}{(1+2\omega)(1-(1-\omega)x_b)} - \frac{1+x_b}{2}\Big) \\
-4(x_b - \log(x_b(1-\omega)) - \frac{1}{2}\log\frac{m_t^2}{m_b^2})\Big(\frac{1}{(1-x_b)_+} - \frac{1+x_b}{2}\Big)\Bigg\}.
\end{aligned}
\tag{4.28}
$$

In Fig 4.2 the b-quark energy distribution in top decay is shown when the mass of the b-quark is ignored (Eq.(4.28)). As it is seen, Eq.(4.28) contains contribution $\sim \frac{\alpha_S(\mu)}{(1-x_b)_+}$, therefore our result diverges in the soft limit $x_b \to 1$. In Fig 4.3, we compare Figs(4.1,4.2) and it is shown that the full inclusion of powers of $\frac{m_b}{m_t}$ has a negligible effect on the x_b spectrum, as we discuss in detail later.

Obviously, the result above (Eq.(4.28)) is not equal to Eq.(3.40) from chapter 3, where we started with $m_b = 0$. As it was mentioned there are some extra finite terms in the new obtained result which the reason for the occurrence of these terms is the different definition of the collinear singular terms in the two approaches. In the previous calculation, the b-quark mass was set to zero from the beginning and the collinearly divergent terms were defined with the help of dimensional regularization. The form of the finite terms is inherent to the chosen regularization procedure. Therefore the extra finite terms (or the subtraction

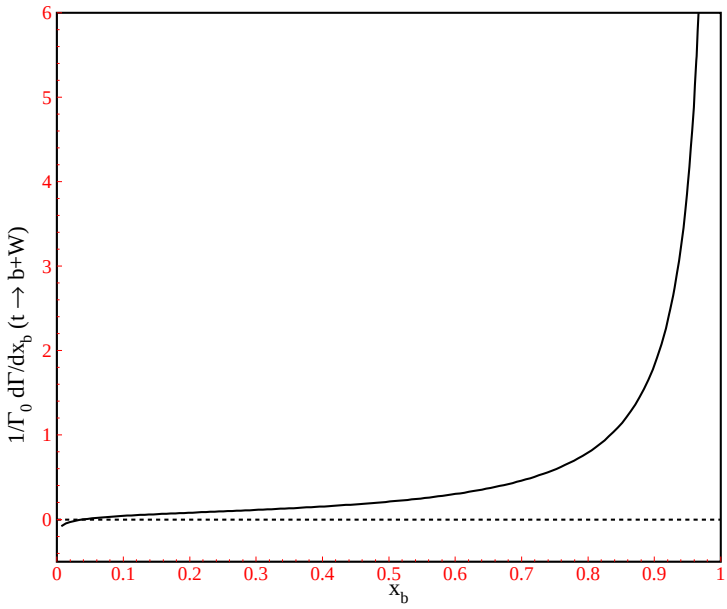

Figure 4.2: b-quark energy distribution in top decay according to the exact NLO calculation, without inclusion of powers of $\frac{m_b}{m_t}$. We set $m_t = 174$ GeV and $m_b = 5$ GeV.

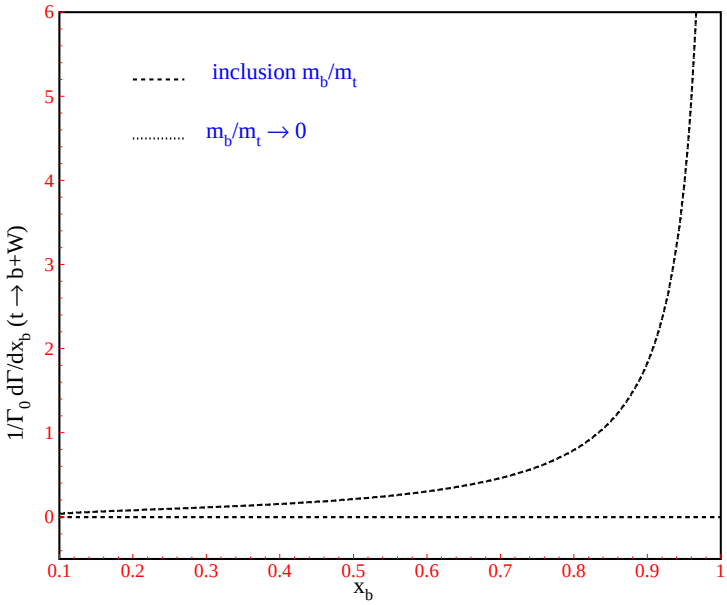

Figure 4.3: b-quark energy distribution in top decay according to the exact NLO calculation, both with and without inclusion of powers of $\frac{m_b}{m_t}$. We set $m_t = 174$ GeV and $m_b = 5$ GeV.

terms) due to the difference between these results, are:

$$\frac{1}{\Gamma_o}\frac{d\Gamma_b^{Sub}}{dx_b} = \lim_{m_b\to 0}\frac{1}{\Gamma_o}\frac{d\tilde{\Gamma}_b}{dx_b} - \frac{1}{\Gamma_o}\frac{d\hat{\Gamma}_b^{\overline{MS}}}{dx_b} \quad =$$

$$\frac{\alpha_s}{2\pi}C_F\Bigg\{\delta(1-x_b)\bigg(2-\frac{3}{2}\log(\frac{m_b^2}{\mu^2})\bigg) - 2(1+x_b^2)\bigg(\frac{\log(1-x_b)}{1-x_b}\bigg)_+$$
$$+\frac{1}{(1-x_b)_+}\bigg(-4x_b^2\log x_b + 2(1-x_b^2)\log(1-\omega) + (1+x_b^2)\log(\frac{\mu^2}{m_t^2}) - 2\log(\frac{m_b^2}{m_t^2})$$
$$+\frac{(1-2\omega)(1-\omega)(x_b^3+x_b)+(1-2\omega)(4\omega-1)x_b^2-1-2\omega}{(1+2\omega)(1-x_b(1-\omega)}\bigg) - (1+x_b)\log\frac{m_t^2}{m_b^2}$$
$$+\frac{4x_b(1-x_b)\omega(1-\omega)}{(1+2\omega)(1-x_b(1-\omega)} + 4\frac{x_b^2}{1-x_b}\log x_b - 2(1+x_b)\log(1-\omega)\Bigg\}.$$

With respect to the definition of "+"-prescription, we can write:

$$\int_0^1 dx(1-x_b^2)\bigg(\frac{\log(1-x_b)}{1-x_b}\bigg)_+ = \int_0^1 dx(1+x_b)\log(1-x_b), \tag{4.29}$$

and

$$\frac{1}{(1-x_b)_+}\big((1+x_b^2)\log\frac{\mu^2}{m_t^2} - 2\log b\big) - (1+x_b)\log\frac{m_t^2}{m_b^2} \quad =$$
$$\bigg(-(1+x_b)+\frac{2}{(1-x_b)_+}\bigg)\log\frac{\mu^2}{m_b^2}.$$

Using Eq.(C.11) the subtraction terms can be simplified to the following terms:

$$\frac{1}{\Gamma_o}\frac{d\Gamma_b^{Sub}}{dx_b} = \frac{\alpha_s}{2\pi}C_F\Bigg\{\delta(1-x_b)\bigg(2+\frac{3}{2}\log(\frac{\mu^2}{m_b^2})\bigg) + \frac{2}{(1-x_b)_+}\big(\log(\frac{\mu^2}{m_b^2})-1\big)$$
$$-4\bigg(\frac{\log(1-x_b)}{1-x_b}\bigg)_+ - (1+x_b)\log\frac{\mu^2}{m_b^2} + (1+x_b)(1+2\log(1-x_b))\Bigg\}$$
$$= \frac{\alpha_s}{2\pi}C_F\bigg[\frac{1+x_b^2}{1-x_b}\bigg(\log\frac{\mu^2}{m_b^2} - 2\log(1-x_b) - 1\bigg)\bigg]_+ . \tag{4.30}$$

In section 4.7 we will prove that the obtained result above is the partonic perturbative fragmentation function $d_{b\to b}(x_b,\mu)$. This function is process independent and can be used in any other heavy-quark production process. The universality of the partonic fragmentation function has been confirmed by performing the same calculations.

4.5 Differential Decay Rate using Fixed x_g in the Massive b-Quark Case

In this section we are interested in calculating the differential width using fixed x_g. As usual we start from Eq.(A.1) and fix the momentum of the real emitted gluon. The differential decay rate is given by:

$$\begin{aligned}\frac{d\tilde{\Gamma}}{dx_g} &= 2^{1-2D}\pi^{\frac{3}{2}-D}\mu^{2(4-D)}\int dE_b\ d\cos\theta\ \delta(\cos\theta-a)\frac{S^{D-3}}{\Gamma[\frac{D}{2}-1]\Gamma[\frac{D-1}{2}]} \\ &\quad\times(p_b m_t x_g)^{D-4}(1-\cos^2\theta)^{\frac{D-4}{2}}\times\overline{|M|^2},\end{aligned} \tag{4.31}$$

where $a=\frac{2E_gE_b+m_t^2+m_b^2-m_W^2-2m_tE_g-2m_tE_b}{2E_gp_b}$.
The real gluon energy range is, see appendix B:

$$\frac{m_tS(1-x_g)}{1-2Sx_g}(1-Sx_g-Sx_g\sqrt{1-F\beta^2})\le E_b\le\frac{m_tS(1-x_g)}{1-2Sx_g}(1-Sx_g+Sx_g\sqrt{1-F\beta^2}),$$

where $F=\frac{(1-2Sx_g)}{(1-x_g)^2}$.
Obviously, since the momentum of the gluon has been fixed there is no soft singularity and calculations can be done in 4-dimensions.
The terms in the squared amplitude $\overline{|M|^2}$ are the sum of Eqs.(4.21,4.23) with $D=4$. Finally, decay width reads:

$$\begin{aligned}\frac{1}{\Gamma_o}\frac{d\tilde{\Gamma}_g}{dx_g} &= \\ &\frac{\alpha_s}{\pi G_0x_g\omega Q}C_F\Bigg\{S^2\Big((1+b+2\omega)(1+(1-x_g)^2)-4S\beta^2(1-x_g)\Big)\Big(-\frac{1}{2}\log b+\log S \\ &+\log(1-x_g)-\frac{1}{2}\log(1-2Sx_g)+\log(1+\sqrt{1-\frac{(1-2Sx_g)\beta^2}{(1-x_g)^2}})\Big)+ \\ &\frac{S^2(1-x_g)}{(1-2Sx_g)^2}\sqrt{1-\frac{(1-2Sx_g)\beta^2}{(1-x_g)^2}}\Big[x_g^3S^2(4S+b+1)+x_g^2S(28S^2-21bS-21S+14b-2) \\ &+Sx_g(-16S\beta^2+24b-32S+24)+4S\beta^2-6b+8S-6\Big]\Bigg\}.\end{aligned} \tag{4.32}$$

4.6 Subtraction Terms for x_g Fixed

The result for $\frac{1}{\Gamma_0}\frac{d\tilde{\Gamma}}{dx_g}$ is converted to the following form in the limit $m_b \to 0$:

$$\lim_{m_b\to 0} \frac{1}{\Gamma_o}\frac{d\tilde{\Gamma}_g}{dx_g} = \frac{\alpha_s}{2\pi}C_F\Bigg\{\frac{1+(1-x_g)^2}{x_g}\Bigg(2\log(1-x_g) - \log\frac{m_b^2}{\mu^2} - \log\frac{\mu^2}{m_t^2} + 2\log(1-\omega) - \log(1-x_g(1-\omega))\Bigg) - \frac{1-x_g}{2x_g(1-x_g(1-\omega))^2(1+2\omega)}\Bigg((1-\omega)^2(2\omega-3)x_g^3 + (1-\omega)(-14\omega^2+7\omega+11)x_g^2 - 16(1-\omega)(1+2\omega)x_g + 8(1+2\omega)\Bigg)\Bigg\}, \tag{4.33}$$

Comparing this result with Eq.(3.47), we realize that they do not coincide and we obtain the following subtraction term :

$$\frac{1}{\Gamma_o}\frac{d\Gamma_g^{Sub}}{dx_g} = \lim_{m_b\to 0}\frac{1}{\Gamma_o}\frac{d\tilde{\Gamma}_g}{dx_g} - \frac{1}{\Gamma_o}\frac{d\hat{\Gamma}_g^{\overline{MS}}}{dx_g} = \frac{\alpha_s}{2\pi}C_F\Bigg\{-\frac{1+(1-x_g)^2}{x_g}(1+2\log x_g - \log\frac{\mu^2}{m_b^2})\Bigg\}. \tag{4.34}$$

We shall need this result when we want to calculate the energy distribution of b-flavored hadrons in top decay, using the general-mass variable-flavor-number scheme.

4.7 b-Quark Fragmentation Function in Top Decay to NLO QCD

For heavy quark production, the quark mass m acts as a regulator for the collinear singularity and allows one to perform perturbative calculations. Therefore the fragmentation of heavy quarks is a collinear-safe process. However, fixed-order differential distributions, like Eq.(4.28), contain terms proportional to $\alpha_s \log\frac{m_t^2}{m_b^2}$ which spoil the convergence of the perturbative expansion and needs to be resummed to all orders to improve the predictions. To achieve this goal, we can follow the approach of perturbative fragmentation functions, originally proposed in [42], which allows to resum these large logarithms.
According to this method, heavy quarks are first produced at large transverse momentum

$m \ll P_T$ (in our process: $m_b \ll m_t$), as if they were massless, and afterward they slow down and fragment into a massive object. The perturbative fragmentation function $D(\mu_F, m)$ expresses the transition of a massless parton into a massive quark at the factorization scale μ_F. We leave a detailed discussion of this procedure to the last part of this section.
Now we turn our attention to Eq.(4.30) and we show that this is the initial condition of the massless b-quark perturbative fragmentation function into the massive one, namely it will be $D_b(x_b, \mu_{0F}, m_b)$.
As we showed, the massless and the massive differential width in the $\overline{MS}$ factorization scheme can be written as:

$$\begin{aligned}
\frac{1}{\Gamma_0}\frac{d\hat{\Gamma}}{dx_b} &= \delta(1-x_b) + \frac{\alpha_s}{2\pi} C_F \hat{A}(x_b) \quad from \quad Eq.(3.40), \\
\frac{1}{\Gamma_0}\frac{d\hat{\Gamma}}{dx_g} &= \frac{\alpha_s}{2\pi} C_F \hat{A}_g(x_g) \qquad\qquad from \quad Eq.(3.46), \\
\frac{1}{\Gamma_0}\frac{d\tilde{\Gamma}}{dx_b} &= \delta(1-x_b) + \frac{\alpha_s}{2\pi} C_F \tilde{A}(x_b) \quad from \quad Eq.(4.26),
\end{aligned} \tag{4.35}$$

and also when μ_{0F} is taken to be of the order of the mass m_b, $D_b(x_b, \mu_{0F}, m_b)$ can not contain large logarithms , it means that $\log(\frac{\mu_0}{m_b})$ is not large with respect to $\frac{1}{\alpha_s}$, while we always assume that $\frac{m_b}{\mu_0}$ is small. Therefore it must be possible to express $D_b(x_b, \mu_{0F}, m_b)$ as a perturbative expansion in power of α_s, see Eqs.(2.45,2.46):

$$\begin{aligned}
D_b(x_b, \mu_{0F}, m_b) &= d_b^{(0)}(x_b) + \frac{\alpha_s}{2\pi} d_b^{(1)}(x_b, \mu_{0F}, m_b) + \mathcal{O}(\alpha_s^2) \\
&= \delta(1-x_b) + \frac{\alpha_s}{2\pi} d_b^{(1)}(x_b, \mu_{0F}, m_b) + \mathcal{O}(\alpha_s^2).
\end{aligned} \tag{4.36}$$

We expect $D_g(x_g)$, expressing the transition of a gluon into a massive b-quark, to be of order α_s, since in order to produce a heavy quark from a gluon the strong coupling constant must enter at least once. i.e.

$$D_g(x_g, \mu_{0F}) = \frac{\alpha_s}{2\pi} d_g^{(1)}(x_g, \mu_{0F}) + \mathcal{O}(\alpha_s^2). \tag{4.37}$$

Following[42], we neglect terms behaving like $(\frac{m_b}{m_t})^p$ in $\frac{1}{\Gamma_o}\frac{d\tilde{\Gamma}_b}{dx_b}$, where $p \geq 1$. Therefore according to Eq.(2.18) the differential width for the production of a massive b quark in top

decay can be expressed via the following convolution:

$$\begin{aligned}\frac{1}{\Gamma_0}\frac{d\tilde{\Gamma}_b}{dx_b}(x_b, m_t, m_W, m_b) &= \frac{1}{\Gamma_0}\frac{d\hat{\Gamma}_i}{dz} \otimes D_{i\to b}(\frac{x_b}{z}) \\ &= \sum_i \int_{x_b}^1 \frac{dz}{z}(\frac{1}{\Gamma_0}\frac{d\hat{\Gamma}_i(z, m_t, m_W, \mu, \mu_F)}{dz}) D_i(\frac{x_b}{z}, \mu_F, m_b),\end{aligned} \tag{4.38}$$

where $\frac{d\hat{\Gamma}_i}{dz}$ is the differential width for the production of a massless parton i in top decay with energy z, which is insensitive to the low-energy feature of the process, and therefore does not depend on the mass of the b-quark. $D_i(\frac{x_b}{z}, \mu_F, m_b)$ is the perturbative fragmentation function for a parton i to fragment into a massive b quark, which is insensitive to the high-energy part of the process, and therefore does not depend on m_t. The scales μ and μ_F are the renormalization and factorization scales respectively. As before we choose the same values for them, $\mu = \mu_F$. The definitions of $d\Gamma$ and D_i are not unique. They depend on the scheme one uses to separate the collinear singularities. For definiteness, we will always refer to the $\overline{MS}$ factorization scheme.

Since we have been assuming $B(t \to bW) = 1$ and the probability to produce a b-quark via the splitting of a secondary gluon is negligible, we shall limit ourselves to considering the perturbative fragmentation of a massless b into a massive b and, on the right side of Eq.(4.38), we shall have only the $i = b$ contribution. Substituting Eqs.(4.35,4.36) in Eq.(4.38) and keeping only the terms up to the order α_s we get:

$$\begin{aligned}\frac{1}{\Gamma_o}\frac{d\tilde{\Gamma}_b}{dx_b}(x_b, m_t, m_W, m_b) &= \\ &\int_{x_b}^1 \frac{dz}{z}\big(\delta(1-z) + \frac{\alpha_s}{2\pi}C_F\hat{A}(z)\big)\Big(\delta(1-\frac{x_b}{z}) + \frac{\alpha_s}{2\pi}d^{(1)}_{b\to b}(\frac{x_b}{z}, \mu_0, m_b)\Big) \\ =&\int_{x_b}^1 \frac{dz}{z}\delta(1-z)\delta(1-\frac{x_b}{z}) + \frac{\alpha_s}{2\pi}C_F\int_{x_b}^1 \frac{dz}{z}\delta(1-\frac{x_b}{z})\hat{A}(z) + \\ &\frac{\alpha_s}{2\pi}\int_{x_b}^1 \frac{dz}{z}\delta(1-z)d^{(1)}_{b\to b}(\frac{x_b}{z}, \mu_0, m_b) + \mathcal{O}(\alpha_s^2).\end{aligned} \tag{4.39}$$

Evaluating the Dirac Delta definition we obtain:

$$\delta(1-x_b) + \frac{\alpha_s}{2\pi}C_F\tilde{A}(x_b) = \delta(1-x_b) + \frac{\alpha_s}{2\pi}C_F\hat{A}(x_b) + \frac{\alpha_s}{2\pi}d^{(1)}_{b\to b}(x_b, \mu_0, m_b), \tag{4.40}$$

therefore:

$$\begin{aligned} d^{(1)}_{b\to b}(x_b,\mu_0,m_b) &= C_F(\tilde{A}(x_b)-\hat{A}(x_b)) \\ &= \frac{2\pi}{\alpha_s}(\frac{1}{\Gamma_o}\frac{d\Gamma^{Sub}_b}{dx_b}), \end{aligned} \tag{4.41}$$

which shows the initial condition for the b-quark perturbative FF is proportional to the subtraction term.

It is simple to show that inserting Eq.(3.40) and the definition of fragmentation function $b \to b$ (Eq.(4.30)) into Eq.(4.38) the massive b-quark differential decay rate, Eq.(4.28), is obtained. In this demonstration the following property of the '+'-distribution is used:

$$-\frac{(1+x_b^2)}{(1-x_b)_+}\log\frac{\mu^2}{m_t^2}+\frac{2x_b}{(1-x_b)_+}\log\frac{\mu^2}{m_b^2}+(1-x_b)\log\frac{\mu^2}{m_b^2}=(1+x_b)\log\frac{m_b^2}{m_t^2}.$$

Now let us explain about the perturbative fragmentation function approach in more detail. We generally apply this method to resum collinear logarithms $\sim \alpha_s(\mu_F)\log(\mu_F^2/\mu_{0F}^2)$ appearing in the fixed order calculations considering the massive quarks, see section 2.4. In our process using the factorization theorem, the differential decay rate to produce a massive b-quark is related to a convolution of the differential decay rate including the massless b-quark with the perturbative fragmentation function, Eq.(4.38). Former is proportional to $\mathcal{O}(\log(\mu_F^2/m_t^2))$ and latter is proportional to $\mathcal{O}(\log(\mu_{0F}^2/m_b^2))$. Assuming $\mu_{0F} \simeq m_b$ and $\mu_F \simeq m_t$ there will be no longer large logarithms in the differential decay rate and considering the splitting function (Eq.(2.32)) at $\mathcal{O}(\alpha_s)$ in the DGLAP equation, one resums the leading logarithms $\sim \alpha_s^n(m_t)\log^n(m_t^2/m_b^2)$ appearing in the perturbative-FF. Accounting for $\mathcal{O}(\alpha_s^2)$ terms in Eq.(2.28) leads to the inclusion of next-to-leading logarithms $\sim \alpha_s^{n+1}(m_t)\log^n(m_t^2/m_b^2)$ as well. Then we can get rid of them.
Furthermore, in the initial condition of perturbative-FF (Eqs.(4.34,4.41)) the coefficient multiplying the strong coupling constant contains terms behave as: $\frac{1}{(1-x_b)_+}$ or $\left(\frac{\log(1-x_b)}{1-x_b}\right)_+$ which are singular once $x_b \to 1$. The soft leading logarithms (LL) $\sim \left(\frac{\log(1-x_b)}{1-x_b}\right)_+$ and the soft NLL $\sim \frac{1}{(1-x_b)_+}$ arise from emitting of soft gluons and in order to obtain a reliable result in the large-x_b region we must resum these logarithms to all order of α_s, see [43]. This feature of the perturbative expansion is due to the fact that in the limit $x_b \to 1$ the phase space for gluon radiation is reduced, so that the usual cancellation of soft divergences is incomplete. In [42] the authors have shown that a modified evolution kernel allows us to

resum all leading logarithms of $1 - x_b$ in the anomalous dimension of the fragmentation function. This modification of the evolution kernel is equal to changing the argument in α_s that is taken to be the maximum virtuality allowed kinematically in the gluon line.

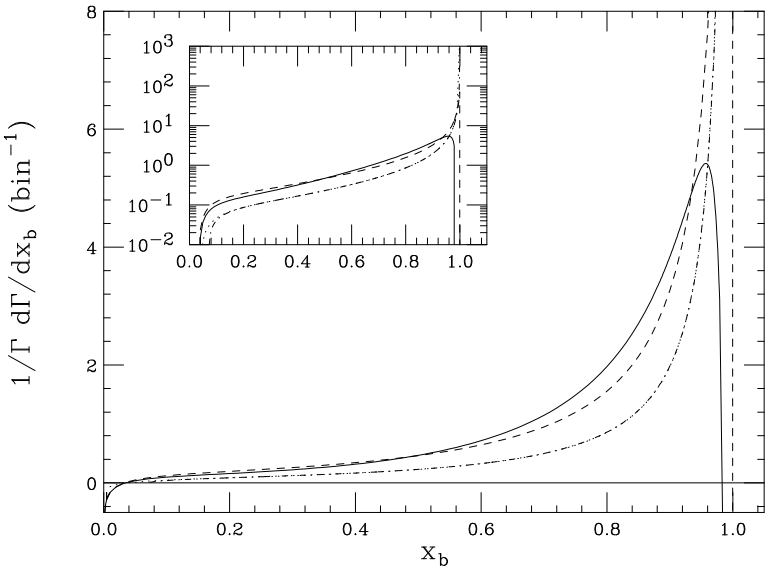

Figure 4.4: b-quark energy distribution in top decay according to the perturbative fragmentation approach, with (solid line) and without (dashes) NLL soft-gluon resummation in the initial condition of D_b, and according to the exact NLO calculation, with (dot-dashes) and without (dots) inclusion of powers of $\frac{m_b}{m_t}$. The initial condition of the fragmentation function is set to $\mu_0 = \mu_{0F} = m_b$ and the final scale is set to $\mu = \mu_F = m_t$

In Fig.4.4, taken from [51], the b-quark energy distribution in top decay is shown via the perturbative fragmentation approach with and without NLL soft gluon resummation in the initial condition of the perturbative fragmentation function. For the sake of comparison, we also show the exact result for a massive b-quark as before, Figs.(4.1,4.2). We note that the use of perturbative fragmentation function has a stronger impact on the x_b distribution. Moreover, the full inclusion of powers of $\frac{m_b}{m_t}$ has a negligible effect on the x_b spectrum; the dot-dashed and dotted lines in Fig.4.4 are indistinguishable. As for the perturbative fragmentation results, the distribution without soft gluon resummation shows a very sharp peak at $x_b \to 1$. This behavior is smoothed out when we resum the soft NLL logarithms in the initial condition of the perturbative fragmentation function, as the b-energy spectrum gets softer and shows the so-called 'Sudakov peak'.

For $x_b \to 0$, the coefficient function(3.40) contains large logarithms $\sim \alpha_s \log x_b$ which have not been resummed yet. Although, in the soft limit $x_b \to 1$, Eq.(3.40) contains contributions of soft LL and NLL as well. Since $\alpha_s(m_b) \approx 2\alpha_s(m_t)$, for $\mu = m_t$ and $\mu_0 = m_b$ such terms are smaller than the similar ones which appear in the initial condition of the perturbative fragmentation function, but nonetheless they would need to be resummed. As explained in [43], once x_b approaches unity, non-perturbative contributions also become important and have to be taken into account.

4.8 B-Hadron Production in Top Quark Decay

In this section we present results for the energy distribution of b-flavored hadrons B as a function of the normalized energy fraction taken away by the B-hadron in top decay. This kinematic variable is defined as: $x_B = \frac{2E_B}{m_t(1-\omega)}$. In this work we consider the transition $b \to B$, where B is either a meson like $B^-(b\overline{u})$ and $B^0(b\overline{d})$ or a baryon containing a b-quark. Our results are not valid for production of meson $B^+(u\overline{b})$, because the meson B^+ will be created in NNLO. Of course, the B^+ meson can be created by the anti-top in the same way as the B^- from top decay.

4.8.1 Non-perturbative Fragmentation

According to the factorization formula (2.18), the cross section of inclusive B-hadron production in top decay

$$t \to b + W^+(g) \to B + X,$$

can be expressed as the convolution of the parton level spectrum with the non-perturbative fragmentation function $D^B(x_B, \mu_F)$, i.e.

$$\frac{1}{\Gamma_0}\frac{d\Gamma}{dx_B}(x_B, m_t, m_W, m_b) = \frac{1}{\Gamma_0}\sum_a \int_{x_{a,min}}^{x_{a,max}} \frac{dx_a}{x_a}\frac{d\Gamma_a}{dx_a}(x_a, m_t, m_W, m_b, \mu, \mu_F) D_a^B(\frac{x_B}{x_a}, \mu_F). \tag{4.42}$$

In the equation above, a stands for the partons b, g and $\frac{1}{\Gamma_0}\frac{d\Gamma_a}{dx_a}$ is the parton-level differential width and D_a^B is the non-perturbative fragmentation function describing the hadronization $a \to B$, which is process independent. As it was generally explained in section 2.3.1, we can extract it from one specific process such as $e^-e^+ \to b\bar{b}$ processes and use it in the b-quark

hadronization in top decay. In order to be applicable fits results to the b-hadronization in top decay, we have to describe the perturbative process $e^-e^+ \to b\overline{b}(g)$ in the same framework as done for $t \to bW(g)$. The factorization scale μ_F is an arbitrary scale that separates the low from the high energy dynamics and like before we set $\mu = \mu_F$.
In fact, the factorization on the right hand side of Eq.(4.42) and the splitting between perturbative and non-perturbative part is somewhat arbitrary and the parameterization of the non-perturbative model indeed depends on the approach which is used to describe the perturbative parton level process and on the values which are chosen for quantities like Λ, m_b and the renormalization and factorization scales. Therefore the partonic decay width $d\Gamma$ is not finite and it is usually defined with a prescription for the subtraction of collinear singularities, like the $\overline{MS}$ prescription that we already used. Also $D_B(x_B, \mu_F)$ is prescription dependent, but the convolution of two terms in Eq.(4.42) is not, so that the physical cross section is scheme independent.
To achieve $D(x_B/z, \mu_F)$ (FF at an arbitrary scale μ_F), we have to solve the DGLAP evolution equations (see Eqs.(2.27,2.28)):

$$\frac{d}{d\log\mu_F^2} D_i(x_B, \mu_F, m_b) = \sum_j \int_{x_B}^1 \frac{dz}{z} P_{ij}\big(\frac{x_B}{z}, \alpha_s(\mu_F)\big) D_j(z, \mu_F, m_b). \tag{4.43}$$

To solve the above equation, we need the function $D(x, \mu_{0F})$ as the initial condition of non-pFF at $\mu = \mu_{0F}$. The solution of Eq.(4.43) has then a power expansion in terms of $\alpha_s(\mu_F)$ which organize correctly all the powers of $\log(\frac{\mu_F}{\mu_{0F}})$ arising in perturbative theory.
The DGLAP equation is however not valid when x_b is small, since due to soft gluon emission the $P_{ij}(x_b, \alpha_s(\mu_F))$ contain terms which behave in the limit $x_b \to 0$ like $(\alpha_S^n/x_b)\log^{2n-1-m} x_b$, where $m = 1, 2, ..., 2n-1$ labels the class of terms, and are therefore unreliable in this limit. This implies that the cross section can not be reliably calculated at small x_B, and the FFs $D_j(z, \mu_0)$ can not be fitted at small x_B.
Several models have been proposed to describe the non-perturbative transition from a quark into a hadron state. These models are suited to determine initial condition (at the starting scale $\mu_{0F} = \mu_0$) of non-pFFs at the DGLAP evolution and in this work we apply them to specify the initial condition of FFs in transition of $b \to B$ and $g \to B$. In the following we explain the most commonly used.

- **The Standard model (S)**[44, 45, 49, 50] consists of a simple power functional form:

$$D(x; \mu_0, \alpha, \beta) \;=\; N x^\alpha (1-x)^\beta, \tag{4.44}$$

with

$$\frac{1}{N} = \frac{1}{B(\mu_F)} \int_{x_{cut}}^{1} (1-x)^{\beta} x^{\alpha} dx. \tag{4.45}$$

The cut x_{cut} excludes the x range where our formalism is not valid and $B(\mu_F)$ is the $b \to B$ branching ratio, we shall explain this cut in more detail later. This form is usually adopted for the FF's of light hadrons. This model has been used in [44, 83] to describe the non-perturbative effects of b-quark fragmentation.

- **The Peterson model (P)**[84] describes the non-perturbative transition of a heavy quark into a heavy hadron according to the following function:

$$D(x, \mu_0, \epsilon) \quad = \quad N \frac{x(1-x)^2}{[(1-x)^2 + \epsilon x]^2}. \tag{4.46}$$

The Peterson form is particularly suitable to describe FFs that peak at large x. It has been used in connection with the fragmentation of heavy quarks, such as c or b quarks into their mesons. It depends only on two parameters N and ϵ.

The coefficients (N, α, β) or (N, ϵ) in the mentioned models should be specified experimentally. They will be investigated later and we shall use these models in our calculation and we also present comparisons with NLO results obtained in two models.

4.8.2 Approaches for NLO Calculations: ZM- and GM-VFNS

In order to calculate the B-hadron production cross section, we need a theoretical framework. The QCD-improved parton model implemented in the $\overline{MS}$ renormalization and factorization scheme is a nice framework. In this framework, three distinct approaches for NLO calculations in perturbative QCD are being used. In the following we explain them in detail.

- **The Massive Scheme** or fixed-flavor-number-scheme (**FFNS**) [71].
  As already mentioned, in the heavy-quark production in high-energetic collisions, because of being small the strong coupling constant ($\alpha_S \ll 1$) the heavy quark production process is considered as a calculable process in perturbative QCD. The mass of the heavy quark acts as a cutoff for the initial- and final state collinear singularities and sets the scale for the perturbative calculations. On this basis, most

of the next-to-leading order QCD calculations have been performed in the past. This approach where the mass of heavy quark m is kept and the number of active flavors (n_f)in the initial state is fixed to $n_f = 3(4)$ for charm(bottom) production is called the FFNS. In this approach the predictions are only reliable in the small region of the transverse momentum p_t of the produced heavy quark in $\gamma\gamma$, γp and $p\overline{p}$ reactions (from $p_t = 0$ to $p_t \geq m$) or when the lepton momentum transfer Q in deep inelastic ep scattering is not much larger than the mass of the heavy quark. However, when p_t(or Q) is much larger than the heavy quark mass, logarithms of the form $\log(\frac{p_t^2}{m^2})$ or $\log(\frac{Q^2}{m^2})$ become large and spoil the convergence of the perturbation series, thus the fixed-order perturbation theory is no longer valid, specially in our case where $Q = m_t \approx 180\text{GeV}$ and $m = m_b \approx 4.5\text{GeV}$. These logarithms can be resummed and the perturbation series can be improved. The resummation of hinted large logarithms is similar to the conventional massless parton model approach which is explained in the following.

- **The Massless Scheme** or zero-mass variable-flavor-number-scheme (**ZM-VFNS**) [48, 72, 75], which is the conventional parton model approach. In the conventional ZM-VFNS calculation, one starts with heavy quark mass $m = 0$ from the beginning, except in the initial conditions for the FFs. Therefore there are no large logarithms $\log \frac{Q^2}{m^2}$ in the partonic differential decay width, for example $\log \frac{m_b^2}{m_t^2}$ in Eqs(3.40,3.47). Since m only enters via the definition of the starting scale μ_0 for the FFs of partons, its precise value is unimportant.

  In this method the collinear singularities are treated with dimensional regularization and they are factorized into the FFs according to the $\overline{MS}$ scheme, as it is usually done in connection with the fragmentation of light quarks into light mesons. In this approach the predictions are reliable only in the region of large transverse momenta, with $p_t \gg m$, or in the large energy Q, with $Q \gg m$. In fact the necessary condition to use the ZM-VFNS is that the energy scale, separating perturbative hard scattering and non-perturbative fragmentation, should be sufficiently large in comparison with the heavy-quark mass. In our work this condition is satisfied.

  In order to be consistent at NLO in Eqs.(3.40,3.47), α_s has to be taken at NLO as Eq.(2.15). In our calculation we adopt the NLO value $\Lambda_{\overline{MS}}^{(5)} = 227$ MeV appropriate for $n_f = 5$, which corresponds to $\alpha_s^{(5)}(m_t) = 0.1071$, i.e this corresponds to

$\alpha_s^{(5)}(m_Z) = 0.1181$.

The partonic cross section calculated in the FFNS (in presence of the mass of heavy quark) in the limit $m \to 0$ is not equal to the corresponding ZM-VFNS cross section, even if the collinear singular terms proportional to $\log(\frac{m^2}{Q^2})$ are subtracted from the obtained FFNS cross section, this point was mentioned in section 4.4. In [42], it was shown that these additional finite terms can be generated in the theory for $m = 0$ with $\overline{MS}$ factorization by convoluting massless cross section with a partonic fragmentation function $d_{Q\to Q}(x, \mu)$. This point was shown in section 4.7 for the special transition $b \to b$.

In [77] for the process $gg \to Q\overline{Q}g$ and $gq \to Q\overline{Q}g$, in [41, 78] for the process $\gamma^\star Q \to Qg($ where $\gamma^\star$ is a space-like virtual photon) and also in [79] for the process $\gamma\gamma \to Q\overline{Q}g$ it has been shown that the finite terms are obtained from a convolution of the corresponding LO cross section with $d_{Q\to Q}(x, \mu)$ and it is has also been confirmed the universality of the partonic FF. The point referred above leads us to apply another approach which is so-called GM-VFNS.

- **The GM-VFNS** or general-mass variable-flavor-number-scheme [76, 77, 79, 80, 81] is much closer to the ZM-VFNS, but keeps all m^2/Q^2 or m^2/p_t^2 power terms in the hard-scattering cross sections. These terms are important in the region of intermediate p_T values, $p_T \geq m$, and we expect these terms to improve our theoretical predictions which were computed in the ZM-VFNS. In this approach we calculate partonic differential decay rate ($d\tilde{\sigma}$) considering the mass of heavy quark. To have a result consistent with massless decay width we subtract the extra finite terms, as explained before, from the obtained massive width. Therefore the desired massive differential width is $d\tilde{\sigma} - d\sigma^{Sub}$ which has to be convoluted with non-pFF in the factorization formula. In our work $d\tilde{\sigma}_b$ and $d\tilde{\sigma}_g$ are given in Eqs.(4.26,4.32) and the convenient subtraction terms can be found in Eqs.(4.30,4.33).

  To evaluate the B-hadron production differential width in GM-VFNS, the b-quark is considered as a heavy quark with mass m_b and the group of light quarks consists of u, d, s, c whose mass is put to zero. Furthermore, the number of active flavors are taken $n_f = 5$ in the strong coupling constant and the DGLAP evolution equations and we need FFs implemented with $n_f = 5$ in the $\overline{MS}$ factorization scheme.

In both approaches mentioned above the notion VFNS was used since the number of active flavors (n_f) depends on the scale which we are using. In our approach, n_f at the scale μ_F is specified by a condition on the value of μ_F. It means that if $\mu_F \leq m_{f+1}$, where f counts the quarks u, d, s, c and b respectively, then the number of active flavors will be $n_f = f$. The transition scales (thresholds) in the evolution equation (4.43) depend on n_f and are taken to be at m_{n_f+1}. In the VFNS the number of active quark flavor is increased by one unit, $n_f \to n_f + 1$, when the factorization scale crosses the transition scale.

In the next section we intend to make some theoretical predictions at the hadron level for top quark decay. Before discussing this subject let us explain the integration bounds in the factorization formula (Eq.(4.42)). Here we consider two cases: the first case is to consider the massive b-quark hadronizing into a bottom-hadron and the other one is hadronization of the massless b-quark into a bottom-hadron. These processes are subjected in ZM- and GM-VFNS.
In the GM scheme, the bounds of integration in x_a [$x_a = 2E_a/(m_t(1+b-\omega))$, $a = b, g$] and x_B [$x_B = 2E_B/(m_t(1+b-\omega))$] now depend on the partonic subprocess and on the fragmenting parton a. In the case of b-quark fragmentation, by defining $\rho_b = 4m_b^2/m_t^2(1+b-\omega)^2$, we have $x_{b,min} = max(x_B, \sqrt{\rho_b}), x_{b,max} = 1$ and $\sqrt{\rho_B} \leq x_B \leq 1$, where $\rho_B = 4m_B^2/m_t^2(1+b-\omega)^2$. In the case of gluon fragmentation we have $x_{g,min} = x_B, x_{g,max} = \beta^2$ and $\sqrt{\rho_B} \leq x_B \leq \beta^2$ with $\beta = \sqrt{1-\rho_b}$.
In the ZM scheme where there are massless partons in the final state ($m_g = m_b = 0$), we have both for the gluon and the b-quark fragmentation $x_{b,min} = x_{g,min} = x_B, \quad x_{b,max} = x_{g,max} = 1$, where $x_a (a = b, g)$ is now $2E_a/m_t(1-\omega)$ and for the variable x_B, which is now $x_B = 2E_B/m_t(1-\omega)$, we have $\sqrt{\rho_B(b=0)} \leq x_B \leq 1$.

4.8.3 Theoretical Predictions at Hadron-level for $t \to B + X$

In this section, at first we numerically analyze the ZM-VFNS predictions. In this approach, we describe the fragmentation of massless b quarks into B mesons by a one-step process characterized in terms of a non-perturbative FF, as is usually done for the fragmentation of u, d and s quarks into light mesons. Afterward we apply GM-VFNS to make predictions of B-hadron production and then we compare the results obtained in both schemes.

To predict the b-quark hadronization properties, we have to specify the coefficients (N, α, β) and (N, ϵ) in Eqs.(4.44,4.46), describing the transition of the b-quark and the

Set			
LO Standard	NLO Standard	LO Peterson	NLO Peterson
N=56.4	N=79.4	N=0.0952	N=0.116
$\alpha = 8.39$	$\alpha = 8.06$	$\epsilon = 0.0126$	$\epsilon = 0.0198$
$\beta = 1.16$	$\beta = 1.45$		

Table 4.1: Fit parameters for the $b \to B$ fragmentation functions according to sets S, P at LO and NLO. All other FFs are taken to be zero at the starting scale $\mu_0 = 2m_b = 10$ GeV.

gluon into a B-hadron. These coefficients are usually determined by fitting the fractional energy distribution of B mesons inclusively produced in e^-e^+ annihilation.

In the literature one can find different methods to extract these coefficients from experimental data. In this work we only use the extracted data for non-pFFs. At first we apply the results of the non-pFFs given in [72]. The authors provide non-perturbative FFs, both at leading and next-to-leading order in $\overline{MS}$ factorization scheme with five massless quark flavors. They are determined by fitting the fractional energy distribution of B-mesons in e^-e^+ collision reported by the OPAL collaboration at CERN LEP1 [82]. They considered the OPAL data on the inclusive production of B^+/B^0 mesons in e^-e^+ annihilation($e^-e^+ \to \gamma, Z \to B^+/B^0 + X$) at the Z-boson resonance as an experimental input with assumption $\mu = \mu_F = m_Z = 91.2GeV$. At LEP1, B mesons were dominantly produced by $Z \to b\overline{b}$ decays, with subsequent fragmentation of the b quarks and anti quarks into B mesons, which decay weakly. The produced B^+ and B^0 mesons were identified via their semileptonic decays containing a fully reconstructed charmed meson. In [72] the starting scales for the FFs of the gluon and the u, d, s, c and b quarks and anti-quarks into B mesons are taken to be $\mu_0 = 2m_b$, with $m_b = 5GeV$. They adopt the LO (NLO) value $\Lambda^{(5)}_{\overline{MS}} = 108$ MeV (227 MeV) in presence of five active quark flavors in their calculations. The FFs of the gluon and the first four quark flavors are assumed to be zero at the starting scale. These FFs are generated through the DGLAP evolution to larger values of μ_F.

In Fig.4.5, from [72], the authors showed that there was a good consistency between the experimental data from the OPAL collaboration and the FFs which they proposed for two different models. The values for the input parameters in Eqs(4.44,4.46) resulting from their LO and NLO fits to the OPAL data are summarized in table.4.1.

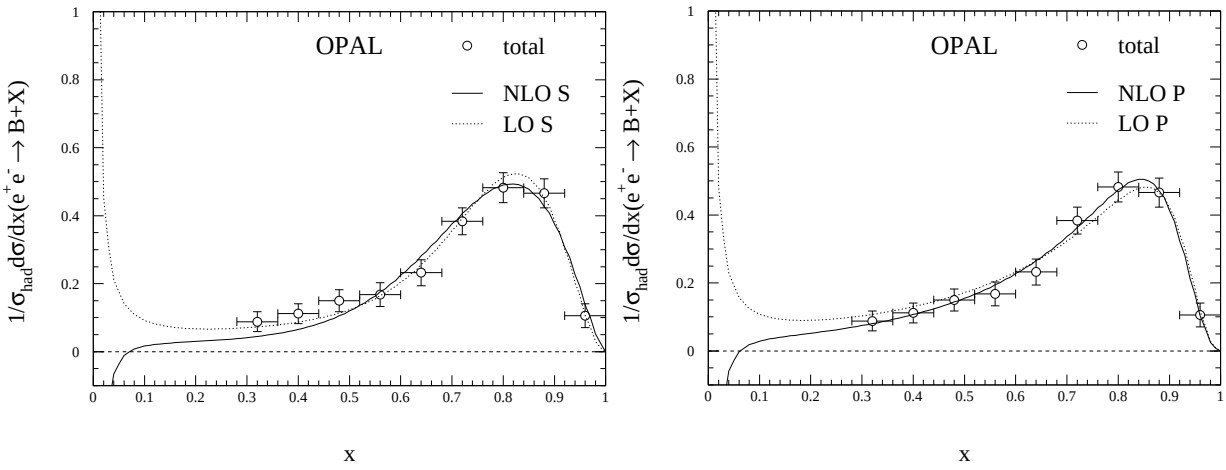

Figure 4.5: The cross section of inclusive B^+/B^--meson production in e^+e^- annihilation at $\mu = M_Z = 91.2$ GeV evaluated with sets LO and NLO Standard ansatz (left hand side), and LO and NLO Peterson ansatz (right hand side), compared with the OPAL data.

Now we apply these parameters in the Peterson and Standard models for our calculation and we depict the B-meson energy distribution, resulting from hadronization of the b-quark and the gluon in the top decay, in x_B and compare the two models. To determine the active flavor number and thresholds we take $m_c = 1.5$ GeV and $m_b = 5.0$ GeV and light quarks to be massless. We choose the renormalization and factorization scales to be $\mu = \mu_F = m_t = 174.0$ GeV in Eqs(3.40,3.46,4.43).

In Fig.4.6 we depict the differential decay rate of inclusive B-meson production in top decay at $\sqrt{s} = m_t$ using the Peterson model. It shows the contributions of the b-quark (dots) and the gluon (dashes) fragmentation into the B-meson in the top decay. We also presented the contribution of both fragmentations (solid line) to the differential decay rate of B-meson production. In this figure our results loose their physical validity at low x_B. In this region, the perturbative treatment is no longer valid. Here, the massless approximation also is not valid. Since B mesons have mass, $m(B) = 5.28$ GeV, they can only be produced for $x_B > x_{min} = \frac{2m_t m_B}{m_t^2 - m_W^2} = 0.07$. Thus, our results should only be considered to be meaningful for $x_B > 0.07$.

In Fig.4.7 we compare the total contributions obtained for the B-meson energy distribution in the variable x_B from the Peterson and the Standard models. As shown, at large x_B the results are approximately the same and there is good agreement between the prediction

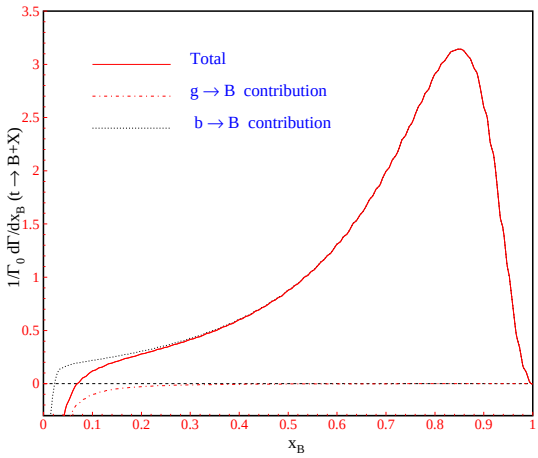

Figure 4.6: x_B spectrum in top decay, with the hadronization modeled according to the Peterson model, with the relevant parameters fitted to the OPAL data. The plotted curves are the contribution of the fragmentation of gluon to B(dot-dashes), the contribution of b fragmentation to the B-meson(dots) and the total contribution to B production(solid line). We set $\mu_F = \mu = m_t$ and $\mu_{0F} = \mu_0 = 2m_b$.

of both models. In our calculation we considered both the contribution of the b-quark fragmentation and the gluon fragmentation to the x_B spectrum, although the contribution of gluon fragmentation , which only enters at NLO, is really negligible. This is shown in Fig.4.6. To study this point in more detail we also investigate the fragmentation functions distribution in x_B. In Fig.4.8, we compare the non-perturbative fragmentation functions of $b \to B$ and $g \to B$ at NLO using the Peterson model fitted to the OPAL data. It is clear that the main contribution of hadronization in the top quark decay is due to the hadronization of the b-quark at NLO.

It is interesting to study the $b \to B$ branching fraction ($\frac{\Gamma(b\to B)}{\Gamma(b\to Hadron)}$), which was already referred in Eq.(4.45). It is defined as:

$$B_b(\mu) = \int_{x_{cut}}^{1} dx D_b(x,\mu), \tag{4.47}$$

where x_{cut} in our work is $x_{cut} = 0.07$.
In table 4.2, we present the value of $B_b(\mu)$ at the threshold $\mu = 2m_b = 10$ GeV and at $\mu = m_t = 174.0$ GeV for the various FF sets. As shown, $B_b(\mu)$ is rather constant under the evolution from $2m_b$ to m_t.

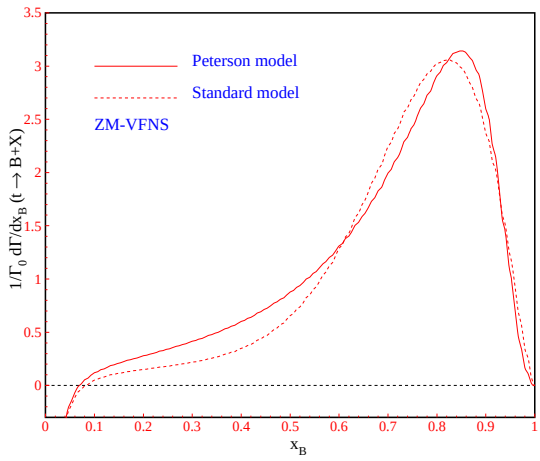

Figure 4.7: Comparison of the Standard and Peterson models in x_B distribution in top quark decay, with the relevant parameters fitted to the OPAL data. The initial factorization scale is like in Fig.4.6.

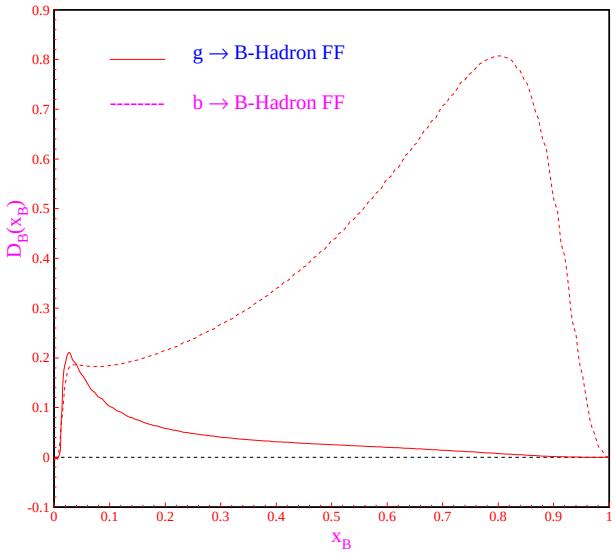

Figure 4.8: Comparison of the non-perturbative fragmentation functions of $b \to B$ and $g \to B$ in the Peterson model fitted to the OPAL data using $\mu_{0F} = 2m_b = 10$ GeV.

Set	$B_b(2m_b)$	$B_b(m_Z)$	$B_b(m_t)$	$\langle x\rangle_b(2m_b)$	$\langle x\rangle_b(m_Z)$	$\langle x\rangle_b(m_t)$
NLO S	0.3836	0.3759	0.3740	0.787	0.663	0.638
NLO P	0.4059	0.3960	0.3937	0.756	0.639	0.615

Table 4.2: $b \to B$ branching fractions and mean B to b momentum fractions evaluated from Eqs.(4.47,4.48) ,respectively, at the starting and the $\mu_F = m_t$ scale using the various FF sets.

Another interesting quantity is the mean B to b momentum fraction,

$$\langle x\rangle_b(\mu) = \frac{1}{B_b(\mu)} \int_{x_{cut}}^{1} dx x D_b(x,\mu). \tag{4.48}$$

Table 4.2 also includes the values of $\langle x\rangle_b(\mu)$ at $\mu = 2m_b = 10$ GeV and $\mu = m_t = 174.0$ GeV evaluated with the various FF sets. As seen, the differences between S and P models in every given scale are negligible. As μ runs from $2m_b$ to m_t, $\langle x\rangle_b(\mu)$ decreases from approximately 0.7 to about 0.6. This shows the μ evolution softens the FFs. These results can be compared with the OPAL experimental result which reads $B_b(m_Z) = 0.405 \pm 0.035(stat) \pm 0.045(syst)$ [73] and $\langle x\rangle_b(m_Z) = 0.695 \pm 0.006(stat) \pm 0.003(syst) \pm 0.007(model)$ [74].

Up to now we were working in the Zero-Mass Variable-Flavor-Number-Scheme, where we started with $m_b = 0$. It is interesting to know the difference between the effects of massless and massive b-quarks in the top quark decay. From now on we use the GM-VFNS in our calculation where the b-quark is considered to be a massive particle. In Fig.4.9, we compare the Peterson and the Standard models for non-perturbative part of top hadronization. This graph can be compared with Fig.4.7 in which the b-quark was a massless quark. This is done in Fig.4.10 where we compare the effects of the b-quark mass in every model. In Fig.4.10, it is seen that in the massless b-quark case, the maximum value of the top quark decay width is about $0.04(bin^{-1})$ higher than the one where the b-quark is considered to be a massive particle. We have to keep in mind that for $x_B < 0.07$ our result is not meaningful. In the left side of Fig.4.10, we compared the x_B distribution in top quark decay both when the b-quark is considered to be a massless particle from the beginning and when it is considered to be a massive one within the Standard hadronization model. In the right hand side of Fig.4.10 the same has been done but using the Peterson model. It is seen that for large values of x_B ($x_B \geq 0.8$), the value of the b-quark mass is immaterial and the results coincide. For the obtained results we used the Peterson and

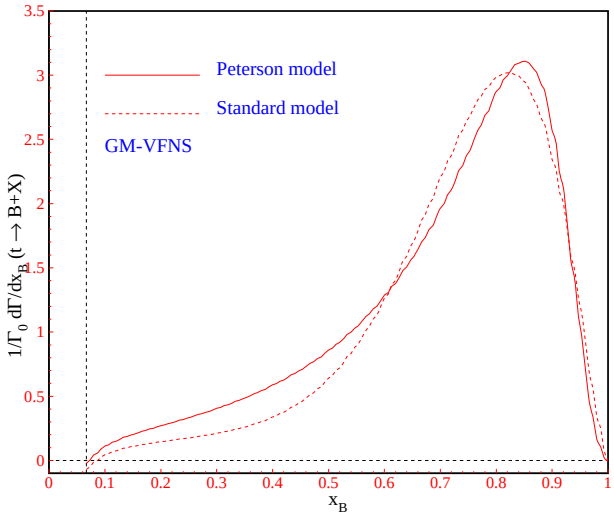

Figure 4.9: Comparison of the Standard and Peterson model in x_B distribution in top quark decay, with the NLO fits using OPAL data with this assumption that b is a massive quark from the beginning and $\mu_{0F} = 2m_b = 10$ GeV.

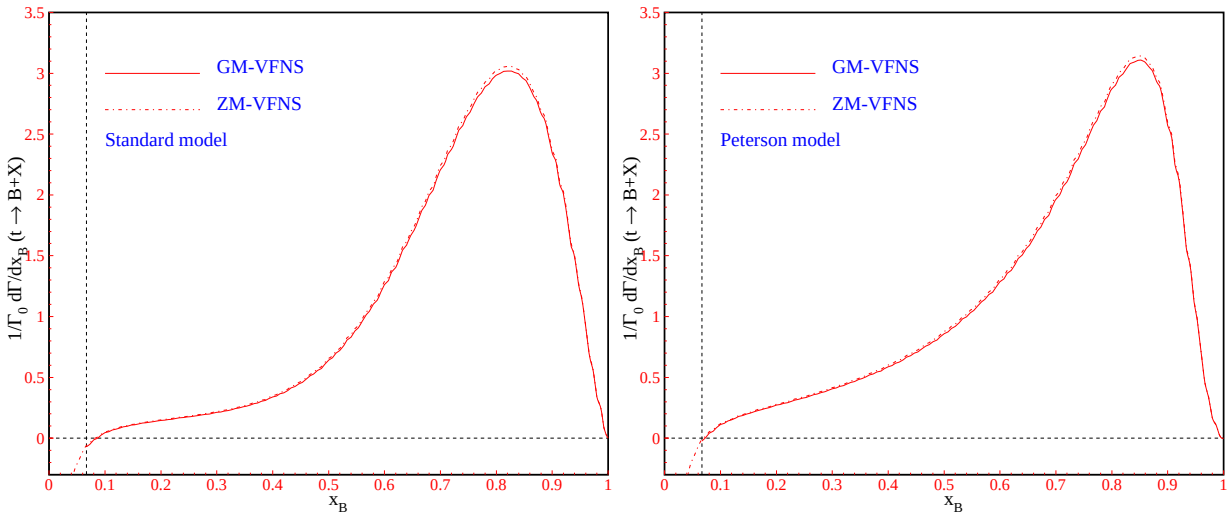

Figure 4.10: Left side: x_B spectrum in top quark decay for the massive (solid line) and massless (dot-dashes) b quarks using the S model for the non-perturbative part.
Right side: x_B spectrum in top quark decay for the massive (solid line) and massless (dot-dashes) b quarks using the P model for the non-perturbative part. In both calculations the initial factorization scale is: $\mu_0 = 10$ GeV.

Standard models extracted in [72]. They showed that the Peterson model yields the best fits using $\mu_0 = 2m_b$ with $m_b = 5$ GeV. This was done by comparison to the Opal experimental data in e^-e^+ annihilation at $\mu_F = \sqrt{s} = m_Z$ with the theoretical predictions.
When new and more precise measurements of the cross section of inclusive B-meson production in e^-e^+ annihilation on the Z-boson resonance have been performed by the ALEPH [64], OPAL [65] and SLD [66] collaborations, the authors in [85] performed a combined fit to these data sets [64, 65, 66] using $\mu_0 = m_b$ with $m_b = 4.5$ GeV. They also adopted the NLO value $\Lambda^{(5)}_{\overline{MS}} = 227$ MeV appropriate for $n_f = 5$. In Fig.4.11, from [85], the authors showed that there was a good consistency between the experimental data from the OPAL, SLD and ALEPH collaborations and the FFs which they proposed for the Standard(Power) ansatz. Table 4.3 contains the new values of the parameters in Eqs.(4.44) and (4.46) obtained through the fits based on the Peterson and Standard ansaetze from [85]. From now on we use these parameters in the P and S models.

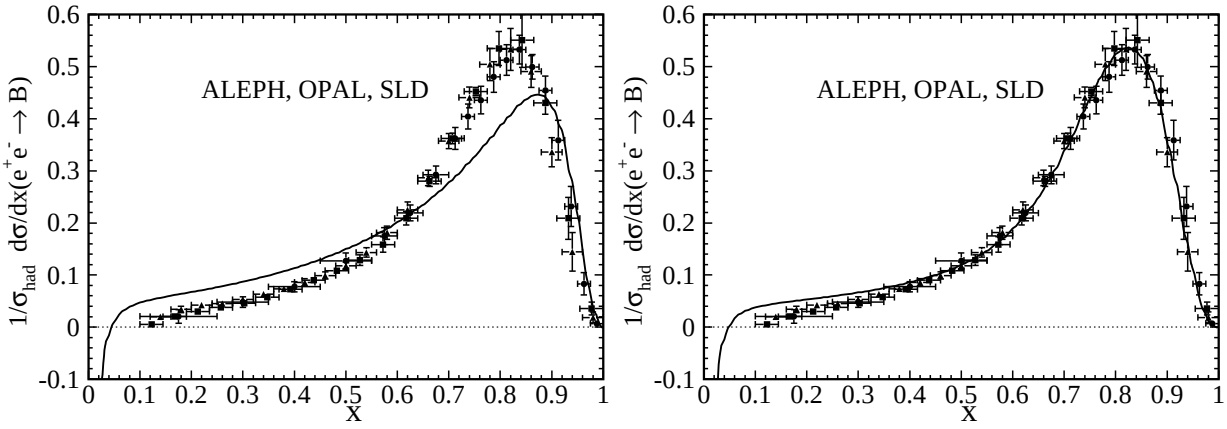

Figure 4.11: Comparisons of the ALEPH (circles), OPAL (squares), and SLD (triangles) data with the NLO fits using the Peterson ansatz (left side) and the Power (Standard) ansatz (right side). The initial factorization scale for all partons is $\mu_0 = m_b = 4.5$ GeV.

While we shift the starting scale from $\mu_0 = 2m_b$ (with $m_b = 5$ GeV) to $\mu_0 = m_b$ (with $m_b = 4.5$ GeV), the gluon and b-quark FFs are smoothed out at $\mu_F = m_t = 174.0$ GeV. This can be seen in Fig.4.12 where the FFs of gluon and b-quark to the B-meson are compared in the different initial scales. In [85], it was shown that the Standard ansatz yields an excellent overall fit to the experimental data points obtained from ALEPH, OPAL and SLD. On the other hand, the Peterson model leads to an incongruous description of

Set	
NLO Standard	NLO Peterson
N=4684.1	N=0.06634
$\alpha = 16.87$	$\epsilon = 0.008548$
$\beta = 2.628$	—

Table 4.3: Fit parameters for the $b \to B$ fragmentation functions according to the sets S, P at the starting scale $\mu_0 = m_b = 4.5$ GeV. All other FFs are taken to be zero at the starting scale, $\mu_0 = 4.5$ GeV, and are generated through the DGLAP evolution.

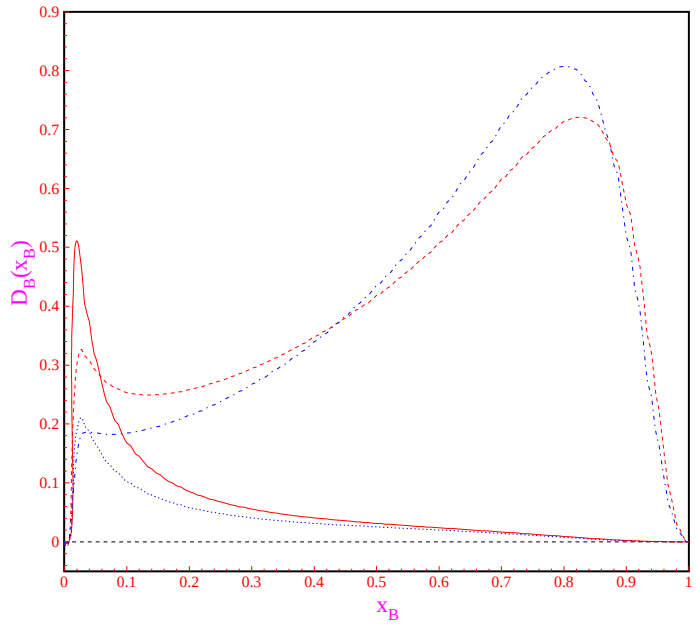

Figure 4.12: Non-perturbative FFs of $b \to B$ (dot-dashes) and $g \to B$ (dots) with initial scale $\mu_0 = 10$ GeV and FFs of $b \to B$ (dashes) and $g \to B$ (solid lines) with initial scale $\mu_0 = 4.5$ GeV. Both are calculated in the Peterson model at $\mu_F = m_t = 174.00$ GeV.

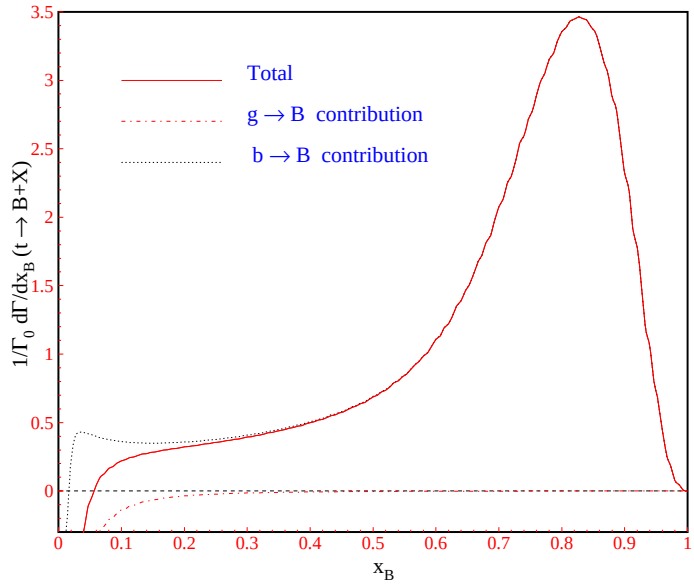

Figure 4.13: x_B spectrum in top decay, with the hadronization modeled according to the Power (Standard) model, with the relevant parameters fitted to the ALEPH, OPAL and SLD data. The plotted curves are the contribution of the fragmentation of gluon to B(dot-dashes), the contribution of b fragmentation to the B-meson(dots) and the total contribution to B production(solid line). We set $\mu_F = \mu = m_t$ and $\mu_{0F} = \mu_0 = m_b = 4.5\text{GeV}$.

the data. This ansatz has only two free parameters, N and ϵ, and is just not flexible enough to account for the very precise experimental data.
In Fig.4.13, using the power (Standard) model with the new fit parameters presented in table 4.3, the contributions of the b-quark fragmentation and the gluon fragmentation to the x_B spectrum are shown. In next step by using new S and P models we depict the B-meson energy distribution in x_B. We compare the two models when the b-quark is considered to be a massless particle and in the next step we consider a massive b-quark in our calculation and compare the results obtained from both ansaetze. In our calculation we assume $m_c = 1.5$ GeV and $m_b = 4.5$ GeV and the factorization and renormalization scale is $\mu = \mu_F = m_t = 174.0$ GeV in Eq(4.43).

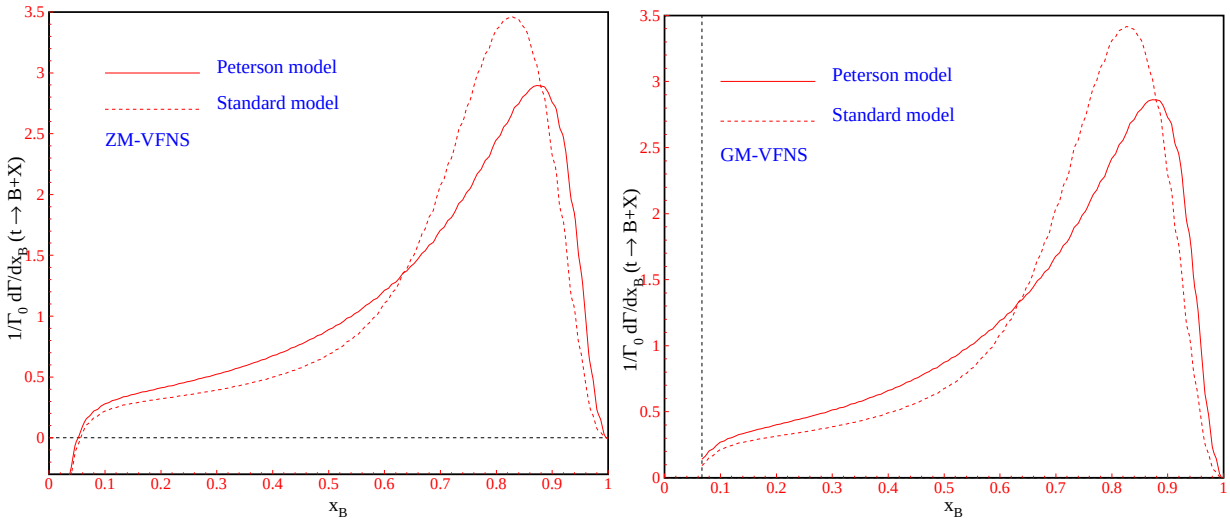

Figure 4.14: Left side: Comparison of the Standard and Peterson models in x_B distribution in top quark decay with the NLO fits . The initial factorization scale is $\mu_0 = 4.5$ GeV and the b-quark is considered to be massless.
Right side: As Figure in the left side but the b-quark is considered to be massive.

In Fig.4.14 we compare the P and S models using the ZM-VFNS and GM-VFNS. As before our result are not valid for $x_B < 0.07$. Comparing Figs(4.7,4.9,4.14), it is seen that when the initial scale μ_0 is changed from 4.5 GeV to 10 GeV a considerable difference exists between the Standard and Peterson models, especially at large x_B. Although these models depend on the experimental data which we use to fit and the different data can

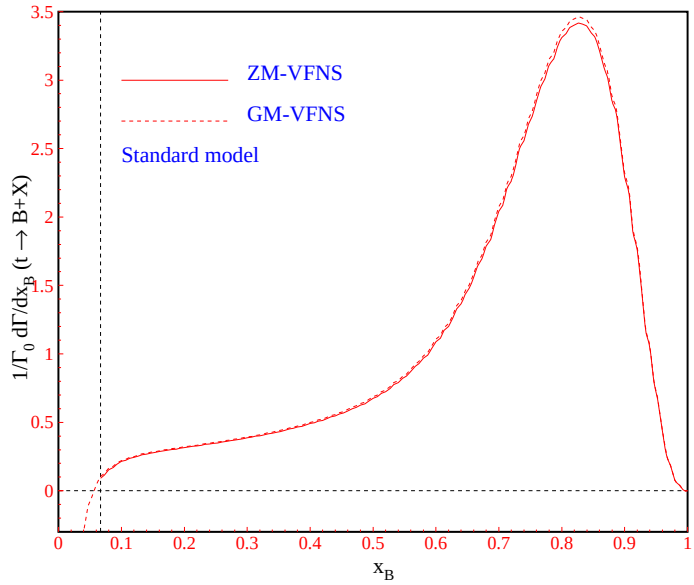

Figure 4.15: Comparison ZM-VFNS and GM-VFNS approaches in x_B distribution in top quark decay using the Standard model. The initial factorization scale is $\mu_0 = m_b = 4.5$ GeV.

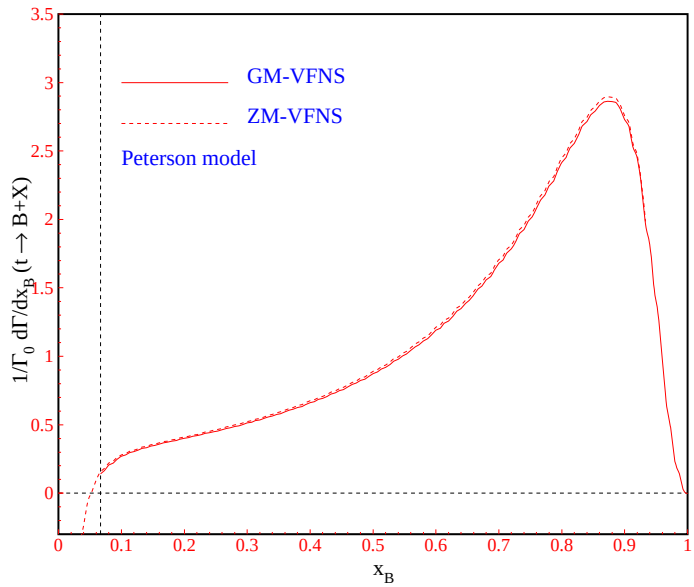

Figure 4.16: As Fig.4.15, using the Peterson model. The initial factorization scale is $\mu_0 = m_b = 4.5$ GeV.

Set	$B_b(m_b)$	$B_b(m_t)$	$\langle x\rangle_b(m_b)$	$\langle x\rangle_b(m_t)$
NLO S	0.40027	0.3870	0.8312	0.617
NLO P	0.40017	0.3848	0.8085	0.603

Table 4.4: branching fractions $B(\mu_F)$ and mean B to b momentum fractions evaluated from Eqs.(4.47,4.48), at the scales $\mu_{0F} = m_b = 4.5$ GeV and $\mu_F = m_t = 174.0$ GeV scales using the various FF sets.

change our fit parameters in models.
In Figs(4.15,4.16) we compare the ZM-VFNS and the GM-VFNS approaches using the Standard and Peterson models for non-perturbative part of B-hadron production in top quark decay, respectively.
As before, it is interesting to study the $b \to B$ branching fraction ($B_b(\mu_F)$) and also the average energy fraction that the B meson receives from the b quark($\langle x\rangle(\mu_F)$), Eqs.(4.47,4.48) respectively. The results are listed in table 4.4. We observe that the Peterson and Standard ansaetze have rather similar results for ($B_b(\mu_F)$) and ($\langle x\rangle(\mu_F)$). The results for the standard model are larger in all scales. When $B_b(\mu_F)$ is practically independent of μ_F, $\langle x\rangle(\mu_F)$ is being smaller through the evolution in μ_F. These results can be compared with the values quoted by ALEPH, OPAL, and SLD, which read $\langle x\rangle_b(m_Z) = 0.7361 \pm 0.0061(stat) \pm 0.0056(syst)$ [64], $0.7193 \pm 0.0016(stat)^{+0.0036}_{-0.0031}(syst)$ [65], and $0.709 \pm 0.003(stat) \pm 0.003(syst) \pm 0.002(model)$ [66], respectively. Of course we have to pay attention to this point that experimental results includes all orders and also contributions from light quarks fragmentation, while ours are evaluated from the $b \to B$ and $g \to B$ FFs at NLO.

Our predictions for the differential decay rate of the B-hadron production in the top quark decay can be compared with the results obtained in [51]. There, to determine the coefficients in the Standard and Peterson models, authors used ALEPH and SLD data from e^-e^+ collisions at the Z pole, i.e. $\sqrt{s} = 91.2$ GeV. Both data sets, ALEPH and SLD, refer to weakly-decaying b-hadrons. The ALEPH data just accounts for B mesons, the SLD set data also consider b-flavored baryons, mainly the Λ_b. In their calculation they used $\overline{MS}$ coefficient functions [86] for e^-e^+ annihilation into massless quarks. They also set $\Lambda^{(5)} = 200$ MeV, $\mu_{0F} = \mu_0 = m_b = 5$ GeV and $\mu = m_t = 175$ GeV and presented that the Standard model leads to excellent fits to both ALEPH and SLD data and the Peterson

model is only consistent with the ALEPH results and is unable to describe the SLD data. There is a good consistency between our result and their result.

4.8.4 Theoretical Predictions to Produce $\pi^{\pm}, p/\overline{p}$ and $K^{\pm}$ in Top Quark Decay

Production of pions, kaons, protons and anti-protons is being studied in $e^{-}e^{+}$ annihilations using time of flight techniques. In [88], the authors showed at 30 GeV center of mass energy at least 40 % of $e^{-}e^{+}$ annihilations into hadrons are estimated to contain baryons. Particle identification was made by means of a time of flight (TOF) measurement between the beam crossing signal and two groups of scintillation counters and to provide $\pi - K$ and $(\pi/K) - p$ sepration they use the Inner Time of Flight counters up to a special momentum. To read more detail see [88]. In [89], it is explained that by comparing the data below and above Charm threshold it is possible to determine directly the c-quark contribution to $\pi^{\pm}$ and $K^{\pm}$ production. These measurements serve as a guide to extract the contribution of all quarks to hadron production when a new flavour threshold is crossed.
In this section we intend to make the theoretical predictions to produce the hadrons $\pi^{\pm}, p/\overline{p}$ and $K^{\pm}$ in fragmenting the b-quark obtained in the top quark decay. In the top quark decay both the b-quark can directly fragment into the b-flavored hadrons and the gluon emitted from the b-quark can produce a pair $q\overline{q}$ and this pair can create a light hadron and the light hadrons can also obtain from B-meson and D-meson decay. Since much precise data from $e^{-}e^{+}$ annihilation exists for the production of the three lightest charged hadrons mentioned above we are interested in the fragmentation processes of the b-quark into $\pi^{\pm}, p/\overline{p}$ and $K^{\pm}$ hadrons. In much of the data from $e^{-}e^{+}$ colliders the observed hadron is identified as one of these hadrons and the extraction of the corresponding individual FFs in these processes are the most precise ones. From a combined use of fragmentation and parton distribution functions in one hadron inclusive deep inelastic scattering information on the initial state parton flavor can be obtained from leading particle effects where a light energetic hadron inside a jet remembers the valance parton.
To study the $\pi^{\pm}, p/\overline{p}$ and $K^{\pm}$-hadron productions of the top quark decay we apply the AKK [87] extraction of fragmentation functions for $\pi^{\pm}, p/\overline{p}, K^{\pm}$ particles at next-to-leading order. They presented a parametrization of non-perturbative fragmentation function describing the production of charged pions, kaons and protons from the gluon and from each of the

quarks. They obtained these functions by fitting to all relevant data sets from e^-e^+ annihilation obtained by the OPAL, DELPHI, SLD and ALEPH Collaboration and also using inclusive hadron production data sets from $pp(\overline{p})$ reactions at BRAHMS, CDF, PHENIX and STAR. In [87] the FFs are parameterized at a starting scale $\mu_0 = \sqrt{2}$ GeV in the form:

$$D_i^{h\pm}(x,\mu_0) = N_i^{h^\pm} x^{a_i^{h^\pm}} (1-x)^{b_i^{h^\pm}} (1 + c_i^{h^\pm}(1-x)^{d_i^{h^\pm}}), \tag{4.49}$$

where $h^\pm$ stands for $\pi^\pm, p/\overline{p}, K^\pm$ and i labels the 11 parton species which produce the observed hadron through fragmentation, being the gluon, the quarks $i = u, d, s, c$ and b and their antiquarks. They also imposed the following constraint in the fits:

$$D_{\overline{q}}^{h\pm}(x,\mu_0) = D_q^{h\pm}(x,\mu_0). \tag{4.50}$$

To ensure a continuous gluon FF at each threshold, for simplicity they set the threshold to the heavy quark masses $m_c = 1.65$ GeV and $m_b = 4.85$ GeV.

The values of all fragmentation function parameters are listed in table.4.5. Since these FFs are parametrized at low factorization scale, extraction of the FFs at each arbitrary energy fraction and factorization scale should be performed using the grids and FORTRAN routines based on solving DGLAP equations with the fitted initial condition. In this part to extract the considered FFs at the desired scale we used Fortran routines which can be found at $http://www.desy.de/\tilde{}simon/AKK.html$. These routines can be used to obtain the fragmentation function sets over the range $0.05 < z < 1$ and $\mu_0^2 < \mu_F^2 < 100000 GeV^2$ with $\mu_0 = \sqrt{2}$. In Figs.(4.17,4.18) we plot the differential decay rate of inclusive $\pi^\pm$-, $K^\pm$- and $p/\overline{p}$-mesons production in top decay at $\mu_0 = m_t$. They show the contributions of the b-quark fragmentation (dot-dashes) and the gluon fragmentation (dashes) to the b-flavored hadrons. We also present the contributions of both fragmentations (solid line) to the differential decay rate of hadrons. In Figs.(4.17,4.19) we also plot the contributions of both fragmentations to the differential decay rate of hadrons on a logarithmic scale.

As it is shown in Fig.4.17, if the normalized energy fraction $x_{\pi^\pm}$ is bigger than 0.62 the probability to produce an inclusive $\pi^\pm$-meson in the top quark decay is negligible and this probability takes the big values in small $x_{\pi^\pm}$. In Fig.(4.18) it is seen that the probability to produce an inclusive $K^\pm$-meson and $p/\overline{p}$ is negligible when $x_{K^\pm} > 0.53$ and $x_{p/\overline{p}} > 0.45$, respectively and these probabilities are considerable in the small energy fractions.

In table 4.6, we present the values of the $b \to \pi^\pm, K^\pm, p/\overline{p}$ branching fractions ($B_b(\mu)$) and the mean $\pi^\pm, K^\pm, p/\overline{p}$ to b momentum fractions ($\langle x \rangle_b(\mu)$) at $\mu_F = 10$ GeV and $\mu_F = m_t = 174$ GeV.

Parameter	$\pi^{\pm}$	$K^{\pm}$	$p/\overline{p}$
N_g	247.80	16.11	16155.68
a_g	1.93	2.13	7.26
b_g	6.14	3.28	9.07
c_g	0.96	0.78	2.04
d_g	-0.53	2.26	-0.43
N_u	0.32	1.66	0.49
a_u	-2.07	0.22	-0.05
b_u	0.96	3.55	1.84
c_u	-0.81	0.50	-0.24
d_u	2.91	-1.74	-0.01
N_d	$= N_u$	3.10	0.03
a_d	$= a_u$	-0.29	-2.61
b_d	$= b_u$	6.71	0.69
c_d	$= c_u$	-0.07	-0.91
d_d	$= d_u$	5.52	0.46
N_s	152607.12	0.82	3574.00
a_s	7.34	-0.04	10.57
b_s	12.29	1.62	16.77
c_s	0 (fixed)	1.16	39.06
d_s	0 (fixed)	0.06	-6.55
N_c	0.33	12.06	43.30
a_c	-2.05	0.99	2.35
b_c	2.61	4.77	9.36
c_c	-0.88	5.45	15.04
d_c	2.13	6.52	13.74
N_b	1.25	15.72	6.81
a_b	-0.45	0.96	0.48
b_b	4.37	7.94	11.89
c_b	17.48	21.05	0.43
d_b	10.79	11.38	0.00

Table 4.5: Values of the charge-sign unidentified FFs parameters at $\mu_{0F} = \sqrt{2}$ GeV by fixing $D_d^{\pi^{\pm}}(x, \mu_F^2) = D_u^{\pi^{\pm}}(x, \mu_F^2)$ and $c_s^{\pi^{\pm}} = d_s^{\pi^{\pm}} = 0$.

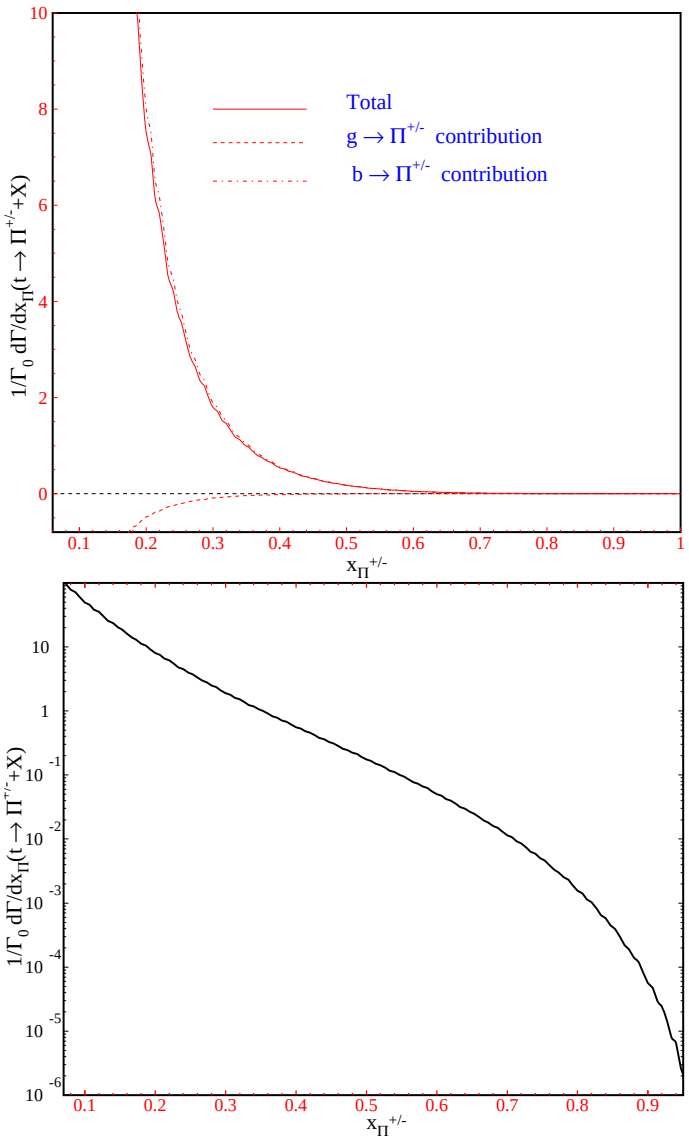

Figure 4.17: Up: $x_{\pi^\pm}$-spectrum of top decay, with the relevant parameters fitted to the OPAL, CDF, PHENIX, BRAHMS and STAR data. The plotted curves are the contributions of the fragmentation of the gluon to $\pi^\pm$ (dashes), b-quark to $\pi^\pm$ (dot-dashes) and the total contribution of them to $\pi^\pm$ (solid line). We set $\mu_F = \mu = m_t$ and $\mu_{0F} = \mu_F = \sqrt{2}$. Down: The total contributions of the fragmenting partons in the $x_{\pi^\pm}$ spectrum of top decay on a logarithmic scale.

Set	$B_b(10GeV)$	$B_b(m_t)$	$\langle x\rangle_b(10GeV)$	$\langle x\rangle_b(m_t)$
$\pi^{\pm}$	0.859	0.784	0.168	0.162
$K^{\pm}$	0.39	0.32	0.174	0.167
$p/\overline{p}$	0.096	0.109	0.175	0.167

Table 4.6: Branching fractions of $b \to b-$flavored hadrons and mean $\pi^{\pm}, K^{\pm}, p/\overline{p}$ to b momentum fractions evaluated from Eqs.(4.47,4.48) ,respectively, at the $\mu_F = 10$ GeV and $\mu_F = m_t = 174$ GeV scales.

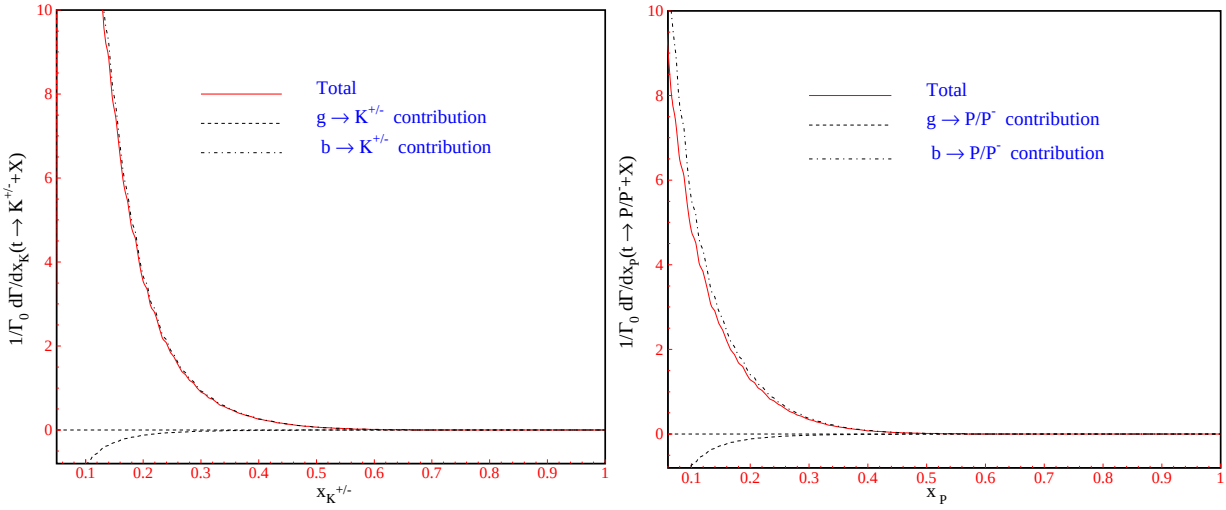

Figure 4.18: Left side: $x_{K^{\pm}}$-spectrum in top decay, with the relevant parameters fitted to the OPAL, CDF, PHENIX, BRAHMS and STAR data. The plotted curves are the contributions of the fragmentation of the gluon(dashes) and the b-quark to $K^{\pm}$ (dot-dashes) and the total contribution of them to $K^{\pm}$. We set the initial and final scales to $\mu_{0F} = \sqrt{2}$ and $\mu_F = \mu = m_t$.
Right side: $x_{p/\overline{p}}$-spectrum in top decay.

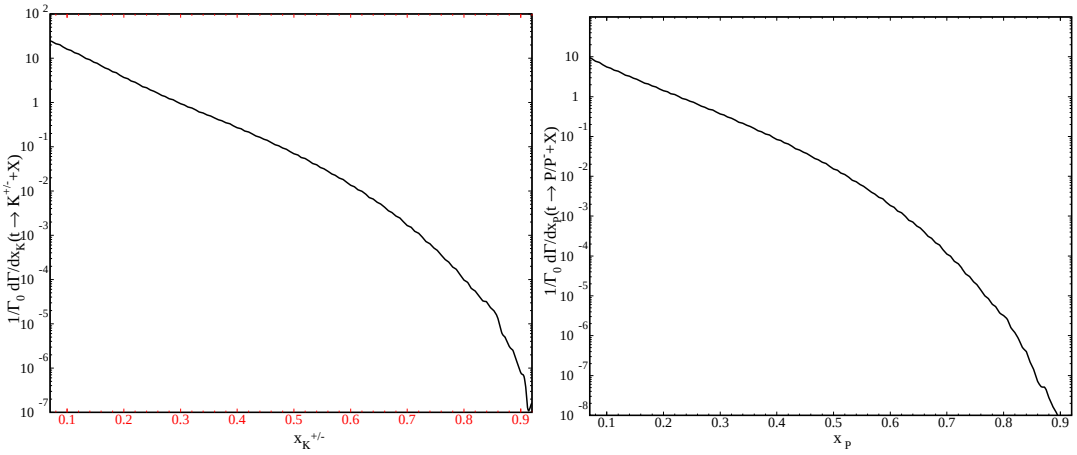

Figure 4.19: Left side: The total contributions of the fragmenting partons in the $x_{K^{\pm}}$ spectrum in top decay on a logarithmic scale, as Fig.4.18.
Right side: The total contributions of the fragmenting partons in the $x_{p/\overline{p}}$ spectrum in top decay on a logarithmic scale, as Fig.4.18.

4.9 The B-hadron Mass Effects and Theoretical Predictions

In the previous results the base of our calculations was to use the factorization theorem. Here we have to point out that the factorization theorem in the form given in Eq.(4.42) can be improved in the presence of a massive quark and a massive hadron, although these effects are negligible, as we shall see. In this section we show how to incorporate the mass effects of the hadron in the energy distribution of the B-hadron produced in the top quark decay process.
According to the factorization formula Eq.(4.42), the decay rate can be expressed via the convolution of the differential width and the fragmentation function:

$$\frac{1}{\Gamma_0}\frac{d\Gamma^B}{dx_B}(x_B, m_t, m_W, m_b) = \frac{1}{\Gamma_0}\sum_{i=b,g}\int_{x_B}^{1}\frac{dz}{z}\frac{d\Gamma_i}{dz}(z, m_t, m_W, m_b, \mu, \mu_F)D_i^B(\frac{x_B}{z}, \mu_F), \tag{4.51}$$

in which the scaling variable x_B is defined: $2E_B/(m_t(1+b-\omega))$. As we pointed out the formula above is valid only for the massless B-hadron and massless partons. Now there are two methods to impose the mass effects of the B-hadron and partons into the equation

above. In the first approach we try to find out the relation between the B-hadron phase space and the parton phase space and in the second way we apply a specific choice of scaling variable using light cone coordinates. The details of the calculation can be found in appendix E.

Therefore, in the presence of the B-hadron and parton masses the experimentally measured observable $(1/\Gamma_0 \times d\Gamma(x_B)/dx_B)$ is related via Eq.(E.25):

$$\frac{1}{\Gamma_0}\frac{d\Gamma^B(x_B, m_t, m_b, m_W)}{dx_B} = \frac{1}{\sqrt{1-\frac{4m_B^2}{m_t^2 x_B^2}}} \times$$
$$\sum_{i=b,g}\int_{y_{B,min(x_B)}}^{y_{B,max(x_B)}} \frac{dy_B}{y_B}\left[(\frac{1}{\Gamma_0}\frac{d\Gamma_i(y_B, m_t, m_i, m_W, \mu^2)}{dy_B})D_i^B(\frac{\eta(x_B)}{y(y_B)}, \mu^2) \times \frac{1}{2}(1+\sqrt{1-\frac{4m_i^2 y_B^2}{m_t^2 x_B^2}})\right], \tag{4.52}$$

in which,

$$\begin{aligned} y_B &= \frac{x_B}{z} \\ D_i^B(\frac{\eta(x_B)}{y(y_B)}) &= D_i^B(\frac{x_B}{y_B} \times \frac{1}{2}(1+\sqrt{1-\frac{4m_i^2 y_B^2}{m_t^2 x_B^2}})) \\ y_{B,max} &= \left(1+\frac{m_i^2-m_B^2}{2m_B^2}(1-\sqrt{1-\frac{4m_B^2}{m_t^2 x_B^2}})\right)^{-1} \\ y_{B,min} &= \frac{x_B}{1+\frac{m_i^2}{m_t^2}}, \end{aligned} \tag{4.53}$$

where m_i stands for the mass of the fragmenting parton, in our calculations $i = b, g$. To prove the equation above we defined $x_B = 2E_B/m_t$, therefore to have the previous scaling variable (defined in section 4.8) this new variable would be divided by the term $1+b-\omega$. According to Eq.(4.52) the effects of hadron mass is to increase the size of the decay rate at small x_B. This point shall be shown in our example later.

Now we show the effects of the B-hadron mass and the b-quark mass on the energy distribution of the B-hadron in the top quark decay using the data in table 4.3 for the S (standard) and the P (peterson) models. In Fig.4.20 we consider the massive b-quark from the beginning and show the effects of the B-hadron mass in the B-hadron energy distribution using GM-VFNS. As it is shown the only considerable effect of the B-hadron mass appears at the small x_B as the mass of the B-hadron increases the decay width at the small x_B (dashed lines in Fig.4.20). In the left side of Fig.4.20 we make these predictions

using the Standards model and in the right side of Fig.4.20 we used the Peterson model. In Fig.4.21 we study the combined effects of the B-hadron mass and the b-quark mass on the energy distribution of the B-hadron and we compare them. As it is seen, the combined effect of the B-hadron mass and the b-quark mass is to increase the size of the decay rate at small x_B and to decrease the size of the decay rate at large x_B. With $m_t = 174$ GeV, $m_b = 4.5$ GeV, $m_W = 80$ GeV and $m_B = 5.28$ GeV, our results are not valid for $x_B < 0.08$.

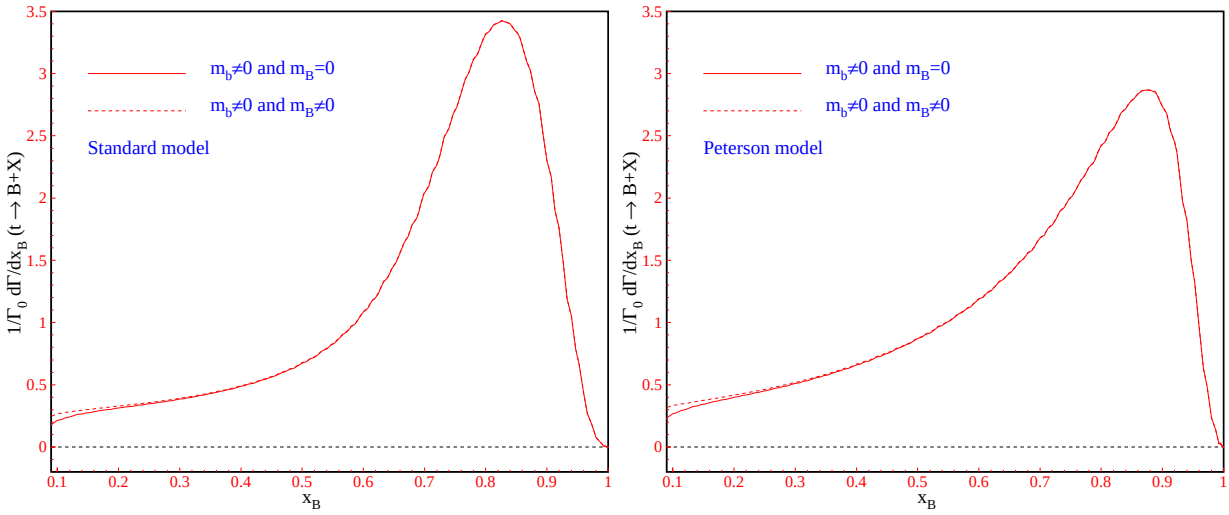

Figure 4.20: Left side: Mass effects of the B-hadron in the energy distribution of the B-hadron in top decay, using the Standard model in presence of the b-quark mass. The initial factorization scale is $\mu_0 = 4.5$ GeV.
Right side: As figure in the left side but using the Peterson model.

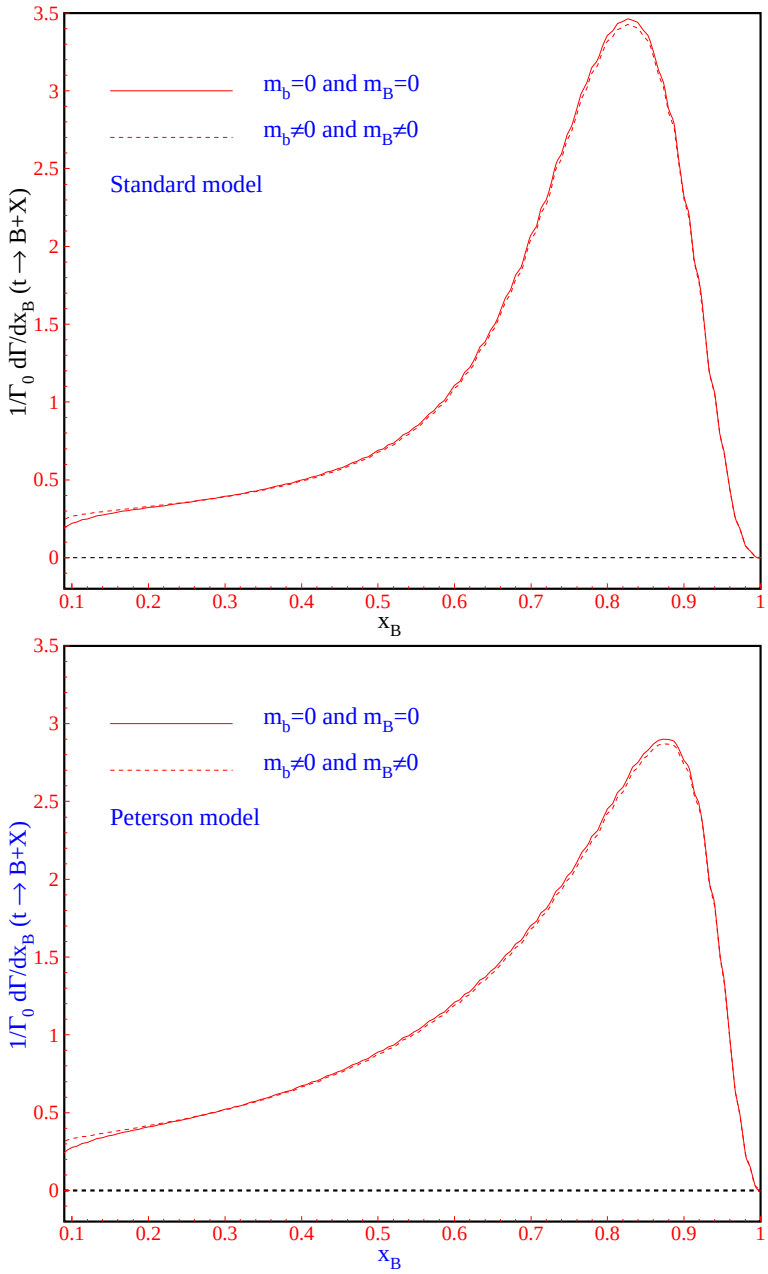

Figure 4.21: Up: Mass effects of the B-hadron and the b-quark in the energy distribution of the B-hadron in top decay, using the Standard model. The initial factorization scale is $\mu_0 = 4.5$ GeV.
Down: As figure above but using the Peterson model.

Chapter 5

W^+-Helicity Fractions in Top Quark Decay

Clearly, to investigate the full structure of partonic interactions one needs to do polarization measurements. Polarization measurements are particularly simple when the particle whose polarization one wants to measure, decays. The angular decay distribution of the decay products reveals information on the state of polarization of the decaying particle. The information contained in the angular decay distribution is maximal when the particle decay is weak. The fact that the angular decay distribution reveals information on the polarization of the decaying particle is sometimes referred to as that the particle decay is self-analyzing.

There are at least two ways to obtain angular decay distributions which we will refer to as *the traditional covariant* and *the helicity amplitudes methods*. In the helicity amplitudes method, one makes use of helicity states for the spinors and the polarization vector of the gauge bosons whereas in the covariant method one evaluates scalar products of four-vectors involving momenta and spin four-vectors in the given references frames. We explain and use these approaches in this chapter in detail. In this work we consider the processes $t \to b + W^+$ and $t \to b + W^+(\to e^+ + \nu_e)$ at LO and NLO, using the helicity amplitudes method for the first process and the covariant way for the second one.

5.1 Helicity Amplitudes for $t \longrightarrow b + W^+$

Since the top quark is heavier than the combined masses of the W^+ boson and the $b-$quark, it will decay into a real W whereas lighter quarks will decay via a virtual W. Because the top quark is so heavy, and the other quarks are so light, the top quark is the only significant source of longitudinal real W bosons. In this section we study correlation of the W^+-boson helicity and decay width in the decay process $t \longrightarrow b + W^+$. Considering Fig.5.1

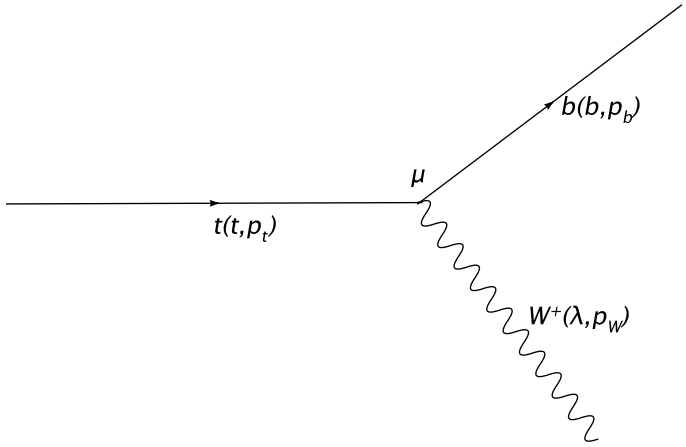

Figure 5.1: Feynman diagram for the decay $t \longrightarrow b + W^+$ at the Born level.

the amplitude of the Born approximation is given by:

$$M^{Born} = \frac{-e}{2\sqrt{2}\sin\theta_W}\epsilon^{\star\mu}(\lambda, p_W)\overline{u}(s_b, p_b)\gamma_\mu(1-\gamma_5)u(s_t, p_t), \tag{5.1}$$

in which $\lambda(= 0, \pm 1)$, s_b and s_t stand for the polarization of the W^+-boson, b-quark and top quark, respectively.

Now we use the helicity states for the spinors and the polarization vector of the gauge boson W^+ with helicity λ in the top quark rest frame. With regards to the momentum four vectors of the W^+-boson propagating along the $\hat{z}$-axis in the top quark rest frame $p^\mu_W = (E_W; 0, 0, \overrightarrow{|p_W|})$, for the polarization four vectors of W^+ we have:

$$\epsilon_\mu(\lambda = 0) = \frac{1}{m_W}\begin{pmatrix} \overrightarrow{|p_W|} \\ 0 \\ 0 \\ E_W \end{pmatrix} \quad \epsilon_\mu(\lambda = \pm 1) = \frac{1}{\sqrt{2}}\begin{pmatrix} 0 \\ 1 \\ \pm i \\ 0 \end{pmatrix}. \tag{5.2}$$

These polarization four vectors satisfy $p_W \cdot \epsilon = 0$ and $\epsilon^2 = -1$. For the helicity spinors we have:

$$u(s_t = 1/2, p_t) = \sqrt{2m_t} \begin{pmatrix} \chi_+ \\ 0 \end{pmatrix} \quad , \qquad u(s_b = 1/2, p_b) = \sqrt{E_b + m_b} \begin{pmatrix} \chi_- \\ \frac{\overrightarrow{|p_b|}}{E_b + m_b} \chi_- \end{pmatrix}$$
$$u(s_t = -1/2, p_t) = \sqrt{2m_t} \begin{pmatrix} \chi_- \\ 0 \end{pmatrix} \quad , \qquad u(s_b = -1/2, p_b) = \sqrt{E_b + m_b} \begin{pmatrix} -\chi_+ \\ \frac{\overrightarrow{|p_b|}}{E_b + m_b} \chi_+ \end{pmatrix}, \tag{5.3}$$

which are solutions of the Dirac equation and χ_+ and χ_- are the Pauli spinors $\chi_+ = (1, 0), \chi_- = (0, 1)$. The spinors above satisfy the orthonormality relations $u^\dagger(r, p).u(r, p) = 2m$. When the top quark and the b-quark are assumed to be unpolarized and the W^+ boson is considered a polarized boson, to obtain the helicity amplitudes squared we start from the following equation:

$$\overline{|M(\lambda)|^2} = \frac{1}{1 + 2s_t} \sum_{s_b, s_t} |M^{Born}|^2 = \frac{1}{2} \sum_{s_b, s_t} (M^{Born} M^{Born\star}), \tag{5.4}$$

where M^{Born} is given in Eq.(5.1), therefore for the helicity amplitudes we obtain:

$$\begin{aligned} \overline{|M(\lambda = 0)|^2} &= \frac{2\pi m_t^2 \alpha}{\omega \sin^2 \theta_W} S(1 + b - 2S\beta^2) \\ \overline{|M(\lambda = +1)|^2} &= \frac{2\pi m_t^2 \alpha}{\sin^2 \theta_W} (S - Q) \\ \overline{|M(\lambda = -1)|^2} &= \frac{2\pi m_t^2 \alpha}{\sin^2 \theta_W} (S + Q), \end{aligned} \tag{5.5}$$

where S, b, β and Q were defined in Eq.(4.1).
In Eq.(5.5), the first term shows the contribution of the W^+ boson polarized longitudinally in the squared matrix element and the second one and the third one show the transverse-plus and the transverse-minus contributions in the matrix element squared $\overline{|M^{Born}(\lambda)|^2}$. The advantage of the helicity amplitudes method is that one can separately identify the three helicity contributions of the W^+ boson.
To obtain the angular decay distribution we start from:

$$\Gamma^{LO} = \Gamma_0 = \frac{(2\pi)^4}{2E_t} \sum_\lambda \int \frac{d^3\mathbf{p}_W}{(2\pi)^3 2E_W} \frac{d^3\mathbf{p}_b}{(2\pi)^3 2E_b} \delta^4(p_t - p_b - p_W) \times \overline{|M^{Born}(\lambda)|^2}. \tag{5.6}$$

Using the top quark rest frame this is simplified to:

$$\Gamma_0 = \frac{\overline{|M^{Born}|^2}}{8\pi m_t^2}(m_t Q). \tag{5.7}$$

Considering Eq.(5.5), we obtain $\Gamma_0 = \Gamma_L + \Gamma_- + \Gamma_+$, where:

$$\begin{aligned}
\Gamma_L &= \Gamma(\lambda = 0) = \frac{m_t Q\alpha}{4\omega \sin^2\theta_W}(S(1+b) - 2b) \\
\Gamma_+ &= \Gamma(\lambda = +1) = \frac{m_t Q\alpha}{4\sin^2\theta_W}(S - Q) \\
\Gamma_- &= \Gamma(\lambda = -1) = \frac{m_t Q\alpha}{4\sin^2\theta_W}(S + Q).
\end{aligned} \tag{5.8}$$

With respect to the Born term rate given in Eq.(4.5), the helicity rates are given in terms of the Born rate as the following:

$$\begin{aligned}
\frac{\Gamma_L}{\Gamma_0} &= \frac{S(1+b) - 2b}{\omega G_0} \\
\frac{\Gamma_+}{\Gamma_0} &= \frac{S - Q}{G_0} \\
\frac{\Gamma_-}{\Gamma_0} &= \frac{S + Q}{G_0},
\end{aligned} \tag{5.9}$$

where S, b, Q and G_0 were defined in Eq.(4.1). These results agree with [91]. If we consider the massless b-quark from the beginning then we obtain:

$$\begin{aligned}
\frac{\Gamma_L}{\Gamma_0} &= \frac{1}{1+2\omega} \\
\frac{\Gamma_+}{\Gamma_0} &= 0 \\
\frac{\Gamma_-}{\Gamma_0} &= \frac{2\omega}{1+2\omega},
\end{aligned} \tag{5.10}$$

which means the contribution of the transverse-plus Born term vanishes in the $m_b = 0$ limit. The $m_b \neq 0$ effects are quite small. This point can be seen using $m_t = 174$ GeV, $m_b = 4.5$ GeV and $m_W = 80$ GeV, where $\Gamma_L/\Gamma_0 = 0.70228$, $\Gamma_+/\Gamma_0 = 0.00033$ and $\Gamma_-/\Gamma_0 = 0.29739$.

5.2 Angular Decay Distribution for $t \to b + W^+(\to e^+ + \nu_e)$ at LO

In this section we study the correlation of the W^+-boson helicity and decay width in the cascade decay process $t \to b + W^+$ followed by $W^+ \to e^+ + \nu_e$ using both the traditional

covariant method and the helicity amplitudes method. At LO the Feynman graph is shown in Fig.5.2 where the W^+-boson is considered as a real particle, i.e. it is considered on shell with $p_W^2 = m_W^2$. The masses of e^+ and ν_e are ignored, i.e: $p_e^2 = p_\nu^2 = 0$.

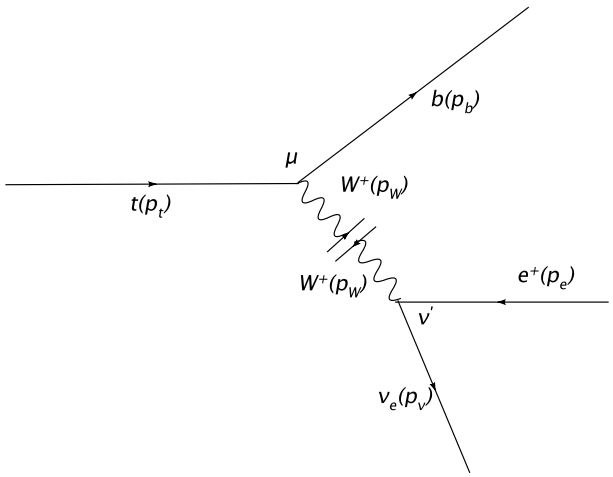

Figure 5.2: Feynman diagram for the decay $t \to b + W^+(\to e^+ + \nu_e)$ at the Born level.

5.2.1 Covariant Approach

In the covariant approach the W^+-boson is considered unpolarized from the beginning and *the mean squared amplitude* for the whole process ($t \to b + W^+(\to e^+ + \nu_e)$) would be evaluated in one frame. We consider the two particles top decay ($t \to b + W^+$) and the two particles W^+-boson decay ($W^+ \to e^+ + \nu_e$) in four space-time dimensions and we start from:

$$d\Gamma^{LO} = d\Gamma^{Had} \times d\Gamma^{Lep}. \tag{5.11}$$

In the equation above the decay rates $d\Gamma^{Had}$(for the hadronic part) and $d\Gamma^{Lep}$(for the leptonic part) are defined as the following:

$$\begin{aligned} d\Gamma^{Had} &= \frac{(2\pi)^4}{2E_t}\frac{d^3\mathbf{p}_W}{(2\pi)^3 2E_W}\frac{d^3\mathbf{p}_b}{(2\pi)^3 2E_b}\delta^4(p_t - p_b - p_W) \times \overline{|M^{Had,Born}|^2} \\ &\Rightarrow \frac{d\Gamma^{Had}}{dx_b} = \frac{Q\delta(1-x_b)}{8\pi m_t}\overline{|M^{Had,Born}|^2}, \\ d\Gamma^{Lep} &= \frac{(2\pi)^4}{2E_W}\frac{d^3\mathbf{p}_e}{(2\pi)^3 2E_e}\frac{d^3\mathbf{p}_\nu}{(2\pi)^3 2E_\nu}\delta^4(p_W - p_e - p_\nu) \times \overline{|M^{Lep,Born}|^2} \\ &\Rightarrow \frac{d\Gamma^{Lep}}{d\cos\theta} = \frac{1}{32\pi m_W}\overline{|M^{Lep,Born}|^2}, \end{aligned} \tag{5.12}$$

where we used the top quark and the W^+ rest frames which are defined in Fig.5.3. The polar angle θ is defined as the angle between the charged-lepton (e^+) momentum in the W^+-rest frame and the W^+ momentum in the top quark rest-frame. In the equation above the amplitudes of the hadronic and leptonic parts of the decay process read:

$$\begin{aligned} M^{Had,Born} &= -\frac{e}{2\sqrt{2}\sin\theta_W}\epsilon^{\star\mu}(\lambda, p_W)\overline{u}(s_b, p_b)\gamma_\mu(1-\gamma_5)u(s_t, p_t) \\ M^{Lep,Born} &= -\frac{e}{2\sqrt{2}\sin\theta_W}\epsilon^{\nu'}(\lambda, p_W)\overline{u}(s_\nu, p_\nu)\gamma_{\nu'}(1-\gamma_5)v(s_e, p_e). \end{aligned} \tag{5.13}$$

Therefore the angular decay distribution is obtained as:

$$\frac{d^2\Gamma^{LO}}{dx_b\; d\cos\theta} = \frac{Q\;\delta(1-x_b)}{256\pi^2 m_t m_W}\overline{|M^{Born}|^2}. \tag{5.14}$$

Now we try to find out the mean squared amplitude for the cascade decay process of the top quark. We start from:

$$\begin{aligned} \overline{|M^{Born}|^2} &= \overline{|M^{Had,Born}\cdot M^{Lep,Born}|^2} = \frac{1}{2}\sum_{\lambda,\lambda',t,b,e,\nu}(M^{Had}M^{Had\star})\cdot(M^{Lep}M^{Lep\star}) \\ &= \frac{e^4}{2\sin^4\theta_W}\sum_{\lambda,\lambda'}\Big(\big[\epsilon^{\nu}(\lambda)\epsilon^{\star\mu'}(\lambda)\big]\cdot\big[\epsilon^{\nu'}(\lambda)\epsilon^{\star\mu}(\lambda)\big]\Big)L_{\mu'\nu'}H_{\mu\nu}, \end{aligned} \tag{5.15}$$

where the hadronic tensor $H_{\mu\nu}$ and the leptonic tensor $L_{\mu'\nu'}$ are defined by:

$$\begin{aligned} H_{\mu\nu} &= \frac{1}{8}\cdot Tr[(\not{p}_b + m_b)\cdot\gamma_\mu(1-\gamma_5)\cdot(\not{p}_t + m_t)\cdot\gamma_\nu(1-\gamma_5)] \\ L_{\mu'\nu'} &= \frac{1}{8}\cdot Tr[\not{p}_\nu\cdot\gamma_{\nu'}(1-\gamma_5)\cdot\not{p}_e\cdot\gamma_{\mu'}(1-\gamma_5)]. \end{aligned} \tag{5.16}$$

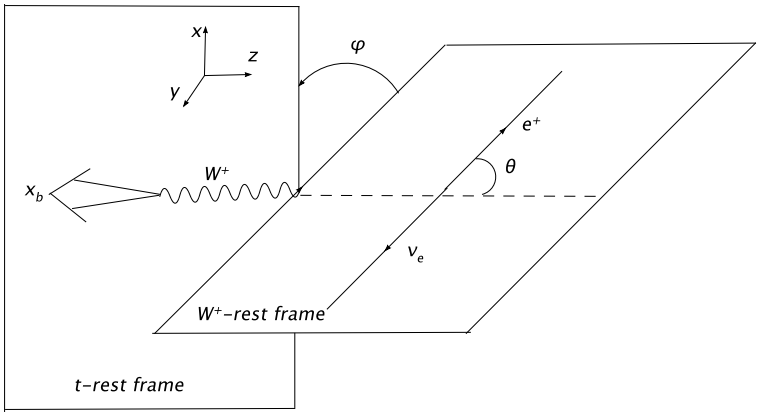

Figure 5.3: Definition of the top quark rest frame and the polar angle θ in the W^+ rest frame.

Using the completeness relation:

$$\sum_{\lambda=0,\pm} \epsilon^{\mu}(\lambda)\epsilon^{\nu\star}(\lambda) = -g^{\mu\nu} + \frac{p_W^{\mu} p_W^{\nu}}{m_W^2}, \tag{5.17}$$

the result above turns into the following result in the case of zero lepton mass:

$$\begin{aligned} \overline{|M^{Born}|^2} &= \frac{8\pi^2\alpha^2}{\sin^4\theta_W}\, L^{\mu\nu} H_{\mu\nu} \\ &= \frac{32\pi^2\alpha^2}{\sin^4\theta_W}(p_b.p_\nu)(p_t.p_e), \end{aligned} \tag{5.18}$$

since $p_W^{\mu} L_{\mu\nu} = p_W^{\nu} L_{\mu\nu} = 0$.
As already mentioned in the covariant method, the invariant $L^{\mu\nu}H_{\mu\nu}$ must be evaluated in one particular frame. Here we choose the top quark rest frame shown in Fig.5.3. In this rest frame for the momentum four-vectors we have:

$$\begin{aligned} p_t^{\mu} &= m_t(1;0,0,0) \\ p_b^{\mu} &= m_t(S;0,0,-Q) \\ p_e^{\mu} &= \frac{m_t}{2}\left(\frac{1+\omega-b}{2} + Q\cos\theta; \sqrt{\omega}\sin\theta, 0, Q + \frac{1+\omega-b}{2}\cos\theta\right) \\ p_\nu^{\mu} &= \frac{m_t}{2}\left(\frac{1+\omega-b}{2} - Q\cos\theta; -\sqrt{\omega}\sin\theta, 0, Q - \frac{1+\omega-b}{2}\cos\theta\right). \end{aligned} \tag{5.19}$$

The details of this calculation can be found in appendix F.
Considering these momenta for the mean squared matrix element (Eq.(5.18)) we have:

$$\begin{aligned}\overline{|M^{Born}|^2} = \frac{16\pi^2\alpha^2}{3\sin^4\theta_W} m_t^4 \Big\{ \frac{1}{2}[(1-b)^2 - \omega(1+b)] \quad . \quad \frac{3}{4}\sin^2\theta + \\ \frac{\omega}{2}[1+b-\omega-2Q] \quad . \quad \frac{3}{8}(1+\cos\theta)^2 + \\ \frac{\omega}{2}[1+b-\omega+2Q] \quad . \quad \frac{3}{8}(1-\cos\theta)^2 \Big\}.\end{aligned} \tag{5.20}$$

This result can be written as:

$$\overline{|M^{Born}|^2} = \frac{16\pi^2\alpha^2}{3\sin^4\theta_W} m_t^4 \big\{ L \cdot \frac{3}{4}\sin^2\theta + T_+ \cdot \frac{3}{8}(1+\cos\theta)^2 + T_- \cdot \frac{3}{8}(1-\cos\theta)^2 \big\}. \tag{5.21}$$

Here we separated the three polarization (or helicity)contributions of the W^+ boson, i.e. L, T_+ and T_- which are the longitudinal, transverse-plus and transverse-minus helicity, respectively. Our result is in complete agreement with [91].
From the obtained amplitude one can conclude that the longitudinal W^+ decay process into a charged lepton(e^+) has an angular distribution which peaks at $\theta = \pi/2$. Form the amplitude (5.21) it is obvious that the charged leptons which are scattered in angles $\theta = 0$ or $\theta = \pi$ are due to the decay of a transverse W^+-boson. The resulting $\cos\theta$ distributions are very distinct for each W^+ helicity state. If one can reconstruct the $\cos\theta$ distribution from top quark decays observed in collider data, these unique shapes can be used for a measurement of W^+ boson polarization and a comparison with theory could be made. There are at least two methods one may use to extract the degree of W^+ boson polarization in top quark decays. In the first method, which was mentioned, one uses the lepton angular distribution, $\cos\theta$, the other one examines the charged lepton p_T distribution, see [92].
Let us go back to Eq.(5.20). In the limit $m_b \to 0$ the Born term is simplified to:

$$\begin{aligned}\overline{|M^{Born}|^2} = \frac{16\pi^2\alpha^2}{3\sin^4\theta_W} m_t^4 \Big\{ \frac{1}{2}[1-\omega] \quad \cdot \quad \frac{3}{4}\sin^2\theta + \\ 0 \quad \cdot \quad \frac{3}{8}(1+\cos\theta)^2 + \\ \omega[1-\omega] \quad \cdot \quad \frac{3}{8}(1-\cos\theta)^2 \Big\}.\end{aligned} \tag{5.22}$$

As it is seen in the massless b-quark case, there is no transverse-plus helicity contribution for the W^+ decay. However in the next section we shall show that in the higher order QCD corrections this contribution vanishes no longer.

Now we are in the situation to write the angular distribution of the differential decay rate for the decay process $t \to X_b + W^+$ followed by $W^+ \to e^+ + \nu_e$. From Eq.(5.14), the normalized differential decay rate can be written as:

$$\begin{aligned}\frac{1}{\Gamma_0'}\frac{d^2\Gamma^{LO}}{dx_b\; d\cos\theta} = \frac{\delta(1-x_b)}{G_0\;\omega}\Big\{ [S(1+b)-2b)] \;\; &\cdot \;\; \frac{3}{4}\sin^2\theta + \\ \omega[S-Q] \;\; &\cdot \;\; \frac{3}{8}(1+\cos\theta)^2 + \\ \omega[S+Q] \;\; &\cdot \;\; \frac{3}{8}(1-\cos\theta)^2\Big\}.\end{aligned} \tag{5.23}$$

In the case $m_b \to 0$ we have:

$$\frac{1}{\Gamma_0'}\frac{d^2\Gamma^{LO}}{dx_b\; d\cos\theta} = \frac{\delta(1-x_b)}{1+2\omega}\left\{\frac{3}{4}\sin^2\theta + 0 + (2\omega)\cdot\frac{3}{8}(1-\cos\theta)^2\right\}. \tag{5.24}$$

In the equations above Γ_0' is the width of the Born process $t \to bW^+(\to e^+\nu_e)$ and it is given by:

$$\Gamma_0' = \frac{m_t m_W \alpha^2}{48\sin^4\theta_W}(QG_0). \tag{5.25}$$

To obtain Γ_0' we would calculate the matrix elements squared $\overline{|M^{Born,Had}|^2}$ and $\overline{|M^{Born,Lep}|^2}$ within their rest frames separately. To explain more precise we start from:

$$\Gamma_0' = \Gamma^{Born,Had} \times \Gamma^{Born,Lep}. \tag{5.26}$$

According to Eq.(5.12) we obtain:

$$\begin{aligned}\Gamma^{Born,Had} &= \frac{Q}{8\pi m_t}\overline{|M^{Born,Had}|^2} \qquad \text{where} \quad \overline{|M^{Born,Had}|^2} = \frac{1}{2}\sum_{\lambda,b,t}(M^{Had}\cdot M^{Had\star}) \\ \Gamma^{Born,Lep} &= \frac{1}{16\pi m_W}\overline{|M^{Born,Lep}|^2} \quad \text{where} \quad \overline{|M^{Born,Lep}|^2} = \frac{1}{3}\sum_{e,\nu,\lambda'}(M^{Lep}\cdot M^{Lep\star}).\end{aligned} \tag{5.27}$$

Using $M^{Born,Had}$ and $M^{Born,Lep}$ defined in Eq.(5.13) and the completeness relation, we have:

$$\begin{aligned}\Gamma^{Born,Had} &= \frac{m_t\alpha}{4\sin^2\theta_W}(QG_0)\\ \Gamma^{Born,Lep} &= \frac{m_W\alpha}{12\sin^2\theta_W}.\end{aligned} \tag{5.28}$$

Therefore the Born level decay rate reads:

$$\Gamma_0' = \frac{m_t m_W\alpha^2}{48\sin^4\theta_W}(QG_0). \tag{5.29}$$

Let us go back to Eq.(5.23). For unpolarized top decay the angular decay distribution is determined by the polarization components of W^+ boson as:

$$\frac{1}{\Gamma_0'}\frac{d\Gamma^{LO}}{d\cos\theta} = \frac{3}{4}\sin^2\theta\ \Gamma_L + \frac{3}{8}(1+\cos\theta)^2\ \Gamma_+ + \frac{3}{8}(1-\cos\theta)^2\ \Gamma_-, \tag{5.30}$$

where $\Gamma_L = 0.702281,\ \Gamma_+ = 0.000321$ and $\Gamma_- = 0.29740$ denote the partial decay rates into the longitudinal, transverse-plus and transverse-minus W^+-boson. The various contributions in Eq.(5.30) are reflected in the shape of the lepton energy spectrum in the rest frame of the top quark. The fact that Γ_+ is predicted to be quite small implies that the lepton spectrum will be soft.
In Fig.5.4 we showed the LO contributions of the longitudinal and transverse-minus W^+-boson in the B-meson energy distribution in the variable x_B using the data given in the table.4.1. In this calculation we adopt the LO value $\Lambda^{(5)} = 108$ Mev appropriate for $n_f = 5$.

5.2.2 Helicity Amplitudes Approach

The $\cos\theta$ dependence of the squared amplitude can be worked out by using the helicity approach. To use this method we start from Eq.(5.18) where we had:

$$\overline{|M^{Born}|^2} = \frac{8\pi^2\alpha^2}{\sin^4\theta_W}\ L^{\mu\nu}H_{\mu\nu}. \tag{5.31}$$

To find out the $\cos\theta$ dependence of $L^{\mu\nu}H_{\mu\nu}$ we use the completeness relation for the polarization four-vectors including the scaler component, i.e:

$$\sum_{\lambda,\lambda'=t,\pm,0}\epsilon^{\mu}(\lambda)\epsilon^{\star\nu}(\lambda')g_{\lambda\lambda'} = g^{\mu\nu}, \tag{5.32}$$

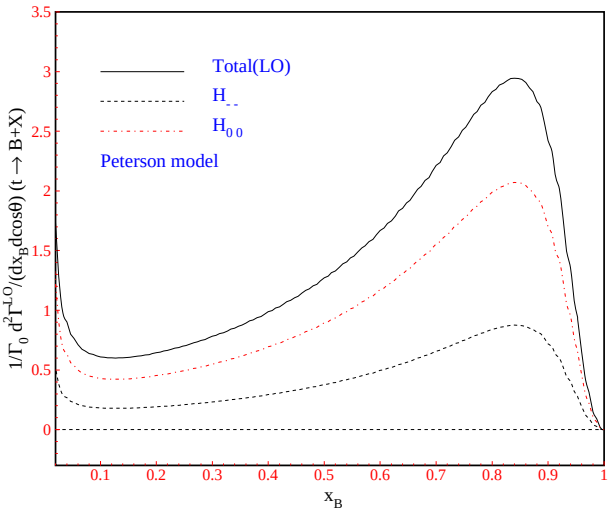

Figure 5.4: Comparison of the LO contributions of the longitudinal and the transverse-minus helicity of the W^+-boson in the B-meson energy distribution using the Peterson model. The solid line shows the summation of all helicity contributions. The initial factorization scale is $\mu_0 = 10.0$ GeV and the b-quark is considered to be massless.

where $\lambda, \lambda' = +, -, 0$ stand for the transverse-plus, transverse-minus and the longitudinal helicity of the W^+-boson and $\lambda, \lambda' = t$ stand for the scalar component of the helicity and the tensor $g_{\lambda\lambda'} = diag(+, -, -, -)$ is the spherical representation of the metric tensor where the components are ordered in the sequence $\lambda, \lambda' = t, \pm, 0$. Therefore we can rewrite the contraction of the lepton and hadron tensor $L^{\mu\nu}H_{\mu\nu}$ as:

$$\begin{aligned} L_{\mu\nu}H^{\mu\nu} &= L^{\mu'\nu'}g_{\mu'\mu}g_{\nu'\nu}H^{\mu\nu} \\ &= \sum_{m,m',n,n'} L^{\mu'\nu'}\epsilon_{\mu'}(m)\epsilon^{\star}_{\mu}(m')g_{mm'}\epsilon^{\star}_{\nu'}(n)\epsilon_{\nu}(n')g_{nn'}H^{\mu\nu} \\ &= \sum_{m,m',n,n'} \Big(L^{\mu'\nu'}\epsilon_{\mu'}(m)\epsilon^{\star}_{\nu'}(n)\Big)\Big(H^{\mu\nu}\epsilon^{\star}_{\mu}(m')\epsilon_{\nu}(n')\Big)g_{mm'}g_{nn'}. \end{aligned} \tag{5.33}$$

Now each parenthesis is an invariant quantity and the nice feature of this representation is that the left bracket can be evaluated in the W^+ rest frame which leads to a $\cos\theta$ dependence. We do not evaluate the scalar contribution of the equation above since this contribution drops out after integration over the azimuthal angle. The result above is

simplified to:

$$L_{\mu\nu}H^{\mu\nu} = L^{\mu'\nu'}\epsilon_{\mu'}(0)\epsilon^{\star}_{\nu'}(0)H_{00} + L^{\mu'\nu'}\epsilon_{\mu'}(+)\epsilon^{\star}_{\nu'}(+)H_{++} + L^{\mu'\nu'}\epsilon_{\mu'}(-)\epsilon^{\star}_{\nu'}(-)H_{--}, \tag{5.34}$$

where we have defined the diagonal hadronic helicity functions $H_{00} = H_L, H_{++}, H_{--}$ according to:

$$H_{mm} = H^{\mu\nu}\epsilon^{\star}_{\mu}(m)\epsilon_{\nu}(m) \qquad m = 0, +, -. \tag{5.35}$$

In the W^+ rest frame (Fig.5.3), one has:

$$\begin{aligned} p^{\mu}_{e^+} &= \frac{m_W}{2}(1; \sin\theta, 0, \cos\theta), \\ p^{\mu}_{\nu_e} &= \frac{m_W}{2}(1; -\sin\theta, 0, -\cos\theta), \\ \epsilon^{\mu}(L) &= (0; 0, 0, 1), \\ \epsilon^{\mu}(\pm) &= \frac{1}{\sqrt{2}}(0; \mp 1, -i, 0), \end{aligned} \tag{5.36}$$

and from Eq.(5.16) we also have:

$$L^{\mu\nu} = p^{\mu}_{e^+}p^{\nu}_{\nu_e} + p^{\nu}_{e^+}p^{\mu}_{\nu_e} - \frac{m^2_W}{2}g^{\mu\nu} - i\epsilon^{\mu\nu\alpha\beta}(p_{e^+})_{\alpha}(p_{\nu_e})_{\beta}, \tag{5.37}$$

therefore with respect to the equations above we obtain:

$$\begin{aligned} &\sum_{\mu',\nu'} L^{\mu'\nu'}\epsilon_{\mu'}(0)\epsilon^{\star}_{\nu'}(0) = L^{33}\epsilon_3(0)\epsilon^{\star}_3(0) = \frac{2}{3}m^2_W\left(\frac{3}{4}\sin^2\theta\right), \\ &\sum_{\mu',\nu'=1,2} L^{\mu'\nu'}\epsilon_{\mu'}(+)\epsilon^{\star}_{\nu'}(+) = \frac{2}{3}m^2_W\left(\frac{3}{8}(1+\cos\theta)^2\right), \\ &\sum_{\mu',\nu'=1,2} L^{\mu'\nu'}\epsilon_{\mu'}(-)\epsilon^{\star}_{\nu'}(-) = \frac{2}{3}m^2_W\left(\frac{3}{8}(1-\cos\theta)^2\right). \end{aligned} \tag{5.38}$$

Now the second parenthesis in Eq.(5.33) should be evaluated in the t-quark rest frame. In this frame we have:

$$\begin{aligned} p^{\mu}_{b} &= \frac{m_t(1-\omega)}{2}(1; 0, 0, -1), \\ p^{\mu}_{W} &= \frac{m_t}{2}(1+\omega; 0, 0, 1-\omega), \\ \epsilon^{\mu}(L) &= \frac{1}{m_W}(|\overrightarrow{p_W}|; 0, 0, E_W), \\ \epsilon^{\mu}(\pm) &= \frac{1}{\sqrt{2}}(0; \mp 1, -i, 0), \end{aligned} \tag{5.39}$$

and from Eq.(5.16), we have:

$$H^{\mu\nu} = p_t^\mu p_b^\nu + p_t^\nu p_b^\mu - (p_t.p_b)g^{\mu\nu} - i\epsilon^{\mu\nu\alpha\beta}(p_t)_\alpha(p_b)_\beta. \tag{5.40}$$

After using the equation above, considering the massless b-quark for the diagonal hadronic helicity structure functions (Eq.(5.35)) we have:

$$H_{00} = \frac{m_t^4}{2m_W^2}(1-\omega) \qquad , H_{++} = 0, \qquad H_{--} = \frac{\omega\ m_t^4}{m_W^2}(1-\omega). \tag{5.41}$$

Then finally we obtain:

$$\begin{aligned}\overline{|M^{Born}|^2} &= \frac{8\pi^2\alpha^2}{\sin^4\theta_W}\ L^{\mu\nu}H_{\mu\nu} \\ &= \frac{16\pi^2\alpha^2}{3\sin^2\theta_W} m_t^4 \Big\{ \frac{1-\omega}{2}\cdot\frac{3}{4}\sin^2\theta + 0 + \omega(1-\omega)\cdot\frac{3}{8}(1-\cos\theta)^2 \Big\}.\end{aligned} \tag{5.42}$$

This result is in agreement with Eq.(5.22) which was calculated via the covariant approach.

5.3 Angular Decay Distribution for $t \to b + W^+(\to e^+ + \nu_e)$ at NLO Using Fixed x_b

In this section we calculate the virtual and real corrections for the cascade top decay and we show that for the NLO QCD corrections the contribution of the transverse-plus helicity of the W^+ vanishes no longer. To extract the singularities we use dimensional regularization as before.

5.3.1 Virtual Gluon Corrections

First we consider the one-loop corrections to the decay width considering the Feynman diagrams depicted in Fig.5.5.

Therefore for the squared amplitude we obtain:

$$\overline{|M^V|^2} = \frac{16\pi^2\alpha^2}{\sin^4\theta_W} L^{\mu\nu}(H^a_{\mu\nu} + H^b_{\mu\nu}), \tag{5.43}$$

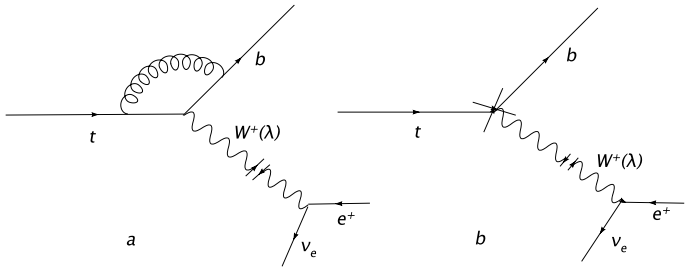

Figure 5.5: Feynman diagrams for the vertex corrections(a) and the renormalization of the fields(b).

where $L^{\mu\nu}$ is given in Eq.(5.16) and,

$$\begin{aligned} H^a_{\mu\nu} &= \frac{1}{8} Tr\big[\not{p}_b \Lambda_\mu (m_t + \not{p}_t)\gamma_\nu (1-\gamma_5)\big] \\ H^b_{\mu\nu} &= \frac{1}{8}(\frac{\delta z_t + \delta z_b}{2}) Tr\big[\not{p}_b \gamma_\mu (1-\gamma_5)(m_t + \not{p}_t)\gamma_\nu (1-\gamma_5)\big], \end{aligned} \tag{5.44}$$

in which Λ_μ, δz_t and δz_b are given in Eqs.(3.7,3.16,3.18), respectively. After using the covariant approach, the contribution of the vertex corrections in the matrix elements reads:

$$\begin{aligned} L^{\mu\nu} H^a_{\mu\nu} &= \alpha_S \frac{\omega(1-\omega)}{6\pi} m_t^4 \bigg[(1-\omega) m_t^2 C_0(m_t^2, 0, m_W^2, m_t^2, 0, 0) - \frac{\omega}{1-\omega} B_0(m_t^2, 0, m_t^2) \\ &\quad + B_0(0,0,0) - \frac{1-3\omega}{2(1-\omega)} B_0(m_W^2, 0, m_t^2) - 1 \bigg] (1-\cos\theta)^2 + \\ &\quad \alpha_S \frac{1-\omega}{6\pi} m_t^4 \bigg[(1-\omega) m_t^2 C_0(m_t^2, 0, m_W^2, m_t^2, 0, 0) - \frac{1+\omega}{2(1-\omega)} B_0(m_t^2, 0, m_t^2) \\ &\quad + B_0(0,0,0) + \frac{\omega}{1-\omega} B_0(m_W^2, 0, m_t^2) - 1 \bigg] \sin^2\theta, \end{aligned} \tag{5.45}$$

and the contribution of the renormalization of the fields reads:

$$L^{\mu\nu} H^b_{\mu\nu} = \frac{m_t^4 (1-\omega)}{8} (\delta z_b + \delta z_t) \bigg[\omega (1-\cos\theta)^2 + \sin^2\theta \bigg]. \tag{5.46}$$

To calculate the contribution of the virtual corrections in the differential decay rate we start from:

$$d\Gamma^{vir} = d\Gamma^{Had,vir} \times d\Gamma^{Lep}. \tag{5.47}$$

After using Eq.(3.5) and Eq.(5.12) we obtain:

$$\frac{d^2\Gamma^{vir}}{dx_b\ d\cos\theta} = \frac{|\overline{M^{vir}}|}{16\pi m_t}\delta(1-x_b)\frac{1-\omega}{32\pi m_W}\Big\{1-\epsilon\big[\gamma_E-\log\frac{4\pi\mu^2}{m_t^2}+2\log(1-\omega)-\frac{2(1+\omega)}{1+2\omega}\big]+ \epsilon^2\big[\frac{1}{2}\big(\gamma_E-\log\frac{4\pi\mu^2}{m_t^2}+2\log(1-\omega)-\frac{2(1+\omega)}{1+2\omega}\big)^2-\frac{\pi^2}{4}+\frac{2(1+\omega)(1+3\omega)}{(1+2\omega)^2}\big]\Big\}, \tag{5.48}$$

with $|\overline{M^{vir}}|$ given in Eq.(5.43). Considering the results above we obtain the following result:

$$\frac{1}{\Gamma_0'}\frac{d^2\Gamma^{vir}}{dx_b\ d\cos\theta} = H_{++}^{Vir}\cdot\frac{3}{8}(1+\cos\theta)^2+H_{--}^{Vir}\cdot\frac{3}{8}(1-\cos\theta)^2+H_{00}^{Vir}\cdot\frac{3}{4}\sin^2\theta. \tag{5.49}$$

For the helicity contributions of the W^+-boson in decay width we have:

$$\begin{aligned} H_{++}^{Vir} &= 0 \\ H_{--}^{Vir} &= \frac{\alpha_S}{2\pi(1+2\omega)}C_f\delta(1-x_b)\big[2(3\omega-1)\log(1-\omega)-2\omega F\big] \\ H_{00}^{Vir} &= \frac{\alpha_S}{2\pi(1+2\omega)}C_f\delta(1-x_b)\big[2\log(1-\omega)-F\big], \end{aligned} \tag{5.50}$$

where F was defined in Eq.(3.22). In the calculation above for the Born level decay rate we used the following formula:

$$\Gamma_0' = \Gamma_0^{Had}\times\Gamma_0^{Lep}, \tag{5.51}$$

where Γ_0^{Lep} was given in Eq.(5.28) and to extract all correct terms we used Eq.(3.2) for Γ_0^{Had}. It is simple to check that Eq.(5.49) is equal to Eq.(3.21) after integration over $\cos\theta$.

5.3.2 Real Gluon Corrections

The Feynman diagrams of the real gluon corrections are shown in Fig.5.6.

There are two methods to calculate the contribution of the real gluon corrections that we will explain in detail. First we explain the helicity amplitudes approach. The whole amplitude for the real gluon correction is given by:

$$M^R = (M_a^{R,Had}+M_b^{R,Had}).M^{Lep}, \tag{5.52}$$

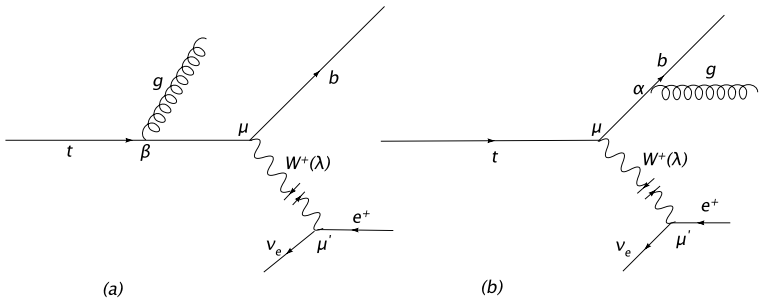

Figure 5.6: Feynman diagrams for the emission of the real gluon.

where the matrix elements $M_a^{R,Had}$, $M_b^{R,Had}$ and M^{Lep} are given in Eqs.(3.23,3.24,5.13). Therefore the mean squared amplitude reads:

$$\overline{|M^R|^2} = \frac{1}{3\times 2}\sum_{spins,color}|M^R|^2 \quad \Rightarrow |\overline{M^R}| = \frac{32\pi^3\alpha^2\alpha_S}{\sin^4\theta_W}C_F\ L^{\mu\nu}H_{\mu\nu}. \tag{5.53}$$

The lepton tensor $L^{\mu\nu}$ was given in Eq.(5.16) and the hadron tensor $H^{\mu\nu}$ equals to $H_a^{\mu\nu} + H_b^{\mu\nu} + 2H_{ab}^{\mu\nu}$ where:

$$\begin{aligned}
H_a^{\mu\nu} &= \\
&\frac{1}{32(p_t.p_g)^2}Tr[-g^{\alpha\beta}\ \not{p}_b\gamma_\mu(1-\gamma_5)(m_t+\not{p}_t-\not{p}_g)\gamma_\beta(m_t+\not{p}_t)\gamma_\alpha(m_t+\not{p}_t-\not{p}_g)(1+\gamma_5)\gamma_\nu],\\
H_b^{\mu\nu} &= \frac{1}{32(p_b.p_g)^2}Tr[-g^{\alpha\gamma}\ \not{p}_b\gamma_\alpha(\not{p}_b+\not{p}_g)\gamma_\mu(1-\gamma_5)(m_t+\not{p}_t)(1+\gamma_5)\gamma_\nu(\not{p}_b+\not{p}_g)\gamma_\gamma],\\
H_{ab}^{\mu\nu} &= \\
&\frac{1}{32(p_t.p_g)(p_b.p_g)}Tr[g^{\gamma\beta}\ \not{p}_b\gamma_\mu(1-\gamma_5)(m_t+\not{p}_t-\not{p}_g)\gamma_\beta(m_t+\not{p}_t)(1+\gamma_5)\gamma_\nu(\not{p}_b+\not{p}_g)\gamma_\gamma].
\end{aligned} \tag{5.54}$$

Applying the procedure which we used in Eq.(5.34) and considering the definition of the polarization vectors of the W^+-boson (Eq.(5.36)), we obtain for the invariant quantity $L^{\mu\nu}H_{\mu\nu}$ in Eq.(5.53):

$$L^{\mu\nu}H_{\mu\nu} = \frac{2}{3}m_W^2\big[\frac{3}{4}H_{00}\sin^2\theta + \frac{3}{8}H_{++}(1+\cos\theta)^2 + \frac{3}{8}H_{--}(1-\cos\theta)^2\big], \tag{5.55}$$

where,

$$\begin{aligned} H_{00} &= H^{\mu\nu}\epsilon^{\star}_{\mu}(0)\epsilon_{\nu}(0) = \frac{1}{m_W^2}\Big(|\overrightarrow{p_W}|^2 H^{00} - E_W|\overrightarrow{p_W}|(H^{03}+H^{30}) + E_W^2 H^{33}\Big), \\ H_{++} &= H^{\mu\nu}\epsilon^{\star}_{\mu}(+)\epsilon_{\nu}(+) = \frac{1}{2}\big(H^{11} + i(H^{12}-H^{21}) + H^{22}\big), \\ H_{--} &= H^{\mu\nu}\epsilon^{\star}_{\mu}(-)\epsilon_{\nu}(-) = \frac{1}{2}\big(H^{11} + i(H^{21}-H^{12}) + H^{22}\big). \end{aligned} \tag{5.56}$$

Now to calculate $H^{00}, H^{03}, H^{30}, \cdots$ we have to specify the general form of the hadron tensor $H^{\mu\nu}$. At first we turn our attention to the matrix γ_5. As we explained in section 3.4, the matrix γ_5 is not well defined in D dimensions and the ordinary anti-commutation relation in 4-dimensions ($\{\gamma_\mu, \gamma_5\} = 0$) produces the ambiguity in D-dimensions. Therefore we employ the Breitenlohner-Maison (BM) scheme for the definition of γ_5 in D-dimensions, as it was explained in section 3.4.

Now we explain the detail of the calculation of the hadron tensor $H^{\mu\nu}$. With respect to

Eq.(5.54) the hadron tensor for the real gluon corrections reads:

$$
\begin{aligned}
H^{\mu\nu} &= H_a^{\mu\nu} + H_b^{\mu\nu} + 2H_{ab}^{\mu\nu} \\
&= \frac{1}{E_g^2(1-\cos\theta)}\Big\{(D-2)[p_t^\mu p_t^\nu - p_W^\mu p_t^\nu - p_b^\mu p_t^\nu + p_b^\mu p_b^\nu + p_b^\mu p_W^\nu] + \\
&(D-4)[p_W^\mu p_W^\nu - p_t^\mu p_W^\nu + p_W^\mu p_b^\nu] + (6-D)p_t^\mu p_b^\nu + \\
&+\frac{i\epsilon^{\mu\nu\alpha\beta}}{m_t E_b} p_g^\alpha p_t^\beta p_b^\gamma [(D-4)p_W^\nu - (D-2)p_t^\nu + (D-6)p_b^\nu] \\
&\frac{m_t}{E_b}[-p_t^\mu p_b^\nu + p_W^\mu p_b^\nu + p_b^\mu p_t^\nu - p_b^\mu p_W^\nu + i\epsilon^{\mu\nu\alpha\beta} p_b^\alpha p_g^\beta] + 2i\epsilon^{\mu\nu\alpha\beta} p_b^\alpha (p_g^\beta - p_t^\beta) - 2E_b m_t g^{\mu\nu}\Big\} \\
&+\frac{1}{E_b E_g(1-\cos\theta)}\Big\{(D-4)[i\epsilon^{\mu\nu\alpha\beta} p_b^\alpha p_g^\beta + p_W^\mu p_b^\nu] \\
&+(1-\frac{D}{2})[i\epsilon^{\mu\nu\alpha\beta} p_g^\alpha p_t^\beta + p_W^\mu p_t^\nu + p_t^\mu p_W^\nu + p_b^\mu p_t^\nu + m_t E_g g^{\mu\nu} - 2p_b^\mu p_b^\nu - 2p_t^\mu p_t^\nu] \\
&+(7-\frac{3}{2}D)p_t^\mu p_b^\nu - 2i\epsilon^{\mu\nu\alpha\beta} p_b^\alpha p_t^\beta - 2m_t E_b g^{\mu\nu}\Big\} \\
&+\frac{1}{E_g^2}\Big\{\frac{2-D}{2}\frac{E_g}{m_t}[2p_b^\mu p_b^\nu + 2p_t^\mu p_t^\nu + p_W^\mu p_b^\nu + p_b^\mu p_W^\nu - p_b^\mu p_t^\nu + i\epsilon^{\mu\nu\alpha\beta} p_b^\alpha p_g^\beta] + \\
&i\epsilon^{\mu\nu\alpha\beta}[p_b^\alpha p_t^\beta - p_b^\alpha p_g^\beta] + \frac{E_g}{m_t}[(\frac{3}{2}D-7)p_t^\mu p_b^\nu + (D-4)p_t^\mu p_W^\nu] + E_g g^{\mu\nu}[2E_b + m_t] + \\
&E_b m_t g^{\mu\nu} - 2p_b^\mu p_b^\nu - p_W^\mu p_b^\nu - p_b^\mu p_W^\nu\Big\} + (1-\cos\theta)\frac{E_b}{m_t} g^{\mu\nu}[1 - \frac{D}{2} - \frac{m_t}{E_g}] + (D-4)g^{\mu\nu},
\end{aligned}
\tag{5.57}
$$

where $\epsilon^{\mu\nu\alpha\beta}$ is the antisymmetric Levi-Civita tensor and it determines the sign in the result of a Dirac trace of four gamma functions and γ_5. By convention $\epsilon^{0123} = 1$ and for every even permutation of $(0,1,2,3)$ the result of this tensor is 1 and for every odd permutation of $(0,1,2,3)$ the result is -1 and it is 0 if any index is repeated.

Now to calculate the transverse-plus, transverse-minus and longitudinal contributions of the helicity amplitude we need to know the four vectors p_t^μ, p_b^μ and p_g^μ in the top quark rest frame, shown in Fig.5.7.

With respect to the definition of θ_R as the angle between the emitting gluon and the b-quark, one has:

$$
\begin{aligned}
p_t^\mu &= (m_t; 0, 0, 0), \\
p_b^\mu &= (E_b; \frac{E_b E_g \sin\theta_R}{|\overrightarrow{p_W}|}, 0, -\frac{E_b(E_b + E_g\cos\theta_R)}{|\overrightarrow{p_W}|}), \\
p_g^\mu &= (E_g; -\frac{E_b E_g \sin\theta_R}{|\overrightarrow{p_W}|}, 0, -\frac{E_g(E_g + E_b\cos\theta_R)}{|\overrightarrow{p_W}|}),
\end{aligned}
\tag{5.58}
$$

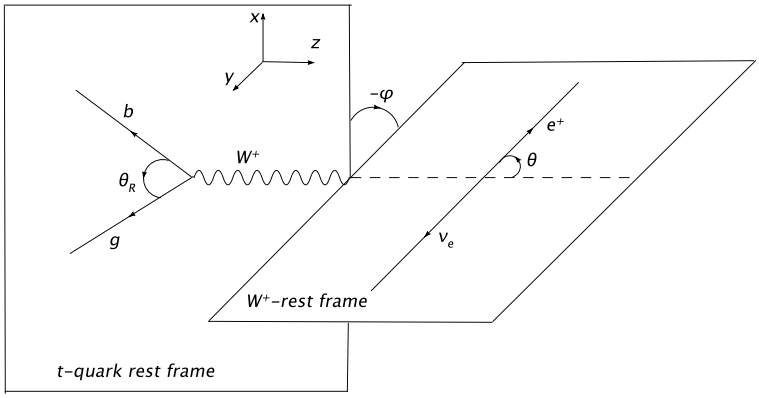

Figure 5.7: Definition of the top quark and the W^+-boson rest frames in NLO calculation.

where $\cos\theta_R = (m_t^2 - m_W^2 - 2m_t(E_b + E_g) + 2E_bE_g)/(2E_bE_g)$.

In the second approach, proposed in [91], to calculate the helicity contributions of the decay rate we use covariant projectors to work out the various helicity components of the W boson. It means, instead of the completeness relation:

$$\sum_{\lambda=0,\pm} \epsilon^{\mu}(\lambda)\epsilon^{\nu\star}(\lambda) = -g^{\mu\nu} + \frac{p_W^{\mu}p_W^{\nu}}{m_W^2}, \tag{5.59}$$

which we already used to calculate the unpolarized differential decay rate, now we use the following relations to extract the longitudinal, transverse-plus and transverse-minus helicities:

$$\begin{aligned}
\epsilon^{\mu}(0)\epsilon^{\nu\star}(0) &= \frac{\omega}{|\overrightarrow{P_W}|^2}\left(p_t^{\mu} - \frac{p_t\cdot p_W}{m_W^2}p_W^{\mu}\right)\left(p_t^{\nu} - \frac{p_t\cdot p_W}{m_W^2}p_W^{\nu}\right), \\
\epsilon^{\mu}(\pm)\epsilon^{\nu\star}(\pm) &= \\
&\frac{1}{2}\Big(- g^{\mu\nu} + \frac{p_W^{\mu}p_W^{\nu}}{m_W^2} - \frac{\omega}{|\overrightarrow{P_W}|^2}\left(p_t^{\mu} - \frac{p_t\cdot p_W}{m_W^2}p_W^{\mu}\right)\left(p_t^{\nu} - \frac{p_t\cdot p_W}{m_W^2}p_W^{\nu}\right) \mp \frac{i\epsilon^{\mu\nu\alpha\beta}}{m_t|\overrightarrow{P_W}|}(p_t)_{\alpha}(p_W)_{\beta}\Big),
\end{aligned} \tag{5.60}$$

where $\epsilon^{0123} = 1$ and $|\overrightarrow{P_W}|^2 = (m_t - E_b - E_g)^2 - m_W^2$.
Now we explain the details of the helicity contributions of the differential decay rate. Using Eqs.(5.53,5.55) we obtain:

$$\frac{1}{\Gamma_0'}\frac{d^2\Gamma^{Real}}{dx_b\ d\cos\theta} = H_{++}^{Real}\cdot\frac{3}{8}(1+\cos\theta)^2 + H_{--}^{Real}\cdot\frac{3}{8}(1-\cos\theta)^2 + H_{00}^{Real}\cdot\frac{3}{4}\sin^2\theta. \tag{5.61}$$

To work out the longitudinal helicity contribution, I used both approaches mentioned above and the results are exactly the same. After using Eq.(3.25,5.51) this result reads:

$$
\begin{aligned}
H_{00}^{Real} &= \frac{\alpha_S}{2\pi(1+2\omega)}C_F\Big\{\frac{\delta(1-x_b)}{\epsilon^2}+ \\
&\frac{1}{\epsilon}\Bigg(\delta(1-x_b)\big[1-\gamma_E-2\log(1-\omega)+\log\frac{4\pi\mu^2}{m_t^2}\big]-\frac{1+x_b^2}{(1-x_b)_+}\Bigg) \\
&+\delta(1-x_b)\Bigg(\frac{1}{2}\big[-\log\frac{4\pi\mu^2}{m_t^2}+2\log(1-\omega)+\gamma_E\big]^2-\gamma_E-\frac{2\omega}{1-\omega}\log\omega-\frac{3\omega}{1+2\omega} \\
&+2Li_2(1-\omega)+\log\frac{4\pi\mu^2}{m_t^2}-2\log(1-\omega)-\frac{\pi^2}{4}\Bigg)+2(1+x_b^2)\Bigg(\frac{\log(1-x_b)}{1-x_b}\Bigg)_+ + \\
&\frac{1}{(1-x_b)_+}\Bigg((1+x_b^2)\Bigg[2\log x_b-\log\frac{4\pi\mu^2}{m_t^2}+2\log(1-\omega)+\gamma_E\Bigg]+ \\
&2(1-\omega)x_b^3+\frac{8\omega^2-4\omega-3}{1+2\omega}x_b^2-2(1+\omega)x_b+\frac{1}{1+2\omega}\Bigg) \\
&-\frac{2x_b(1-x_b)(2-x_b(1-\omega))^2}{(1-\omega)x_b^2-4x_b+4}+\frac{2\sqrt{\omega}}{(\omega-1)((1-\omega)x_b^2-4x_b+4)^2}\Bigg(\\
&(1+\sqrt{\omega})^2(x_b(1-\sqrt{\omega})^2+2\sqrt{\omega})(x_b^2(1-\omega)+x_b(\sqrt{\omega}-3)+2)^2\log(1-x_b(1-\sqrt{\omega}))- \\
&(1-\sqrt{\omega})^2(x_b(1+\sqrt{\omega})^2-2\sqrt{\omega})(x_b^2(1-\omega)-x_b(\sqrt{\omega}+3)+2)^2\log|1-x_b(1+\sqrt{\omega})|\Bigg)\Big\}.
\end{aligned}
\tag{5.62}
$$

Our main aim is to calculate the angular distribution of the differential decay rate for the decay process $t\to X_b+W^+$ followed by $W^+\to e^++\nu_e$ with α_S corrections using fixed x_b. Therefore we define:

$$
\frac{1}{\Gamma_0'}\frac{d^2\hat{\Gamma}}{dx_b\ d\cos\theta}=\hat{H}_{++}\cdot\frac{3}{8}(1+\cos\theta)^2+\hat{H}_{--}\cdot\frac{3}{8}(1-\cos\theta)^2+\hat{H}_{00}\cdot\frac{3}{4}\sin^2\theta. \tag{5.63}
$$

For the contribution of the decay width into a longitudinal W^+-boson, we have to sum up Eq.(5.50) and Eq.(5.62). Therefore we obtain:

$$
\begin{aligned}
\hat{H}_{00} &= \frac{1}{1+2\omega}\delta(1-x_b)+ \\
&\frac{\alpha_S}{2\pi(1+2\omega)}C_F\Big\{(-\frac{1}{\epsilon}+\gamma_E-\log 4\pi)\Bigg(\frac{3}{2}\delta(1-x_b)+\frac{1+x_b^2}{(1-x_b)_+}\Bigg)+\hat{B}(x_b)\Big\},
\end{aligned}
\tag{5.64}
$$

where,

$$
\begin{aligned}
\hat{B}(x_b) \;=\; & \\
\delta(1-x_b)\Bigg(& -\frac{3}{2}\log\frac{\mu^2}{m_t^2} + 2\log\omega\log(1-\omega) + \frac{2\omega}{\omega-1}\log\omega + 4Li_2(1-\omega) - \frac{2\pi^2}{3} - 3\frac{2+5\omega}{1+2\omega}\Bigg) \\
& + \frac{1}{(1-x_b)_+}\Bigg((1+x_b^2)\big[2\log x_b - \log\frac{\mu^2}{m_t^2} + 2\log(1-\omega)\big] + 2(1-\omega)x_b^3 + \\
& \frac{8\omega^2-4\omega-3}{1+2\omega}x_b^2 - 2(1+\omega)x_b + \frac{1}{1+2\omega}\Bigg) + 2(1+x_b^2)\left(\frac{\log(1-x_b)}{1-x_b}\right)_+ \\
& - \frac{2x_b(1-x_b)(2-x_b(1-\omega))^2}{(1-\omega)x_b^2-4x_b+4} + \frac{2\sqrt{\omega}}{(\omega-1)((1-\omega)x_b^2-4x_b+4)^2}\Bigg(\\
& (1+\sqrt{\omega})^2(x_b(1-\sqrt{\omega})^2+2\sqrt{\omega})(x_b^2(1-\omega)+x_b(\sqrt{\omega}-3)+2)^2\log(1-x_b(1-\sqrt{\omega})) - \\
& (1-\sqrt{\omega})^2(x_b(1+\sqrt{\omega})^2-2\sqrt{\omega})(x_b^2(1-\omega)-x_b(\sqrt{\omega}+3)+2)^2\log|1-x_b(1+\sqrt{\omega})|\Bigg).
\end{aligned}
\tag{5.65}
$$

According to the explanation expressed in section 3.6, in order to get the $\overline{MS}$-subtracted coefficient function we shall have to subtract from Eq.(5.64) the $\mathcal{O}(\alpha_s)$ term multiplying the characteristic $\overline{MS}$ constant $(\frac{1}{\epsilon} - \gamma_E + \log 4\pi)$. The obtained result above after integrating over $x_b (0 \leq x_b \leq 1)$ can be compared with the result given in [91], see appendix G. To obtain the result above and to compare with the result given in [91] we used the following relations between the Spence Functions:

$$
\begin{aligned}
Li_2(x^2) &= 2\big(Li_2(x) + Li_2(-x)\big) \\
Li_2(1-x^2) &= \frac{\pi^2}{6} - Li_2(x^2) - 2\log x\log(1-x^2).
\end{aligned}
\tag{5.66}
$$

Now we use the second approach to calculate the transverse-minus component of the hadron tensor in the real gluon correction. Defining $R = \log(1+(S-1)x_b+\sqrt{S(Sx_b^2-2x_b+2)})$, $T = \log(-2S^2x_b^3+4Sx_b^2-(1+3S)x_b+1+|2Sx_b^2-2x_b+1|\sqrt{S(Sx_b^2-2x_b+2)})$ and $D = \log((1-S)x_b^2 - x_b + 1/2 + |2Sx_b^2-2x_b+1|/2)$ and also $M = \log(2S^2x_b^2 - S(1+2x_b) +$

$1 - S|2Sx_b^2 - 2x_b + 1|)$ where $S = (1-\omega)/2$, we obtain the following results:

$$
\begin{aligned}
H_{--}^{Real} \;=\; & \frac{\alpha_S\;\omega}{\pi(1+2\omega)} C_F \Bigg\{ \frac{\delta(1-x_b)}{\epsilon^2} + \\
& \frac{1}{\epsilon}\Bigg(\delta(1-x_b)\big[1-\gamma_E - 2\log(1-\omega) + \log\frac{4\pi\mu^2}{m_t^2}\big] - \frac{1+x_b^2}{(1-x_b)_+} \Bigg) \\
& + \delta(1-x_b)\Bigg(\frac{1}{2}\big[-\log\frac{4\pi\mu^2}{m_t^2} + 2\log(1-\omega) + \gamma_E\big]^2 + \frac{3}{4}(1-18\omega) - \\
& \gamma_E - \frac{2\omega}{1-\omega}\log\omega + \log\frac{4\pi\mu^2}{m_t^2} - 2\log(1-\omega) \\
& + 2Li_2(1-\omega) - \frac{\pi^2}{4} \Bigg) + (1+x_b^2+2x_b^3)\Bigg(\frac{\log(1-x_b)}{1-x_b} \Bigg)_+ \\
& + \frac{1}{(1-x_b)_+}\Bigg((1+x_b^2)\Bigg[2\log x_b - \log\frac{4\pi\mu^2}{m_t^2} + 2\log(1-\omega) + \gamma_E \Bigg] - Dx_b^3 + \\
& \frac{x_b^3\sqrt{1-\omega}}{\sqrt{(1-\omega)x_b^2 - 4x_b + 4}}\big(T-R\big) \Bigg) \\
& + (\frac{1+\omega}{1-\omega} - x_b)\Bigg(\log(1-x_b(1-\omega)) - M + \log\omega \Bigg) + \\
& (-\frac{D}{2} + \log(1-x_b))\big(1 + x_b + 2x_b^2\big) + \frac{(x_b(1+\omega)-2)|(1-\omega)x_b^2 - 2x_b + 1|}{(1-x_b)(1-\omega)((\omega-1)x_b^2 + 4x_b - 4)} \\
& + \frac{1}{2(1-x_b)(1+2\omega)((1-\omega)x_b^2 - 4x_b + 4)(1-x_b(1-\omega))}\Bigg(-(1-2\omega)(1-\omega)^2 x_b^5 \\
& + (\omega-1)(4\omega^2 + 12\omega - 5)x_b^4 - (10\omega^3 - 21\omega^2 - 2\omega + 21)x_b^3 + \\
& (-66\omega^2 + 75\omega + 47)x_b^2 + 2\frac{20\omega^3 - 80\omega^2 + 31\omega + 23}{\omega - 1}x_b + 4\frac{14\omega^2 - 7\omega - 4}{\omega - 1} \Bigg) + \\
& \frac{1}{2\sqrt{\omega}(\omega-1)((1-\omega)x_b^2 - 4x_b + 4)^2}\Bigg(\\
& (1-\sqrt{\omega})^2(x_b(1+\sqrt{\omega})^2 - 2\sqrt{\omega})(x_b^2(1-\omega) - x_b(\sqrt{\omega}+3) + 2)^2 \log|1 - x_b(1+\sqrt{\omega})| - \\
& (1+\sqrt{\omega})^2(x_b(1-\sqrt{\omega})^2 + 2\sqrt{\omega})(x_b^2(1-\omega) + x_b(\sqrt{\omega}-3) + 2)^2 \log(1 - x_b(1-\sqrt{\omega})) \Bigg) \\
& + \frac{R-T}{2(((1-\omega)x_b^2 - 4x_b + 4)(1-\omega))^{\frac{3}{2}}} \times \\
& \Bigg((\omega-1)^3 x_b^4 + (\omega-3)(\omega-1)^2 x_b^3 + 2(\omega-13)(\omega-1)x_b^2 - 4(\omega^2 - 8\omega + 9)x_b + 8 \Bigg) \Bigg\}.
\end{aligned}
\tag{5.67}
$$

After summing up Eq.(5.50) and Eq.(5.67) for the transverse-minus helicity rates we obtain:

$$\begin{aligned}\hat{H}_{--} &= \frac{2\omega}{1+2\omega}\delta(1-x_b)+\\ &\frac{\alpha_S\omega}{\pi(1+2\omega)}C_F\Big\{(-\frac{1}{\epsilon}+\gamma_E-\log 4\pi)\Big(\frac{3}{2}\delta(1-x_b)+\frac{1+x_b^2}{(1-x_b)_+}\Big)+\frac{\hat{C}(x_b)}{2}\Big\},\end{aligned} \tag{5.68}$$

where,

$$\begin{aligned}\hat{C}(x_b) &= \delta(1-x_b)\Big(-\frac{3(7+18\omega)}{2(1+2\omega)}-\frac{4\omega}{1-\omega}\log\omega-3\log\frac{\mu^2}{m_t^2}\\ &-\frac{2(1-\omega)}{\omega}\log(1-\omega)+4\log\omega\log(1-\omega)+8Li_2(1-\omega)-\frac{4\pi^2}{3}\Big)+\\ &+\frac{2}{(1-x_b)_+}\Big((1+x_b^2)\Big[2\log x_b-\log\frac{\mu^2}{m_t^2}+2\log(1-\omega)\Big]-Dx_b^3+\\ &\frac{x_b^3\sqrt{1-\omega}}{\sqrt{(1-\omega)x_b^2-4x_b+4}}\big(T-R\big)\Big)+2(1+x_b^2+2x_b^3)\Big(\frac{\log(1-x_b)}{1-x_b}\Big)_+ +\\ &(-D+2\log(1-x_b))\big(1+x_b+2x_b^2\big)+2\frac{(x_b(1+\omega)-2)|(1-\omega)x_b^2-2x_b+1|}{(1-x_b)(1-\omega)((\omega-1)x_b^2+4x_b-4)}\\ &+2(\frac{1+\omega}{1-\omega}-x_b)\Big(\log(1-x_b(1-\omega))-M+\log\omega\Big)+\\ &+\frac{1}{(1-x_b)(1+2\omega)((1-\omega)x_b^2-4x_b+4)(1-x_b(1-\omega))}\Big(-(1-2\omega)(1-\omega)^2x_b^5\\ &+(\omega-1)(4\omega^2+12\omega-5)x_b^4-(10\omega^3-21\omega^2-2\omega+21)x_b^3+\\ &(-66\omega^2+75\omega+47)x_b^2+2\frac{20\omega^3-80\omega^2+31\omega+23}{\omega-1}x_b+4\frac{14\omega^2-7\omega-4}{\omega-1}\Big)+\\ &\frac{1}{\sqrt{\omega}(\omega-1)((1-\omega)x_b^2-4x_b+4)^2}\Big(\\ &(1-\sqrt{\omega})^2(x_b(1+\sqrt{\omega})^2-2\sqrt{\omega})(x_b^2(1-\omega)-x_b(\sqrt{\omega}+3)+2)^2\log|1-x_b(1+\sqrt{\omega})|-\\ &(1+\sqrt{\omega})^2(x_b(1-\sqrt{\omega})^2+2\sqrt{\omega})(x_b^2(1-\omega)+x_b(\sqrt{\omega}-3)+2)^2\log(1-x_b(1-\sqrt{\omega}))\Big)\\ &+\frac{R-T}{(((1-\omega)x_b^2-4x_b+4)(1-\omega))^{\frac{3}{2}}}\times\\ &\Big((\omega-1)^3x_b^4+(\omega-3)(\omega-1)^2x_b^3+2(\omega-13)(\omega-1)x_b^2-4(\omega^2-8\omega+9)x_b+8\Big).\end{aligned} \tag{5.69}$$

The obtained result above after integrating over x_b can be found in appendix G.

As it is seen in Eq.(5.50), the contribution of the transverse-plus helicity in the virtual

correction vanishes, but in the real gluon correction this contribution is no longer zero. We used the second approach to calculate this contribution as well. The result reads:

$$
\begin{aligned}
\hat{H}_{++} \;=\; & \\
& \frac{\alpha_S\omega}{2\pi(1+2\omega)}C_F\Big\{\frac{3}{2}\delta(1-x_b)+2(1+x_b^2-2x_b^3)\left(\frac{\log(1-x_b)}{1-x_b}\right)_+ \\
& +\frac{2}{(1-x_b)_+}\left(Dx_b^3+\frac{(R-T)\sqrt{1-\omega}x_b^3}{\sqrt{(1-\omega)x_b^2-4x_b+4}}\right)+(1+x_b+2x_b^2)(D-2\log(1-x_b)) \\
& +2(x_b-\frac{1+\omega}{1-\omega})\big(-M+\log(1-x_b(1-\omega))+\log\omega\big) \\
& +\frac{1}{(1-x_b)((1-\omega)x_b^2-4x_b+4)(1-x_b(1-\omega))}\Bigg((1-\omega)^2x_b^5+ \\
& (1-\omega)(2\omega-9)x_b^4+3(\omega-7)(\omega-1)x_b^3-\frac{27\omega^2-46\omega+19}{1-\omega}x_b^2 \\
& +2\frac{6\omega^2-11\omega+3}{1-\omega}x_b+4\frac{\omega}{1-\omega}\Bigg)-2\frac{(x_b(\omega+1)-2)|(1-\omega)x_b^2-2x_b+1|}{(1-x_b)(1-\omega)((\omega-1)x_b^2+4x_b-4)} \\
& +\frac{1}{\sqrt{\omega}(\omega-1)((1-\omega)x_b^2-4x_b+4)^2}\Bigg(\\
& (1-\sqrt{\omega})^2(x_b(1+\sqrt{\omega})^2-2\sqrt{\omega})(x_b^2(1-\omega)-x_b(\sqrt{\omega}+3)+2)^2\log|1-x_b(1+\sqrt{\omega})|- \\
& (1+\sqrt{\omega})^2(x_b(1-\sqrt{\omega})^2+2\sqrt{\omega})(x_b^2(1-\omega)+x_b(\sqrt{\omega}-3)+2)^2\log(1-x_b(1-\sqrt{\omega}))\Bigg) \\
& +\frac{T-R}{(((1-\omega)x_b^2-4x_b+4)(1-\omega))^{\frac{3}{2}}}\times \\
& \Big((\omega-1)^3x_b^4+(\omega-3)(\omega-1)^2x_b^3+2(\omega-13)(\omega-1)x_b^2-4(\omega^2-8\omega+9)x_b+8\Big)\Big\}.
\end{aligned}
\tag{5.70}
$$

These results are in agreement with [91] after integration over x_b, see appendix G.
In the calculations above, the factor $\overrightarrow{|p_W|}^{-n}(n=1,2,3)$ in the mean squared helicity amplitudes makes the phase space integration more difficult than in the unpolarized integration width and new classes of phase space integrals appear in our calculation. For example we have the three following terms in the squared helicity amplitude of the transverse-plus

component of the differential decay rate:

$$\frac{f(x_b)}{x_g^2\sqrt{(1-Sx_b-Sx_g)^2-\omega}},$$
$$\frac{g(x_b,x_g)}{(1-x_b-x_g)\sqrt{(1-Sx_b-Sx_g)^2-\omega}},$$
$$\frac{h(x_b)}{x_g(1-x_b-x_g)\sqrt{(1-Sx_b-Sx_g)^2-\omega}}, \tag{5.71}$$

where $f(x_b)=x_b^2$, $g(x_b,x_g)=S(8x_b^2+(D+2)x_bx_g+(D-2)x_g^2)/2$ and $h(x_b)=2Sx_b^3$. The first of the above terms includes the soft singularity (when $x_g\to 0$) and the second term includes the collinear singularity as we will explain in detail in the following. According to Eq.(A.3) and the definition of the b-quark and the gluon energy fraction:

$$\begin{aligned} x_b &= \frac{2E_b}{m_t(1-\omega)} \\ x_g &= \frac{2E_g}{m_t(1-\omega)}, \end{aligned}$$

we obtain: $\cos\theta=(1-x_b-x_g+2Sx_bx_g)/(2Sx_bx_g)$ thus $1-\cos\theta\propto 1-x_b-x_g$, so that if $\theta\to 0$ then $x_g\to 1-x_b$. Therefore in the second of the above terms when $x_g\to 1-x_b$ the collinear singularities will appear. The third of the above terms includes both singularities. To obtain the contribution of the real gluon correction in the total differential decay width and to extract all the singularities we have to use the D-dimensional phase space integration (Eq.(3.30)) replacing the terms above in $\overline{|M^R|^2}$ in Eq.(3.30). But the problem is the solution of these integrals is very difficult and we could not find a suitable software to calculate these phase spaces integrals. For this reason we used a trick to work out these integrals. At first we turn our attention to the first of the terms (5.71). The 4-dimensional integral over $x_g(\propto E_g)$ of this term is divergent because of the factor $1/x_g^2$. Now our trick is to subtract an add the term:

$$\frac{f(x_b)}{x_g^2\sqrt{(1-Sx_b)^2-\omega}},$$

to Eq.(5.71), i.e.:

$$\frac{f(x_b)}{x_g^2\sqrt{(1-Sx_b-Sx_g)^2-\omega}} = \left[\frac{f(x_b)}{x_g^2\sqrt{(1-Sx_b-Sx_g)^2-\omega}}-\frac{f(x_b)}{x_g^2\sqrt{(1-Sx_b)^2-\omega}}\right]_{D=4}+\left.\frac{f(x_b)}{x_g^2\sqrt{(1-Sx_b)^2-\omega}}\right|_{D\neq 4}. \tag{5.72}$$

Then the squared bracket is free of soft singularities and it can be calculated in 4 dimensions. This point can be understood by expanding this difference in x_g and it will be obvious that the result is free of $1/x_g^2$, so that this difference can be calculated in 4 dimensions. The second term in (5.72) can now be solved in D dimensional phase space by using Mathematica and it gives us all correct singularities.

Now we turn our attention to the second term in Eq.(5.71). If we use the four dimensional phase space for these terms of the squared amplitude, these terms diverge logarithmically when integrating over x_g in the limit $x_g \to 1 - x_b$. For these terms we subtract and add the following term:

$$\frac{g(x_b, x_g)}{(1 - x_b - x_g)\sqrt{(1-S)^2 - \omega}},$$

to the main term. Therefore their difference (the first bracket in Eq.(5.73)) is free of collinear singularities and it can be considered in 4-dimensions but the remaining term in Eq.(5.73) must be solved in D dimensional phase space:

$$\begin{aligned}\frac{g(x_b, x_g)}{(1 - x_b - x_g)\sqrt{(1 - Sx_b - Sx_g)^2 - \omega}} \quad &= \\ \left[\frac{g(x_b, x_g)}{(1 - x_b - x_g)\sqrt{(1 - Sx_b - Sx_g)^2 - \omega}} \quad - \quad \frac{g(x_b, x_g)}{(1 - x_b - x_g)\sqrt{(1-S)^2 - \omega}}\right]_{D=4} &+ \\ \left.\frac{g(x_b, x_g)}{(1 - x_b - x_g)\sqrt{(1-S)^2 - \omega}}\right|_{D\neq 4} &.\end{aligned} \tag{5.73}$$

For the third term in Eq.(5.71), at first we decompose it in the following form:

$$\begin{aligned}\frac{h(x_b)}{x_g(1 - x_b - x_g)\sqrt{(1 - Sx_b - Sx_g)^2 - \omega}} \quad &= \\ \frac{1}{1 - x_b}\left(\frac{1}{x_g} + \frac{1}{1 - x_b - x_g}\right)&\frac{h(x_b)}{\sqrt{(1 - Sx_b - Sx_g)^2 - \omega}},\end{aligned}$$

and we then use the previous tricks to extract all singularities and to work out the finite terms. This term creates the singularity proportional to $\propto 1/\epsilon^2$.

5.4 Angular Decay Distribution for $t \to b + W^+(\to e^+ + \nu_e)$ at NLO Using Fixed x_g

To study the angular decay distribution of the cascade decay of the top quark ($t \to b + W^+(\to e^+ + \nu_e)$) precisely, we have to specify the angular differential width for the production of a gluon in the top quark decay with the scaled energy fraction of the gluon (x_g). To calculate these contributions we start with the phase space integral given in Eq.(3.42) using the b-quark energy range given in Eq.(3.43). As we explained in section 3.7, when the momentum of the real gluon is fixed there will be no soft singularity and in conclusion there will be no the plus description in our result, because these terms arise after integration over the real gluon phase space.

Now we intend to calculate the angular distribution of the differential decay rate for the cascade decay of the top quark with α_s corrections using fixed x_g. As before, we define:

$$\frac{1}{\Gamma_0'}\frac{d^2\hat{\Gamma}}{dx_g\; d\cos\theta} = \hat{I}_{++}\cdot\frac{3}{8}(1+\cos\theta)^2 + \hat{I}_{--}\cdot\frac{3}{8}(1-\cos\theta)^2 + \hat{I}_{00}\cdot\frac{3}{4}\sin^2\theta, \tag{5.74}$$

and to work out the helicity contributions we apply the approach explained in the previous section. Therefore for the longitudinal helicity contribution in the total decay width we have:

$$\hat{I}_{00} = \frac{\alpha_s}{2\pi(1+2\omega)}C_F\Big\{\frac{1+(1-x_g)^2}{x_g}\Big(-\frac{1}{\epsilon}+\gamma_E-\log 4\pi\Big)+\hat{B}_1(x_g)\Big\}, \tag{5.75}$$

where,

$$\begin{aligned}
\hat{B}_1(x_g) \;=\; & \frac{1+(1-x_g)^2}{x_g}\Big(-\log\frac{\mu^2}{m_t^2}+2\log x_g+2\log(1-x_g)+2\log(1-\omega)\Big)\\
&+\frac{2\sqrt{\omega}}{x_g^2(1-\omega)^3}\Big((x_g(\sqrt{\omega}-1)+1)^2(x_g(\sqrt{\omega}-1)^2-2)(1+\sqrt{\omega})^4\log(1-x_g(1-\sqrt{\omega}))\\
&-(x_g(\sqrt{\omega}+1)-1)^2(x_g(\sqrt{\omega}+1)^2-2)(1-\sqrt{\omega})^4\log|1-x_g(1+\sqrt{\omega})|\Big)\\
&+\frac{1}{2(1+2\omega)(1-(1-\omega)x_g)^2}\Big(-(1-\omega)^2(1+6\omega)x_g^3+2(1-\omega)(6\omega^2+19\omega+3)x_g^2\\
&-(-18\omega^3+15\omega^2+84\omega+13)x_g+4\frac{8\omega^3+2\omega^2-19\omega-3}{\omega-1}+4\frac{4\omega^2+7\omega+1}{x_g(\omega-1)}\Big)-\\
&\log(1-(1-\omega)x_g)\Big(x_g+2\frac{(2\omega^2-5\omega-1)}{1-\omega}+\frac{6\omega^2+24\omega+2}{x_g(1-\omega)^2}+16\frac{\omega(1+\omega)}{x_g^2(\omega-1)^3}\Big).
\end{aligned} \tag{5.76}$$

In order to obtain the the $\overline{MS}$-subtracted coefficient function we have to subtract from Eq.(5.75) the $\mathcal{O}(\alpha_s)$ term multiplying the characteristic $\overline{MS}$ constant $(\frac{1}{\epsilon} - \gamma_E + \log 4\pi)$. Considering $S = (1-\omega)/2$ and by defining $N = \log((1-S)x_g^2 - x_g + |2Sx_g^2 - 2x_g + 1|/2 + 1/2)$ and $F = \log(2S^2x_g^2 - S(1+2x_g) - S|2Sx_g^2 - 2x_g + 1| + 1)$, for the transverse-minus helicity contribution we have:

$$\hat{I}_{--} = \frac{\alpha_s \omega}{\pi(1+2\omega)} C_F \Big\{ \frac{1+(1-x_g)^2}{x_g} \Big(-\frac{1}{\epsilon} + \gamma_E - \log 4\pi \Big) + \hat{B}_2(x_g) \Big\}, \tag{5.77}$$

where,

$$\begin{aligned}
\hat{B}_2(x_g) \;=\; & \frac{1+(1-x_g)^2}{x_g} \Bigg(-\log\frac{\mu^2}{m_t^2} + 2\log x_g + 2\log(1-x_g) + 2\log(1-\omega) \\
& -\frac{N}{2} + 2\frac{1+\omega}{1+2\omega} \Bigg) - \frac{F}{2} \Big(x_g - \frac{2}{1-\omega} - 2\frac{\omega^2-3\omega-1}{x_g(1-\omega)^2} + 8\frac{\omega}{x_g^2(\omega-1)^3} \Big) \\
& + \frac{1}{2x_g^2(1-\omega)^3\sqrt{\omega}} \Bigg((x_g(\sqrt{\omega}+1)-1)^2 (x_g(\sqrt{\omega}+1)^2 - 2)(1-\sqrt{\omega})^4 \log|1 - x_g(1+\sqrt{\omega})| \\
& -(x_g(\sqrt{\omega}-1)+1)^2 (x_g(\sqrt{\omega}-1)^2 - 2)(1+\sqrt{\omega})^4 \log(1 - x_g(1-\sqrt{\omega})) \Bigg) + \\
& \Big(\frac{x_g}{2} + \frac{1}{\omega-1} - \frac{\omega^2-3\omega-1}{x_g(1-\omega)^2} + 4\frac{\omega}{x_g^2(\omega-1)^3} \Big) \log\omega + \\
& \Big(\frac{3}{\omega-1} + \frac{-2\omega^2+6\omega+7}{x_g(1-\omega)^2} + 4\frac{1+2\omega}{x_g^2(\omega-1)^3} \Big) \log(1-(1-\omega)x_g) + \\
& \frac{|(1-\omega)x_g^2 - 2x_g + 1|}{4(1-(1-\omega)x_g)^2} \Bigg(-(1-\omega)x_g + 2(\omega+2) - 7\frac{1+\omega}{x_g(1-\omega)} + 4\frac{1+\omega}{x_g^2(1-\omega)^2} \Bigg) - \\
& \frac{1}{4(1-(1-\omega)x_g)^2} \Bigg((1-\omega)^2 x_g^3 + 2(1-\omega)(7\omega-5)x_g^2 + 2(9\omega^2 - 27\omega + 11)x_g + \\
& 2\frac{-21\omega^2+32\omega-7}{1-\omega} - 3\frac{9\omega+1}{x_g(1-\omega)} + 4\frac{1+\omega}{x_g^2(1-\omega)^2} \Bigg).
\end{aligned} \tag{5.78}$$

The new logarithms N and F which we used in the obtained result above are the same as the logarithms D and M which we defined in the previous section, respectively, but the variable x_b is now replaced by x_g.

For the transverse-plus helicity contribution we also obtain:

$$\begin{aligned}
\hat{I}_{++} &= \frac{\alpha_s\omega}{\pi(1+2\omega)}C_F\Big\{\frac{F}{2}\big(x_g-\frac{2}{1-\omega}-2\frac{\omega^2-3\omega-1}{x_g(1-\omega)^2}+8\frac{\omega}{x_g^2(\omega-1)^3}\big)\\
&+\frac{1}{2x_g^2(1-\omega)^3\sqrt{\omega}}\Big((x_g(\sqrt{\omega}+1)-1)^2(x_g(\sqrt{\omega}+1)^2-2)(1-\sqrt{\omega})^4\log|1-x_g(1+\sqrt{\omega})|\\
&\quad-(x_g(\sqrt{\omega}-1)+1)^2(x_g(\sqrt{\omega}-1)^2-2)(1+\sqrt{\omega})^4\log(1-x_g(1-\sqrt{\omega}))\Big)-\\
&\quad\big(\frac{x_g}{2}+\frac{1}{\omega-1}-\frac{\omega^2-3\omega-1}{x_g(1-\omega)^2}+4\frac{\omega}{x_g^2(\omega-1)^3}\big)\log\omega+\frac{1+(1-x_g)^2}{2x_g}N+\\
&\quad\big(-x_g-\frac{1}{1-\omega}+\frac{5}{x_g(1-\omega)^2}+\frac{4}{x_g^2(\omega-1)^3}\big)\log(1-(1-\omega)x_g)\\
&\quad-\frac{|(1-\omega)x_g^2-2x_g+1|}{4(1-(1-\omega)x_g)^2}\Big(-(1-\omega)x_g+2(\omega+2)-7\frac{1+\omega}{x_g(1-\omega)}+4\frac{1+\omega}{x_g^2(1-\omega)^2}\Big)\\
&\quad+\frac{1}{4(1-(1-\omega)x_g)^2}\Big(3(1-\omega)^2x_g^3-2(1-\omega)(7-\omega)x_g^2+2(2\omega^2-5\omega+12)x_g+\\
&\quad2\frac{-5\omega^2+8\omega-7}{1-\omega}-\frac{11\omega+3}{x_g(1-\omega)}+4\frac{1+\omega}{x_g^2(1-\omega)^2}\Big)\Big\}.
\end{aligned}\tag{5.79}$$

It is simple to show that after integrating over $\cos\theta$ in Eq.(5.74) we will obtain Eq.(3.46). As we pointed out, in the calculations above we only deal with the collinear singularities and to extract these singularities we have to work at D-dimensions like before. In calculation of the transverse-plus and the transverse-minus helicity contributions the phase space integrals include terms like the second term given in Eq.(5.71) which are not calculable simply. Therefore we used the trick which was explained in the last part of the previous section. In the next section we will study the numerical results for the helicity contributions of the top quark decay width and we shall make some predictions about the energy distribution of the B-hadron produced in each helicity of the W^+-boson in the top quark decay.

5.5 Numerical Results

In the last two sections we calculated the angular distribution of the differential decay width to produce a b-quark or a gluon in the cascade decay process $t\to b+W^+(\to e^++\nu_e)$. In Eqs.(5.63,5.74) we showed that the differential decay widths can be written in the following

forms:

$$\frac{1}{\Gamma_0'}\frac{d^2\hat{\Gamma}}{dx_b\ d\cos\theta} = \hat{H}_{++}\cdot\frac{3}{8}(1+\cos\theta)^2 + \hat{H}_{--}\cdot\frac{3}{8}(1-\cos\theta)^2 + \hat{H}_{00}\cdot\frac{3}{4}\sin^2\theta, \qquad (5.80)$$

and,

$$\frac{1}{\Gamma_0'}\frac{d^2\hat{\Gamma}}{dx_g\ d\cos\theta} = \hat{I}_{++}\cdot\frac{3}{8}(1+\cos\theta)^2 + \hat{I}_{--}\cdot\frac{3}{8}(1-\cos\theta)^2 + \hat{I}_{00}\cdot\frac{3}{4}\sin^2\theta, \qquad (5.81)$$

where $\hat{H}_{++}(\hat{I}_{+}), \hat{H}_{--}(\hat{I}_{--})$ and $\hat{H}_{00}(\hat{I}_{00})$ stand for the transverse-plus and the transverse-minus and the longitudinal helicity components of the differential decay rate, respectively. These components are given in Eqs(5.64,5.68,5.70,5.75,5.77,5.79). As we already defined, the angle θ denotes the polar angle between the W^+ momentum direction and the outgoing positron (see Fig.5.7). In our calculations the b-quark is considered a massless parton from the beginning.
It is simple to show that after integrating over $\cos\theta$ $(-1 \leq \cos\theta \leq 1)$ in Eq.(5.80) and Eq.(5.81) we obtain Eq.(3.38) and Eq.(3.46) where the W^+-boson was considered an unpolarized particle from the beginning.

Now we are in the situation to make predictions about the energy distribution of the B-hadron produced in each case of helicity of the W^+-boson in the top quark decay. To make the predictions we use the ZM-VFNS scheme which was explained in section 4.8.2. In Fig.5.8, considering the helicity components of the W^+-boson we depict the differential decay rate of inclusive B-hadron production in top decay at $\sqrt{s} = m_t$ using the Peterson model. As it is seen the contribution of the transverse-plus helicity is tiny and to make this more obvious we plot it in Fig.5.9. As we pointed out in section 5.2, assuming $m_b = 0$ from the beginning the contribution of the transverse-plus helicity of the W^+-boson in the differential decay rate is zero at the leading order (LO) calculation of the differential decay width. In Fig.5.8 we can also see that for each x_B the sum of the contributions of the individual helicity components of the W^+-boson is equal to the total value which we got from the calculation of unpolarized W^+-boson. In the following we will discuss numerical results for additional interesting quantities. As before, we set $m_t = 174$ GeV and $m_W = 80$ GeV and for the strong coupling constant we use $\alpha_s(m_t) = 0.1071$ which was evolved from

$\alpha_s(m_Z) = 0.1181$ (see section 2.1.4), therefore one has:

$$\begin{aligned}
\int_0^1 dx_b\ \hat{H}_{00} &= 0.635937, \\
\int_0^1 dx_b\ \hat{H}_{--} &= 0.277517, \\
\int_0^1 dx_b\ \hat{H}_{++} &= 0.000928,
\end{aligned} \tag{5.82}$$

see appendix G. Considering the above results, Eq.(5.80) after integrating over x_b can be written as:

$$F(\cos\theta) = \frac{1}{\Gamma_0'}\frac{d\hat{\Gamma}}{d\cos\theta} = 0.000348(1+\cos\theta)^2 + 0.104069(1-\cos\theta)^2 + 0.476953\sin^2\theta. \tag{5.83}$$

So that we can calculate the following quantities:

$$\begin{aligned}
\int_{-1}^1 d\cos\theta\ F(\cos\theta) &= 0.9143, \\
\int_{-1}^1 d\cos\theta\ F(\cos\theta)\cos\theta &= -0.1383, \\
\int_{-1}^1 d\cos\theta\ F(\cos\theta)\cos^2\theta &= 0.2386.
\end{aligned} \tag{5.84}$$

We close this discussion by stating that we have presented results on the $\mathcal{O}(\alpha_s)$ radiative corrections to the three helicity rates in unpolarized top quark decay which can be determined from doing an angular analysis on the decay products or from an analysis of the shape of the lepton spectrum. The radiative corrections to the unpolarized transverse-minus and longitudinal rates are sizable and the radiative correction to the transverse-plus rate is very small.

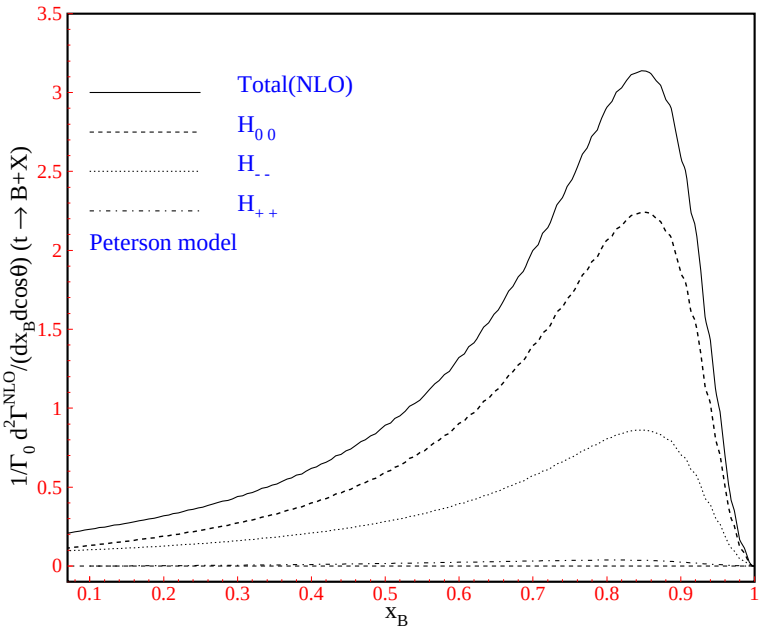

Figure 5.8: Comparison of the NLO contributions of the longitudinal and the transverse-minus and the transverse-plus helicity of the W^+-boson in the B-hadron energy distribution using the Peterson model. The solid line shows the summation of all helicity contributions. The initial factorization scale is $\mu_0 = 10.0$ GeV and the b-quark is considered to be massless.

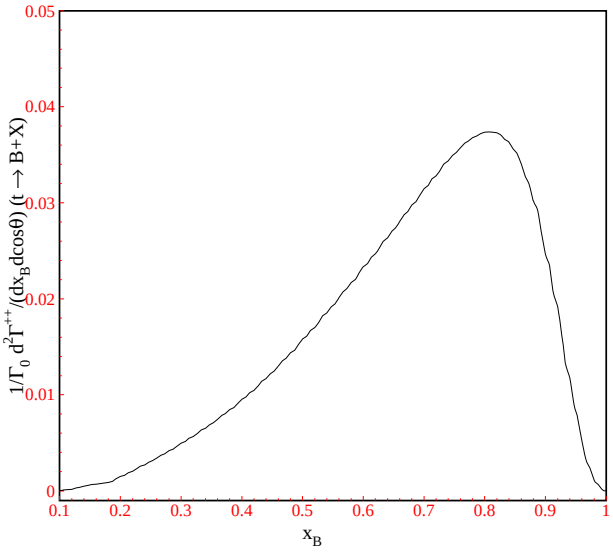

Figure 5.9: The NLO contributions of the transverse-plus helicity of the W^+-boson in the B-hadron energy distribution using the Peterson model.

Chapter 6

Summary and Conclusions

To perform accurate studies of the top-quark properties and a precise measurement of its mass at the Tevatron accelerator and, in future, at the LHC and at the Linear Collider, a reliable description of the b-quark fragmentation in top quark decay, $t \to bW$, will be necessary. As shown in [94], the b-fragmentation is one of the sources of uncertainty in the top mass measurement at the Tevatron.

In this work we calculated the normalized differential decay rate of production of a b-quark in top decay ($\frac{1}{\Gamma_0}\frac{d\Gamma}{dx_b}$). It can be observed that one has:

$$\frac{1}{\sigma}\frac{d\sigma}{dx_b} = \frac{1}{\Gamma}\frac{d\Gamma}{dx_b} \ ,$$

where $\frac{1}{\sigma}\frac{d\sigma}{dx_b}$ is the normalized differential cross-section for the production of a b quark with energy fraction x_b from decay of t-quarks, independently of the production mechanism. Our result will then be applicable to $p\overline{p}$ (Tevatron), pp (LHC) or e^-e^+ (Linear Colider) collisions.

In this thesis, at first, we discussed the b-quark fragmentation in top decay in NLO QCD using the perturbative fragmentation method, which resums large logarithms $\sim \log(\frac{m_t^2}{m_b^2})$ appearing in the fixed-order massive calculation. We compared the NLO differential decay rate of top decay with respect to the energy fraction of b-quark (x_b) for a massless b- and a massive b-quark, but neglecting contributions proportional to powers of the ratio $\frac{m_b}{m_t}$. The obtained subtraction term from the difference of them is consistent with the expression of the initial condition for the b-quark perturbative FF, Eq.(4.30). We then compared the results for the distribution of the b-quark energy fraction both in the fixed-order approach and in the perturbative FF approach, see Fig.4.4. We found that the perturbative FF

approach has a remarkable effect on the parton level distribution, especially when x_b approaches unity.

In the next step we studied and made theoretical predictions for the energy distributions of b-flavored hadron in top decay using the two of most important hadronization models. We used the B-meson FFs [72, 85] fitted by the e^-e^+ data from ALEPH, OPAL and SLD in two different initial scales of factorization: $\mu_0 = m_b = 4.5$ GeV and $\mu_0 = 2m_b = 10$ GeV. According to the factorization theorem, the universality of the obtained B-meson FFs from e^-e^+ collision are guaranteed and we used them in the non-perturbative part of the hinted hadronization process.

In this work, we applied the QCD improved parton model within two distinct approaches, the ZM-VFNS and GM-VFNS. We used them and compared the results obtained from these schemes. In [72, 75], it is shown that the ZM-VFNS predictions are found to agree with the CDF data from Tevatron runs IA and I [96]. The necessary condition to use the ZM-VFNS is that the energy scale, separating perturbative hard scattering and non-perturbative fragmentation (final state factorization scale μ_F), should be sufficiently large in comparison with the b-quark mass. It was really in our calculation ($m_t \gg m_b$). We also obtained the $b \to B$ branching fraction and the average energy fraction that the B meson receives from the b quark using the S and P models within the different initial scales. The results are approximately same and they are in good agreement with experimental data as we expect. The results should be independent of the chosen initial scales. It will be interesting to use the present approach to perform predictions of other observable relying on the b-fragmentation in top decay, such as invariant mass distribution used in [95] to fit the top mass value. We also made the theoretical predictions to produce some other hadrons such as: $\pi^{\pm}, p/\overline{p}$ and $K^{\pm}$ in fragmenting the b-quark obtained in top quark decay where we applied the AKK [87] extraction of fragmentation functions for $\pi^{\pm}, p/\overline{p}$ and $K^{\pm}$ particles at NLO. We also investigated the B-hadron mass effect on the energy distribution of the B-hadron using the improved factorization formula.

In the last chapter we studied the helicity contributions of W^+-boson in the top quark decay. We showed that the contribution of the transverse-plus helicity of the W^+-boson is negligible in the top quark decay and most produced charged leptons in the W^+-boson decay are due to a W^+-boson with a longitudinal or transverse-minus helicity. We also made the theoretical prediction for the energy distributions of b-flavored hadron in unpolarized top decay considering the polarized W^+-boson. It will be interesting to study these

contributions in NNLO QCD.

Appendix A

Phase Space for Top Decay at NLO

In this appendix we intend to explain about the differential decay rate formula of the three particles top decay ($t \to bWg$) in D space-time dimensions. The mass of interacting particles are labeled by m_W, m_t and m_b for the W^+-boson, t- and b-quark.
For the real correction contributions to the differential decay rate ($d\Gamma^R$), one has:

$$\begin{aligned} d\Gamma^R &= \frac{\mu^{2(4-D)}}{2m_t}\frac{d^{D-1}\mathbf{p}_W}{(2\pi)^{D-1}2E_W}\frac{d^{D-1}\mathbf{p}_g}{(2\pi)^{D-1}2E_g}\frac{d^{D-1}\mathbf{p}_b}{(2\pi)^{D-1}2E_b} \\ &\quad (2\pi)^D\delta^D(p_t - p_W - p_g - p_b) \times \overline{|M^R|^2} \\ &= \frac{\mu^{2(4-D)}}{2m_t}\overline{|M^R|^2}dPS(p_t, p_b, p_g, p_W), \end{aligned} \tag{A.1}$$

where the matrix element $\overline{|M^R|}^2$ is given in Eqs.(3.27,3.29,3.32,3.35) and the phase space element dPS is defined as:

$$dPS = \frac{d^{D-1}\mathbf{p}_W}{(2\pi)^{D-1}2E_W}\frac{d^{D-1}\mathbf{p}_g}{(2\pi)^{D-1}2E_g}\frac{d^{D-1}\mathbf{p}_b}{(2\pi)^{D-1}2E_b}(2\pi)^D\delta^D(p_t - p_W - p_g - p_b).$$

To simplify our calculations, we choose the p_t-rest frame where $\overrightarrow{p} = 0$. We also select the Z-axis in the direction of the momentum vector of the b-quark ($\overrightarrow{p_b}$). Considering the massless b-quark the momentum vectors of incoming and outgoing particles in D-dimensions wil be:

$$p_t^\mu = (m_t, \vec{0}) = (m_t, 0, 0, \cdots, 0) \qquad p_b^\mu = (E_b, 0, 0, \cdots, E_b) \qquad p_W^\mu = (E_W, \overrightarrow{p_W})$$

$$p_g^\mu = (E_g, 0, 0, \cdots, E_g \sin\theta_{gb} \sin\phi_{gb}, E_g \sin\theta_{gb} \cos\phi_{gb}, Eg \cos\theta_{gb}),$$

where $|\overrightarrow{p_b}| = E_b$ and $|\overrightarrow{p_g}| = E_g$ and θ_{gb} is the scattering angle between the gluon and the b-quark, from now on we denote as θ.

In D-dimension we can also write:

$$d^{D-1}\mathbf{p}_g = |\overrightarrow{p_g}|^{D-2} d|\overrightarrow{p_g}| d\Omega_g \quad \text{where} \quad d\Omega_g = \frac{2\pi^{D/2-1}}{\Gamma[D/2-1]} \sin^{D-3}\theta d\theta,$$

$$d^{D-1}\mathbf{p}_b = |\overrightarrow{p_b}|^{D-2} d|\overrightarrow{p_b}| d\Omega_b \quad \text{where} \quad \int d\Omega_b = \frac{2\pi^{\frac{D-1}{2}}}{\Gamma[\frac{D-1}{2}]},$$

and

$$\int d^{D-1}\mathbf{p}_W \delta^D(p_t - p_W - p_b - p_g) = \delta(m_t - E_W - E_b - E_g).$$

Therefore the Phase Space element reads:

$$dPS = \frac{\pi^{\frac{3}{2}-D}}{2^{2D-2}} \frac{(E_g E_b)^{D-4}}{\Gamma[\frac{D}{2}-1]\Gamma[\frac{D-1}{2}]} \delta(\cos\theta - a) \sin^{D-3}\theta d\theta dE_g dE_b, \tag{A.2}$$

where,

$$a = \frac{2E_g E_b + m_t^2 - m_W^2 - 2m_t E_g - 2m_t E_b}{2E_g E_b}. \tag{A.3}$$

Therefore the differential decay rate for the three particle decay can be written as:

$$\begin{aligned} \frac{d\hat{\Gamma}}{dx_b} &= 2^{4-3D}\pi^{\frac{3}{2}-D}\mu^{2(4-D)} \int dE_g \; d\cos\theta \; \delta(\cos\theta - a) \frac{(1-\omega)^{D-3}}{\Gamma[\frac{D}{2}-1]\Gamma[\frac{D-1}{2}]} \\ &\quad \times (E_g m_t x_b)^{D-4} (1-\cos^2\theta)^{\frac{D-4}{2}} \times \overline{|M^R|^2}, \end{aligned} \tag{A.4}$$

where x_b is the normalized b-quark energy fraction as already defined in section 3.1.

Appendix B

Determination of energy variations range of b-quark and gluon in top decay

Kinematically a decay process $p \rightarrow p_1 + p_2 + p_3$ (Fig.B.1) depends on two independent variables. It can be also related by crossing to $2 \rightarrow 2$(e.g. $p + p_{\overline{1}} \rightarrow p_2 + p_3$) although in both considerations the number of invariant variables must be the same. Our main aim in this appendix is to determine values of these variables. To be obvious, at first we explain the notion of the invariant and non-invariant variables in the process $1 \rightarrow 3$.

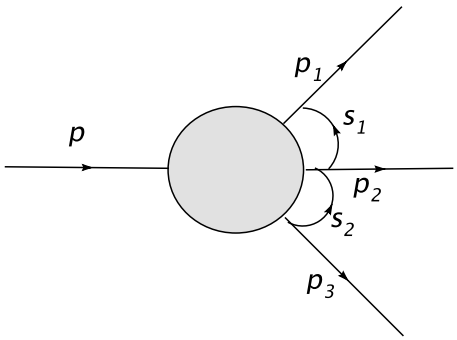

Figure B.1: Three-particle decay $p \rightarrow p_1 + p_2 + p_3$ with invariant variables S_1 and S_2

B.1 Invariant Variables

As in $2 \rightarrow 2$ scattering, it is suitable to choose s, t and u as invariant variables. This quantities are positive in the decay channel and we take the following form for them:

$$s_1 = (p_1 + p_2)^2 = (p - p_3)^2,$$

$$s_2 = (p_2 + p_3)^2 = (p - p_1)^2,$$

$$s_3 = (p_1 + p_3)^2 = (p - p_2)^2.$$

The value of these variables would be the same in each selected frame.

B.2 Non-invariant Variables

In the process $1 \rightarrow 3$ (Fig.B.1) non-invariant variables are three-momenta of outgoing particles and angels and the value of these variables depend on the chosen frame. To define these variables one has to specify a specific Lorentz frame. The convenient frame is the rest frame of the decaying system or overall CMS which is defined as the frame in which $\overrightarrow{p} = \overrightarrow{p_1} + \overrightarrow{p_2} + \overrightarrow{p_3} = 0$(Fig.B.2). To determine the non-invariant variables

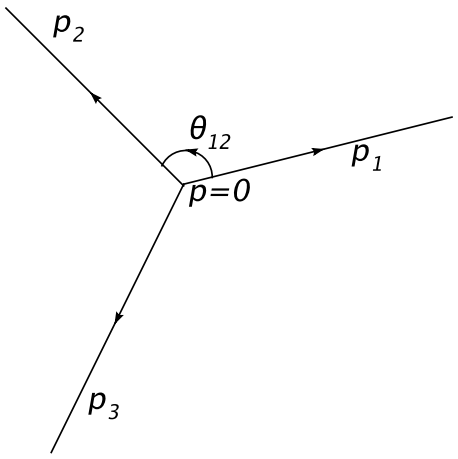

Figure B.2: Rest frame of the decaying system (p=0)

(three momenta) at first we have to specify the physical values of s_1 and s_2 (or s_3). To determine the values of s_1 and s_2 (and in conclusion p_1 and p_2) we apply the method

introduced in [61]. In this approach we consider the *basic four-particle kinematic function* $G(s_1, s_2, s, m_2^2, m_1^2, m_3^2)$(Nyborg, 1965a), with the following definition:

$$G(x,y,z,u,v,w) = x^2y+xy^2+z^2u+zu^2+v^2w+vw^2+xzw+xuv+vyz-wyz+yzw+yuw-$$

$$xy(z+u+w+v)-zu(x+y+v+w)-vw(x+y+z+u).$$

This function satisfies the following condition:

$$G(s_1, s_2, s, m_2^2, m_1^2, m_3^2) \leq 0.$$

To see more details refer to [61].
To determine the energy variations range of the gluon and the b-quark in the top decay we have to solve the equation above. Here we consider the special values of masses as we have in our calculation:

B.3 Two Masses Vanish

If we consider the massless b-quark in the top decay therefore in the p_t-rest frame we have to solve the following equation:

$$G(m_t^2 - 2m_tE_g, m_t^2 - 2m_tE_b, m_t^2, m_W^2, 0, 0) \leq 0,$$

where $s_1 = (p_t - p_g)^2$, $s_2 = (p_t - p_b)^2$ and $s = m_t^2$. After solving this equation in terms of E_b or E_g, we obtain:

$$\frac{m_t(1-\omega)(1-x_b)}{2} \leq E_g \leq \frac{m_t(1-\omega)(1-x_b)}{2(1-x_b(1-\omega))}$$

and

$$\frac{m_t(1-\omega)(1-x_g)}{2} \leq E_b \leq \frac{m_t(1-\omega)(1-x_g)}{2(1-x_g(1-\omega))}.$$

B.4 One Mass Vanishes

If we consider the massive b-quark in the top decay, therefore the *basic four-particle kinematic function* which has to be solved is:

$$G(m_t^2 - 2m_tE_g, m_t^2 + m_b^2 - 2m_tE_b, m_t^2, m_W^2, m_b^2, 0) \leq 0.$$

After solving this equation we obtain:

$$\frac{m_t S(1-x_b)(1-Sx_b-S\sqrt{x_b^2-\beta^2})}{1+b-2Sx_b} \leq E_g \leq \frac{m_t S(1-x_b)(1-Sx_b+S\sqrt{x_b^2-\beta^2})}{1+b-2Sx_b},$$

or in terms of E_b we have:

$$\frac{m_t S(1-x_g)}{1-2Sx_g}(1-Sx_g-Sx_g\sqrt{1-F\beta^2}) \leq E_b \leq \frac{m_t S(1-x_g)}{1-2Sx_g}(1-Sx_g+Sx_g\sqrt{1-F\beta^2}),$$

where: $F = \frac{(1-2Sx_g)}{(1-x_g)^2}$.

Appendix C

+-Description $\big[f(x)\big]_+$

The +-description of a function $f(x)$, which is singular at $x = 1$, is expressed by $\big[f(x)\big]_+$ and the definition of $\big[f(x)\big]_+$ is expressed by:

$$\int_0^1 dx g(x)\big[f(x)\big]_+ = \int_0^1 d\,x f(x)\big[g(x) - g(1)\big], \tag{C.1}$$

where g is a sufficiently regular function, consequently:

$$\int_0^1 dx\big[f(x)\big]_+ = 0. \tag{C.2}$$

We can also take the +-description of a function which is singular at $x = 0$. For example for the following functions:

$$\frac{1}{\big[x\big]_+} \qquad \textbf{and} \qquad \left[\frac{\log(x)}{x}\right]_+, \tag{C.3}$$

which are singular at x=0, according to Eq.(C.1) we can write:

$$\int_0^1 dx \frac{1}{[x]_+} g(x) = \int_0^1 dx \frac{\big[g(x) - g(0)\big]}{x}, \tag{C.4}$$

$$\int_0^1 dx \left[\frac{\log(x)}{x}\right]_+ g(x) = \int_0^1 dx \frac{\log(x)}{x}\big[g(x) - g(0)\big]. \tag{C.5}$$

The analytic form of the $+-$function is written as:

$$[f(x)]_+ = \lim_{\beta\to 0}\left[\int_0^1 dx f(x)\theta(1-\beta) + \delta(1-x-\beta)\int_0^\beta dy f(y)\right], \tag{C.6}$$

in which $\theta(x)$ is step function.
The +-descriptions which appear during the calculation of the real gluon corrections are:

$$\frac{1}{\big[1-x\big]_+} \qquad \textbf{and} \qquad \left[\frac{\log(1-x)}{1-x}\right]_+, \tag{C.7}$$

which have singularities at $x = 1$. Using Eq.(C.1) these forms can be written in the following normal form:

$$\int_0^1 dx \frac{1}{[1-x]_+} g(x) = \int_0^1 dx \frac{\big[g(x)-g(1)\big]}{1-x}, \tag{C.8}$$

and,

$$\int_0^1 dx \left[\frac{\log(1-x)}{1-x}\right]_+ g(x) = \int_0^1 dx \frac{\log(1-x)}{1-x}\big[g(x)-g(1)\big]. \tag{C.9}$$

The plus prescriptions are strictly distributions; for $x < 1$ they can be thought as the function itself, i.e.

$$[f(x)]_+ = f(x) \qquad for \quad x < 1. \tag{C.10}$$

Using Eq.(C.1), one can easily prove the following important distributional identities:

$$\begin{aligned}
[f(x)]_+ g(x) &= f(x)g(x) - (g(1)\int_0^1 f(y)dy)\delta(1-x), \\
[f(x)g(x)]_+ &= [f(x)]_+ g(x) - (\int_0^1 [f(y)]_+ g(y)dy)\delta(1-x), \\
[f(x)]_+ g(x) &= [f(x)]_+ g(1) + f(x)(g(x)-g(1)).
\end{aligned} \tag{C.11}$$

As an example, using the above relations, one can write the spiting function $P_{qq}^{(0)}(x)$ as:

$$P_{qq}^{(0)}(x) = C_F\big[\frac{1+x^2}{1-x}\big]_+ = C_F\big(\frac{2}{(1-x)_+} - (1+x) + \frac{3}{2}\delta(1-x)\big). \tag{C.12}$$

Sometimes, we encounter the integration range which is not from 0 to 1 but from an arbitrary $A < 1$ to 1. We introduce a more general +-description $[f(x)]_A$ and it satisfies:

$$\int_A^1 dx [f(x)]_A g(x) = \int_A^1 dx f(x)[g(x)-g(1)], \tag{C.13}$$

and,

$$\int_A^1 dx [f(x)]_A = 0. \tag{C.14}$$

Now we need to find out the relation between $[f(x)]_+$ and $[f(x)]_A$. Setting

$$[f(x)]_+ = [f(x)]_A + C\delta(1-x), \tag{C.15}$$

and keeping the principle integration formula Eq.(C.1),we can find out the relevant C. After some calculation we obtain a general formula for the coefficient C for a $[f(x)]_A$

$$C = -\int_0^A dy f(y). \tag{C.16}$$

An given example is the following functions:

$$\frac{1}{[1-x]_A} \quad \textbf{and} \quad \left[\frac{\log(1-x)}{1-x}\right]_A. \tag{C.17}$$

Applying Eqs.(C.15,C.16) or calculating the coefficient C directly keeping the principle integration, Eq.(C.1), we obtain the following formula:

$$\frac{1}{[1-x]_+} = \frac{1}{[1-x]_A} + \log(1-A)\delta(1-x), \tag{C.18}$$

$$\tag{C.19}$$

$$\left[\frac{\log(1-x)}{1-x}\right]_+ = \left[\frac{\log(1-x)}{1-x}\right]_A + \frac{1}{2}\log^2(1-A)\delta(1-x). \tag{C.20}$$

Appendix D

Calculation of Differential Decay Rate due to Real Corrections

In this appendix we want to explain about factors of singularities to differential decay rate and the contribution of the terms in the squared amplitude to the decay width. We consider two cases. Once the b-quark is considered to be a massless particle in the top decay process and in the other case the b-quark is considered as a massive particle from the beginning.

D.1 Massless b-Quark

To simplify our calculation in section 3.5, we classified the terms into $\overline{|M^R|^2}$ to the four groups. For the first type (Eq.(3.27)) we don't deal with any singularity and if we plug

these terms into Eq.(3.25) and integrate over E_g and $\cos\theta$ we obtain:

$$\frac{d\hat{\Gamma}^{Real,1}}{dx_b} = \frac{2^{8\epsilon}\pi^{4\epsilon-\frac{1}{2}}\mu^{2\epsilon}m_t^{1-4\epsilon}\alpha\alpha_s}{\sin^2\theta_w(1-x_b(1-\omega))^{-\epsilon}}\cdot\frac{(1-x_b)^{-2\epsilon}(1-\omega)^{-2\epsilon}}{\Gamma(1-2\epsilon)\Gamma(\frac{3}{2}-\epsilon)}$$
$$\times\Bigg\{\frac{2^{2\epsilon}\pi^{\frac{1}{2}}(1-\omega)^{-2\epsilon}\Gamma(1-2\epsilon)}{\Gamma(\frac{3}{2}-\epsilon)(1-x_b(1-\omega))^2}\cdot\Bigg[\frac{-x_b^{1-2\epsilon}}{96}(2\epsilon^2-\epsilon-1)(1-\omega)^3+\frac{x_b^{2-2\epsilon}}{192}\Bigg((4\epsilon^2-\epsilon-3)\omega^4$$
$$+(-20\epsilon^2+7\epsilon+17)\omega^3+(36\epsilon^2-16\epsilon-36)\omega^2+(-28\epsilon^2+16\epsilon+36)\omega+(8\epsilon^2-7\epsilon-17)$$
$$+\frac{1}{\omega}(\epsilon+3)\Bigg)+\frac{x_b^{3-2\epsilon}}{96}\Bigg((-2\epsilon^2+\epsilon+3)\omega^4+(8\epsilon^2-5\epsilon-15)\omega^3+(-12\epsilon^2+10\epsilon+30)\omega^2+$$
$$(8\epsilon^2-10\epsilon-30)\omega+(-2\epsilon^2+5\epsilon+15)-\frac{1}{\omega}(\epsilon+3)\Bigg)+\frac{x_b^{4-2\epsilon}}{192}(\epsilon+3)\frac{(1-\omega)^5}{\omega}\Bigg]+$$
$$\frac{(1-\omega)^2\Gamma(1-\epsilon)}{48}{}_2F_1[\epsilon,2\epsilon;1+\epsilon;1-x_b(1-\omega)]\Bigg[\frac{2x_b^2(1-\omega)}{\omega\epsilon}+x_b\big(-2\epsilon+\frac{1+4\omega}{\omega}-\frac{4}{\omega\epsilon}\big)$$
$$+2\epsilon-\frac{1+4\omega}{\omega}+\frac{1+2\omega}{\omega\epsilon}\big)\Bigg]+\frac{\Gamma(1-\epsilon)(1-\omega)^2}{12\omega(1+\epsilon)}{}_2F_1[\epsilon,1+2\epsilon;2+\epsilon;1-x_b(1-\omega)]\times$$
$$\Bigg[-(1-\omega)x_b^2+(2-\omega)x_b+1\Bigg]+\frac{\Gamma(1-2\epsilon)\Gamma(1+\epsilon)(1-\omega)^2}{48\omega(1-x_b(1-\omega))^\epsilon}\Bigg(-2(1-\omega)x_b^2(\frac{1}{\epsilon}-1)$$
$$-(2\omega+7)x_b+\frac{3x_b}{\epsilon}+2\epsilon\omega x_b-2\epsilon\omega-\frac{1+2\omega}{\epsilon}+4\omega+5\Bigg)\Bigg\}. \qquad \text{(D.1)}$$

Here we can expand the appeared Hypergeometric functions as:

$${}_2F_1[\epsilon,2\epsilon;1+\epsilon;1-x_b(1-\omega)]=1+\mathcal{O}(\epsilon^2),$$
$${}_2F_1[\epsilon,2\epsilon+1;2+\epsilon;1-x_b(1-\omega)]=1+\big(\frac{x_b(1-\omega)\log(x_b(1-\omega))}{1-x_b(1-\omega)}+1\big)\epsilon+\mathcal{O}(\epsilon^2).$$

For the second group (Eq.(3.29)) we obtain:

$$\frac{d\hat{\Gamma}^{Real,2}}{dx_b}=$$
$$\frac{2^{10\epsilon}\pi^{4\epsilon}\mu^{2\epsilon}m_t^{1-4\epsilon}\alpha\alpha_s}{192\omega\sin^2\theta_w(1-x_b(1-\omega))^{2-\epsilon}}\cdot\frac{(1-x_b)^{1-2\epsilon}(1-\omega)^{2-4\epsilon}}{\Gamma^2(\frac{3}{2}-\epsilon)}\times\Bigg\{(1-\omega)^3x_b^{3-2\epsilon}\big(\epsilon+\frac{4}{\epsilon}-5\big)$$
$$+(1-\omega)^2x_b^{2-2\epsilon}\big(4\omega\epsilon^2-(11\omega+5)\epsilon-\frac{2(2\omega+5)}{\epsilon}+11\omega+19\big)$$
$$+(1-\omega)x_b^{1-2\epsilon}\big(-12\omega\epsilon^2+2(15\omega+4)\epsilon-\frac{8(\omega+1)}{\epsilon}-2(13\omega+10)\big)$$
$$+x_b^{-2\epsilon}\big(8\omega\epsilon^2-4(1+5\omega)\epsilon-\frac{2(1+2\omega)}{\epsilon}+2(3+8\omega)\big)\Bigg\}. \qquad \text{(D.2)}$$

If we expand the result above in ϵ, we will have the collinear singularity which appears as the $\frac{1}{\epsilon}$-term in Eq.(3.31).
If we plug the group of third terms (Eg.(3.32)) into Eq.(3.25) we will have:

$$\frac{d\hat{\Gamma}^{Real,3}}{dx_b} =$$
$$\frac{2^{8\epsilon}\pi^{4\epsilon-\frac{1}{2}}\mu^{2\epsilon}m_t^{1-4\epsilon}\alpha\alpha_s}{24\omega\sin^2\theta_w}\cdot\frac{(1-\omega)^{1-2\epsilon}}{\Gamma(\frac{3}{2}-\epsilon)}\times\Bigg\{(1-x_b)^{-1-2\epsilon}\Bigg[\Bigg(x_b^3(1-\omega)^2-2x_b^2(1-\omega)(2-\omega)$$
$$+x_b(\omega+6)(1-\omega)+2\epsilon\omega(1-\omega)x_b+4\epsilon\omega-2(\omega+2)\Bigg)\Gamma(1+\epsilon)+\Bigg(-2x_b^3(1-\omega)^2$$
$$-2x_b^2(1-\omega)(2\omega-3)-2x_b(1-\omega)(4+\omega)+4\epsilon\omega(1-\omega)x_b-4\epsilon\omega$$
$$+2(2+\omega)\Bigg)\frac{\Gamma(1-\epsilon)(1-x_b(1-\omega))^\epsilon}{(1+\epsilon)\Gamma(1-2\epsilon)}{}_2F_1[\epsilon,1+2\epsilon;2+\epsilon;1-x_b(1-\omega)]\Bigg]$$
$$+(1-x_b)^{-2\epsilon}\Bigg[\Bigg(\frac{2x_b^2(1-\omega)^2}{\epsilon}+x_b(1-\omega)(2\omega-\frac{2+\omega}{\epsilon})\Bigg)\Gamma(1+\epsilon)+\Bigg(-\frac{2(1-\omega)x_b^2}{\epsilon}$$
$$+\frac{(\omega+2)x_b}{\epsilon}-2\omega x_b\Bigg)\frac{(1-\omega)\Gamma(1-\epsilon)(1-x_b(1-\omega))^\epsilon}{(1+\epsilon)\Gamma(1-2\epsilon)}{}_2F_1[\epsilon,2\epsilon;1+\epsilon;1-x_b(1-\omega)]\Bigg]\Bigg\}. \tag{D.3}$$

The obtained Hypergeometric functions can be expanded in ϵ as:

$$\begin{aligned}
{}_2F_1[\epsilon,1+2\epsilon;2+\epsilon;1-x_b(1-\omega)] &= 1+\epsilon\Big(\frac{x_b(1-\omega)\log(x_b(1-\omega))}{1-x_b(1-\omega)}+1\Big)+ \\
&\quad \frac{\epsilon^2\,x_b(1-\omega)}{1-x_b(1-\omega)}\Bigg(-\log^2(x_b(1-\omega))+\log(x_b(1-\omega))+ \\
&\quad \frac{2-x_b(1-\omega)}{x_b(1-\omega)}Li_2(1-x_b(1-\omega))\Bigg)+\mathcal{O}(\epsilon^3) \\
{}_2F_1[\epsilon,2\epsilon;1+\epsilon;1-x_b(1-\omega)] &= 1+2\epsilon^2Li_2(1-x_b(1-\omega))+\mathcal{O}(\epsilon^3).
\end{aligned}$$

Obviously, there are terms with the coefficient $(1-x_b)^{-1-2\epsilon}$. If we want to integrate over x_b, we will encounter a difficulty in the limit $x_b\to 1$. Thus, before integration over x_b we have to apply Eq.(3.33).
To close this discussion we plug the fourth group of terms into the equation for the differential decay rate and integrate over E_g. Therefore we have both the collinear and the soft

singularities and we obtain the following result:

$$\frac{d\hat{\Gamma}^{Real,4}}{dx_b} =$$
$$\frac{2^{8\epsilon}\pi^{4\epsilon-\frac{1}{2}}\mu^{2\epsilon}m_t^{1-4\epsilon}\alpha\alpha_s}{24\omega\sin^2\theta_w}\cdot\frac{(1-\omega)^{2-2\epsilon}}{\Gamma(\frac{3}{2}-\epsilon)}(1-x_b)^{-1-2\epsilon}\Bigg\{\Bigg(\frac{(1-\omega)x_b^3}{\epsilon}-\frac{(2+\omega)x_b^2}{\epsilon}+2\omega x_b^2\Bigg)\Gamma(1+\epsilon)$$
$$+\Bigg[(1-\omega)^{1-2\epsilon}\Bigg(-\frac{2(1-\omega)x_b^{3-2\epsilon}}{\epsilon}+(\frac{4-\omega}{\epsilon}-2\omega)x_b^{2-2\epsilon}+(-\frac{2+\omega}{\epsilon}+2\omega)x_b^{1-2\epsilon}\Bigg)+$$
$$\Bigg(-2(1-\omega)^2x_b^4+2(1-\omega)(3+\omega)x_b^3-4\omega(1-\omega)\epsilon x_b^3-2(2+\omega)x_b^2+4\omega\epsilon x_b^2\Bigg)\times$$
$$\frac{{}_2F_1[1+\epsilon,1+2\epsilon;2+\epsilon;1-x_b(1-\omega)]}{1+\epsilon}\Bigg]\frac{\Gamma(1-\epsilon)(1-x_b(1-\omega))^\epsilon}{\Gamma(1-2\epsilon)\Gamma(\frac{3}{2}-\epsilon)}\Bigg\}, \tag{D.4}$$

where the given Hypergeometric function can be expanded in ϵ as:

$${}_2F_1[1+\epsilon,1+2\epsilon;2+\epsilon;1-x_b(1-\omega)] = -\frac{\log(x_b(1-\omega))}{1-x_b(1-\omega)}+\frac{\epsilon}{1-x_b(1-\omega)}\Bigg(\log^2(x_b(1-\omega))$$
$$-\log(x_b(1-\omega))-Li_2(1-x_b(1-\omega))\Bigg)+\frac{\epsilon^2}{1-x_b(1-\omega)}\Bigg(-\frac{2\log^3(x_b(1-\omega))}{3}+$$
$$\log^2(x_b(1-\omega))\log(1-x_b(1-\omega))+\log^2(x_b(1-\omega))+2Li_2(1-x_b(1-\omega))\log(x_b(1-\omega))-$$
$$\frac{\pi^2\log(x_b(1-\omega))}{3}-Li_2(1-x_b(1-\omega))+Li_3(1-x_b(1-\omega))+2Li_3(x_b(1-\omega))-2\zeta(3)\Bigg)+\mathcal{O}(\epsilon^3).$$

This time all terms in Eq.(D.4) have the coefficient $(1-x_b)^{-1-2\epsilon}$ discussed before, which we have to treat like the term in the third group according to Eq.(3.33) and then expand them in ϵ.

D.2 Massive b-quark

As we already explained in section 4.2.3, when we consider the b-quark as a massive particle in the top quark decay the only singularities arise from the emission of the soft gluon. In this case we do not deal with the collinear singularities, this was why we classified the terms in $\overline{|M|^2}$ to two groups, section 4.2.3. The first group includes no factor of singularity, for this reason we would investigate them in 4-dimension phase space. But the terms in the second group (Eq.(4.23)) have the factor of E_g in their denominators. Therefore when $E_g \to 0$ (which corresponds to the limit $x_b \to 1$), the soft singularity appears. These singularities are obtained to replace the term $(1-x_b)^{-1-2\epsilon}$ by the +-function definition.

In the following we show them in detail.

$$\frac{d\tilde{\Gamma}^{Real,2}}{dx_b} = \frac{2^{4\epsilon-2}\pi^{2\epsilon-\frac{1}{2}}\mu^{4\epsilon}m_t^{1-4\epsilon}\alpha\alpha_s}{3\omega\sin^2\theta_w}\cdot\frac{S^{1-2\epsilon}(1+b-2Sx_b)^{\epsilon}}{\Gamma(\frac{3}{2}-\epsilon)}(1-x_b)^{-1-2\epsilon}\times$$
$$\big(2b(1-S)+S(2S(2-x_b)x_b+2\epsilon\omega-\omega-2)\big)\Bigg\{\big(\frac{4^{\epsilon}x_b\Gamma(\epsilon+\frac{1}{2})}{\sqrt{\pi}\epsilon}\big)\times$$
$$\Bigg(-(S(x_b-\sqrt{x_b^2-\beta^2})-1)^{-2\epsilon}\ {}_2F_1[2\epsilon,\epsilon;1+\epsilon;\frac{1-S(x_b+\sqrt{x_b^2-b^2})}{1+S(\sqrt{x_b^2-\beta^2}-x_b)}]+$$
$$(S(x_b+\sqrt{x_b^2-\beta^2})-1)^{-2\epsilon}\ {}_2F_1[2\epsilon,\epsilon;1+\epsilon;\frac{S(x_b-\sqrt{x_b^2-\beta^2})-1}{S(\sqrt{x_b^2-\beta^2}+x_b)-1}]$$
$$-(b+S(\sqrt{x_b^2-\beta^2}-x_b))^{-2\epsilon}\ {}_2F_1[2\epsilon,\epsilon;1+\epsilon;\frac{b-S(x_b+\sqrt{x_b^2-b^2})}{b+S(\sqrt{x_b^2-\beta^2}-x_b)}]+$$
$$(b-S(x_b+\sqrt{x_b^2-\beta^2}))^{-2\epsilon}\ {}_2F_1[2\epsilon,\epsilon;1+\epsilon;\frac{b-S(x_b-\sqrt{x_b^2-b^2})}{b-S(\sqrt{x_b^2-\beta^2}+x_b)}]\Bigg)+$$
$$\big(\frac{(1+b-2Sx_b)\Gamma(2+2\epsilon)}{S(1+2\epsilon)\Gamma(2+\epsilon)}\big)\times$$
$$\Bigg((S(x_b-\sqrt{x_b^2-\beta^2})-1)^{-2\epsilon-1}\ {}_2F_1[1+2\epsilon,\epsilon;2+\epsilon;\frac{1-S(x_b+\sqrt{x_b^2-b^2})}{1+S(\sqrt{x_b^2-\beta^2}-x_b)}]+$$
$$-(S(x_b+\sqrt{x_b^2-\beta^2})-1)^{-2\epsilon-1}\ {}_2F_1[1+2\epsilon,\epsilon;2+\epsilon;\frac{S(x_b-\sqrt{x_b^2-\beta^2})-1}{S(\sqrt{x_b^2-\beta^2}+x_b)-1}]+$$
$$-b(b+S(\sqrt{x_b^2-\beta^2}-x_b))^{-2\epsilon-1}\ {}_2F_1[1+2\epsilon,\epsilon;2+\epsilon;\frac{b-S(x_b+\sqrt{x_b^2-b^2})}{b+S(\sqrt{x_b^2-\beta^2}-x_b)}]+$$
$$b(b-S(x_b+\sqrt{x_b^2-\beta^2}))^{-2\epsilon-1}\ {}_2F_1[1+2\epsilon,\epsilon;2+\epsilon;\frac{b-S(x_b-\sqrt{x_b^2-b^2})}{b-S(\sqrt{x_b^2-\beta^2}+x_b)}]\Bigg)\Bigg\}. \quad \text{(D.5)}$$

After applying the definition of the new +-prescription defined in section 4.2.3, we expand them in ϵ and we obtain Eq.(4.24).

Appendix E

Factorization Theorem in Presence of Hadron Mass

An interesting aspect of calculating hadron production cross section is the effect of hadron mass. In this appendix we want to obtain the relevant factorization formula for these cases. Here we explain two different approaches and show that both yield the same results.

E.0.1 Light Cone Vectors Approach

In section 4.8.3, to calculate the energy distribution of the B-hadron in top decay we used the following factorization formula, which is true only in the case that the B-hadron and fragmenting parton are massless:

$$d\Gamma^{Had}(x_B, m_t, m_W, m_b) = \sum_{i=b,g} \int_{x_B}^{1} dz \; d\hat{\Gamma}_i(\frac{x_B}{z}, m_t, m_i, m_W, \mu^2) D_i^B(z, \mu^2), \tag{E.1}$$

in which the normalized variables were defined as: $z = \frac{2p_t.q}{s(1+b-\omega)}$ and $x_B = \frac{2p_t.p_B}{s(1+b-\omega)}$ with $s = m_t^2$ and q stands for the momentum of the partons(the b-quark and the real gluon in our calculation).
In top quark decay, choosing the top quark rest frame and taking the z-axis to be in the direction of the fragmenting parton, the momenta read:

$$p_t^\mu = (m_t, \overrightarrow{0}) \quad q^\mu = (q^0, 0, 0, q^0) \quad p_B^\mu = (p_B^0, 0, 0, p_B^0). \tag{E.2}$$

Now to incorporate the effects of the B-hadron mass it is useful to work with light cone coordinates, in which any 4-vectors V is written in the form $V^\mu = (V^+, V^-, \overrightarrow{V_T})$ with

$V^{\pm} = (1/\sqrt{2})(V^0 \pm V^3)$ and $\overrightarrow{V_T} = (V^1, V^2)$ instead of the normal four vectors $V^\mu = (V^0, V^1, V^2, V^3)$, [97]. In this new coordinates it can easily be verified that Lorentz invariant scalar products have the form:

$$\begin{aligned} V \cdot W &= V^+W^- + V^-W^+ - \overrightarrow{V_T} \cdot \overrightarrow{W_T} \\ V \cdot V &= 2V^+V^- - V_T^2. \end{aligned} \tag{E.3}$$

Therefore, in these coordinates the light cone four vectors of Eq.(E.2) read:

$$\begin{aligned} p_t^\mu &= (p_t^+, p_t^-, \overrightarrow{0}) = (\frac{m_t}{\sqrt{2}}, \frac{m_t}{\sqrt{2}}, \overrightarrow{0}) \\ q^\mu &= (q^+, 0, \overrightarrow{0}) = (\sqrt{2}\, q^0, 0, \overrightarrow{0}) \\ p_B^\mu &= (p_B^+, 0, \overrightarrow{0}) = (\sqrt{2}\, p_B^0, 0, \overrightarrow{0}), \end{aligned} \tag{E.4}$$

for example, $s = p_t^2 = 2p_t^+p_t^-$.

From now on, we use the light cone variables $\eta = 2p_t \cdot p_B/s = p_B^+/p_t^+$ and $k = 2p_t \cdot q/s = q^+/p_t^+$. For incorporating the effects of parton mass and the B-hadron mass the variable k and the scaling variable η are more convenient than z and x_B, respectively. Although in the absence of hadron mass and parton mass they are identical to x_B and z except for the coefficient $(1 + b - \omega)$ in the denominators of x_B and z. Now we verify the effects of hadron mass and parton mass in the differential decay rate of the top quark using the factorization formula.

In light cone coordinates the fundamental factorization formula reads:

$$d\Gamma^B(\eta, m_t, m_W, m_b) = \sum_i \int_\eta^1 dk\; d\Gamma_i(\frac{\eta}{k}, m_t, m_i, m_W, \mu^2) D_i^B(k, \mu^2), \tag{E.5}$$

where the variables η and k are defined in light cone coordinates. With $\eta = p_B^+/p_t^+$ and $y = \eta/k = p_B^+/q^+$ in the presence of the B-hadron mass and parton mass, the momenta take the following form:

$$\begin{aligned} p_t^\mu &= (p_t^+, p_t^-, \overrightarrow{0}) = (\frac{m_t}{\sqrt{2}}, \frac{m_t}{\sqrt{2}}, \overrightarrow{0}) \\ q^\mu &= (q^+, q^-, \overrightarrow{0}) = (\frac{m_t\, \eta}{\sqrt{2}\, y}, \frac{y\, m_q^2}{\sqrt{2}\, m_t \eta}, \overrightarrow{0}) \\ p_B^\mu &= (p_B^+, p_B^-, \overrightarrow{0}) = (\frac{m_t}{\sqrt{2}}\eta, \frac{m_B^2}{\sqrt{2}\, m_t \eta}, \overrightarrow{0}). \end{aligned} \tag{E.6}$$

Now to obtain the differential decay rate to produce the B-hadron from top quark decay we use the factorization formula in light cone coordinates, Eq.(E.5). Using $k = \eta/y$ we have:

$$\frac{1}{\Gamma_0}\frac{d\Gamma^B(\eta, m_t, m_b, m_W)}{d\eta} = \sum_{i=b,g}\int_\eta^1 \frac{dy}{y}\left(\frac{1}{\Gamma_0}\frac{d\Gamma_i(y, m_t, m_i, m_W, \mu^2)}{dy}\right)D_i^B\left(\frac{\eta}{y}, \mu^2\right). \tag{E.7}$$

The energy fraction and the observable measured in experiments are given by $x_B = 2p_0^B/m_t$ and $1/\Gamma_0(d\Gamma^B/dx_B)$, respectively. Therefore we have to specify the relation between the two scaling variables x_B and η in the presence of the hadron mass. With respect to the momentum four vectors of the B-hadron in light cone coordinates, $p_B^\mu = ((p_B^0+|\overrightarrow{p_B}|)/\sqrt{2}, (p_B^0-|\overrightarrow{p_B}|)/\sqrt{2}, \overrightarrow{0})$, and comparing with Eq.(E.6) we obtain:

$$\begin{aligned} p_0^B &= \frac{m_t\ \eta}{2}\left(1 + \frac{m_B^2}{m_t^2\ \eta^2}\right) \\ |\overrightarrow{p_B}| &= \frac{m_t\ \eta}{2}\left(1 - \frac{m_B^2}{m_t^2\ \eta^2}\right). \end{aligned} \tag{E.8}$$

Using $p_0^B = (m_t x_B)/2$, thus:

$$\eta(x_B) = \frac{x_B}{2}\Big(1 + \sqrt{1 - \frac{4m_B^2}{m_t^2\ x_B^2}}\Big), \tag{E.9}$$

so that Eq.(E.7) is now related to the measured observable $1/\Gamma_0(d\Gamma/dx_B)$ via:

$$\frac{1}{\Gamma_0}\frac{d\Gamma^B(x_B, m_t, m_b, m_W)}{dx_B} = \left(\frac{1}{\Gamma_0}\frac{d\Gamma^B(\eta(x_B), m_t, m_b, m_W)}{d\eta}\right)\frac{d\eta(x_B)}{dx_B}, \tag{E.10}$$

where $d\eta(x_B)/dx_B = (1-m_B^2/(m_t\eta(x_B))^2)^{-1} = (1+\sqrt{1-4m_B^2/(m_t^2x_B^2)})/(2\sqrt{1-4m_B^2/(m_t^2x_B^2)})$. The final result reads:

$$\frac{1}{\Gamma_0}\frac{d\Gamma}{dx_B}(x_B, m_t, m_b, m_W) = \frac{1}{1-\frac{m_B^2}{m_t^2\eta^2(x_B)}}\sum_{i=b,g}\int_{\eta(x_B)}^1 \frac{dy}{y}\Big(\frac{1}{\Gamma_0}\frac{d\Gamma_i}{dy}(y, m_t, m_i, m_W, \mu^2)\Big)D_i^B\left(\frac{\eta(x_B)}{y}, \mu^2\right). \tag{E.11}$$

Therefore in the presence of the B-hadron mass the general form of the factorization formula is preserved except for a global factor. Note the two variables x_B and η in Eq.(E.9) are approximately equal when $m_B << m_t x_B$, i.e. hadron mass effects can not be neglected when x_B is too small.

E.0.2 Phase Space Approach

In the second approach we verify the previous result by finding the relation between the phase spaces of the B-hadron and the parton. As before we work in the top quark rest frame. To extract the relation between the B-hadron and parton phase space we now define $y = (p_B^0 + |\overrightarrow{p_B}|)/(q^0 + |\overrightarrow{q}|)$, $k = (q^0 + |\overrightarrow{q}|)/m_t$ and $y = \eta/k$, therefore:

$$p_B^0 + |\overrightarrow{p_B}| = y(q^0 + |\overrightarrow{q}|) \Rightarrow \frac{dp_B^0}{dq^0} = \frac{|\overrightarrow{p_B}|}{|\overrightarrow{q}|}. \tag{E.12}$$

We are working in the rest frame where the fragmenting parton momentum ($\overrightarrow{q}$) is parallel to $\overrightarrow{p_B}$ thus $d\Omega_B = d\Omega_q = d\Omega$. Since $d^3\mathbf{p}_B = |\overrightarrow{p_B}|^2\ d|\overrightarrow{p_B}|d\Omega$ we have:

$$\frac{d^3\mathbf{p}_B}{p_B^0} = \frac{d^3\mathbf{q}}{q^0} \times \frac{|\overrightarrow{p_B}|^2}{|\overrightarrow{q}|^2}. \tag{E.13}$$

Now with respect to the following relations:

$$\begin{cases} p_B^0 + |\overrightarrow{p_B}| = m_t y k \\ \\ {p_B^0}^2 - |\overrightarrow{p_B}|^2 = m_B^2 \Rightarrow p_B^0 - |\overrightarrow{p_B}| = \frac{m_B^2}{m_t y k} \end{cases} \Longrightarrow |\overrightarrow{p_B}| = \tfrac{m_t y k}{2}(1 - \tfrac{m_B^2}{m_t^2 y^2 k^2}), \tag{E.14}$$

and

$$\begin{cases} q^0 + |\overrightarrow{q}| = m_t k \\ \\ {q^0}^2 - |\overrightarrow{q}|^2 = m_q^2 \Rightarrow q^0 - |\overrightarrow{q}| = \frac{m_q^2}{m_t k} \end{cases} \Longrightarrow \begin{array}{c} |\overrightarrow{q}| = \frac{m_t k}{2}(1 - \frac{m_q^2}{m_t^2 k^2}) \\ \\ q^0 = \frac{m_t k}{2}(1 + \frac{m_q^2}{m_t^2 k^2}), \end{array} \tag{E.15}$$

Eq.(E.13) is simplified to:

$$\frac{d^3\mathbf{p}_B}{p_B^0} = \frac{d^3\mathbf{q}}{q^0} \times y^2 \times \frac{(1 - \frac{m_B^2}{m_t^2 y^2 k^2})^2}{(1 - \frac{m_q^2}{m_t^2 k^2})^2}. \tag{E.16}$$

Now to incorporate hadron mass effects, we use the general form of the factorization theorem,

$$d\Gamma^B(\eta, m_t, m_W, m_b) = \sum_{i=b,g} \int_\eta^1 dk\ d\Gamma_i(\frac{\eta}{k}, m_t, m_W, m_i, \mu^2) D_i^B(k, \mu^2). \tag{E.17}$$

As the partonic differential decay rate $d^3\Gamma$ is proportional to $\overline{|M|^2}d^3\mathbf{q}/q^0$, the hadronic differential decay rate can be written as:

$$\frac{d^3\Gamma^B}{d\mathbf{p}_B^3} = \sum_{i=b,g}\int_\eta^1 dk\ (\frac{d^3\Gamma_i(\frac{\eta}{k}, m_t, m_W, m_i, \mu^2)}{d\mathbf{q^3}})(\frac{d^3\mathbf{q}}{d^3\mathbf{p}_B})D_i^B(k,\mu^2)$$
$$\Rightarrow \quad \frac{d^2\Gamma}{|\overrightarrow{p_B}|^2 d|\overrightarrow{p_B}|d\Omega_B} = \sum_{i=b,g}\int_\eta^1 dk\ (\frac{d^2\Gamma_i(\frac{\eta}{k}, m_t, m_W, m_i, \mu^2)}{|\overrightarrow{q}|^2 d|\overrightarrow{q}|d\Omega_q})(\frac{d^3\mathbf{q}}{d^3\mathbf{p}_B})D_i^B(k,\mu^2), \tag{E.18}$$

where $d^3\mathbf{q}/d^3\mathbf{p}_B$ is given in Eq.(E.16) and from Eq.(E.15) it can be easily shown that $d|\overrightarrow{q}| = q^0(dk/k)$. Now we define the experimentally measured variable $x_B = (2p_B^0)/\sqrt{s} = (2p_B^0)/m_t$ therefore $|\overrightarrow{p_B}| = (m_t x_B/2)\sqrt{1-4m_B^2/(m_t^2 x_B^2)}$ and $d|\overrightarrow{p_B}| = m_t^2 x_B dx_B/(4|\overrightarrow{p_B}|)$. Now Eq.(E.18) is simplified to:

$$\frac{d\Gamma^B(x_B, m_t, m_b, m_W)}{dx_B} = \frac{1}{1-\frac{m_B^2}{m_t^2\eta^2(x_B)}}\sum_{i=b,g}\int_{\eta(x_B)}^1 \frac{dy}{y}\ (\frac{d\Gamma_i(y, m_t, m_i, m_W, \mu^2)}{dy})D_i^B(\frac{\eta(x_B)}{y},\mu^2), \tag{E.19}$$

where $\eta(x_B) = x_B(1+\sqrt{1-4m_B^2/(m_t x_B)^2})/2$. The advantage of our definition of the variables is that we again get the same factorization formula (Eq.(E.11)).

In Chapters 3 and 4 we calculated the partonic decay rate by defining the variables $z = 2q^0/(m_t(1+b-\omega))$, $x_B = 2p_B^0/(m_t(1+b-\omega))$. Now to simplify more, we define the new scaling variables $z = 2q^0/m_t$, $x_B = 2p_B^0/m_t$ which would be divided by the coefficient $1+b-\omega$, later. Defining these new variables if we want to make use of the previous results for the differential decay rate calculated in Chapters 3 and 4, we have to specify the relations between the new (z, x_B) and old (k, η) variables and express the new form of the factorization formula for this case. We now define $y_B = p_B^0/q^0$ and we start from the definition of the variable y and obtain:

$$y = \frac{p_B^0 + |\overrightarrow{p_B}|}{q^0 + |\overrightarrow{q}|} \Rightarrow y = y_B\frac{1+\sqrt{1-\frac{4m_B^2}{m_t^2x_B^2}}}{1+\sqrt{1-\frac{4m_q^2y_B^2}{m_t^2x_B^2}}}. \tag{E.20}$$

Therefore it is simple to show that:

$$\frac{dy_B}{y_B} = \frac{dy}{y}\times(\sqrt{1-\frac{4m_q^2y_B^2}{m_t^2x_B^2}}). \tag{E.21}$$

We can also show that the relation between the phase space of the B-hadron and partons is now expressed via the following expression instead of Eq.(E.16):

$$\frac{d^3\mathbf{p}_B}{p_B^0} = \frac{d^3\mathbf{q}}{q^0} \times y_B^2 \times \frac{\sqrt{1-\frac{4m_B^2}{m_t^2 x_B^2}}}{\sqrt{1-\frac{4m_q^2 y_B^2}{m_t^2 x_B^2}}}. \tag{E.22}$$

From Eq.(E.21) the previous partonic differential decay rate in Eq.(E.19) is now expressed as:

$$\begin{aligned}\frac{d\Gamma_i(y, m_t, m_W, m_i, \mu^2)}{dy} &= \frac{d\Gamma_i(y_B(y), m_t, m_W, m_i, \mu^2)}{dy_B} \times \frac{dy_B}{dy} \\ &= \frac{d\Gamma_i(y_B(y), m_t, m_W, m_i, \mu^2)}{dy_B} \times \frac{(1+\sqrt{1-\frac{4m_i^2 y_B^2}{m_t^2 x_B^2}})\sqrt{1-\frac{4m_i^2 y_B^2}{m_t^2 x_B^2}}}{1+\sqrt{1-\frac{4m_B^2}{m_t^2 x_B^2}}}.\end{aligned} \tag{E.23}$$

In Eq.(E.22) m_q stands for the mass of the fragmenting parton that from Eq.(E.23) on, we label it by m_i.

Considering the equation above, the result E.19 is now converted to:

$$\begin{aligned}\frac{d\Gamma^B(x_B, m_t, m_b, m_W)}{dx_B} &= \frac{1}{1-\frac{m_B^2}{m_t^2 \eta^2(x_B)}} \times \\ &\sum_{i=b,g} \int_{y_{B,min(x_B)}}^{y_{B,max(x_B)}} \frac{dy_B}{y_B} \left(\frac{d\Gamma_i(y_B(y), m_t, m_i, m_W, \mu^2)}{dy_B}\right) D_i^B\left(\frac{\eta(x_B)}{y(y_B)}, \mu^2\right) \frac{1+\sqrt{1-\frac{4m_i^2 y_B^2}{m_t^2 x_B^2}}}{1+\sqrt{1-\frac{4m_B^2}{m_t^2 x_B^2}}}.\end{aligned} \tag{E.24}$$

Therefore to calculate the differential decay rate for producting the massive B-hadron from top quark decay considering massive partons we have to use the following formula:

$$\begin{aligned}\frac{d\Gamma^B(x_B, m_t, m_b, m_W)}{dx_B} &= \frac{1}{\sqrt{1-\frac{4m_B^2}{m_t^2 x_B^2}}} \times \\ &\sum_{i=b,g} \int_{y_{B,min(x_B)}}^{y_{B,max(x_B)}} \frac{dy_B}{y_B} \left[\left(\frac{d\Gamma_i(y_B(y), m_t, m_i, m_W, \mu^2)}{dy_B}\right) D_i^B\left(\frac{\eta(x_B)}{y(y_B)}, \mu^2\right) \frac{1}{2}\left(1+\sqrt{1-\frac{4m_i^2 y_B^2}{m_t^2 x_B^2}}\right)\right],\end{aligned} \tag{E.25}$$

where,

$$D_i^B\left(\frac{\eta(x_B)}{y(y_B)}\right) = D_i^B\left(\frac{x_B}{y_B} \times \frac{1}{2}\left(1+\sqrt{1-\frac{4m_i^2 y_B^2}{m_t^2 x_B^2}}\right)\right). \tag{E.26}$$

Solving Eq.(E.20) we obtain the integration bounds:

$$y_B = \frac{2Ay}{A^2 + \frac{4m_i^2}{m_t^2 x_B^2} y^2} \Rightarrow \begin{cases} y_{B,max} = (1 + \frac{m_i^2 - m_B^2}{2m_B^2}(1 - \sqrt{1 - \frac{4m_B^2}{m_t^2 x_B^2}}))^{-1} \\ \\ y_{B,min} = \frac{x_B}{1 + \frac{m_i^2}{m_t^2}}, \end{cases} \tag{E.27}$$

where $A = 1 + \sqrt{1 - \frac{4m_B^2}{m_t^2 x_B^2}}$.

Appendix F

Rest Frames for Cascade Decay of $t \to X_b + W^+(\to e^+ + \nu_e)$

In this appendix we want to study and find out the connection between the two different rest frames needed for our calculation in the cascade decay $t \to X_b + W^+(\to e^+ + \nu_e)$. As we saw in Eq.(5.18) on the one hand in the covariant approach the invariant $L^{\mu\nu}H_{\mu\nu} = 4(P_b.P_\nu)(P_t.P_{e^+})$ must be evaluated in one particular frame where we choose the top quark rest frame. On the other hand we want to calculate the angular decay distribution for the top quark by the polar angle θ, which is measured in the W^+ rest frame where the lepton pair emerges back-to-back, Fig.5.3. The two desired rest frames are shown in Fig.F.1. In the top quark rest frame the four vectors of momenta are written as:

$$\begin{aligned} P_t^{\star,\mu} &= m_t(1;0,0,0) \\ P_b^{\star,\mu} &= m_t(S;0,0,-Q) \\ P_W^{\star,\mu} &= \frac{m_t}{2}(1-b+\omega;0,0,2Q) \\ P_e^{\star,\mu} &= (E_e^\star;A,0,B), \end{aligned} \tag{F.1}$$

and in the W^+-boson rest frame the four vectors of momenta needed, are:

$$\begin{aligned} P_e^{R,\mu} &= \frac{m_W}{2}(1;\sin\theta^R,0,\cos\theta^R) \\ P_\nu^{R,\mu} &= \frac{m_W}{2}(1;-\sin\theta^R,0,-\cos\theta^R) \\ P_b^{R,\mu} &= (E_b;0,0,|\overrightarrow{p_b}|). \end{aligned} \tag{F.2}$$

To calculate the $P_e^{\star,\mu}$ and $P_\nu^{\star,\mu}$ four vectors we consider two invariant variables $(P_b+P_\nu)^2$ and $(P_b+P_e)^2$ and calculate them in the two rest frames mentioned above and by comparing

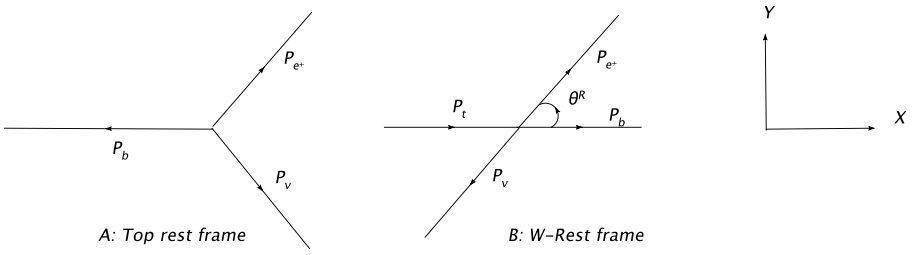

Figure F.1: Rest frame of the decaying system ($p_t = 0$) and the system formed by the particles e^+ and ν_e

them we extract our parameters. In the following we show the details of calculation:

$$\begin{aligned}(P_b^{\star,\mu} + P_\nu^{\star,\mu})^2 &= m_t^2 - 2\ m_t\ E_e^\star; \qquad \text{in t-quark rest frame,}\\ (P_b^{R,\mu} + P_\nu^{R,\mu})^2 &= m_t^2\big(S + Q\cos\theta^R\big); \quad \text{in W-rest frame.}\end{aligned} \tag{F.3}$$

We have to pay attention to the point that the angle θ defined in Fig.5.3 is different to the angle θ^R in Fig.F.1. We have to exchange the angle θ^R with θ as: $\theta^R \to \pi - \theta$. Then Eq.(F.3) yields:

$$E_e^\star = \frac{m_t}{2}\Big(\frac{1-b+\omega}{2} + Q\ \cos\theta\Big). \tag{F.4}$$

In the next step we consider the invariant variable $(P_b + P_e)^2$ in the two rest frames:

$$\begin{aligned}(P_b^{\star,\mu} + P_e^{\star,\mu})^2 &= m_t^2\Big(b + \frac{2B\ Q}{m_t} + S\Big(\frac{1-b+\omega}{2} + Q\cos\theta\Big)\Big); \quad \text{in the t-quark rest frame,}\\ (P_b^{R,\mu} + P_e^{R,\mu})^2 &= m_t^2\big(S + Q\ \cos\theta\big); \qquad\qquad\qquad\qquad \text{in the W-rest frame.}\end{aligned} \tag{F.5}$$

After comparing them we have: $B = m_t(Q + (1-b+\omega)/2\ \cos\theta)/2$. Since the positron is considered massless ($P_{e^+}^2 = 0$) we obtain $A = m_W/2 \cdot \sin\theta$. Therefore in the top quark rest frame for the positron momentum four-vector we have:

$$P_e^{\star,\mu} = \frac{m_t}{2}\Big(\frac{1-b+\omega}{2} + Q\cos\theta; \sqrt{\omega}\sin\theta, 0, Q + \frac{1-b+\omega}{2}\cos\theta\Big). \tag{F.6}$$

For the electron-nutrino momentum four-vector we have:

$$\begin{aligned}&P_\nu^{\star,\mu} = P_W^{\star,\mu} - P_e^{\star,\mu} \Longrightarrow\\ &P_\nu^{\star,\mu} = \frac{m_t}{2}\Big(\frac{1-b+\omega}{2} - Q\cos\theta; -\sqrt{\omega}\sin\theta, 0, Q - \frac{1-b+\omega}{2}\cos\theta\Big).\end{aligned} \tag{F.7}$$

Appendix G

Helicity Components of Cascade Decay Rate of Top Decay

In section 5.3.2 we calculated the angular decay distribution of the cascade decay process $t \to b + W^+(\to e^+ + \nu_e)$ and in Eq.(5.63) we showed that the differential decay width can be written in the following form:

$$\frac{1}{\Gamma_0'}\frac{d^2\hat{\Gamma}}{dx_b\ d\cos\theta} = \hat{H}_{++}\cdot\frac{3}{8}(1+\cos\theta)^2 + \hat{H}_{--}\cdot\frac{3}{8}(1-\cos\theta)^2 + \hat{H}_{00}\cdot\frac{3}{4}\sin^2\theta, \qquad \text{(G.1)}$$

where $\hat{H}_{++}, \hat{H}_{--}$ and $\hat{H}_{00}$ are the transverse-plus and the transverse-minus and the longitudinal helicity components of the differential decay, respectively. This components were calculated in Eqs(5.64,5.68,5.70). Now to obtain the individual helicity components of top decay rate, in Eqs(5.64,5.68,5.70) we have to integrate over $x_b (0 \le x_b \le 1)$. We start from Eq.(5.64), therefore after integrating over x_b we obtain the following result:

$$\begin{aligned}
\hat{\Gamma}_{00} \;=\; & \frac{1}{1+2\omega} + \frac{\alpha_S}{2\pi}C_F\frac{\omega}{(1-\omega)^2(1+2\omega)}\Big\{\frac{(1-\omega)(-4\omega^2+47\omega+5)}{2\omega} - \frac{2\omega^2+5\omega+1}{\omega}\frac{2\pi^2}{3} + \\
& 8(1+2\omega)\log\omega - \frac{3(1-\omega)^2}{\omega}\log(1-\omega) - (1-\sqrt{\omega})^2\frac{\omega^{\frac{3}{2}}+6\omega-\sqrt{\omega}+2}{\omega}\log(1-\sqrt{\omega})\log\omega \\
& -(1+\sqrt{\omega})^2\frac{-\omega^{\frac{3}{2}}+6\omega+\sqrt{\omega}+2}{\omega}\log(1+\sqrt{\omega})\log\omega \\
& -2(1-\sqrt{\omega})^2\frac{\omega^{\frac{3}{2}}+8\omega+3\sqrt{\omega}+4}{\omega}Li_2(\sqrt{\omega}) - 2(1+\sqrt{\omega})^2\frac{-\omega^{\frac{3}{2}}+8\omega-3\sqrt{\omega}+4}{\omega}Li_2(-\sqrt{\omega})\Big\},
\end{aligned} \qquad \text{(G.2)}$$

where we defined $\hat{\Gamma}_{00} = \int_0^1 dx_b\ \hat{H}_{00}$. This result is in good agreement with [91] where the authors defined $\hat{\Gamma}_L = \hat{\Gamma}_{00}$.

Now we turn our attention to Eq.(5.68). After integrating over x_b the result reads:

$$\begin{aligned}\hat{\Gamma}_{--} &= \frac{2\omega}{1+2\omega}+\frac{\alpha_S}{2\pi}C_F\frac{\omega}{(1-\omega)^2(1+2\omega)}\Big\{-\frac{1}{2}(1-\sqrt{\omega})(\omega^{\frac{3}{2}}-7\omega+33\sqrt{\omega}+13)+\\ &\frac{-2\omega^2+4\omega+3}{3}\pi^2-\frac{2(1-\omega)(1-4\omega)}{\omega}\log(1+\sqrt{\omega})-\frac{2(1-\omega)^2(1+2\omega)}{\omega}\log(1-\sqrt{\omega})\\ &-(-2\omega^2+7\omega+5)\log\omega-\frac{(1-\sqrt{\omega})^2}{2\sqrt{\omega}}(4\omega^{\frac{3}{2}}+7\omega+5)\log\omega\log(1-\sqrt{\omega})+\\ &\frac{(1+\sqrt{\omega})^2}{2\sqrt{\omega}}(-4\omega^{\frac{3}{2}}+7\omega+5)\log\omega\log(1+\sqrt{\omega})-\\ &\frac{12\omega^{\frac{5}{2}}-\omega^2-26\omega^{\frac{3}{2}}+12\omega-2\sqrt{\omega}+5}{\sqrt{\omega}}Li_2(\sqrt{\omega})+\\ &\frac{-4\omega^{\frac{5}{2}}-\omega^2+6\omega^{\frac{3}{2}}+12\omega+2\sqrt{\omega}+5}{\sqrt{\omega}}Li_2(-\sqrt{\omega})\Big\}.\end{aligned} \tag{G.3}$$

As before we defined $\hat{\Gamma}_{--}=\int_0^1 dx_b\ \hat{H}_{--}$.
Now for the contribution of the transverse-plus helicity to the top quark decay rate, Eq.(5.70) after integrating over x_b reads:

$$\begin{aligned}\hat{\Gamma}_{++} &= \frac{\alpha_S}{2\pi}C_F\frac{\omega}{(1-\omega)^2(1+2\omega)}\Big\{-\frac{1}{2}(1-\sqrt{\omega})(\omega^{\frac{3}{2}}+9\omega+5\sqrt{\omega}+25)+\frac{(-2\omega^2+6\omega+7)\pi^2}{3}\\ &-(-2\omega^2+7\omega+5)\log\omega-2(2\omega^2-7\omega+5)\log(1+\sqrt{\omega})-\\ &\frac{(1-\sqrt{\omega})^2}{2\sqrt{\omega}}(4\omega^{\frac{3}{2}}+7\omega+5)\log\omega\log(1-\sqrt{\omega})+\\ &\frac{(1+\sqrt{\omega})^2}{2\sqrt{\omega}}(-4\omega^{\frac{3}{2}}+7\omega+5)\log\omega\log(1+\sqrt{\omega})-\\ &+\frac{4\omega^{\frac{5}{2}}-\omega^2-10\omega^{\frac{3}{2}}+12\omega-10\sqrt{\omega}+5}{\sqrt{\omega}}Li_2(\sqrt{\omega})\\ &\frac{-12\omega^{\frac{5}{2}}-\omega^2+30\omega^{\frac{3}{2}}+12\omega+10\sqrt{\omega}+5}{\sqrt{\omega}}Li_2(-\sqrt{\omega})\Big\},\end{aligned} \tag{G.4}$$

where we defined $\hat{\Gamma}_{++}=\int_0^1 dx_b\ \hat{H}_{++}$. This result is in perfect agreement with [91]. We

can also show that Eq.(3.38) after integrating over x_b reads:

$$\begin{aligned}\hat{\Gamma} &= 1+\frac{\alpha_S}{2\pi}C_F\frac{\omega}{(1-\omega)^2(1+2\omega)}\Big\{\frac{(1-\omega)(-6\omega^2+9\omega+5)}{2\omega}-2(-2\omega^2-\omega+1)\log\omega- \\ &\frac{(1-\omega)^2(5+4\omega)}{\omega}\log(1-\omega)-2\frac{(1-\omega)^2(1+2\omega)}{\omega}\Big(\log\omega\log(1-\omega)+\frac{\pi^2}{3}\Big) \\ &-8\frac{(1-\omega)^2(1+2\omega)}{\omega}\Big(Li_2(\sqrt{\omega})+Li_2(-\sqrt{\omega})\Big)\Big\}. \qquad \text{(G.5)}\end{aligned}$$

Summing up Eqs.(G.2,G.3,G.4), one can show that the total rate (Eq.(G.5)) is the summation of all helicity contributions, i.e.:

$$\hat{\Gamma}=\hat{\Gamma}_{00}+\hat{\Gamma}_{++}+\hat{\Gamma}_{--}. \qquad \text{(G.6)}$$

Bibliography

[1] S. Weinberg, Phys. Rev. Lett. 19 (1967) 1264; A. Salaam, in Elementary particle Physics, ed. N. Svartholm (Almqvist and Wiksells, Stockholm, 1968), p.367.

[2] [CDF Collaboration], arXiv:hep-ex/0703034.

[3] M. Martinez and R. Miquel, Eur. Phys. J. C **27** (2003) 49 [arXiv:hep-ph/0207315].

[4] K. Hagiwara et al, Phys. Rev. D 66 (2002) 010001.

[5] T. Muta, "Foundations of quantum chromodynamics. Second edition," World Sci. Lect. Notes Phys. **57** (1998) 1.

[6] R. K. Ellis, W. J. Stirling and B. R. Webber, "QCD and Collider Physics," Cambridge Univ. Press, 1996.

[7] A. Bassetto, M. Ciafaloni and G. Marchesini, Phys. Rept. **100** (1983) 201.

[8] Y. L. Dokshitzer, D. Diakonov and S. I. Troian, Phys. Rept. **58** (1980) 269.

[9] Yu. L. Dokshitzer, V. A. Khoze, A. H. Mueller and S. I. Troyan, *Basic of Perturbative QCD, Editions Frontieres*, Gif-sur-Yvette, 1991.

[10] M. Gell-Mann, Phys. Lett. **8** (1964) 214; G. Zweig, Preprints CERN-TH 401 and 412.

[11] M. Han and Y. Nambu, Phys. Rev. **139B** (1965) 1006; M. Gell-Mann, Acta Phys. Austriaca Suppl. 9 (1972) 733.

[12] R. P. Feynman, Phys. Rev. Lett. **23** (1969) 1415.

[13] J. D. Bjorken, Phys. Rev. **179** (1969) 1547.

[14] M. Breidenbach *et al.*, Phys. Rev. Lett. **23** (1969) 935.

[15] C. G. Callan and D. J. Gross, Phys. Rev. Lett. **22** (1969) 156.

[16] G. 't Hooft, Nucl. Phys. B 33 (1971) 173.

[17] H. Fritzsch, M.Gell-Mann and H. Leutwyler, Phys.Lett. B 47 (1973) 365.

[18] O. V. Tarasov, A. A. Vladimirov and A. Yu. Zharkov, Phys. Lett. B 93 (1980) 429;
S.A.Larin and J. A. M. Vermaseren , Phys. Lett. B 303(1993) 334;
T. van Ritbergen, J. A. M. Vermaseren and S. A. Larin, Phys. Lett. B 400 (1997) 379

[19] W. Bernreuther, Ann. Phys (NY) 151 (1983) 127; Erratum Nucl. Phys. B 513 (1998) 758.

[20] D.I.Gross and F. Wilczek, Phys. Rev. D 8 (1973) 3497; H. D. Politzer, Phys. Rev. Lett. 26 (1973) 1346

[21] S. Catani, M. L. Mangano and P. Nason, JHEP 9807 (1998) 024.

[22] W. J. Marciano, Phys. Rev. D **29** (1984) 580.

[23] J. C. Collins, D. E. Soper and G. Sterman, in *Perturbative* QCD, edited by A. H. Mueller (World Scientific, Singapore, 1989), P.1.

[24] J. C. Collins, Phys. Rev. D 66 (1998) 094002.

[25] J. C. Collins and D. E. Soper, Nucl. Phys. B 194 (1982) 445.

[26] G. Curci, W. Furmanski and R. Petronzio, Nucl. Phys. B 175 (1980) 27;
W. Furmanski and R. Petronzio, Phys. Lett. B97 (1980) 437.

[27] M. Gluck, E. Reya and A. Vogt, Eur. Phys. J. C 5 (1998) 461.

[28] S. Libby and G. Sterman, Phys. Rev. D 18 (1978) 3252; 18 (1978) 4737.

[29] G. Altarelli and G. Parisi, Nucl. Phys. B 126 (1977) 298.

[30] V. N. Gribov and L. N. Lipatov, Sov. J. Nucl. Phys. 15 (1972) 438;
L. N. Lipatov, Sov. J. Nucl. Phys. 20 (1975) 94;
Yu. L. Dokshitzer, Sov. Phys. JETP 46 (1977) 641.

[31] E. G. Floratos, D. A. Ross and C. T. Sachrajda, Nucl. Phys. B **129** (1977) 66 [Erratum-ibid. B **139** (1978) 545].

[32] A. Gonzalez-Arroyo, C. Lopez and F. J. Yndurain, Nucl. Phys. B **153** (1979) 161.

[33] E. G. Floratos, C. Kounnas and R. Lacaze, Nucl. Phys. B **192** (1981) 417.

[34] G. Curci, W. Furmanski and R. Petronzio, Nucl. Phys. B **175** (1980) 27.

[35] E. G. Floratos, D. A. Ross and C. T. Sachrajda, Nucl. Phys. B 129 (1977) 66; ibid. B 139 (1978) 545 (erratum); ibid. B 152 (1979) 493; A. Gonzales-Arroyo, C. Lopez and F. J. Yndurainn, Nucl. Phys. B 153 (1979) 161; E. G. Floratos, R. Lacaze and C. Kounnas, Nucl. Phys. B 192 (1981) 417.

[36] G. Sterman, Phys. Rev. D 17 (1978) 2773; ibid 2789.

[37] F. Bloch and A. Nordsieck, Phys. Rev. 52 (1937) 54; A. Nordsieck, Phys. Rev. 52 (1937) 59.

[38] T. Kinoshita, J. Math. phys. 3 (1962) 650; T. D. Lee and M. Nauenberg, Phys. Rev. 133 (1964) 1545.

[39] S. Weinberg, Phys. Rev. 140B (1965) 516.

[40] S. Catani and M. Grazzini, Nucl. Phys. B 570 (2000) 287.

[41] S. Kretzer and I. Schienbein, Phys. Rev. D 58 (1998) 094035.

[42] B. Mele and P. Nason, Nucl. Phys. B 361 (1991) 626.

[43] M. Cacciari and S. Catani, Nucl. Phys. B 617 (2001) 253.

[44] G. Colangelo and P. Nason, Phys. Lett. B 285 (1992) 167.

[45] M. Cacciari and M. Greco, Phys. Rev. D 55 (1997) 7134.

[46] P. Nason and C. Oleari, Nucl. Phys. B 565 (2002) 245.

[47] M. Cacciari and P. Nason, Phys. Rev. Lett. 89 (2002) 122003.

[48] M. Cacciari and M. Greco, Nucl. Phys. B 421 (1994) 530.

[49] M. Cacciari, M. Greco, S. Rolli and A. Tanzini, Phys. Rev. D 55 (1997) 2736.

[50] M. Cacciari and M. Greco, Z. Phys. C 69 (1996) 459.

[51] G. Corcella and A. D. Mitov, Nucl. Phys. B 623 (2002) 247.

[52] S. Keller and E. Laenen, Phys. Rev. D 59 (1999) 114004.

[53] CDF Collaboration, T.Affolder et al., Phys. Rev. Lett.**86** (2001) 3233.

[54] L. Zwirner, Ph.D Thesis,Hamburg University,2003

[55] G. 't Hooft and M.Veltman,Nucl. Phys. B44 189 (1972).

[56] M. Chanowitz, M. Furman, and I. Hinchliffe, Nucl. Phys. B159 225 (1979).

[57] P.Breitenlohner and D.Maison, Commu. Math. Phys. 52 11 (1977).

[58] J. G. Krner, G. Schuler, G. Kramer and B. Lampe, Phys. Lett. B **164** (1985) 136.

[59] S. Dittmaier, Nucl. Phys. B **675** (2003) 447

[60] L. Mihaila, Ph.D Thesis,Hamburg University,2002

[61] E.Byckling, K.Kajantie, "Particle Kinematics," John Wiley and Sons. (1973).

[62] G. t' Hooft, Nucl. Phys. B**61** (1973) 455.

[63] C. S. Li and R. J. Oakes, Phys. Rev. D **43** (1991) 855.

[64] A. Heister *et al.* [ALEPH Collaboration], Phys. Lett. B **512** (2001) 30 [arXiv:hep-ex/0106051].

[65] G. Abbiendi *et al.* [OPAL Collaboration], Eur. Phys. J. C **29** (2003) 463 [arXiv:hep-ex/0210031].

[66] K. Abe *et al.* [SLD Collaboration], Phys. Rev. Lett. **84** (2000) 4300; Phys. Rev. D 65, 092006 (2002); 66, 079905 (E) (2002) [arXiv:hep-ex/9912058].

[67] Harry Bateman, "Higher Transcendental Functions", McGRAW-HILL BOOK COMPANY, INC. 1953.

[68] T. Huber and D. Maitre, Comput. Phys. Commun. **175** (2006) 122 [arXiv:hep-ph/0507094].

[69] L. Lewin, "Dilogarithms and Associated Functions", MacDonald, London, 1958.

[70] S. Moch and P. Uwer, Comput. Phys. Commun. **174** (2006) 759 [arXiv:math-ph/0508008].

[71] P. Nason, S. Dawson, and R.K. Ellis, Nucl. Phys. **B303**, 607 (1988); **B327**, 49 (1989); **B335**, 260(E) (1989);W. Beenakker, H. Kuijf, W. L. van Neerven and J. Smith, Phys. Rev. D **40** (1989) 54; W. Beenakker, W.L. van Neerven, R. Meng, G.A.Schuler, and J. Smith, Nucl. Phys. **B351**, 507 (1991); I. Bojak and M. Stratmann, Phys. Rev. D **67**, 034010 (2003).

[72] J. Binnewies, B. A. Kniehl and G. Kramer, Phys. Rev. D **58** (1998) 034016 [arXiv:hep-ph/9802231].

[73] R. Akers *et al.* [OPAL Collaboration], Z. Phys. C **67** (1995) 57.

[74] G. Alexander *et al.* [OPAL Collaboration], Phys. Lett. B **364** (1995) 93.

[75] B. A. Kniehl and G. Kramer, Phys. Rev. D **60** (1999) 014006 [arXiv:hep-ph/9901348].

[76] G. Kramer and H. Spiesberger, Eur. Phys. J. C **38** (2004) 309 [arXiv:hep-ph/0311062].

[77] B. A. Kniehl, G. Kramer, I. Schienbein and H. Spiesberger, Phys. Rev. D **71** (2005) 014018 [arXiv:hep-ph/0410289].

[78] S. Kretzer and I. Schienbein, Phys. Rev. D **59** (1999) 054004 [arXiv:hep-ph/9808375].

[79] G. Kramer and H. Spiesberger, Eur. Phys. J. C **22** (2001) 289 [arXiv:hep-ph/0109167].

[80] B. A. Kniehl, G. Kramer, I. Schienbein and H. Spiesberger, Eur. Phys. J. C **41** (2005) 199 [arXiv:hep-ph/0502194].

[81] B. A. Kniehl, G. Kramer, I. Schienbein and H. Spiesberger, Phys. Rev. Lett. **96** (2006) 012001 [arXiv:hep-ph/0508129].

[82] G. Alexander *et al.* [OPAL Collaboration], Phys. Lett. B **364** (1995) 93.

[83] B. Mele and P. Nason, Phys. Lett. B **245** (1990) 635.

[84] C. Peterson, D. Schlatter, I. Schmitt and P. M. Zerwas, Phys. Rev. D **27** (1983) 105.

[85] B. A. Kniehl, G. Kramer, I. Schienbein and H. Spiesberger, Phys. Rev. D **77** (2008) 014011 [arXiv:0705.4392 [hep-ph]].

[86] P. Nason and B. R. Webber, Nucl. Phys. B **421** (1994) 473; ibid. B480 (1996) 755 (erratum).

[87] S. Albino, B. A. Kniehl and G. Kramer, Nucl. Phys. B **803** (2008) 42 [arXiv:0803.2768 [hep-ph]].

[88] R. Brandelik *et al.* [TASSO Collaboration], Phys. Lett. B **94** (1980) 444.

[89] R. Brandelik *et al.* [DASP Collaboration], Nucl. Phys. B **148** (1979) 189.

[90] J. G. Krner and M. C. Mauser, Lect. Notes Phys. **647** (2004) 212 [arXiv:hep-ph/0306082].

[91] M. Fischer, S. Groote, J. G. Krner and M. C. Mauser, Phys. Rev. D **63** (2001) 031501 [arXiv:hep-ph/0011075].

[92] T. N. Vickey, Ph.D Thesis, "Measurement of W boson polarization in top quark decay," CITATION = UMI-31-60963-MC.

[93] H. S. Do, S. Groote, J. G. Krner and M. C. Mauser, Phys. Rev. D **67** (2003) 091501 [arXiv:hep-ph/0209185].

[94] B. Abbott *et al.* [D0 Collaboration], Phys. Rev. D **58** (1998) 052001;
A. A. Affolder *et al.* [CDF Collaboration], Phys. Rev. D **63** (2001) 032003.

[95] A. Kharchilava, Phys. Lett. B **476** (2000) 73;
G. Corcella, J. Phys. G26 (2000) 634;
G. Corcella, M.L. Mangano and M.H. Seymour, JHEP 0007 (2000) 004.

[96] F. Abe *et al.* [CDF Collaboration], Phys. Rev. Lett. **75** (1995) 1451, Phys. Rev. D **65**,052005 (2002) .

[97] J. C. Collins, "Light-cone variables, rapidity and all that," arXiv:hep-ph/9705393.

ACKNOWLEDGMENTS

First of all I would like to thank my supervisor Professor Bernd A. Kniehl for opening the doors of perturbative QCD to me and also for offering me the opportunity to work on this interesting title. I am particularly grateful to Professor G. Kramer for his helpful advices during my research. I would also like to thank my spouse and my child to accompany me during our staying in Hamburg. I am also grateful to Mathias Butenschön for very useful discussions on QCD and also for every pleasant time which we had together. I would also like to thank Dr. Simon Albino for the helpful discussions on the effect of the B-hadron mass on the energy distribution of B-hadron obtained in decay processe. And finally I am grateful to my father who motivated me to continue my studies.